



UNIVERSITEIT • STELLENBOSCH • UNIVERSITY
jou kennisvenoot • your knowledge partner

Soil Formation on the Namaqualand Coastal Plain



by
Michele Louise Francis

Submitted to the Department of Soil Science
in part fulfilment of the requirements for the degree of

Doctor of Philosophy in Agriculture

UNIVERSITY OF STELLENBOSCH

Supervisors: M. V. Fey and F. Ellis

March 2008

© University of Stellenbosch 2008

Declaration

I, Michele Louise Francis, declare that this dissertation is my own work, except where otherwise stated. It is being submitted for the degree Doctor of Philosophy in Agriculture at the University of Stellenbosch and it has not been submitted before for any degree or examination, at any other university.

Signature of Author

Stellenbosch
March 2008

Abstract

The (semi-)arid Namaqualand region on the west coast of South Africa is well-known for its spring flower displays. Due to the aridity of the region, soils research has lagged behind that of the more agriculturally productive parts of South Africa. However, rehabilitation efforts after the hundred or so years of mining, coupled with the increasing ecology and biodiversity research, have prompted a recent interest in Namaqualand soils as a substrate for plant growth. The area is also notable for the abundance of heuweltjies. Much of the previous heuweltjie-work focussed on biogenic aspects such as their spacing, origin and age, but although heuweltjies are in fact a soil feature, there have been few published studies on the soil forming processes within heuweltjies. However, the depositional history of the sediments on the Namaqualand coastal plain is well constrained, which is in stark contrast to the paucity of data on their subsequent pedogenesis. Given that the regolith has been subaerially exposed in some parts for much of the Neogene, the soil formation forms an important part of the sediments' history. The primary aim of this thesis, therefore, was to examine the soil features of the Namaqualand coastal plain to further the understanding of pedogenesis in the region.

The regolith of the northern Namaqualand coastal plain, often ten or more metres deep, comprises successive late Tertiary marine packages, each deposited during sea-level regression. The surface soil horizons formed from an aeolian parent material. The relatively low CaCO_3 in the aeolian sands dictated the pedogenic pathway in these deposits. The non-calcareous pathway lead to clay-rich, redder apedal horizons that show a stronger structure with depth, and generally rest directly on marine sands via a subtle discontinuity that suggests pedogenesis continues into the underlying marine facies. The calcareous pathway lead to similar clay-rich, redder apedal B horizons, but which differ in that they are calcareous,

and rest on a calcrete horizon often via a stoneline of rounded pebbles. Deeper in the profile, there is generally a regular alteration of sedimentary units, with the upper shoreface facies showing reddening, and the lower shoreface sands remaining pale. This seems to be a function of the grain size, since the upper shoreface materials are coarser, and the redder parts of the lower shoreface are also associated with slightly coarser sands. In some strata the oxidation of glauconite-rich sediments resulted in an orange colour. In an area with abundant heuweltjies, a strongly-cemented calcretized nest was present about 2 m deep within a silica cemented, locally calcareous dorbank profile. Vertical termite burrows are present up to 12 m deep, and appear to have been conduits for preferential vertical flow. Soil formation and termite activity is at least as old as the Last Interglacial. E horizons may have formed in a wetter Last Interglacial paleoclimate, but they are still active in the present day.

The Namaqualand coastal plain, with its extensive areas of calcrete development, is almost a textbook setting for calcrete development by inorganic processes. However, these calcretes also show microscale biogenic features. These include M rods, MA rods, and fungal filaments. Abiotic alpha-fabric seems dominant in mature calcrete horizons, and beta-fabric in calcareous nodules in a calcic B horizon above calcrete. The apparent absence of Mg-calcite and dolomite, and abundance of sepiolite in the calcretes of coastal Namaqualand suggests that these Mg-rich clay minerals are the main Mg-bearing phase. Deformation (pseudo-anticlines) in the calcrete appear to result primarily from the displacive effect of calcite crystallization. Although evidence of shrink/swell behaviour is present in the form of accommodating planes, it does not appear to be as volumetrically significant as displacive calcite.

Indurated light-coloured horizons that resembled calcrete but are non- to mildly calcareous, break with a conchoidal fracture, resist slaking in both acid and alkali, turn methyl-orange purple, and show a bulk-soil sepiolite XRD peak are similar to palygorskite-cemented material ('palycrete') from Spain and Portugal, and so were tentatively named 'sepiocrete'. Sepiolite and palygorskite are often reported from arid region soils but there has been no recorded cementation of soils by sepiolite. The degree of induration in some of these horizons suggest that amorphous silica could play a role in cementation, and so this thesis compares the two silica-cemented horizons encountered in Namaqualand (silcrete and dorbank (petroduric)) to these 'sepiocrete' horizons. Both silica and sepiolite are

present in the matrix, although the degree to which silica and sepiolite dominate seems to vary even within same horizon. It seems most probable that both contribute to the structural properties of the horizon. Sepiolitic horizons do not form a diagnostic horizon in the World Reference Base, Soil Taxonomy, or the South African system. To fit the existing soil classification schemes, the terms 'sepiolitic' and 'petrosepiolitic' (in the same sense as 'calciic' and 'petrocalciic') would be appropriate. The term 'sepiolitic' should be used for horizons which: contain sepiolite in amounts great enough for it to be detected by XRD in the bulk soil, peds (a fractured surface and not just the cutan) cling strongly to the wetted tongue, and methyl orange turns from orange to purple-pink over most of a fragmented surface. The term can be easily be applied as a adjective to other hardpans where sepiolite is significant but not necessarily cementing, such as 'sepiolitic' petrocalciic/petroduric. If the horizon is in addition to the above criteria cemented to such a degree that it will slake neither in acid (so cannot be classified as petrocalciic) nor in alkali (and so cannot be classified as petroduric) then the term 'petrosepiolitic' would be appropriate. The 'sepiolitic' criteria distinguish the 'petrosepiolitic' horizon from a 'silcrete', a silica-cemented horizon which does not fit the definition of petroduric.

Sepiolite is more prominent than palygorskite in the XRD traces. The $<0.08 \mu\text{m}$ fraction is the only size fraction where palygorskite could be detected before acetate treatment. It is unlikely that these fibrous clay minerals are inherited from either the marine or aeolian parent materials, they appear to be pedogenic in origin. Sepiolite and palygorskite are associated with the presence of calcite in the soil profile. Trends in MgO , Al_2O_3 and SiO_2 show that the soil clay fractions lie on a mixing line between sepiolite and mica end-members, with a contribution from smectite, and is consistent with the XRD and TEM results. There is a good correlation between Fe_2O_3 and TiO_2 , which can be attributed to the ubiquitously presence of mica. There was no TEM evidence of fibrous mineral degradation to sheet silicates, nor for the evolution of mica laterally to a fibrous mineral. SEM analyses show that much of the sepiolite/palygorskite occurs as fringed sheets, but higher magnification often revealed these sheets to be composed of fibres. These are found coating (rather than evolving from) mica/illite particles, as free-standing mats, and are common on the grain-side of cutans. Some of these textures suggest illuviation of the fibrous clay minerals, but another explanation may be that sites such as that immediately adjacent

to silicate grains have the highest concentration of silica for their formation. There was no conclusive evidence for or against the presence of kerolite in the clay fraction, although it does not appear to be a dominant phase in the $<2 \mu\text{m}$ fraction.

The hypothesis was that the permeable upper horizons in Namaqualand soils constitute a shallow ephemeral aquifer, which can be considered the pedogenic analogue of the saline lake environments in which sepiolite typically forms. The chemical evolution of the soil solution and clay mineral genesis could therefore be considered in the same terms as the geochemical evolution of closed-basin brines. The Namaqualand coastal plain, like other maritime areas, shows a trend of decreasing pH, increasing Ca and increasing Mg with increasing evaporation. This can be explained by their seawater-influenced initial ratios, and is consistent with the ‘chemical divides’ of the Hardie-Eugster model of brine evolution. Halite remains undersaturated at all concentrations in the saturated paste extracts. At higher concentrations, gypsum reaches saturation, and sulfate is removed from solution. H_4SiO_4 activity remains unchanged for all levels of evaporation and pH. Calcite remains close to saturation, and is only dependent on the HCO_3^- activity and pH for the range of Cl^- activity encountered. Most of the soils for which there is a positive sepiolite identification show a positive sepiolite saturation index. The sepiolite saturation index is independent of Mg^{2+} and H_4SiO_4 and only increases with increasing pH. Evidence of the pH control on sepiolite saturation is that sepiolite is commonly associated with calcareous horizons. Sepiolite precipitation is therefore more likely to be triggered when a solution encounters a pH barrier than by the concentration of ions by evaporation. The effect of a pH change on the sepiolite saturation index is much greater than that of the effect on calcite. The marine-influenced high Mg coupled with the Hardie-Eugster model of brine evolution offers an explanation for sepiolite-dominance at the coast, and palygorskite-dominance inland. Coastal areas, unlike continental areas, have $\text{Mg} > \text{HCO}_3^-$ initially, which results in an increasing Mg trend with evaporation during the precipitation of sepiolite according to the Hardie-Eugster scheme. The result is that after sepiolite precipitation is initiated by a geochemical pH-barrier, Mg levels will rise causing the increasing $(\text{Mg} + \text{Si})/\text{Al}$ ratio to continue to favour sepiolite precipitation. This suggests that once sepiolite has begun to precipitate, the subsequent salinity with its accompanying Mg increase makes substantial palygorskite formation unlikely to follow.

The hardpan horizons in heuweltjies commonly grade from a ‘sepiolitic’ petrocalcic in the centre through ‘sepiolitic’/‘petrosepiolitic’ to the petroduric horizon on the edges. Noteworthy sepiolite-related pedofeatures in the calcrete include ‘ooids’ with successive sepiolite (hydrophilic and therefore a precipitational substrate) and micrite/acicular calcite layers in the coatings; and limpid yellow nodules with pseudo-negative uniaxial interference figures. They superficially resemble the spherulites in the fresh termite frass. Their fibrous nature and low birefringence, together with the low Ca, high Mg, Si composition, and molar Mg/Si ratios consistent with sepiolite. The pedogenesis of the hardpans in the heuweltjie is proposed to be as follows: enrichment of cations such as Ca and Mg in the heuweltjie centre caused by termite foraging results in calcite and clay authigenesis in the centre of the heuweltjie, leaving the precipitation of pure silica to occur on the periphery. The decaying organic matter concentrated in the centre of the mound by the termites is sufficient to supply the components for calcite precipitation in the centre of the heuweltjie. Following calcite precipitation, the pH is suitable for sepiolite precipitation. The movement of the Mg-Si enriched water downslope, coupled with the decrease in HCO_3^- and increase in Mg^{2+} due to sepiolite precipitation, allows for the precipitation of the ‘sepiolitic’ zone on the outer side of the calcrete, and extend beyond the calcrete in some heuweltjies.

The Namaqualand coastal plain is well positioned for further work on its regolith, particularly because of the mining excavations which provide excellent exposures of well-defined layers of the regolith down to bedrock. Soil formation and termite activity is at least as old as the Last Interglacial, and so more detailed work would further the understanding of the subaerial alteration history in southern Africa, as well as providing better-constrained information on the Namaqualand soils that can be used by land-use management and biosphere studies.

Uittreksel

Die (semi) ariede Namakwaland streek teen die Weskus van Suid-Afrika is bekend vir sy pragtige lentebloem. Vanweë die dorre geaardheid van die streek het grondnavorsing, wat veral op landboukundig-produktiewe dele van Suid-Afrika gefokus het, hier agterweë gebly. Nietemin, rehabilitasie pogings na die sowat honderd jaar se myn van diamante, gekoppel aan die toenemende belangstelling in ekologiese- en biodiversiteitsnavorsing, het die huidige belangstelling in Namakwalandse grond as 'n substraat vir plantegroei, aangewakker. Die streek is ook bekend vir sy oorfloed van “heuweltjies” (lae hope of knoppe in die landskap), wat algemeen aanvaar word dat dit deur die grasdraertermiet *Micrhorodotermes viator*, met debatteerbare bydraes deur ander diere, veroorsaak word. Meeste van die vorige werk op heuweltjies het op biogenetiese aspekte soos spasiëring, oorsprong en ouderdom gefokus. Alhoewel heuweltjies grootliks 'n grondgeaardheid het, is min gepubliseerde werk aangaande die grondvormingsprosesse hiervan gedoen. Die geskiedenis van die sediment afsettings van die Namakwalandse kusgebied is redelik bekend, in teenstelling met die skaarste aan data oor hulle daaropvolgende pedogenese. Omdat die regoliet gedurende sommige tye van die Neogeen aan die atmosfeer blootgestel was, maak grondvorming 'n belangrike deel uit van die geskiedenis van die sedimente. Die hoofdoel van hierdie proefskrif was daarom om die grondkenmerke van die sedimente op die Namakwalandse kusgebied te ondersoek sodat hulle pedogenese beter verstaan kan word.

Die regoliet van die noordelike Namakwalandse kusgebied, dikwels tien of meer meters dik, bestaan uit opeenvolgende lae van mariene oorsprong wat afgesit is gedurende seevlak terugtrekkings in die Laat Tersiêre tydperk. Die oppervlak grondhorisonte het vanaf eoliese moedermateriaal gevorm. Die relatiewe lae CaCO_3 inhoud in die eoliese sande het die pedogenetiese rigting in die af-

settings bepaal wat gelei het tot 'n meer kleiryke, apedale horison wat sterker struktuurontwikkeling met diepte toon. Soortgelyke horisonte is teenwoordig in paleosols onder 'n duinveld wat tot die Laaste Glasiële Maksimum dateer is. Die apedale horisonte rus f direk op mariene sande via 'n subtiele diskontinuiteit wat beteken dat pedogenese ook in die onderliggende mariene materiale plaasgevind het of op kalkkreet, dikwels via 'n kliplyn of geronde rolstene. Dieper in die profiel is daar 'n algemene dog gereelde verandering van die verskillende sedimentêre lae, met die growwer lae wat meer rooi en die fyner sande wat bleek kleure vertoon. In sommige van die lae het die oksidasie van gloukoniet-ryke sedimente 'n oranje kleur veroorsaak.

Die Namakwalandse kusvlakte, met ekstensiewe areas van kalkkreet ontwikkeling, is moontlik 'n teksboek voorbeeld vir kalkkreet ontwikkeling deur anorganiese prosesse. Nietemin toon hierdie kalkcrete ook mikroskaal biogenetiese kenmerke. Dit sluit in M stawe, MA stawe en swamfilamente. Dit wil voorkom asof abiotiese alfa-raamwerk oorheers in die ouer kalkkreet horisonte terwyl beta-raamwerk geassosieer word met die kalkhoudende en kalsiese B horisonte wat bokant kalkkreet voorkom. Die skynbare afwesigheid van Mg-ryke kalkkreet en dolomiet en die volopheid van sepioliet in die kalkcrete van die Namakwalandse kusgebied, dui aan dat hierdie Mg-ryke kleimineraal die hoof Mg-draende fase verteenwoordig. Deformasie (vals antikliene) in die kalkkreet blyk die resultaat te wees van die verplasende effek van kalsiet kristallisering. Alhoewel bewyse van swel/krimp gedrag voorkom in die vorm van akkommoderende vlakke, wil dit voorkom dat dit nie so volumetries belangrik is as die van verplasende kalkkreet.

Verharde liggekleurde horisonte wat lyk soos kalkkreet maar wat nie- tot swak kalkhoudend is, wat in konkoïdale patrone verbrokkel, wat nie verslemp in suur of alkali, wat pers verkleur in metiel-oranje en in 'n bulk grondmonster sepioliet XSD pieke vertoon, skyn vergelykbaar te wees met die paligorskiet-gesementeerde materiaal ("palikreet") wat in Spanje en Portugal beskryf is. Dit word hier voorlopig "sepiokreet" genoem. Beide silika en sepioliet is teenwoordig in die matriks, alhoewel die mate wat silika en sepioliet domineer selfs binne die dieselfde horison skyn te verskil. Dit is baie moontlik dat beide van hulle bydra tot die struktureienskappe van die horison. Sepiolitiese horisonte vorm nie 'n diagnostiese horison in die World Reference Base, Soil Taxonomy of die Suid-Afrikaanse Taksonomiese Grondklassifikasiesisteme nie. Om in die bestaande grondklassifikasiesisteme geakkommodeer te word, word voorgestel dat die terme "sepiolities"

en hardebank sepioliet (op dieselfde wyse as “kalsies” en “petrokalsies” of hardebank karbonaathorison tans), gebruik word.

Sepioliet pieke is meer prominent as die van paligorskiet op die XSD aanwysers van die kleiner as $2 \mu\text{m}$ fraksie. Die $<0.08 \mu\text{m}$ fraksie was die enigste groottefraksie waarin paligorskiet bespeur kon word voor asetaat behandeling. Dit is onwaarskynlik dat hierdie veselkleiminerale geerf kon gewees het van of die mariene of die eoliese moedermateriale. Hulle blyk van pedologiese oorsprong te wees. Tendense in die MgO , Al_2O_3 en SiO_2 inhoud toon dat die grond se kleifraaksie lê op 'n gemengde lyn tussen sepioliet en mika endlede, met 'n bydrae van smektiet, wat in ooreenstemming is met XSD en TEM resultate. Daar is 'n sterk korrelasie tussen Fe_2O_3 en TiO_2 inhoud, wat toegeskryf kan word aan die alomteenwoordige mika. Daar was geen TEM bewys van veselmineraal afbraak na plaatsilikate; ook nie die evolusie van mika lateraal na 'n veselmineraal toe nie. Daar was geen bevestigende bewyse vir of teen die teenwoordigheid van keroliet in die kleifraaksie nie, alhoewel dit wil voorkom dat dit nie 'n dominante fase van die kleifraaksie uitmaak nie.

Die hipotese word voorgestel dat die deurlatende boonste horisonte in gronde van Namakwaland eintlik 'n vlak kortstondige waterdraer (akwifer) kan vorm, wat die pedogenetiese analoog is met 'n sout-meer omgewing waarin sepioliet tipies sal vorm. Die chemiese evolusie van die grondoplossing kan daarom in dieselfde terme as die geochemiese evolusie van geslote kom pekel(sout)water beskou word. Haliel het onderversadig gebly by alle konsentrasies in die versadigde pasta ekstraksies. By hoër konsentrasie het gips versadiging bereik en sulfaat word dan uit die oplossing verwyder. Die aktiwiteit van H_4SiO_4 het onveranderd gebly by alle vlakke van verdamping. Kalsiet bly naby aan versadiging en is slegs afhanklik van die HCO_3^- aktiwiteit en pH vir die reeks van Cl^- aktiwiteite wat aangetref is. Meeste van die gronde waarin sepioliet aangetref is, het 'n positiewe sepioliet versadigingsindeks getoon. Die sepioliet versadigingsindeks is onafhanklik van Mg^{2+} en H_4SiO_4 en neem slegs toe met toename in pH. Bewyse van pH beheer by sepioliet versadiging is dat sepioliet slegs met kalkhoudende horisonte geassosieer word. Sepioliet presipitasie sal daarom meer geredelik plaasvind wanneer 'n oplossing 'n pH verandering ondervind as by die konsentrasie van ione deur verdamping. Die mariene-geaffekteerde hoë Mg gekoppel met die Hardie-Eugster model van pekelwater gedrag, bied 'n verklaring vir die oorheersing van sepioliet teen die kus en paligorskiet verder binneland toe. Kusgebiede, in teenstelling

met kontinentale gebiede, het $Mg > HCO_3^-$ aanvanklik, Mg vlakke sal styg wat die $(Mg+Si)/Al$ verhouding sal bevoordeel vir die presipitasie van sepioliet. Dit beteken dat as sepioliet eers begin presipiteer, die gepaardgaande saliniteit, met verhoging in Mg, betekenisvolle paligorskiet vorming onwaarskynlik sal maak.

Die hardebank horisonte in heuweltjies algemeen wissel van 'n "sepiolitiese" petrokalsies naby die middel, deur "sepiolities"/"petrosepiolities" na 'n petroduriese (dorbank) horison op die rand. Opmerkzaam is dat sepioliet-verwante pedomaaksels in kalkreet soos olietkorrels insluit. Hulle vorming kan mees waarskynlik verklaar word deur die hidrofiliese/hidrofobiese membraanteorie vir stilstaande water te gebruik, gegewe die opeenvolgende sepioliet (hidofilies en daarom 'n presipiterende substraat) en mikriet/naaldvormige kalsiet lae in die bedekkings, en sterk hidrofobiese organiese materiaal in die heuweltjie. Ietwat van 'n raaisel is die deurskynende geel nodules met vals-negatiewe eenassige interferensiefigure. Laasgenoemde lyk soos sferoliete in vars termiet uitwerpsels. Hulle veselagtige geaardheid en lae dubbelbreking, tesame met die lae Ca en hoë Mg en Si inhoude en hoë molare Mg/Si verhouding, is ooreenstemmend met di van sepioliet. Dit word voorgestel dat die vorming van die hardebanke in die heuweltjie as volg plaasgevind het: Verryking met katione soos Ca en Mg in die middel van die heuweltjie deur termiete wat plantmateriaal ingebring het en wat kalsiet en klei deur outigenese in die middel van die heuweltjie veroorsaak het. Die afbrekende organiese materiaal wat aangesamel het in die middel van die heuweltjie was genoeg om die komponente vir kalsiet presipitasie te kon verskaf. Na hierdie organiese materiaal geïnisieerde kalsiet presipitasie, was die pH geskik vir sepioliet presipetasie. Die beweging van die Mg-Si-verrykte water verder heuvel afwaarts, gekoppel aan die verlaging van die HCO_3^- en toename in Mg^{2+} a.g.v. sepioliet presipitasie, veroorsaak die presipetasie van die sepiolitiese sone nader aand die buitenste sone van die heuweltjie met die presipitasie van silika op die rand van die heuweltjie.

Die Namakwalandse kusgebied is goed geposisioneer vir verdere werk betreffende die regoliet, veral a.g.v. die mynaktiwiteite waar diep uitgrawings goeie blootstelling van goed-gedefinieerde lae tot op vaste rots blootlê. Grondvorming en termiet-aktiwiteite is tenminste so oud as die Laaste Interglasiale Tydperk. Verdere werk hierop sal die geskiedenis van die sub-blootgestelde grondoppervlak se veranderings in Suidelike Afrika help verklaar. Dit kan ook help met 'n beter begrip van die dikwels verstrengelde informasie wat aangaande Na-

makwaland bestaan, asook help met landgebruiksbestuur en biosfeer studies. Bykomend sal mikromorfologiese studies wat die verwantskap tussen kalsiet, sepioliet/paligorskiet en silika fases in meer heuweltjies bestudeer, die algemene model wat in hierdie proefskrif gestel word, verder verfyn.

Acknowledgements

This thesis spanned two continents and six years from its beginnings as a Master's degree, and so the list of people who have provided support directly and indirectly is long. I particularly need to thank my family, two members of which have known life no other way, for their patience with it.

Thanks are due to De Beers Namaqualand Mines, in particular the Environmental Department for facilitating this thesis project. People who went out of their way to help me during the sampling stages, and are owed a special thanks, are: Paul Kruger for his enthusiastic help in the field; Charlaine Kruger for making this project possible; Jenny van der Westhuizen for co-ordinating all aspects of the Kleinzee visits; Russel Nicol for his assistance with my visits to the Koningnaas Complex; John Fulton for producing the map of sample locations; the Geology Department for permission to publish the results and their help with the stratigraphy, in particular Andy Grills, Neale Baartjies and Marthinus Prinsloo for taking the time to assist me; John Pether for agreeing to spend a day in the field with me at very short notice; and the late Hendrik Prinsloo for the many thought-provoking discussions and his assistance in the field.

Many people from outside the Soil Science department were involved in the data collection. Electron Microscope images were taken by Mr N. Steenkamp and Esmé Spicer and myself at the University of Stellenbosch Geology Department, and Belinda White and Vijay Bandu at the University of KwaZulu-Natal (Pietermaritzburg campus). XRF analyses were done by Esmé Spicer at the University of Stellenbosch Geology Department. The thin sections were prepared by Montserrat Antúnez Pujol from the University of Lleida, Spain, and David Wilson from the University of Cape Town. Thanks are also due to Remy Bucher at the iThemba Labs Materials Research Group, Somerset West, for running many, many XRD samples.

Thanks are also due to the staff in the Soil Science Department at the University of Stellenbosch: Annatjie French for the Admin, the Laboratory Staff Judy Smith, Kamiela Crombie and Herschel Achilles for their help with some of the analyses; Tanya Medinski for the carbon and nitrogen analyses; Matt Gordon for the cation and anion analyses, and his patience with the samples and my repeated requests for sometimes large amounts of chemicals; and Herschel Achilles and Kenneth Davidse Jr. for moving the sample crates around, particularly given my refusal to down-size the sample volumes.

I would like to particularly thank Richard O'Brien for his generous assistance with the XRD, his advice on all aspects of the clay extraction and identification, and for kindly running some of my samples when I could not. He was the first one to identify almost mono-minerallic sepiolite in the clay fraction.

Friends who helped freely with some of the more labor-intensive chemical analyses are Cathy Dowding, Ailsa Hardie, Arne Henrichsen, Tanya Medinski, and Jason Salzwedel. Students who helped during their vacation work in the Soil Science department are Nicolette van der Merwe, who did acetate pre-treatments and clay separations, and Thami Vilakhazi, who did particle size analysis, clay separations and ran some of the samples on the XRD at the University of Stellenbosch Geology Department.

Thanks are also due to Willem de Clercq for constructing the resin impregnator in the University of Stellenbosch Soil Science department; Jeffrey Hughes for taking the time to give a lot of advice about clay minerals; John Compton for advice on pCO₂ conversions; David L. Parkhurst for answering queries about setting up the PHREEQC runs; Georges Stoops for remotely diagnosing a problem with the microscope set-up; Andrei Rozanov for helping to identify phytoliths; Anthony Mills and Antoni Milewski for their assistance with the question of oxalate in the vegetation, and Tim Francis for his help with soil forming processes in sediments on the East Coast of South Africa.

Much credit is due to Rosa Poch for her generous assistance with the sampling and thin section descriptions; to Jan Lambrechts and Freddie Ellis for locating the 'sepiocretes' and heuweltjies, the sampling trips, and many discussions; to Martin Fey for his seemingly never-ending patience with questions of an editorial nature. I am indebted to Freddie Ellis for translating the Abstract.

I thank my supervisors, Professor Martin Fey and Dr Freddie Ellis, for the opportunity they gave me to work in the Soil Science Department and for their continuing enthusiasm, a lot of advice and guidance, and most of all their faith in my ability to finish.

Financial support for this project was received from De Beers Namaqualand Mines Limited, the National Research Foundation (Grant number 2047381), and Eskom's Tertiary Support Program (TESP).

*I dedicate this thesis to Arne Henrichsen. Without his help with everything else,
this thesis would not have been written.*

Contents

Introduction	1
1 Silica- and sepiolite- cemented duricrusts on the west coast of South Africa	4
1.1 Introduction	4
1.1.1 Silica-cemented horizons	5
1.1.2 ‘Sepiocrete’	6
1.2 Materials and methods	8
1.2.1 Site description	8
Coastal plain; BMC: profiles SK11 and KV196T	8
Knersvlakte: profile KNERS	13
1.2.2 Laboratory methods	14
1.3 Results and discussion	15
1.3.1 Slaking behaviour	15
Dorbank (petroduric)	15
‘Sepiocrete’	18
1.3.2 Mineralogy	19
Dorbank (petroduric)	19
‘Sepiocrete’	22

1.3.3	Micromorphology	24
	Dorbank (petroduric)	24
	‘Sepiocrete’	27
1.3.4	Genesis	32
	Dorbank (petroduric)	32
	‘Sepiocrete’	35
1.3.5	Classification	37
	Dorbank (petroduric)	37
	‘Sepiocrete’	38
1.4	Summary and conclusions	40
1.4.1	Dorbank (petroduric)	40
1.4.2	‘Sepiocrete’	41
2	Soil formation in sediments of the Namaqualand coastal plain	43
2.1	Introduction	43
2.2	Site description	45
2.2.1	Climate	45
	Temperature	46
	Moisture	46
	Rainfall	46
	Evaporation	47
	Topography	47
	Microrelief	47
	Soil Permeability	49
2.2.2	Regolith	49

2.2.3	Bedrock geology and morphology	50
2.3	Methods	50
2.4	Results and discussion	52
2.4.1	A horizons	53
2.4.2	B horizons	60
	Age	62
2.4.3	Eluvial horizons	63
2.4.4	Cemented horizons	65
	Calcite-cemented horizons	65
	Silica-cemented horizons	67
	Sepiocrete and sil-sepiocrete intergrades	67
2.4.5	Marine sediments	68
2.4.6	Biological activity	70
	Tunnels	71
	Roots	71
	Termites	71
2.5	Conclusions	74
3	‘Pseudo-anticlines’ and biogenic features in sepiolite-containing calcrete in Namaqualand	76
3.1	Introduction	76
3.2	Materials and methods	78
3.3	Results and discussion	79
3.3.1	Composition	79
	Carbonates	79

Clays	80
3.3.2 Morphology and micromorphology	82
‘Pseudo-anticlines’	82
Biogenic fabric	85
3.4 Conclusions	88
4 Clay mineral occurrences in Aridisols on the west coast of South Africa (Namaqualand)	90
4.1 Introduction	90
4.2 Materials and methods	92
4.3 Results and discussion	94
4.3.1 Effect of milling and acetate pretreatments on clay fraction	94
4.3.2 Clay mineral variations in soil profiles	95
4.3.3 Kerolite	106
4.3.4 Chemical composition of clay fraction	106
4.3.5 Sepiolite/palygorskite modes of occurrence	109
4.3.6 Palygorskite/sepiolite transformation	109
4.4 Conclusions	112
5 Brine evolution and geochemical barriers: mineral formation in Namaqualand soils	115
5.1 Introduction	115
5.2 Materials and methods	119
5.3 Results and discussion	122
5.3.1 Chloride as a proxy for evaporative concentration	125
5.3.2 Marine-influenced initial ratios and subsequent evaporation trends	131

5.3.3	pH control of sepiolite equilibrium	134
5.3.4	Coastal sepiolite and inland palygorskite in Namaqualand	137
5.3.5	Summary of mineral genesis on the Namaqualand coastal plain	139
	Halite and gypsum	140
	Calcite	140
	Sepiolite-palygorskite	140
	Silica	142
	pH variation and its potential to affect the genesis of calcic, sepiolitic and duric soils	142
5.4	Conclusions	142
6	Micromorphology, mineralogy and genesis of soils associated with a Namaqualand ‘heuweltjie’	145
6.1	Introduction	145
6.2	Materials and methods	148
6.3	Results and discussion	151
6.3.1	Profile descriptions	151
6.3.2	Clay mineralogy	153
	Calcrete in centre of heuweltjie: samples 2A, 2B, 2C	153
	‘Sepiolitic’ pedocutanic (argic) 7.5 m from centre of heuweltjie: sample 2D	154
	Dorbank (petroduric) at edge of heuweltjie	154
6.3.3	Micromorphology of excrement and exit towers: Stellen- bosch heuweltjie	156
6.3.4	Micromorphology of the heuweltjie at Papendorp	159
	Biological activity	182

Horizon over calcrete in the heuweltjie centre	182
Calcrete in the heuweltjie centre	183
Calcareous ooids and peloids	183
Limpid nodules	186
Pseudo-negative uniaxial ‘spherulites’	186
Possible Other Morphological Forms	187
Composition	188
‘Sepiolitic’ pedocutanic (argic) midway to edge of heuweltjie (sample 2D)	190
Dorbank (petroduric) at heuweltjie edge; sample 1.3	191
6.3.5 Heuweltjie formation	192
Organic matter as a source of ions for calcrete formation .	192
Source of ions for sepiolite/palygorskite formation	194
Leaching and redistribution of ions within the heuweltjie: zoning of sepiolite and dorbank (petroduric)	194
6.4 Conclusions	196
Summary of findings and recommendations for further work	198
References	203
A Photographs of soil profiles: BMC and KNC	231

List of Figures

1.1	Location of sample areas	9
1.2	Location of profiles KV196T, SK11 and their farm names within the Buffels Marine Complex (BMC) mining area	12
1.3	Photograph: dorbank (petroduric) cutan on ‘sepiocrete’	17
1.4	Photograph: ‘sepiocrete’	18
1.5	XRD traces of clay fractions from profile KV196T	20
1.6	XRD traces of clay fractions from the Knersvlakte profile KNERS	21
1.7	TEM image: amorphous material coating clay grain	22
1.8	XRD traces of clay fractions from profile SK11	23
1.9	Photomicrographs: typical views of silica in dorbank (petroduric) horizons.	26
1.10	Optical and SEM images of neoformed and illuviated smectite and silica in dorbank (petroduric) fragments	28
1.11	Optical and SEM images of granular microstructure in ‘sepiocrete’	29
1.12	SEM images: HCl etching of ‘sepiocrete’	31
1.13	SEM images: HCl etching of ‘sepiocrete’ continued	32
1.14	Optical and SEM images of silica in ‘sepiocrete’	33
1.15	SEM: broken sponge spicule in dorbank (petroduric) fragments.	35
2.1	Location of field area.	45

2.2	Location of sample areas	48
2.3	Generalized regolith profile	53
2.4	Archaeological site buried by regic sands	60
2.5	Dune plume north of Swartlintjies River: interpretation.	62
2.6	Photograph: Possible vertical termite burrows that have become conduits for preferential flow.	66
2.7	Photograph: probable hematite ‘halos’ in lower shoreface sands . .	69
2.8	Photograph: termite nest, 1.7 m deep below calcrete.	72
2.9	Photograph: strongly-cemented, calcareous hive 2 m deep within dorbank.	73
2.10	Photograph: Possible vertical termite burrows now conduits for preferential flow in lower shoreface sands.	73
3.1	XRD traces: Nature of the carbonates in calcrete	80
3.2	XRD traces: clay fraction mineralogy	81
3.3	XRD trace: sepiolite cutan on calcrete	83
3.4	Photomicrographs: displacive, replacive and needle fibre calcite; clay textures in calcrete	84
3.5	SEM images: Biogenic calcite in calcite nodules from a neocar- bonate B horizon overlying calcrete	87
3.6	SEM images: HCl-etched filaments and fibrous clay minerals . . .	88
4.1	XRD traces of clay fraction from profile 6868	97
4.2	XRD traces of clay fraction from profile AK61H	100
4.3	XRD traces of clay fraction from profile AK1/TRIG	101
4.4	XRD traces of clay fraction from profile LKC1-5	102
4.5	XRD traces of clay fraction from profile OBT	103

4.6	XRD traces of clay fraction from profile SL4-1	104
4.7	TEM images of clay fractions	105
4.8	Trends in total element composition of clay fractions: MgO+Al ₂ O ₃ vs SiO ₂ ; Al ₂ O ₃ vs K ₂ O; Fe ₂ O ₃ vs TiO ₂	108
4.9	SEM images of sepiolite/palygorskite occurrences in calcareous nodules from 6869/iv	110
4.10	TEM images of sepiolite/palygorskite fibres and fibre bundles in 6869/iv	112
5.1	Variation of ion activities with Cl ⁻ as a proxy for evaporative concentration in saturated paste extracts	123
5.2	Variation of mineral saturation indices with Cl ⁻ as a proxy for evaporative concentration in saturated paste extracts	126
5.3	Variation of mineral saturation indices (SI) with pH in saturated paste extracts	128
5.4	Variation of mineral saturation indices (SI) with activity of com- ponent ion in saturated paste extracts	129
5.5	Variation of mineral saturation indices (SI) with activity of com- ponent ion in saturated paste extracts (continued)	136
5.6	Variations in saturation indices with pCO ₂	138
6.1	Location of Papendorp heuweltjie	148
6.2	Photographs of sample locations within heuweltjie	150
6.3	XRD traces of white palygorskite/sepiolite cutans and associated calcrete from the centre of heuweltjies from Worcester and Oudt- shoorn.	153
6.4	XRD traces of clay fraction from Papendorp heuweltjie	155
6.5	TEM image of ‘sepiolitic’ pedocutanic (argic) sample 2D and dor- bank (petroduric) sample 1.3.	156

6.6	Photomicrographs of termite excrement from an active heuweltjie on the south side of Papegaaiberg (Stellenbosch)	157
6.7	Photomicrographs of termite exit tunnels from active heuweltjie on the south side of Papegaaiberg (Stellenbosch)	158
6.8	Photomicrographs from the centre of the heuweltjie: neocutanic B (sample 2.2) and calcrete (2A).	166
6.9	Continued - photomicrographs from the centre of the heuweltjie: calcrete (2A).	167
6.10	Continued - photomicrographs from the centre of the heuweltjie: calcrete (2A).	168
6.11	HCl etching of peloids and limpid nodule with pseudo-negative uniaxial interference figures in sample 2A, calcrete in centre of heuweltjie	169
6.12	Photomicrographs and corresponding SEM (backscatter electron) images from calcrete (2A) in centre of heuweltjie	170
6.13	SEM (backscatter electron) images of fragments and thin sections from calcrete (2A) in centre of heuweltjie	171
6.14	Photomicrographs from 2 m away from the centre of the heuweltjie: calcrete (2B).	172
6.15	Continued - photomicrographs from 2 m away from the centre of the heuweltjie: calcrete (2B).	173
6.16	Continued - photomicrographs from 2 m away from the centre of the heuweltjie: calcrete (2B).	174
6.17	Continued - photomicrographs from 2 m away from the centre of the heuweltjie: calcrete (2B).	175
6.18	Photomicrographs from 3.2 m away from the centre of the heuweltjie: calcrete (2C).	176
6.19	Continued - photomicrographs from 3.2 m away from the centre of the heuweltjie: calcrete (2C).	177

6.20	Photomicrographs from 7.5 m away from the centre of the heuweltjie: non-calcareous ‘sepiolitic’ pedocutanic (argic) (2D).	178
6.21	Continued - photomicrographs from 7.5 m away from the centre of the heuweltjie: non-calcareous ‘sepiolitic’ pedocutanic (argic) (2D).	179
6.22	Continued - photomicrographs from 7.5 m away from the centre of the heuweltjie: non-calcareous ‘sepiolitic’ pedocutanic (argic) (2D).	180
6.23	Photomicrographs of dorbank (petroduric, sample 1.3) at the edge of the heuweltjie (8 m from 2D)	181
6.24	Inferred water movement through the heuweltjie.	195
	Plate: Profile 6869	232
	Plate: Profile AK1	233
	Plate: Profile AK61H	234
	Plate: Profile DL88	235
	Plate: Profile KV196T	236
	Plate: Profile KV220PRN	237
	Plate: Profile LKC1-5	238
	Plate: Profile OBT	239
	Plate: Profile SK11	240
	Plate: Profile SL4-1	241
	Plate: Profile SN30	242
	Plate: Profile SNT60	243
	Plate: Profile SPNT	244
	Plate: Profile TP231L	245
	Plate: Profile TP266Q	246

List of Tables

1.1	Profile descriptions	16
1.2	Thin section descriptions	25
1.3	Profile chemistry	34
1.4	XRF analyses	38
2.1	Profile descriptions.	54
2.2	Redness rating: soil profile comparison	64
4.1	Clay mineral variation down profiles.	96
5.1	Composition of saturated paste extracts	124
5.2	Ion-concentration trends in maritime and continental water systems	132
6.1	Profile descriptions from Papendorp heuweltjie	152
6.2	Thin section descriptions of samples from Table 6.1. Abbreviations: c/f: coarse/fine; diam.: diameter; incl.: including; max.: maximum; occ.: occasional; OIL: oblique incident light; PPL: plane polarised light; XPL: cross polarised light.	160

Introduction

This study was conceived in order to examine in greater detail the 100 km stretch of coast that was mapped by F. Ellis and J. J. N. Lambrechts for the De Beers Namaqualand Mines rehabilitation program, as characterisation and classification of all horizons within the regolith before disturbance assists in understanding the new soil forming processes that have begun on the surfaces of the mine dumps. The study area was subsequently expanded to encompass additional heuweltjies and ‘sepiocretes’. The Namaqualand region has been receiving an increasing amount of attention since the commencement of this thesis. This has culminated in a Special Issue of the Journal of Arid Environments on Sustainable Land Use in Namaqualand (September 2007, Volume 70, Issue 4, Pages 561-846), and although the body of literature on Namaqualand is by no means limited to this volume, the reader unfamiliar with Namaqualand is urged to consult it as an introduction to the present state of knowledge. Many of the premises (particularly in terms of the influence of climate on floral kingdoms and ecosystem functioning) outlined in the Special Issue were presupposed in this thesis.

The thesis is presented as a collection of papers that are intended to be submitted for publication. Each Chapter has therefore been formulated that it can be read as a ‘stand-alone’ paper, with reference to the work in previous Chapters. This means, however, that there is some overlap in the ‘Materials and Methods’ section of each chapter. The aims of each Chapter is outlined below.

During the initial field work light-coloured horizons were encountered that resembled calcrete but were non-calcareous, broke with a conchoidal fracture and were resistant to slaking in both acid and alkali. Further examination showed them to contain a large amount of sepiolite, and they were tentatively named ‘sepiocretes’. The aim of Chapter 1 (*Silica- and sepiolite-cemented duricrusts on the west coast of South Africa*), was to derive a name for these horizons based

on their cementing agent. Since amorphous silica could also have played a role in cementing the ‘sepiocrete’ horizons, Chapter 1 compares the two known types of silica-cemented horizons encountered in Namaqualand to these ‘sepiocrete’ horizons.

The aim of Chapter 2 (*Soil formation in sediments of the Namaqualand coastal plain*), was to describe and characterise the general soil forming features, both current soils and paleosols, in the regolith down to bedrock. The mining excavations tens of metres deep down to bedrock have provided an opportunity to examine soil formation in a regolith that has been subaerially exposed in some parts for much of the Neogene.

The aims of Chapter 3 (*‘Pseudo-anticlines’ and biogenic features in sepiolite-containing calcrete in Namaqualand*) were to describe the micromorphology, mineralogy and genesis of calcretes on the Namaqualand coastal plain, including the development of pseudo-anticline structures. Biogenic processes, however, are increasingly being seen as important to calcrete genesis, and so a particular aim was to establish whether there was a biogenic contribution to calcrete formation, and to distinguish the fibrous clay minerals sepiolite and/or palygorskite from similar biogenic needle fibre calcite.

Chapter 4 (*Clay mineral occurrences in Aridisols on the west coast of South Africa (Namaqualand)*) focuses on the clay mineralogy of the soils. The aims of this Chapter were to evaluate the effect of pretreatments on the sepiolite and palygorskite peaks, and particularly to concentrate kerolite if present; examine the clay mineral associations throughout the profile including the marine parent materials to establish which, if any, were inherited phases; and to examine the morphology and modes of occurrence of the fibrous clay minerals in Namaqualand soils, especially for evidence of disintegration or transformation into sheet silicates.

Chapter 5 (*Brine evolution and geochemical barriers: mineral formation in Namaqualand soils*) is based on the hypothesis that the permeable upper horizons in Namaqualand soils constitute a shallow ephemeral aquifer, which can be considered as a pedogenic analogue of the saline lake environments in which sepiolite typically forms. The chemical evolution of the soil solution and clay mineral genesis could therefore be considered in the same terms as the geochemical evolution of closed-basin brines. The aim was to apply the principles of brine evolution, particularly the Hardie-Eugster model, to sepiolite genesis in arid soils of the Namaqualand

coastal plain. The Hardie-Eugster model is based on the effect mineral precipitation has on brine evolution, which is determined by the initial ratio of the component ions in the solution. It was conceived as a means of understanding the evolution of closed-basin brines, and has since been applied to a diverse range of environments, from saline soil seeps to coastal pans and calcrete genesis.

Chapter 6 (*Micromorphology, mineralogy and genesis of soils associated with a Namaqualand Heuweltjie*) is the first detailed micromorphological study through one of the heuweltjie (Mima-like) mounds that are ubiquitous in the region. The aim was to use soil micromorphology and the principles of brine evolution from Chapter 5 to help explain soil formation within the heuweltjie, particularly the relationship between the (petro)calcic, '(petro)sepiolitic' and petroduric horizons.

Chapter 1

Silica- and sepiolite- cemented duricrusts on the west coast of South Africa

1.1 Introduction

The arid Namaqualand region on the west coast of South Africa has been recognised for its exceptionally high species diversity and endemism (Cowling and Hilton-Taylor, 1999; Cowling et al., 1999), and the region has been receiving increasing attention as a result. It is the focus of a Special Issue of the *Journal of Arid Environments* (2007). A summary of the landscape and climate and their effect on vegetation diversity is given by Desmet (2007). Soils knowledge, however, has lagged behind the biodiversity interest. With the exception of a study of the clay mineralogy of Namaqualand soils (Singer et al., 1995), soils information was generally limited to Land Type Surveys (Land Type Survey Staff, 1987), unpublished irrigation reports, work by Ellis (1988), and an outline by Watkeys (1999).

Francis et al. (2007) summarised the key characteristics of Namaqualand soils. They noted the presence of three types of hardpans: reddish brown, silica-cemented horizons which slake in alkali; calcium carbonate-cemented horizons which slake in acid; and a cemented horizon they referred to as 'sepiocrete', an indurated light-coloured horizon that resembles calcrete but is non- to mildly

calcareous, breaks with a conchoidal fracture, is resistant to slaking in both acid and alkali and reacts positively to methyl orange in the field (Mifsud et al., 1979). XRD analysis of the bulk soil shows a sepiolite peak. They are commonly associated with calcrete in ‘heuweltjies’ (hillocks; circular features having a different vegetation pattern and raised (1 to 2.5 m) surface, 10 to 20 m diameter, usually attributed to termites). The material is similar to the palygorskite-cemented material (‘palycrete’) described by Rodas et al. (1994) and Stahr et al. (2000), and Sauer et al. (submitted). Sepiolite and palygorskite are often reported from arid region soils and is commonly found in calcretes (Vanden Heuvel, 1964; Singer and Norrish, 1974; Yaalon and Wieder, 1976; Elprince et al., 1979; Hay and Wiggins, 1980; Watts, 1980; Singer and Galan, 1984; Singer, 1989; Blank and Fosberg, 1991; Monger and Daugherty, 1991; Verrecchia and Le Coustumer, 1996; Singer, 2002; Neaman and Singer, 2004; Owliaie et al., 2006), but there has been no recorded cementation of soils by sepiolite.

This Chapter describes these ‘sepiocretes’ and their genesis, and attempts to derive a name for these horizons based on their cementing agent. Since Francis et al. (2007) and F. Netterberg (pers. comm., 2003) suggested that amorphous silica could also play a role in cementing the ‘sepiocrete’ horizons, this Chapter describes and compares the two types of silica-cemented horizons encountered in Namaqualand to these ‘sepiocrete’ horizons.

1.1.1 Silica-cemented horizons

Two morphologically distinct silica-cemented horizons occur in southern Africa: ‘dorbank’ in the South African Classification System (Soil Classification Working Group, 1991), equivalent to the ‘duripan’ of Soil Taxonomy (Soil Survey Staff, 1999) and ‘petroduric’ of the World Reference Base (1998), and ‘silcretes’. Although both are the result of silica cementation, their general morphology and genesis in southern Africa differ (Ellis and Lambrechts, 1994). There is much less information available on the genesis and morphology of ‘dorbank’ (Ellis and Schloms, 1982; Ellis, 1988; Ellis and Lambrechts, 1994) than ‘silcrete’ (such as Summerfield, 1983a; Partridge and Maud, 1987). Two morphological types of dorbank (petroduric horizons) occur: a massive type, and one with a platy or laminated structure (Ellis and Lambrechts, 1994). The layers in the platy type are from a few millimetres to 0.3 m thick, and may show vertical cracks. Of-

ten coatings or thin layers of calcium carbonate occur between the plates. The massive dorbank varies in thickness from 1 to 5 m or more.

In regions where both silcrete and dorbank are found, silcrete occurs as cappings on the oldest landscape positions, with dorbank on lower lying erosion surfaces (Ellis and Lambrechts, 1994). Ellis and Lambrechts (1994) found that the high correlation ($r^2 = 63$) between dorbank distribution and the aridity index may indicate that dorbank developed under present arid climates, or similar paleoclimates, in contrast to silcrete ($r^2 = 19$). Dorbank is strikingly similar to the ‘red-brown hardpans’ of Australia described by both Litchfield and Mabbutt (1962) and Chartres (1985), both of whom also draw a distinction between these and silcrete.

Unlike the dorbanks, South African silcretes are characteristically pale in colour, which suggests silica accumulation and cementation under hydromorphic conditions in sandy materials (Ellis and Lambrechts, 1994). They are usually 1 to 2 m thick, massive, and very hard. They are commonly associated with Tertiary erosion surfaces and occur as remnant cappings (flat topped mesas) in the landscape (Partridge and Maud, 1987), where they are referred to as weathering profile silcretes by Summerfield (1983a). These are usually associated with pale coloured deeply weathered saprolite (‘pallid zone’) up to 20 m thick, composed primarily of kaolinite and illite with variable amounts of detrital quartz. Silcrete also occurs as non-weathering profile silcretes (Summerfield, 1983a), such as the Cenozoic Kalahari Beds. These have formed through silicification of various host sediments, especially calcretes and playa sediments (Summerfield, 1983a). The author observed similar silicification of lower shoreface facies marine sands (Pether et al., 2000) near the base of deep regolith in mining excavations (De Beers Namaqualand Mines) on the Namaqualand coastal plain.

1.1.2 ‘Sepiocrete’

Similar materials have been encountered in southern Africa before, but they have not been classified and no systematic study has been undertaken. Palygorskite-rich hardpans that macroscopically resembled calcretes, but were generally non-calcareous, and did not slake in 30% NaOH, were documented from Botswana (Runtu) by Netterberg (1969), who noted that the cementing medium was prob-

ably chalcedonic and opaline silica. There are also materials which look like calcretes but contain no carbonate at the Elandsfontein (near Hopefield) fossil site (Netterbeg, pers. comm., 2003), a white disintegrating material associated with dorbank in a heuweltjie near Ebenhaeser ($31^{\circ}35'50''\text{S}$ $18^{\circ}16'45''\text{E}$, road to Papendorp), with minor calcite and very abundant sepiolite (1.25 nm peak on a bulk sample XRD trace) (Ellis, unpublished data), and is present in some heuweltjies around the Worcester area of the Western Cape and Oudtshoorn in the Eastern Cape.

Francis et al. (2007) suggested interlocking fibrous sepiolite crystals could provide an explanation for the cementation of the 'sepiocrete' horizons. Brecciated sepiolite lutites in the Esquivias deposit (Madrid Basin) are "cemented with sepiolite" (Pozo and Casas, 1999, p. 400). The addition of 10% sepiolite to cement increased both the compressive and bending strengths of the mortar (Kavas et al., 2004). Bain (1971) noted that massive authigenic sepiolite formed in playa lakes dries to an extremely tough and coherent material. Mosaddeghi et al. (2006) evaluated the tensile strength of artificial mixtures of sand–palygorskite–calcite, and found that the effect of 5% palygorskite was approximately similar to that of 30% CaCO_3 . They suggested that this might be due to the fibrous structure and the higher surface area of palygorskite as compared to CaCO_3 , and that the fibrous units could act as binding bridges around and between the sand particles. This strong and non-friable nature is not restricted to sepiolite/palygorskite: non-slaking kaolin (flint clay) that breaks with a conchoidal fracture was described by Keller (1982, p. 30) which "when immersed in water remains intact, firm "rock-like" indefinitely . . . it withstands weathering for years on the outcrop or in a stockpile." Keller (1982) attributed its resistance to slaking to tightly interlocking, randomly oriented, compact packages and sheaves of kaolin crystals exhibiting a mutual-boundary texture.

Francis et al. (2007) and Netterberg (pers. comm., 2003) suggested that amorphous silica could also play a role in cementing the 'sepiocrete' horizons. Interestingly, Keller (1982) noted that although siliceous cement may have increased certain hydrothermal kaolins' resistance to slaking, no independent field or laboratory evidence had demonstrated that free silica served as a cement in typical flint clay of sedimentary origin.

Massive sepiolite is sometimes called ‘meerschaum’ (from German meaning ‘sea-froth’ (Hay et al., 1995)), especially in the gem trade when it occurs in compact masses or nodules (Sariiz and Isik, 1995). In Eskişehir, Turkey, high-quality sepiolite nodules were formed by alteration of magnesite nodules at shallow burial under alkaline conditions (Ece and Çoban, 1994). Other major sepiolite deposits include the Hekimhan region of Turkey (Yalçın and Bozkaya, 1995), Kenya (Hay et al., 1995), Somalia (Singer et al., 1998) and Spain, all of which formed in a paleolacustrine environment. There is abundant published information on these and other sepiolite-palygorskite occurrences (Weaver and Beck, 1977; Singer and Galan, 1984; Jones and Galan, 1988; Singer et al., 1992; Torres-Ruíz et al., 1994; Akbulut and Kadir, 2003; Jamoussi et al., 2003; Zaaboub et al., 2005, among others).

1.2 Materials and methods

One typical dorbank (petroduric horizon) and two ‘sepiocrete’ profiles were used to examine the genesis and cementing agents of these duricrust samples. Sampling was done in the Knersvlakte (KNERS, Figure 1.1), and in the Buffels Marine Complex (BMC) (De Beers Consolidated Mines Ltd - Namaqualand Mines) in the Kleinzee-Port Nolloth area in the northern part of the (semi-)arid Namaqualand coastal plain (KV196T and SK11).

1.2.1 Site description

Coastal plain; BMC: profiles SK11 and KV196T

On the Namaqualand coast, the prevailing winds are very strong southerly (occasionally gale force), with occasional berg (east) wind conditions, especially during winter. Temperatures increase markedly during berg wind conditions, which may persist for longer than a week. As a result, the average maximum temperature from February to October (late summer to spring) is over 30° C, with April and October experiencing temperatures of 38° C. In contrast, the average maximum temperature from November to January is 25° C (late spring to summer). Minimum temperatures from March to October are around 6° C,

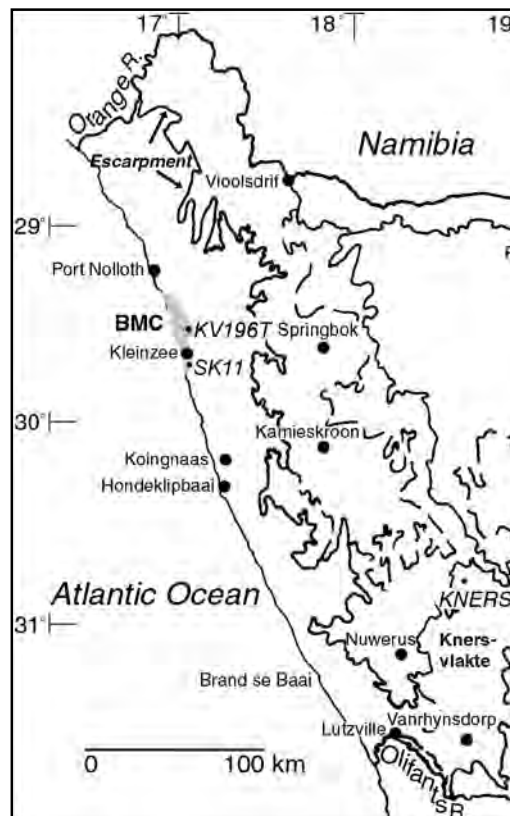


Figure 1.1: Location of Buffels Marine Complex (BMC) mining area, KV196T, SK11, and the Knersvlakte sampling site (KNERS). The escarpment (arrowed, dark lines) forms the eastern edge of the coastal plain. Modified from Ellis (1988).

with July dropping to 3° C. From November to April the minimum is around 10° C (D.B.C.M., 2000, data collected at Kleinzee, July 1995 to March 1997).

The Namaqualand coastal plain receives less than 150 mm winter rainfall annually, with the figure increasing southwards. Crucially for both plant growth and water movement through the soil, the climate is characterised by highly reliable rainfall when compared to other arid regions with similar mean annual precipitation (Desmet, 2007). It typically arrives as widespread, gentle showers (average rainfall event 6 mm, P. Carrick unpublished data, cited by Desmet (2007)). Drought conditions are rare, and rainfall is higher than average about once every 10 years, causing ephemeral rivers to flow. Flood events occurred in the Buffels River, for example, in 1945, 1961, 1962, 1963, 1976, 1980, 1986, 1996 and 1997 (D.B.C.M., 2000). Paleoclimates of the northern Namaqualand region are not that well constrained, but the consensus for the greater area seems to be that it was wetter during the Last Glacial (Van Zinderen Bakker, 1976; Tankard and Rogers, 1978; Parkington et al., 2000).

Coastal fog adds significantly to the total precipitation. Data from the Pilot Fog Study at Kleinsee for the period July to October 1995 showed that the highest precipitation due to fog occurred during August. The total fog recorded during this period was 1001 mm (D.B.C.M., 2000). Tinley (1985; in D.B.C.M., 2000) estimated that the plants may trap up to 300 mm of fog per annum.

That evapotranspiration greatly exceeds precipitation in Namaqualand is reflected by a vegetation cover (Sandveld bioregion (Desmet, 2007)) of approximately 60%, as well as the presence of saline pans and ephemeral rivers, and areas with salt efflorescence and crusts at the soil surface. The evaporation rate is of the order of 2 m per year. The evaporation rate is higher than expected for a coastal area due to the wind regime, but is reduced by the regular occurrence of coastal fog (D.B.C.M., 2000).

The regolith of the Buffels Marine Complex comprises successive late Tertiary marine packages, each deposited during sea-level regression (Pether, 1994). Some rest on kaolinized paleochannel sediments, described in detail by Pether (1994), who concluded that they were laid down as a quartzo-feldspathic sediment in a fluvial environment, and subsequently deeply weathered, with extensive alteration of feldspar to kaolinite. These sediments are described in greater detail by Tankard (1966), Tankard (1975), Pether (1994), and Pether et al. (2000). De Villiers and Cadman (2001) favoured an early Tertiary age for this channel north of the Swartlinter River, although it may also contain reworked Cretaceous material (Pether et al., 2000; De Villiers and Cadman, 2001).

The marine packages overlying the kaolinised paleochannel sediments are arranged *en echelon* down the bedrock gradient, from oldest and highest inland to youngest and lowest at the coast. Each package is named after the elevation of its transgressive maximum as represented in the Hondeklip Bay area (Pether, 1994; Pether et al., 2000). The 90 m package is ca. 18 - 16 Ma, the 50 m package early Pliocene, and the 30 m package not well constrained, but ca. 3.3 Ma or younger (Pether et al., 2000). The 30 m package is transgressed by younger littoral deposits up to about 10 m a.m.s.l. (Pether et al., 2000). The sand fraction is dominated by quartz and feldspar, lesser glauconite and phosphatic shell fragments, and variable amounts of heavy minerals (garnet, magnetite, ilmenite, biotite, sphene, amphibole, epidote, kyanite (rare) and zircon (rare)) (Pether, 1994). The marine packages are capped by recent aeolian deposits.

Coastal dunefields originate at the mouth of the rivers and extend inland in a northerly direction. In places, older soil profiles are overlain by aeolian sands. Soil formation has taken place in aeolian, 'sheetwash', and marine-deposited sediments.

Soils within the broader context of Namaqualand are summarized by Francis et al. (2007) and Desmet (2007). Soils on the Namaqualand coastal plain in the vicinity of the Buffels Marine Complex sampling sites can be classified into the Aridisol and Entisol orders of Soil Taxonomy (Soil Survey Staff, 1999). Greater detail is presented in Chapter 2. In summary, the Entisol order, in which the only expression of soil formation is the presence of vegetation and a darkening of the A horizon, is represented by Quaternary aeolian sands. These regic sands are classified as the Namib Form in the South African classification system (Soil Classification Working Group, 1991). The grey sands are of most recent aeolian origin and closest to the coast, the red sands are the oldest and furthest inland, and the yellow sands usually occupy an intermediate zone between red and grey. Although described as deep sands there is abundant evidence (even though mostly incipient) of differentiation into horizons (for example bleaching, clay illuviation and secondary cementing by silica and carbonate), such that the more stable landscapes display many typical Aridisol features noted by Buol et al. (1997): surface soil crusts a few millimetres thick are common; somewhat altered subsurface horizons where the original stratification has been obliterated by mixing; argillic subsurface horizons with a higher clay content than the overlying horizon; eluvial horizons; horizons of carbonate accumulation that vary from calcic to petrocalcic (which are generally on the order of 1 m thickness); red-brown silica-cemented horizons (petroduric in Soil Taxonomy or dorbank in the South African classification system), which may contain a significant amount of calcium carbonate and gypsum and are commonly 1 to 2 m thick. Gypsic and petrogypsic soils occur in the northern part.

Profile KV196T is classified as the Garies Form (Orthic A - Red apedal B - Dorbank) in the South African classification system (Soil Classification Working Group, 1991). It is located adjacent to and in a mine excavation in the Buffels Marine Complex on the farm Kareedoornvlei 177 (see Figure 1.2), on the 95 m terrace cut into silcrete, 118 m a.m.s.l. (GPS), Terrain unit: crest. It is further inland than SK11 (Figure 1.1). The profile is pictured in Appendix A.

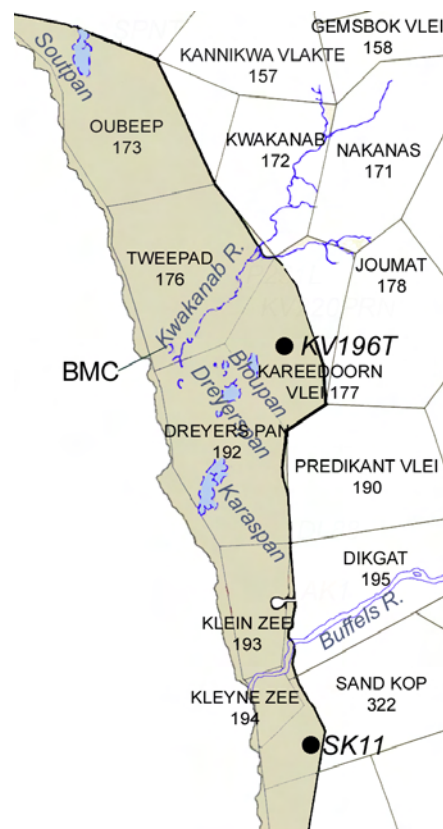


Figure 1.2: Location of profiles KV196T, SK11 and their farm names within the Buffels Marine Complex (BMC) mining area

Profile SK11 is classified as the Pinedene Form (Orthic A - Yellow-brown apedal B - Signs of Wetness) in the South African classification system. It is located adjacent to and in a mine excavation in the Buffels Marine Complex on the farm Sand Kop 322 (see Figure 1.2), on the 65 m terrace, 60 m a.m.s.l. (GPS). Terrain unit: footslope. It is pictured in Appendix A.

Fieldwork took place in February 2002. Profiles to bedrock were examined and sampled. Samples were named according to the mining excavation to which they were closest, the prefix being the farm name. Sample sites were selected to be representative of each terrace and marine package. Samples (approximately 2 kg) of each horizon were taken from the sidewalls of the mining excavations and from soil pits dug in the undisturbed areas nearby. The soil morphology was described in the field. A 10% solution of HCl was used to test for carbonate, and 30% H₂O₂ for manganese. Colour was described using a Munsell colour chart (Munsell Color Company, 1975). Horizons falling within 1.5 m of the surface were treated as diagnostic horizons for classification purposes. Those occurring deeper

in the profile were described, but treated as non-diagnostic and no consideration given to their position in the profile.

Knersvlakte: profile KNERS

Like the Buffels Marine Complex to the north, the Knersvlakte receives a reliable winter rainfall (May-August) of between 100 and 175 mm (Schmiedel and Jürgens (1999), using data from Weather Bureau (1988)). However, unlike the Buffels Marine Complex, models show the climate of the Knersvlakte remained as dry as present back to the Last Glacial Maximum (Desmet (2007), citing data from Midgley et al. (2001)).

The Knersvlakte forms the southern part of Namaqualand, just north of the Olifant's River (Figure 1.1). It is a part of the Succulent Karoo bioregion (Desmet, 2007), in contrast to the Sandveld bioregion of the area around the Buffels Marine Complex. This area occupies a broad plain created by the proto-Orange River some 20 million years ago and almost completely cuts the continuity of the African escarpment, creating a very distinct physical boundary between the sandstone and shale sedimentary rocks of the Cape Fold Mountains to the south, and the predominately igneous landscape of Namaqualand to the north (Desmet, 2007). The Knersvlakte consists of fluvial sediments (Pickford and Senut, 1997), and gypsum at depth that is mined in some places. The area is underlain by shales, phyllites and limestones of the Nama Group and is streaked by numerous quartz veins (Schmiedel and Jürgens, 1999), that have weathered to give rise to the distinctive, white, quartz gravel surface (pictured in (Schmiedel and Jürgens, 1999)). It is characterised by shallow soils overlying dorbank horizons (Francis et al., 2007).

The Knersvlakte profile (KNERS) was located 53 km east of Kliprand turnoff on N7, at 30° 48' 47.3" S, 18° 43' 25.3" E, 554 m a.m.s.l. (GPS). Terrain unit: extensive plain. Borrow pit, upper horizons removed (disturbed). It was associated with an old (inactive) heuweltjie, and in the vicinity of an alkali intrusive. Field-work took place in June 2004. Samples (approximately 2 kg) were taken of each hardpan horizon. The soil morphology was described in the field. A 10% solution of HCl was used to test for carbonate, and 30% H₂O₂ for manganese. Colour was described using a Munsell colour chart (Munsell Color Company, 1975).

1.2.2 Laboratory methods

Slaking tests were devised to distinguish silica- from carbonate-cemented hardpan horizons. These tests were based on the WRB (1998) definition of petroduric, petrocalcic and fragic horizons. A fragment a few centimetres in diameter was submerged in water, 5M HCl or 6M NaOH and gently heated on a waterbath for four days. More solution was added when necessary. Samples which did not slake were then subjected to alternating 5M HCl and 6M NaOH treatments. Thin sections for optical microscopy from the Knersvlakte profile were impregnated with a polyester resin and ground without water, and the samples from the KV196T profile impregnated with an epoxy resin. Fine grained calcite was identified by effervescence in 1M HCl under the optical microscope. Uncoated fragments and thin sections were observed before and after etching in 1M HCl using a Philips Xl30 environmental scanning electron microscope (ESEM) in low vacuum and with an energy dispersive X-ray analysis system (EDX). High vacuum SEM was done on Au-coated fragments using a Leo 1430VP SEM-EDX system. Major element composition of bulk samples was determined by x-ray fluorescence (XRF). For chemical and mineralogical (x-ray diffraction, XRD) analysis, samples were air-dried, crushed in a pestle and mortar (unless specified as milled, where samples were milled for 5 minutes using a stainless steel ball mill) and passed through a 2 mm sieve. The >2 mm cement was sorted from the >2 mm pebbles and recrushed, to minimise shattering of detrital pebbles/gravel. For XRD analysis, the <2 μm fractions of the bulk samples were separated by dispersion (shaking briefly by hand, raising the pH to approximately 10 with Na_2CO_3) and settling. The 1 to 0.08 μm and <0.08 μm fractions were separated by centrifugation. The clay suspension was flocculated by the addition of MgCl_2 , after lowering the pH to 5 to 7 with HCl to prevent the precipitation of brucite and/or clay destruction. The clay suspension was then Mg-, Ca- or K-saturated, concentrated by centrifugation, and sedimented (or smeared, many of the sepiolite-rich samples developed ‘mudcracks’) onto a glass slide. XRD analyses were done with a stepsize of 0.05 degrees and steptime of 40 seconds, using a Bruker D8 Advance Powder Diffractometer with a graphite monochromator, 40 kV and 40 mA. Ethylene glycol was sprayed lightly onto the surface of the Mg-saturated sample slides.

The <2 mm fraction was used for chemical analyses. The pH and electrical con-

ductivity (EC) were measured in a 20 g to 50 mL soil-water mixture. Saturated paste extracts were prepared for all samples except the Knersvlakte profile, since it was truncated so only the duricrust was exposed at the surface. They were prepared with a 300 g sample, to which approximately 100 g (depending on the clay content) of water was added to form a saturated paste, and equilibrated for 24 hours. The pH of the saturated paste was measured directly. The solution from the saturated paste was extracted under vacuum. Electrical conductivity (EC) was measured with a calibrated conductivity meter; alkalinity by potentiometric titration to pH 4.5 with 0.01M HCl; major cations by atomic absorption spectroscopy; major anions by ion chromatography; Si using the blue silicimolybdous acid procedure of Weaver et al. (1968), and dithionite-citrate-bicarbonate extractable Fe using the method of Mehra and Jackson (1960).

1.3 Results and discussion

Descriptions of a typical dorbank (petroduric) profile (KV196T), and two ‘sepiocrete’ profiles (SK11; KNERS) are given in Table 1.1. Typical examples of dorbank and ‘sepiocrete’ (from the Knersvlakte profile) are shown in Figures 1.3 and 1.4. Dorbank (petroduric) occurring in the KV196T profile is the massive type, and the Knersvlakte profile the platy type, and forms prominent cutans on the ‘sepiocrete’. In the ‘sepiocrete’ samples, water applied from a dropper spreads nearly instantly away along very fine cracks, usually in a dendritic pattern. This tendency for water to flow along preferential flow paths may explain the development of the sepiolite veins (arrowed in Figure 1.4).

1.3.1 Slaking behaviour

Dorbank (petroduric)

In this study, even if they effervesced in HCl, the dorbank horizons consistently slaked only in concentrated NaOH (Table 1.1). In comparison, a typical weathering-profile silcrete (non-calcareous) capping a hill near the town of Kleinzee did not slake in prolonged contact with heated concentrated NaOH. This suggests the cement in the dorbank is amorphous silica, compared to a more crystalline form in the silcrete. It also reveals that iron oxides are not the

Table 1.1: Profile descriptions. Roman numerals indicate different facies. Blank fields: *not detected*, except slaking tests: *not tested*, texture and consistency: *not applicable*. Abbreviations: *abun.*-abundant; *alt.*-alternating; *ang.*-angular; *bio.*-biological; *c.*-coarse; *cont.*-continuous; *diam.*-diameter; *f.*-fine; *frag.*-fragment; *med.*-medium; *mod.*-moderate; *occ.*-occasional; *O.M.*-organic matter; *qtz*-quartz; *sec.*-seconds; *sl.*-slight; *v.*-very; *w.*-with.

Depth (m)	Horizon (Soil Classification Working Group, 1991)	Munsell colour		Field Texture	>2mm Frag-ments	Structure		Consistency		Wet	Efferves-cence HCl	Slake (0-no, 5=full)		Water absorp-tion HCl/ NaOH (sec.)	Transition	Other Features
		Dry	Moist			Dry	Moist	HCl	NaOH							
Silicic Duricrust																
<i>KV1967: Gariés Form (Orthic A - Red apedal B - Dorbank), BMC (farm Kareedoorvlei 177), 95m terrace cut into silcrete, 118mamsl (GPS). Terrain unit: crest. Adjacent to mine excavation.</i>																
/A 0-	Orthic A	5YR 4/6	5YR 3/4	F. med. sand		Weak, med. ang. blocky	Loose	Loose	Loose	Non-plastic, non-sticky	None	0	>20	Clear, smooth	Abun. O.M., many roots	
/B 0.2-0.45	B1	7.5YR 5/6	5YR 3/4	F. med. sand		Weak, med. ang. blocky	Loose	Loose	Loose	Non-plastic, non-sticky	None	0	1	Not reached	Few roots	
<i>KV1967: New profile, upper material removed by mining. May be continuous with sample B. Mining excavation</i>																
/1 ±1-	B2	5YR 5/6	5YR 4/6	F. med. sand		Weak to mod., c., ang. blocky	Loose	Loose	Loose	Non-plastic, non-sticky	None	0	1	Diffuse, smooth	Bedding or wind erosion	
/2 1.3-	C1	5YR 5/6	5YR 4/6	Med. sand		Nodular	Hard	Firm	Firm		None	0	3	Abrupt, smooth	Mn on, in ped; abun, white dis-peised non-calcareous material	
/3 1.45-	C2	5YR 6/4	5YR 4/6	Med. sand		Nodular	Hard	Firm	Firm		None	0	8	Gradual, smooth wavy		
/4 1.6-	C3	5YR 5/6	5YR 4/6			Nodular	Sl. hard	Sl. firm	Sl. firm		Strong	0	3	Abrupt, wavy		
/5 1.8-	C4	Hardpan + Soft carbonate	5YR 8/1	5YR 6/4		Laminar to massive	Loose	Loose	Loose	Sl. plastic, non-sl. sticky	Strong	0	2	Abrupt, tonguing		
/6 2-?	C5	Soft dorbank	5YR 5/6	5YR 4/6		Nodular to massive	Loose	Loose	Loose	Sl. plastic, sticky	None	3-4	4	Obscured	Gypsum spots	
/7 ?-3.5	C6	Soft dorbank	5YR 5/6	5YR 5/6		Massive	St. hard-hard	Sl. firm	Friable-v. sl. firm		None	5	2	Obscured		
/8 ±3.5-	C7	Dorbank	5YR 5/6	5YR 5/6		Massive	Soft-hard	Friable	Soft-hard	Non-plastic, non-sticky	None	0	2	Obscured	Gypsum along fractures	
/9 ±4.5-	C8	Dorbank	7.5YR 6/4	7.5YR 5/6		Massive to vesicular	Hard	V. firm	V. firm		None	0	2-4	Gradual, unclear		
/10 ±6-±10	IC9	Marine deposit	5YR 5/6	5YR 5/6	Med. sand	Mod., med.-c.ang. blocky	Loose	Loose	Loose	Non-plastic, sl. sticky	None	0	3	Abrupt to bedrock	Salty taste	
Sepiolitic Duricrust																
<i>a) SK11: Pineferre Form (Orthic A - Yellow-brown apedal B - Signs of Wetness), BMC (farm Sand Kop 322, 65m terrace, 60mamsl (GPS). Terrain unit: footslope. Adjacent to mine.</i>																
/A 0-	Orthic A	7.5YR 5/5	7.5YR 3/4	Med.-f. sand		Single grain apedal	Loose	Loose	Loose	Non-plastic, non-sticky	None	0	4	Abrupt, smooth	Bio. crust, O.M., occ. droppings; many roots	
/B 0.2-	B	Yellow-brown apedal B	7.5YR 6/6	7.5YR 4/6	Med.-f. sand	Weak, f. blocky	Loose	Loose	Loose	Non-plastic, non-sticky	None	0	2	Clear, smooth	Few roots	
/C 0.6-	E	Gleyed sand	7.5YR 6/4	7.5YR 5/4	Med. sand	Apedal single grain	Loose	Loose	Loose	Non-plastic, non-sticky	None	0	1	Abrupt, smooth		
/D 0.65-	B2	Neocutanic	7.5YR 5/6	7.5YR 4/6	Loamy sand	Weak, c., ang. blocky	Sl. hard	Loose	Loose	Sl. plastic, sticky	None	2-3	2-3	Abrupt, smooth	Few roots; few clay cutans	
<i>SK11: New profile, 30 m away, upper material removed by mining. Mining excavation.</i>																
/1 0.01-	IC1	'Sepiocrete'	10YR 7/3	10YR 6/4		Laminar calcrete	V. hard	V. firm	V. firm		Strong	0	0-1	Gradual, wavy	Diffuse Mn coating some peds	
/6 0.45-	IC2	Blocky calcitrized sediment	10YR 7/4	7.5YR 5/6	Loamy sand	Strong, c., blocky to prismatic	Hard-v. hard	Firm-v. firm	Firm-v. firm		V. strong	0	2-3	Gradual, wavy	Mn spots on peds; calcite cutans	
/3 0.9-1.1	IC3	Hardpan carbonate	10YR 8/3	7.5YR 7/6		Laminar	V. hard	Firm-v. firm	Firm-v. firm		Strong	2-3	3	Clear, wavy	Mn spots on some peds	
/9 0.9-1.1	IC3	Hardpan carbonate	10YR 8/3	7.5YR 7/6		Laminar	V. hard	Firm-v. firm	Firm-v. firm		Strong	3	2-3	Clear, wavy	Mn spots on some peds	
/4 1.1-1.15	III C4	Neocarbonate	7.5YR 6/4	7.5YR 5/6	Med. sand	Weak, ang. blocky	Loose	Loose	Loose	Non-plastic, non-sticky	Strong	0	1	Clear, wavy		
/4b 1.15-1.5	III C5	Neocarbonate	10YR 7/4	10YR 6/4	Loamy sand	Weak, c. blocky	Loose	Loose	Loose	Sl. plastic, sl. sticky	Mod.	0	1	Clear, wavy to sample 7		
/5 0.8-1.5	IV C5	Termitic nest	10YR 6/4	10YR 5/6	Loamy sand	Mod., c., blocky	Firm	Loose	Loose	Sl. plastic, sl. sticky	Local	0	3	Diffuse	Occ. Mn; chert frag.; calcite cutans	
/7 1.5->2.2	IV C6	Sedimentary	5YR 7/4	10YR 6/3	Sandy loam	Local	Firm	Loose	Loose	Sl. plastic, sl. sticky	Local	0	3	Not reached		
<i>b) KNERS: Knersvlakte, 53 km E of Kliprand turnoff on N7. 30°48'47.3" S, 18°43'25.3" E, 564 mamsl (GPS). Terrain unit: extensive plain. Borrow pit, upper horizons removed.</i>																
Profile 1																
/A -0.1	'Sepiocrete'	5YR 8/2	7.5YR 6.5/6		Abun.	Massive	V. hard	V. firm	V. firm		Mod.-sl.	1	0		Sepiolite cutan	
/1 -0.15	Dorbank cutan few cm thick on Kners2'	5YR 7/6	5YR 5/6			Laminar coating	V. hard	Firm	Firm		None	0	5	>20	Cutan to Kners 2	
/2 -0.15	'Sepiocrete'	5YR 8/3	7.5YR 6/6		Mod.	Massive	V. hard	Firm-v. firm	Firm-v. firm		Slight	2-3	0	5	Many cracks	
Profile 2: From opposite side of borrow pit.																
/5 -0.15	Dorbank	5YR 6/6	5YR 5/6		Abun. qtz	Platy to blocky	Hard	Firm	Firm		None	0	5	15	Abun. cracks; occ. Mn; few roots; sepiolite cutan	
/4 -1	'Sepiocrete'	5YR 8/2	7.5YR 6.5/6		Abun. qtz	Massive	V. hard	V. firm	V. firm		Mod.-sl.	0	0-1	5	Sepiolite cutan	



(a) Profile showing area magnified in (b)



(b) Scale bar 1 cm

Figure 1.3: Reddish-brown dorbank (petroduric) forming cutan (KNERS/1) on white 'sepiocrete' (KNERS/2) from the Knersvlakte (Profile 1, described in Table 1.1). Hammer is 30 cm long.

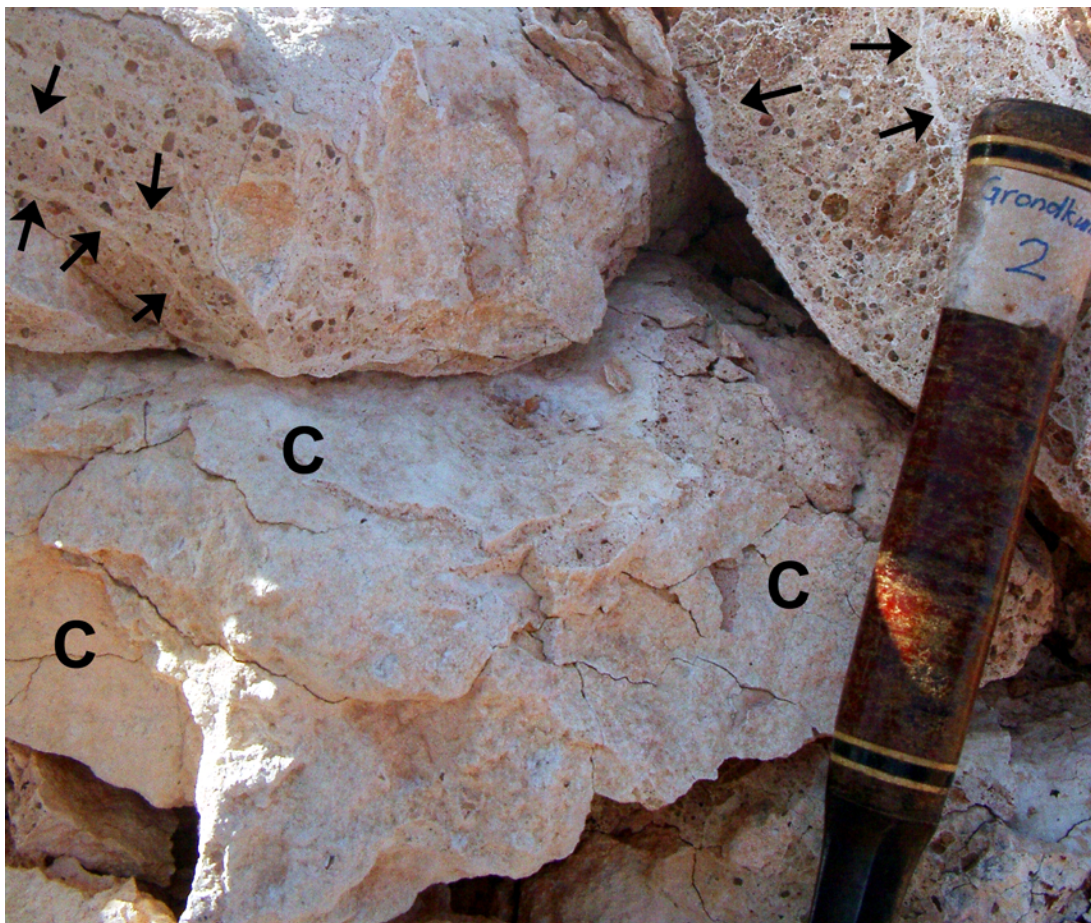


Figure 1.4: White ‘sepiocrete’ from the Knersvlakte (Profile 2), KNERS/4 described in Table 1.1. Sepiolite veins arrowed. Lower fragment partially coated by white, non-calcareous sepiolite cutan (C). Hammer handle 15 cm long.

cementing agent in dorbank. Despite their red-brown colour (Table 1.1), the dithionite-citrate-bicarbonate extractable Fe (Mehra and Jackson, 1960) content of KV196T/8 was only 0.4%. This is consistent with the range found by Chartres (1985, p. 329) for red-brown hardpans in Australia.

‘Sepiocrete’

SK11/E was the only example where partial slaking occurring in prolonged water treatments. The remaining ‘sepiocrete’ horizons were generally non- to locally calcareous (Table 1.1), suggesting calcite is not the primary cement. HCl treatments did not result in slaking, nor did NaOH treatments. Partial slaking was observed when alkali/acid treatments were alternated. This is in contrast to the dorbank samples, which slaked in NaOH even if calcareous. This may

suggest that the cement in ‘sepiocrete’ is not solely amorphous silica. However, Martínez-Ramírez et al. (1996) noted that the addition of sepiolite to a pH 12.4 NaOH solution caused the pH to be reduced to 8.6. Although the experimental methodologies were different in that the NaOH solution was refreshed on drying, and was more concentrated compared to Martínez-Ramírez et al. (1996), the pH was not measured and the possibility exists that the presence of sepiolite caused a reduction in pH sufficient to reduce the solubility of silica.

However, a weathering profile silcrete (similar to that described by Summerfield (1983a)) also did not slake in concentrated NaOH under the same experimental conditions. This suggests that in addition to sepiolite content, the degree of silica crystallinity and/or impregnation and/or total amount of secondary silica also plays a role in dictating whether slaking of a particular sample will occur.

The slaking tests established that calcite was not the primary cement in ‘sepiocrete’, but were inconclusive in determining whether silica or sepiolite formed the cementing agent.

1.3.2 Mineralogy

Dorbank (petroduric)

The clay fraction of dorbank profile KV196T contains smectite, and also mica/illite (Figure 1.5). The dorbank samples in the Knersvlakte profile (KNERS/1 and KNERS/5 in Figure 1.6) contain sepiolite, and possibly palygorskite.

With the exception of the non-calcareous KV196T/4, the dorbank horizons show broad, low peaks of the clay minerals, a characteristic noted by both Flach et al. (1969) and Blank and Fosberg (1991), who attributed it to disordered siliceous coatings masking the clay minerals. Figure 1.7 confirms that very fine material coats some clay grains.

Amorphous silica (broad opal-A peak at 0.41-0.403 nm (Drees et al., 1989)) does not appear in any quantity on the diffraction patterns of profile KV196T, despite its presence as cementing agent being suggested by slaking only in strong alkali. KV196T/2 is the only horizon that shows a broad rise of the background in the 0.4 nm vicinity. The amorphous silica peak is more apparent in the Knersvlakte

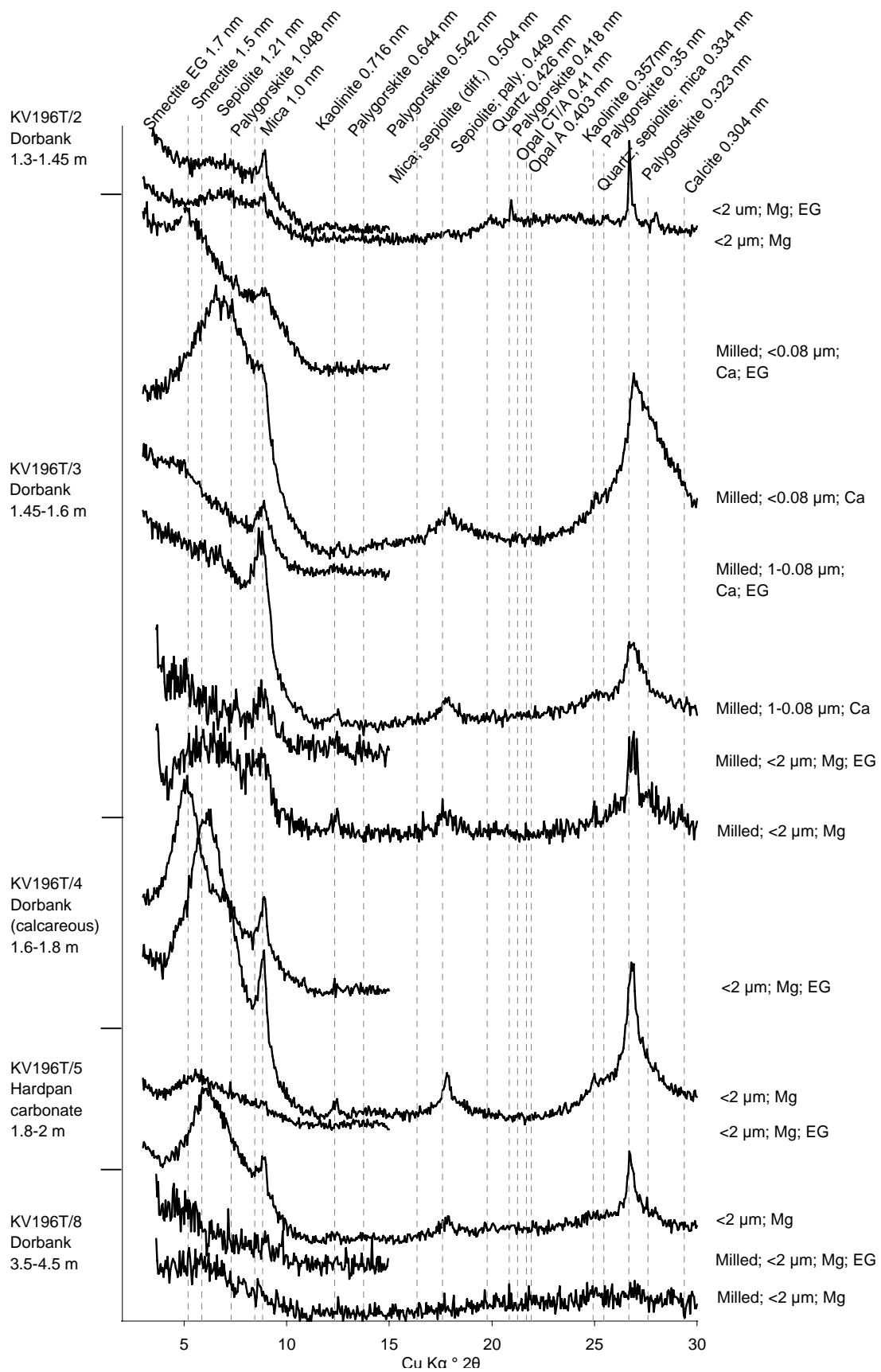


Figure 1.5: XRD traces of Mg- or Ca- saturated clay fractions from selected horizons in profile KV196T. Diff: diffuse; EG: ethylene glycol.

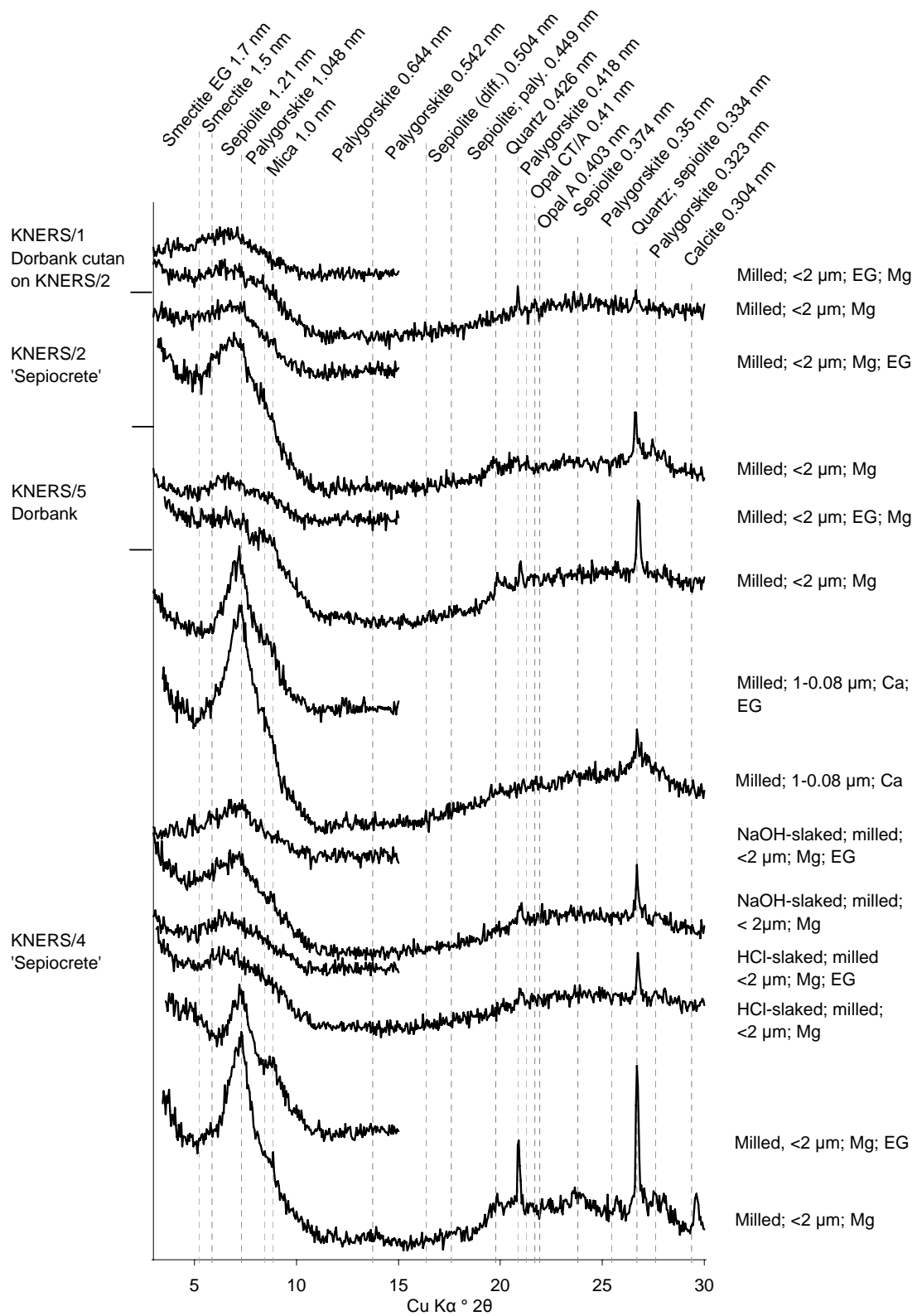


Figure 1.6: XRD traces of Mg- or Ca- saturated clay fractions from selected horizons in the Knersvlakte profile KNERS. Diff: diffuse; EG: ethylene glycol.

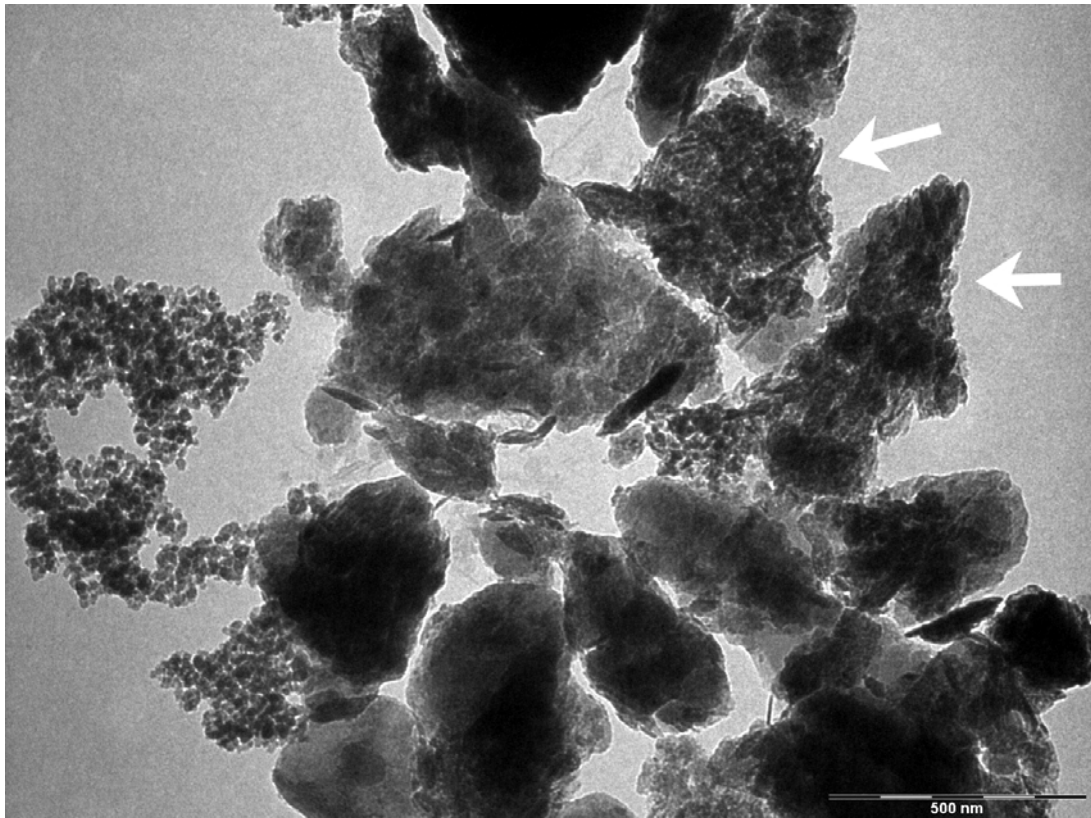


Figure 1.7: TEM image showing very fine material (such as on the left) coating clay grains (top right) in dorbank (petroduric) KNERS/5 (milled).

profile than KV196T. There seems to be a small opal-C/T peak at 0.41 nm in KV196T/8 and /3, and KNERS/1 and possibly /5. Quartz is present in the clay fraction. Since quartz is ubiquitous in the marine sands that form the parent material, and the clay fraction was liberated by milling, there is a large detrital component which cannot be distinguished from authigenic silica.

‘Sepiocrete’

SK11/E, the non-calcareous ‘sepiocrete’ that slaked partially after prolonged soaking in water (Table 1.1), is the only horizon within the SK11 profile that contains monominerallic sepiolite in the clay fraction (Figure 1.8). Amorphous silica does not appear in the clay fraction. The other horizons in the profile contain smectite, kaolinite and mica/illite in addition to sepiolite. Palygorskite appears to be a minor constituent, with the 0.664 nm peak best defined in the $<1 \mu\text{m}$ fractions (Figure 1.8).

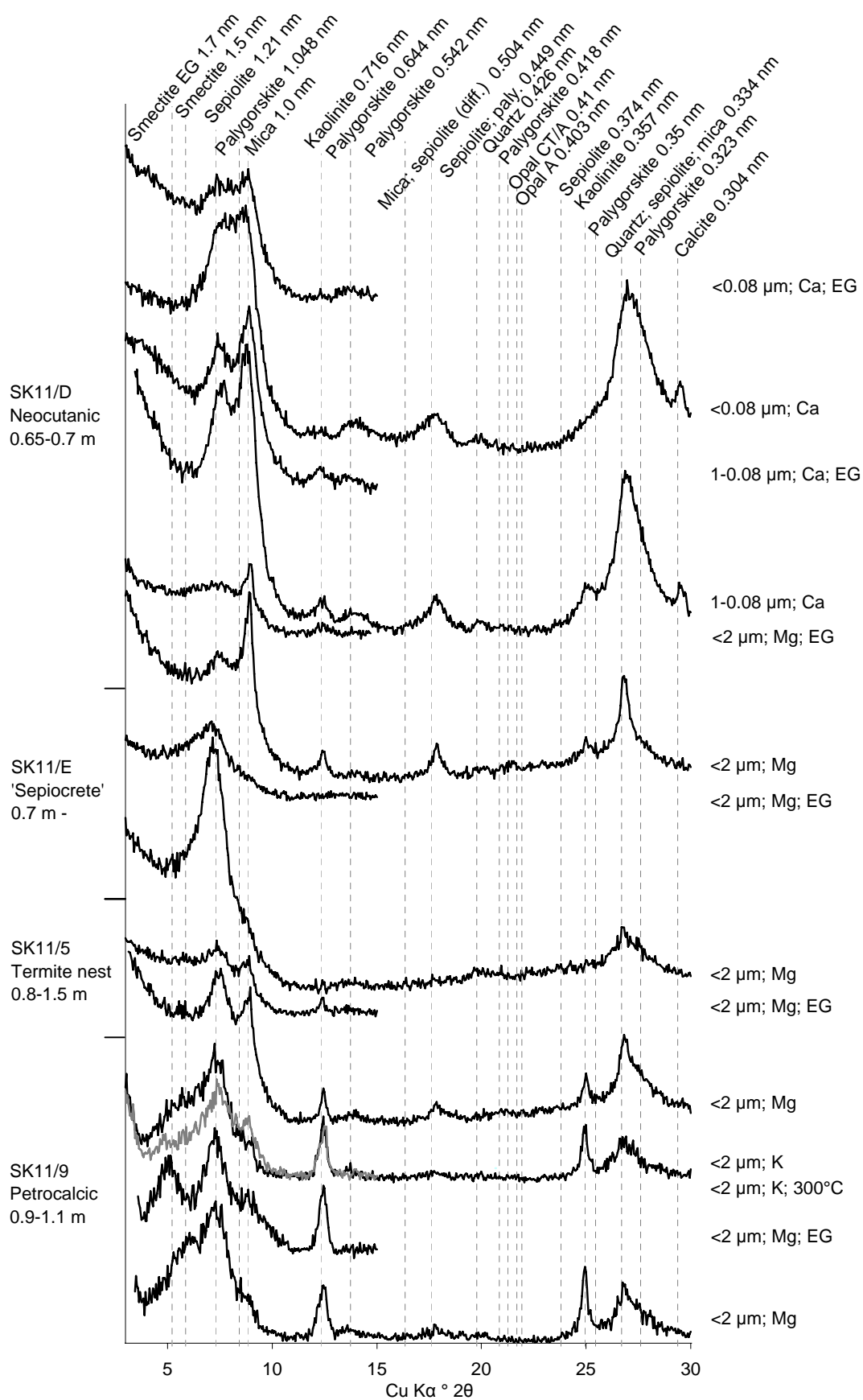


Figure 1.8: XRD traces of Mg-, K- or Ca- saturated clay fractions from selected horizons in profile SK11. EG: ethylene glycol.

XRD traces of the clay fraction of the ‘sepiocrete’ samples in the Knersvlakte profile (Figure 1.6) show strong sepiolite peaks in all size fractions. These are not as clear on the dorbank horizons KNERS/1 and KNERS/5, but this may be a function of disordered siliceous coatings masking the clay minerals in dorbank (Flach et al., 1969; Blank and Fosberg, 1991). Palygorskite is much less prominent than sepiolite in the $<2 \mu\text{m}$ fraction. Both the dorbank and ‘sepiocrete’ horizons in the Knersvlakte profile show a very broad amorphous silica peak emerging on the background at around 0.4 nm, although it is slightly less expressed in KNERS/1 and KNERS/2. This amorphous silica peak is more apparent in this profile than either KV196T (Figure 1.5) or SK11 (Figure 1.8). As with the dorbank, the quartz peaks are likely to have a largely detrital component which cannot be distinguished from authigenic silica.

The $<2 \mu\text{m}$ fraction of partially slaked ‘sepiocrete’ from KNERS/4 was milled and analysed. The HCl treatment caused a significant broadening of the sepiolite peak (Figure 1.6), suggesting the sepiolite was partially destroyed by the acid attack, and consistent with the findings of Gozález et al. (1984) and Dékány et al. (1999). The 0.4 nm amorphous silica peak was not affected by acid treatment. The NaOH treatment also caused a slight broadening of the sepiolite peak, but not to the same degree as the acid treatment. The alkali treatment did not seem to have affected the 0.4 nm amorphous silica peak either, suggesting the alkali treatment was insufficient to remove the silica from these samples.

1.3.3 Micromorphology

Dorbank (petroduric)

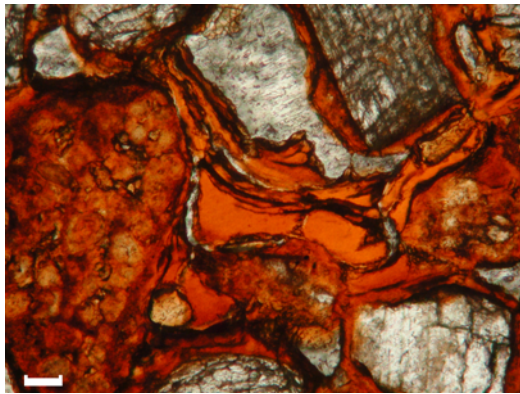
The dorbank micromass is generally dominated by the reddish orange colour imparted by Fe (hydr)oxides, with strongly oriented clay more prominent than amorphous silica in many places (Table 1.2). The amorphous silica is generally clear and yellowish, and is generally isotropic. It may be that it has been masked by the colour of the Fe. Spherulites (crystal aggregations with an approximately circular outline and a permanent cross of extinction in crossed polarized light (Canti, 1997)) are present, some have an isotropic core and appear to be silica (Figures 1.9(a)-(b)), others show pseudo-negative uniaxial interference colours and concentric banding under crossed-polarisers (Figures 1.9(c)-(e)). Summer-

field (1983a) observed spherulites with pseudo-uniaxial extinction crosses comprised of length-fast chalcedony in a vugh-fill in South African silcrete. The orientation of the crystals making up the spherulites in the Namaqualand samples, however, could not be resolved with certainty. Laminated and layer-coated nodules and aggregates are present in KNERS/5 (Figure 1.9(f)-(g)), which are remarkably similar to the compound 'glaebular aggregates' from silcretes in the Riversdale-Albertina area shown by Summerfield (1983a, p. 903).

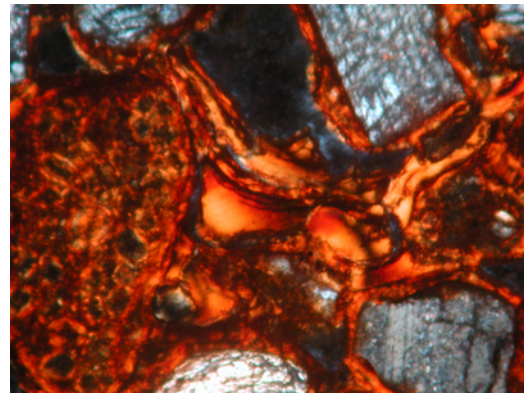
Table 1.2: Thin section descriptions. Abbreviations: diam.: diameter; incl.: including; max.: maximum; occ.: occasional; OIL: oblique incident light; ppl: plane polarised light; xpl: cross polarised light.

<u>Kleinsee, dorbank, sample KV196T/4.</u>	<u>Knersvlakte, dorbank cutan, sample KNERS/1.</u>	<u>Knersvlakte, 'sepiocrete' sample KNERS/2.</u>	<u>Knersvlakte, dorbank, sample KNERS/5.</u>
1 vertical section 20 x 40 mm; thickness ~ 30-35 µm.	3 vertical sections 50 x 40 mm; thickness ~ 30-35 µm.	3 vertical sections 50 x 40 mm; thickness ~ 30-35 µm.	3 vertical sections 50 x 40 mm; thickness ~ 30-35 µm.
Micro-structure Vughy microstructure.	Micro-structure Channel and vughy microstructure.	Micro-structure Weakly separated granular to massive microstructure. Granules 0.6 - 0.05 mm diam.	Micro-structure Vughy microstructure.
Groundmass c/f limit: 5µm c/f ratio: 8:1 c/f-related distribution: chito-gefuric.	Groundmass c/f limit: 5µm c/f ratio: 9:1 c/f-related distribution: close porphyric.	Groundmass c/f limit: 5µm c/f ratio: 1:8 c/f related-distribution: open porphyric.	Groundmass c/f limit: 5µm c/f ratio: 8:1 c/f related-distribution: chito-gefuric to close porphyric.
Coarse Material Subrounded quartz, less feldspar, minor opaques, mica. Grains ~0.4 - 0.03mm.	Coarse Material Predominantly subangular quartz, also opaques. 5mm diam. common, to 0.2 mm.	Coarse Material Predominantly subangular quartz, also opaques, feldspar, garnet. 1mm diam. common, to 0.5 mm.	Coarse Material Subrounded quartz, less feldspar, minor opaques, mica. Grains ~1cm - 0.02mm, orientated ~ with long axis horizontal.
Micromass PPL: Limpid, orange-brown. Comprises Fe-stained silica, and/or clay, some pure silica. Although sample slakes only in NaOH, pure silica in the matrix is difficult to discern, it may be very fine-grained. XPL: Granostriated b-fabric.	Micromass PPL: Banded dark orange predominantly speckled; some limpid layers. Generally orientated parallel to grain edges or to channels. Laminated (with very fine dark bands) and entire lamination "crenulated". Dispersed fine calcite, grey, Mn, mammilate, dispersed. XPL: Granostriated b-fabric.	Micromass PPL: Speckled grey-yellow. Seems to be predominantly sepiolite, locally covered by finely dispersed grey secondary calcite which projects into tiny voids giving a crystallitic b-fabric, and locally some silica. XPL: Speckled b-fabric dominant, locally cross-hatched and crystallitic.	Micromass PPL: Limpid to speckled, reddish-orange-brown. Comprises Fe-stained silica, and/or clay, some pure silica interspersed. XPL: Granostriated b-fabric.
Pedofeatures Grains coated by amorphous Fe-oxides incl. hematite (red in OIL). Also over this are clay coatings, and amorphous (isotropic) silica, which tends to be concentrated on the outer edges and intergrain areas. Coatings are length-slow. Dense infillings of clays, forming microlaminated crescent coatings. In some cases they appear to seal the void and no further vertical illuviation occurs below. Silica is over the clay. Spherulites (with pseudo-negative uniaxial interference colours).	Pedofeatures Coatings: Some grains have an edge that seems to be coated with orientated silica. "Crenulated" clay layers very common, layers orientated parallel to grains and filling interstices, in some cases the inter-coating areas are filled with amorphous silica. Channels: generally branching downwards, may be root channels, <0.4 mm diam, accommodating faces, rough textured sides, sometimes side-branching chambers. Channels and chambers appear to be coated and/or filled with decomposed organic material, generally 0.02mm diam., often occurring as aggregates, and usually associated with fine grey calcite (often only distinguishable by effervescence with HCl), in some places resolved as needle fibre calcite.	Pedofeatures Channels lined and filled with sepiolite, arranged in fan-like bundles. Speckled, grey, laminated calcic pendants and cappings. Discreet subangular limpid yellow clay (silica?) nodules (300 - 70 µm) which have a cross-striated or isotropic b-fabric and very low (first order) interference colours, occasionally will show pseudo-negative uniaxial interference colours, may be coated with micrite, orientated clay or silica (isotropic). Coatings: Quartz and clay particles coated with micrite (mixed with clay) hypocoatings, some are coated with isotropic silica and Fe.	Pedofeatures Coatings: Grains coated by amorphous Fe-oxides incl. hematite (red in OIL). Clay, silica may be masked by the colour of the Fe oxides. The coatings are length-slow. Crescent coatings, not always associated with voids, the voids may have been completely filled. Spherical, rounded peds 0.5 - 1cm, also elongated and large irregular (~ 5cm) peds with laminated (limpid to speckled with silt-sized quartz) reddish-orange-brown coatings. Some are aggregate features, laminated and layer-coated nodules enclosed with other matrix material within a larger laminated and layer-coated nodule. Spherulites: some show pseudo-negative uniaxial interference figures, some have an isotropic core, others concentric banding.

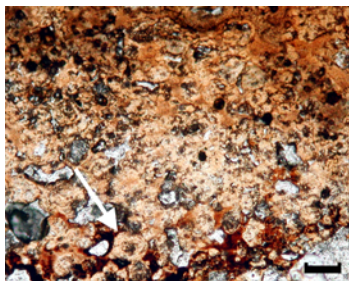
Illuviation of clay has been a dominant soil forming process, with strong ori-



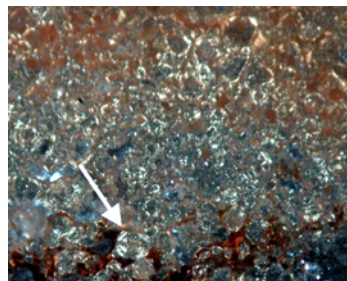
(a) Spherulites (left), limpid crescent coating, amorphous silica (isotropic). KNERS/3, ppl. Scale bar 0.1 mm.



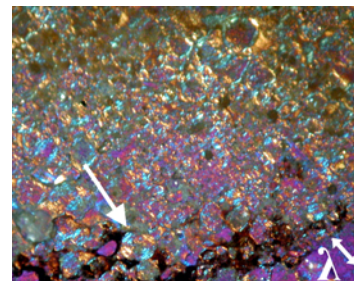
(b) Same view as (a), xpl.



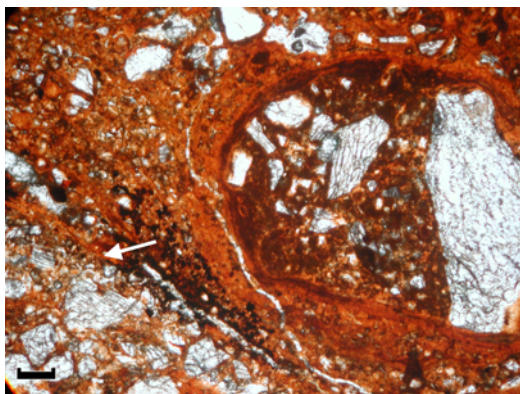
(c) Spherulites. KNERS/5, ppl. Scale bar 0.1 mm.



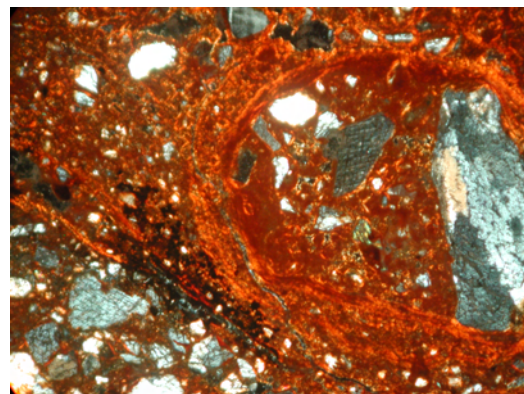
(d) Same as (c), xpl.



(e) Same as (c), xpl, λ plate, fast direction indicated.



(f) Portion of complex aggregate (border with matrix arrowed). KNERS/5, ppl. Scale bar 0.2 mm.



(g) Same view as (f), xpl.

Figure 1.9: Typical views of silica in dorbank (petroduric) horizons. Way-up is top of page.

entation of clay parallel to grains and crescent coatings on the lower part of voids common (Figures 1.9(a)-(b)). Figure 1.10(a)-(b) shows a void blocked by clay-coated grains, resulting in a crescent coating forming on top and no further illuviation into the lower part of the void. Sullivan (1994) obtained optically ori-

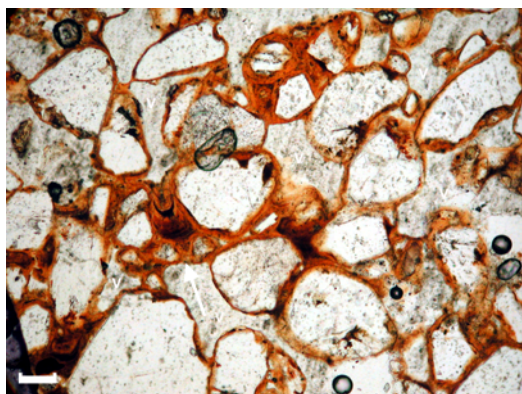
ented clay coatings on coarse quartz sand by passing smectitic clay suspensions through sand columns. These coatings were not removed by subsequent passage of water, suggesting that the dominant clay deposition mechanism involves the retention of suspensions on sand surfaces by capillary and adsorption forces. It appears that clay illuviation occurred before silica precipitation in the dorbank horizons, since the silica is generally (although not exclusively) concentrated on the void side of the clay coatings (Figures 1.9(a)-(b), 1.10(a)-(b)), similar to that described by Litchfield and Mabbutt (1962) for red-brown hardpans in Western Australia. Layering suggestive of illuviation is evident in Figure 1.10(c), the composition of which (Figure 1.10(d)) is consistent with montmorillonite clay, silica and the reddish orange colour imparted by Fe (hydr)oxides.

Smectite neoformation also appears to be present. SEM images of a fragment of KV196T/3 (Figure 1.10(f)) are similar to images of neoformed smectite in Borchardt (1989, p. 680). The composition (Figure 1.10(e)) is very Mg-rich for a smectite: it is closer to that of saponite than montmorillonite. The XRD trace shows the broad peak of an expandable phase (Figure 1.5), as well as mica and kaolinite peaks. The mica and kaolinite alone could not account for the high Mg content. The horizon KV196T/3 occurs fairly high up in the profile (Table 1.1), and it may be that the clay is neoformed in the upper part, and illuviated downwards together with silica and more Al-rich smectite to form harder, more laminated horizons like KV196T/8 (Figure 1.10(c)).

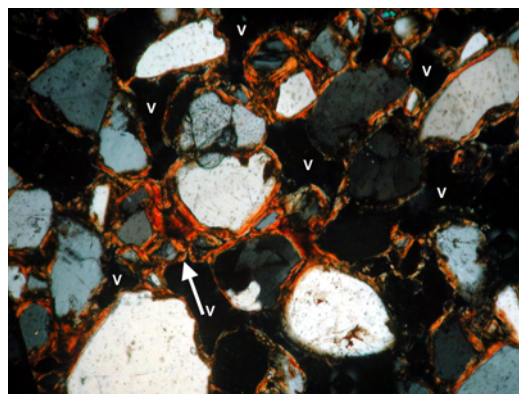
‘Sepiocrete’

The micromorphology of typical ‘sepocrete’ is given in Table 1.2. They are distinctly different from dorbank horizons, the most obvious being the granular microstructure, the micrite-rich matrix, and the lack of crescent clay coatings (Figure 1.11). Prolate calcite crystals (length-slow) project into the inter-granule areas (Figures 1.11(a)-(b)).

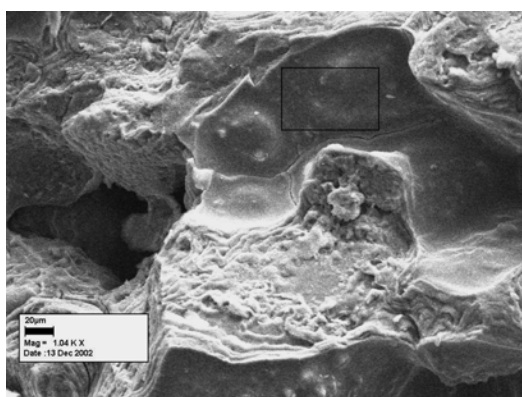
Although the colour and localised effervescence in HCl resemble calcrete in the field, calcite is not the primary cement: Figures 1.12 and 1.13 shows a fragment from KNERS/4 before and after etching in 1M HCl for 30 seconds, until effervescence ceased. Effervescence was only observed in the lower part of the fragment where pitting developed (area C in Figure 1.12(b)). Before etching, the calcite was present in the form of finely dispersed, less than 2 μm particles, consistent with the low Ca content (Figure 1.12(d)). After etching, most of the calcite was



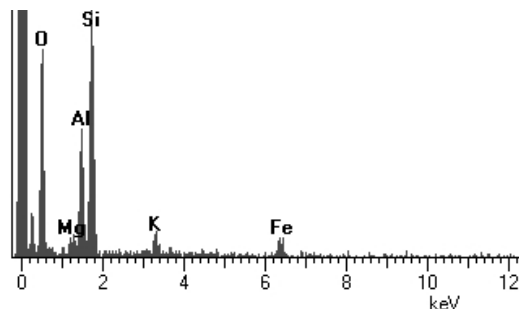
(a) Crescent coating developed above blocked void (v). Scale bar 0.1 mm. Way-up is top of page. KV196T/4, ppl.



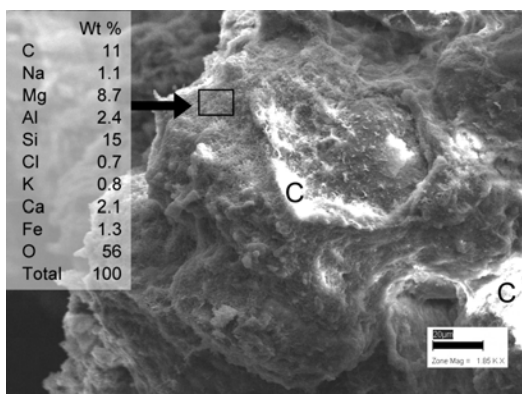
(b) Same view as (a),xpl.



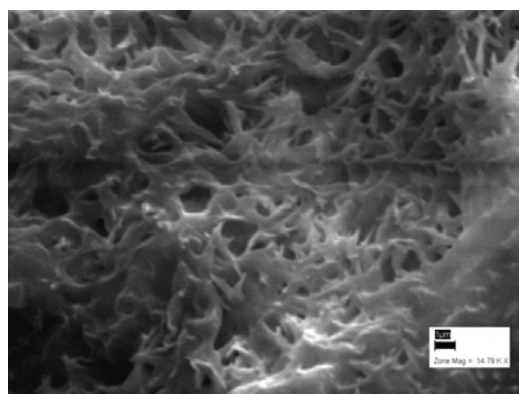
(c) Layering in dorbank, KV196T/8. Scale bar 20 μm .



(d) Spectrum of square in (c).



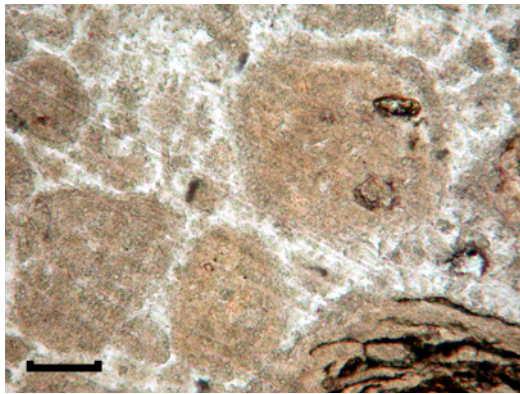
(e) Layering and neoformed clay, KV196T/3. Scale bar 20 μm . C: charging.



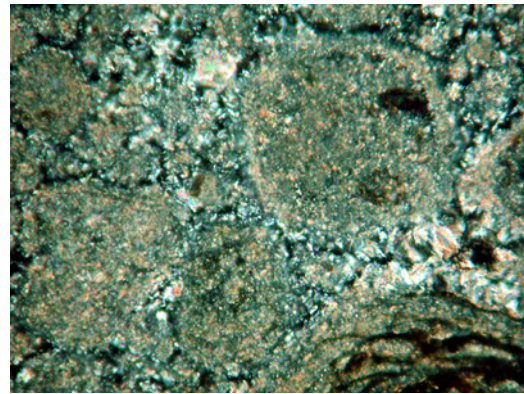
(f) Magnification of square indicated in (e). Scale bar 1 μm .

Figure 1.10: Neoformed and illuviated smectite and silica in dorbank (petroduric) fragments.

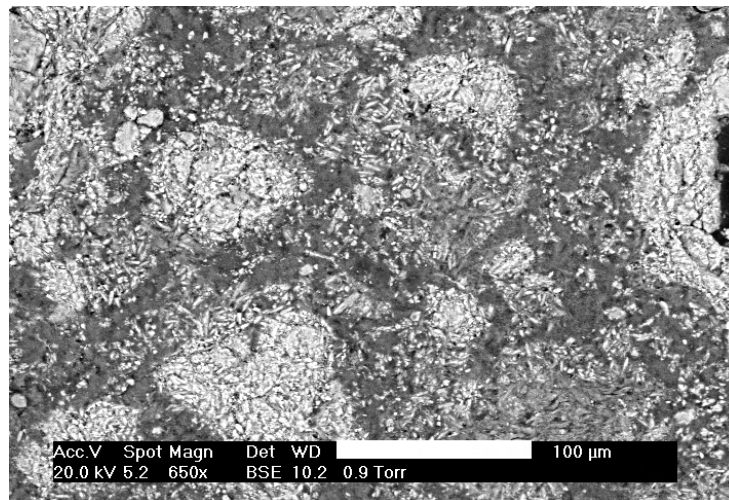
removed. The sample remained very firm (Figure 1.12(b)), which shows calcite is not the primary cement in these samples, and the micrite causing the speckled b-fabric observed with the optical microscope is an accessory feature.



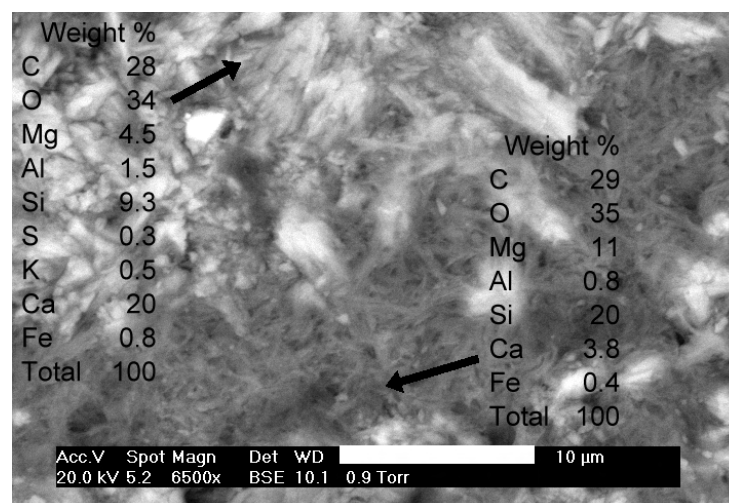
(a) Granular microstructure. Scale bar 0.1 mm, Knors/2, ppl. Way-up is top of page.



(b) Same view as (a), xpl.



(c) Thin section, SEM image of microstructure. Scale bar 100 μm , KNERS/2.



(d) Magnification of (c). Scale bar 10 μm .

Figure 1.11: Optical and SEM images of granular microstructure in 'sepiocrete'.

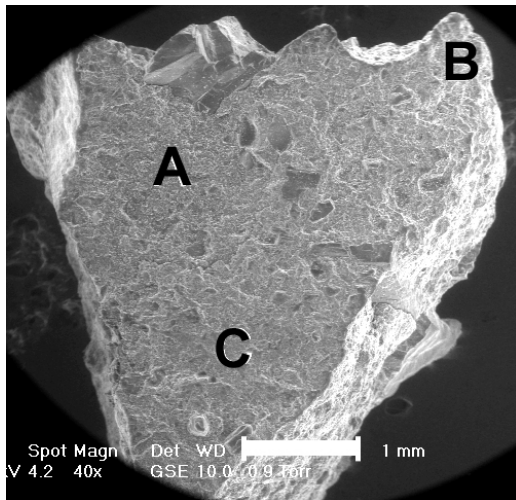
The high Mg/Si ratio of the fibres both pre- and post etching (Figure 1.12(d), (f)) is consistent with molar Mg/Si of 0.67 for sepiolite (Stoessel, 1988). An interlocking, subparallel morphology is present over much of the sample (Figures 1.12(c), (e), 1.13(b), (c)), perhaps contributing to the induration as suggested by Francis et al. (2007).

It is sometimes difficult to distinguish sepiolite from silica with certainty under the optical microscope, given the low birefringence of sepiolite (as in Figures 1.14(a)-(b)). Sepiolite appears to form the matrix areas (Figures 1.11, 1.12, 1.13, 1.14(d)), whereas the silica is localised: Figures 1.13(c)-(d) show morphology suggestive of localised amorphous silica. Elemental mapping in Figure 1.14(c) shows the laminar area to be Si-dominant, and poorer in Mg than comparative mapping of sepiolite-rich areas like Figures 1.11(d) and 1.14(d).

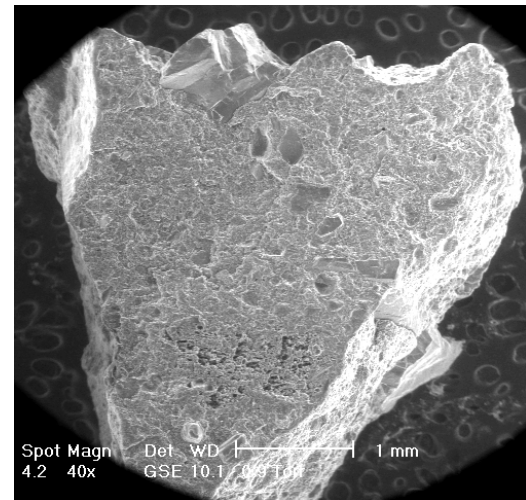
Pedofeatures similar to the sepiolite/silica indicated in Figure 1.14(a) have been recorded in Sardinia, Italy in >2.7 Ma buried paleosols (Usai and Dalrymple, 2003). They suggested that the “milky pedofeatures” as they termed them, were made of different phases of silica such as inorganic opal-A, opal-C and opal-CT, but mainly composed of opal-C. They noted that slight and local birefringence in colourless white-milky pedofeatures has been previously described for opal-CT by Drees et al. (1989). Although silica was the main constituent of the “milky pedofeatures” (reaching 67% of the total weight), the remaining constituents were \approx 25% Al₂O₃, 5% MgO, 2 to 4.6% Fe₂O₃ and 2% CaO, which they attributed to chemisorbed impurities to silica (Drees et al., 1989) or analytical imprecision.

The tapering texture of some sepiolite fibres (seen in Figures 1.12(c), 1.13(a), (c) and (d)) is similar to that observed by Khoury et al. (1982), Blank and Fosberg (1991) and Akbulut and Kadir (2003). The wider ‘root’ of the tapering structure suggests that that crystal growth is from the substrate into the void, with a greater number of shorter fibres growing at the base and fewer fibres reaching greater lengths growing into the void.

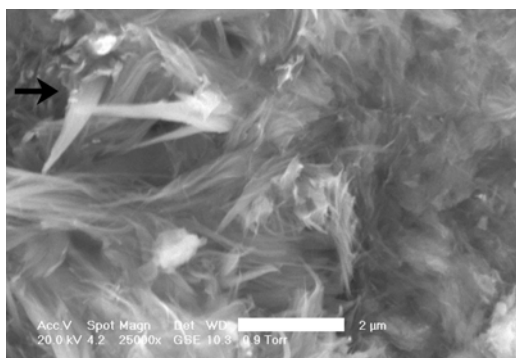
The micromorphology of the ‘sepiocrete’ shows that calcite is not the cementing agent. Whether sepiolite or silica forms the primary cementing agent is not as clear: while most of the intergrain area seems to be composed of pure sepiolite, there are areas that seem to be composed of dense laminar silica. It remains speculative which has had the greater influence: the pervasive sepiolite matrix with its interlocking fibres, or the more localised silica with its ability to indurate a sample to a very firm consistency.



(a) Before etching. Scale bar 1 mm.



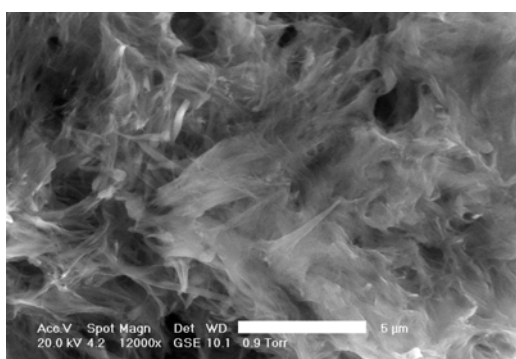
(b) After etching

(c) Before etching area B. Scale bar 2 μm .

Weight %

C	32
O	39
Na	1.3
Mg	8.4
Al	0.7
Si	13
Cl	1.6
K	0.3
Ca	3.7
Fe	0.4
Total	100
m Mg/Si	0.74

(d) EDX analysis of (c)

(e) After etching area B. Scale bar 5 μm .

Weight %

C	34
O	37
Na	1.1
Mg	9.2
Al	0.9
Si	15
Cl	1.7
K	0.2
Ca	0.7
Fe	0.5
Total	100
m Mg/Si	0.72

(f) EDX analysis of (e)

Figure 1.12: SEM images: 1M HCl etching of 'sepiocrete' KNERS/4. EDX analysis semi-quantitative. Mg/Si ratios are molar ratios. Continued in Figure 1.13.

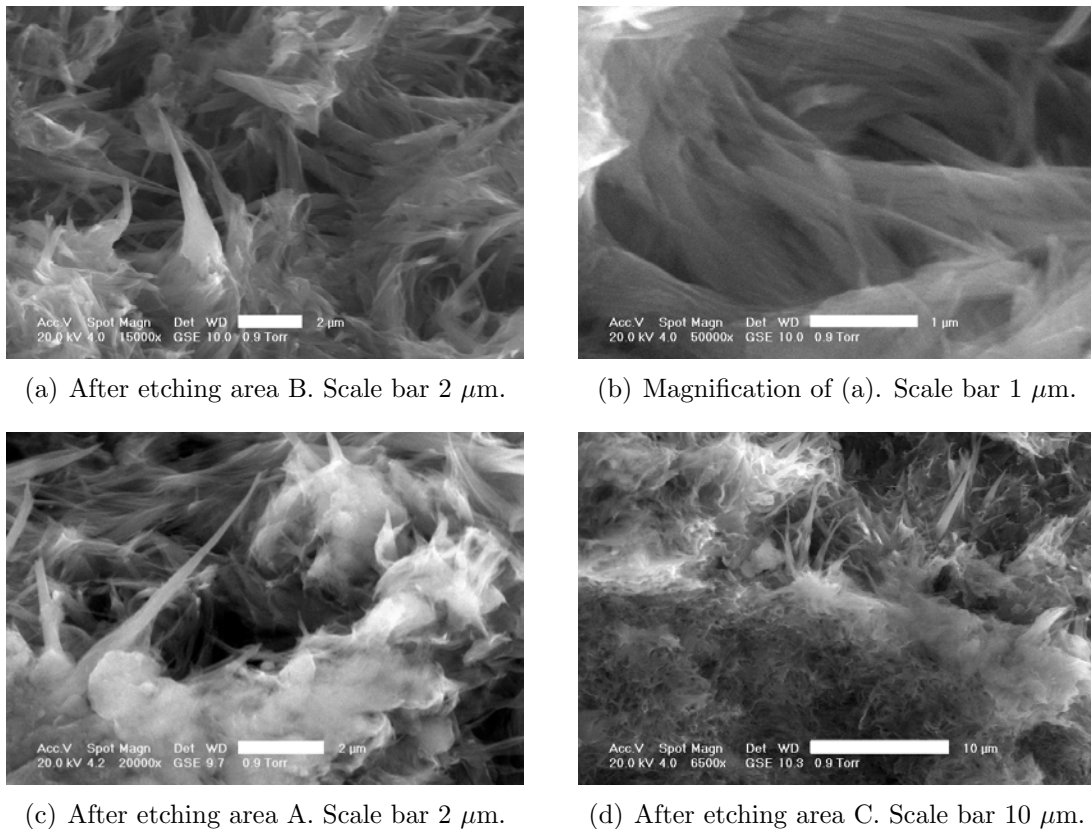
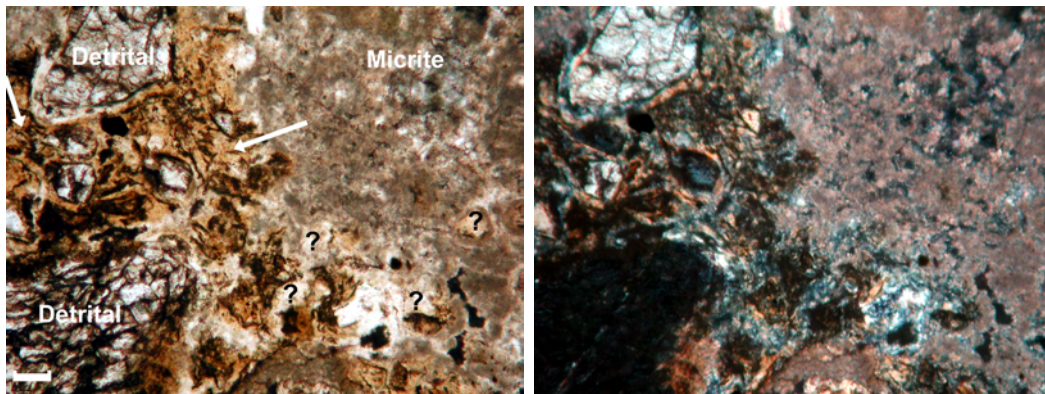


Figure 1.13: Continued from Figure 1.12 - SEM images: 1M HCl etching of 'sepiocrete' KNERS/4.

1.3.4 Genesis

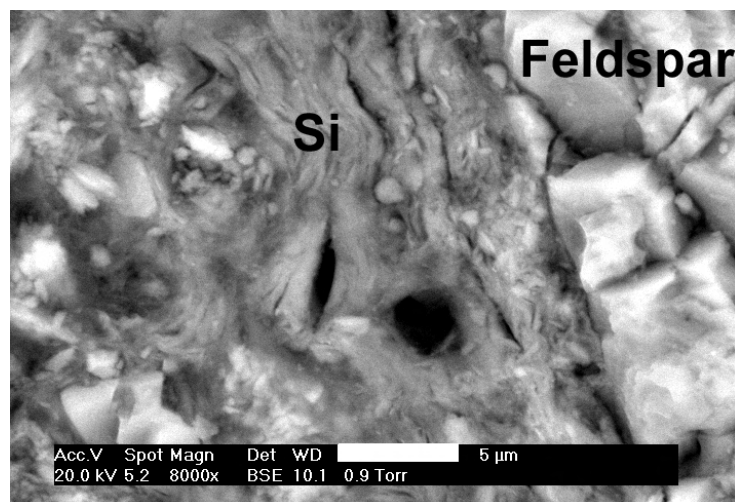
Dorbank (petroduric)

Dorbank (petroduric) genesis may be explained by the high pH of the upper horizons (Table 1.3) which may increase the solubility and mobility of silica, while the sodic environment may contribute to clay dispersion (Ellis, 1988; Ellis and Lambrechts, 1994), and facilitate the hydrolytic exchange of Na^+ , with an associated rise in pH when the soils are submerged in water (McBride, 1994, p.91-95). Under the prevailing low rainfall conditions, the soluble silica would not leach through the profile but rather accumulate in the subsoil. The loci of silica deposition in duric soils depends on both the depth of water movement and the amount of adsorption surface area (Chadwick et al., 1987), and it seems likely that the abundance of illuviated clay in the pore spaces provided a large adsorption area for silica, and is consistent with the thin section observations that clay illuviation occurred before silica precipitation. The dorbank horizons have

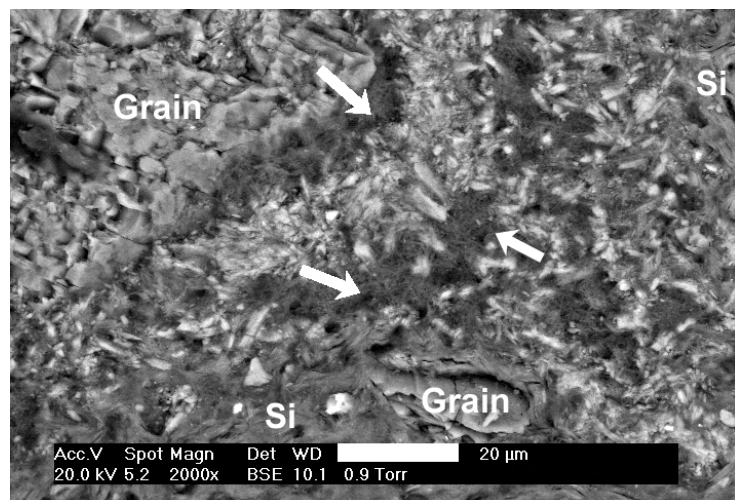


(a) Amorphous silica (arrowed); ?: sepiolite/silica. Scale bar 0.1 mm, ppl. Way-up is top of page.

(b) Same view as (a), xpl.



(c) Thin section, SEM image of laminar silica (Si). Scale bar 5 μm .



(d) Thin section, SEM image of laminar silica (Si), interstitial sepiolite (white arrows) and calcite (white, prolate). Scale bar 20 μm .

Figure 1.14: Optical and SEM images of silica in 'sepiocrete' KNERS/4.

Table 1.3: Chemistry of selected horizons described in Table 1.1 (n/a: not analysed).

			pH	EC*	pH	EC*	HCO ₃ ⁻	Cl ⁻	SO ₄ ²⁻	Ca ²⁺	Mg ²⁺	Na ⁺	K ⁺	Si	Mg/Si	SAR [#]
			1: 2.5		Saturated paste extract *											
Silicic Duricrust: dorbank; Profile KV196T:																
/A	0-0.2 m	Orthic A	8.6	0.75	n/a	n/a	n/a	n/a	n/a	n/a	n/a	n/a	n/a	n/a	n/a	n/a
/B	0.2->0.45 m	Red apedal B	10.2	0.16	n/a	n/a	n/a	n/a	n/a	n/a	n/a	n/a	n/a	n/a	n/a	n/a
/1	±1-1.3 m	Red apedal B	10.1	0.09	9.3	0.78	6.6	2.7	0.66	0.17	0.11	5.7	0.81	0.71	0.16	15
/2	1.3-1.45 m	Dorbank	8.8	0.84	8.0	7.8	2.3	80	11	9.5	14	100	1.5	1.4	9.7	29
/3	1.45-1.6 m	Dorbank	8.7	0.03	7.8	19	0.58	223	28	25	40	174	1.9	0.67	59	31
/4	1.6-1.8 m	Calcareous dorbank	8.6	0.06	8.0	38	1.8	418	79	0.87	88	429	4.4	0.29	300	64
/5	1.8-2 m	Hardpan/Soft carbonate	8.4	0.03	8.2	7.2	2.24	45	78	60	15	51	2.2	0.75	20	8
/6	2 - ? m	Soft dorbank	8.5	0.09	n/a	n/a	n/a	n/a	n/a	n/a	n/a	n/a	n/a	n/a	n/a	n/a
/7	? - 3.5 m	Soft dorbank	9.0	1.1	8.2	9.0	3.0	90	11	6.6	8.4	123	1.8	1.3	6.5	45
/8	± 3.5-±4.5 m	Dorbank	8.5	0.02	8.0	11	0.16	56	91	25	14	96	1.4	0.42	34	22
/9	±4.5- ±6 m	Dorbank	8.2	0.06	7.7	38	1.6	478	68	53	84	588	6.1	1.5	57	71
/10	± 6- ± 10 m	Marine deposit	7.6	0.07	n/a	n/a	n/a	n/a	n/a	n/a	n/a	n/a	n/a	n/a	n/a	n/a
Sepiolitic Duricrust: 'sepiocrete'; Profile SK11:																
/A	0-0.2 m	Orthic A	9.1	0.14	8.5	1.4	7.3	8.2	1.9	5.8	2.9	16	0.94	0.55	5.3	8
/B	0.2-0.6 m	Yellow-brown apedal B	9.2	0.06	8.6	0.60	4.6	2.6	0.39	2.2	1.2	6.3	0.68	0.35	3.4	5
/C	0.6-0.65 m	Gleyed sand	9.1	0.08	8.2	0.72	3.7	4.4	0.50	1.6	1.0	8.8	1.0	0.39	2.7	8
/D	0.65-0.7 m	Neocutanic	8.7	1.3	7.9	9.4	4.1	88	4.3	3.7	6.2	78	2.3	0.60	10	35
/E	0.7- m	'Sepiocrete'	8.4	0.03	n/a	n/a	n/a	n/a	n/a	n/a	n/a	n/a	n/a	n/a	n/a	n/a
/1	0.01-0.45 m	'Sepiocrete'	8.7	0.04	n/a	n/a	n/a	n/a	n/a	n/a	n/a	n/a	n/a	n/a	n/a	n/a
/6	0.45-0.9 m	Blocky calc. sed.	9.1	0.02	n/a	n/a	n/a	n/a	n/a	n/a	n/a	n/a	n/a	n/a	n/a	n/a
/3	0.9-1.1 m	Hardpan carbonate	9.2	0.02	n/a	n/a	n/a	n/a	n/a	n/a	n/a	n/a	n/a	n/a	n/a	n/a
/9	0.9-1.1 m	Hardpan carbonate	8.8	3.6	8.0	19	0.23	290	29	21	30	177	2.7	1.3	24	35
/4	1.1-1.15 m	Neocarbonate	8.9	0.04	n/a	n/a	n/a	n/a	n/a	n/a	n/a	n/a	n/a	n/a	n/a	n/a
/4b	1.15-1.5 m	Neocarbonate	8.7	2.5	n/a	n/a	n/a	n/a	n/a	n/a	n/a	n/a	n/a	n/a	n/a	n/a
/5	0.8-1.5 m	Termite nest	8.9	2.6	n/a	n/a	n/a	n/a	n/a	n/a	n/a	n/a	n/a	n/a	n/a	n/a
/7	1.5- >2.2 m	Sedimentary	8.4	6.3	n/a	n/a	n/a	n/a	n/a	n/a	n/a	n/a	n/a	n/a	n/a	n/a

*EC: mS/cm; cations, anions: mmol/L; Si: mmol/L. # SAR: Sodium adsorption ratio $Na/((Ca + Mg)/2)^{0.5}$

a low water permeability (Table 1.1). It also provides the slow silica-saturated pore water flow rates (Summerfield, 1983b), which are needed for the shift toward equilibrium and subsequent silica precipitation.

Although most of the clay in the dorbank profile KV196T is strongly oriented and illuvial in origin, there appears to be a neoformed Mg-rich smectite in horizon KV196T/3 (Figure 1.10(f)). Borchardt (1989) noted that saponites are seldom found in soils, and appear to be inherited from the parent material. The Namaqualand coastal plain, however, is a Mg-rich environment (Table 1.3). Inglès et al. (1998) found diagenetic Mg-rich smectites in the Ebro Basin, an environment of high alkalinity, silica, magnesium and water stagnation favourable to the formation of these minerals. Hay et al. (1986) found them in the Armagosa desert, and noted that pre-existing sheet silicates such as montmorillonite can form a template for the precipitation of Mg-smectite, or it may precipitate directly from solution. Jones and Galan (1988) noted that trioctahedral smectite precipitation is favoured over sepiolite or palygorskite in an environment with the highest pH (> 9.5), a high (Mg+Fe)/Si ratio (rather than high (Mg+Si)/Al), and highest the alkali salinity.

A broken sponge spicule is evident in horizon KV196T/3 (Figure 1.15). Sponge spicules often occur in ponded or poorly drained environments (Drees et al., 1989). Although the dryness and red colour of the dorbank profile KV196T (Table 1.1) suggest a well aerated environment, Francis et al. (2007) showed how textural discontinuities in typical Aridisols in Namaqualand can subtly modify water infiltration and enhance water storage in the profile. The change from a nodular to a massive structure around 2 m depth (Table 1.1) is accompanied by an EC maximum (Table 1.3). This, together with the presence of the sponge spicule, suggests a periodically water-saturated environment, the composition of which (Table 1.3) is favourable to Mg smectite clay neoformation.

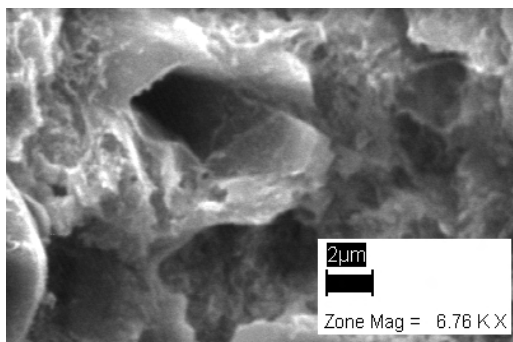


Figure 1.15: SEM: broken sponge spicule in dorbank (petroduric) fragments.

‘Sepiocrete’

Clay dispersion and migration are not as prominent as in the dorbank horizons, perhaps due to their lower SAR (Table 1.3). The pH of sepiolite-bearing horizons is consistent with Jones and Galan (1988), in that sepiolite formation is favoured over palygorskite and trioctahedral smectite in the 8-9.5 pH range.

Rodas et al. (1994) defined ‘palycrete’ as generally having more than 65 % palygorskite. It may be that when an horizon is enriched to such a degree with fibrous clay minerals they have the potential to cause a greater induration than when they occur as an accessory mineral (in calcrete for example), particularly where they display a morphology of intergrown mats and bundles of fibres (Figures 1.11(d), 1.13(b)). A possible mechanism for preferential sepiolite enrichment could be decalcification (Vanden Heuvel, 1964), since sepiolite is closely associated with calcite in Namaqualand soils (M.L. Francis, unpub. data), as in New

Mexico (Vanden Heuvel, 1964), and together with palygorskite is a common mineral in the clay fraction of calcretes (for example Netterberg, 1969; Vanden Heuvel, 1964; Singer and Norrish, 1974; Yaalon and Wieder, 1976; Elprince et al., 1979; Hay and Wiggins, 1980; Watts, 1980; Singer and Galan, 1984; Singer, 1989; Blank and Fosberg, 1991; Monger and Daugherty, 1991; Verrecchia and Le Coustumer, 1996; Singer, 2002; Neaman and Singer, 2004; Owliaie et al., 2006). Netterberg (pers. comm., 2003) suggested that some ‘sepiocrete’ may have originated as decalcified calcrete. Evidence in support of this hypothesis are the presence of calcic pendants and cappings from the KNERS profile (Table 1.2), indicating mobilisation of calcite; and in profile SK11 the calcic horizons occur below the sepiolite-rich and ‘sepiocrete’ horizons (Table 1.1), which may suggest preferential leaching of calcite to the lower part of the profile. Whether the calcite was originally present as a calcic or a petrocalcic horizon is not resolved.

In the KNERS profile it appears the amorphous silica is overlying the sepiolite fibres (Figure 1.13(c)), which suggests that sepiolite precipitated first, followed by silica. This is not so clear from Figure 1.14, where the silica seems to be associated with mineral grains. The timing and precise mechanism of silica precipitation in the ‘sepiocrete’ is difficult to resolve: in the case of KNERS, it may have occurred during the phase that formed the dorbank cutans and overlying dorbank, although there is little micromorphological evidence of illuviation into the ‘sepiocrete’, and this cannot be ubiquitously applied to all ‘sepiocrete’ containing profiles, since not all are overlain by dorbank.

Figures 1.13(c)-(d) do not clearly resolve whether sepiolite or silica precipitated first, although Figure 1.13(c) could be interpreted as the amorphous silica overlying the sepiolite fibres. The association of sepiolite and silica has been noted before: Blank and Fosberg (1991) observed sepiolite crystals radiating outward from laminae of opaline silica in duripans in Idaho, and suggested that some sepiolite forms via the addition of Mg to opal, and Hay and Wiggins (1980) observed opal replacing sepiolite (and calcite) in calcrete of the southwestern United States. A possibility may be a process similar to the pseudomorphic replacement of sepiolite by opal in deposits in the Madrid Basin, Spain (Bustillo and Alonso-Zarza, 2007), which preserved the fibrous microstructure and striated birefringence of the sepiolite. Bustillo and Bustillo (2000) suggested that silicification could occur as a function of the sepiolite precipitation, as initial precipitation of sepiolite depleted the solution in Mg. However, Table 1.3 shows

that the Mg is present in excess of the amount of Si required to form sepiolite (using an Mg/Si ratio of 0.67), and thus the Mg will not be depleted relative to Si during sepiolite precipitation (Eugster and Jones, 1979).

Several examples of etched quartz grains are present in both 'sepiocrete' profiles in SK11/1 and KNERS/4 (not shown), which suggests the localised dissolution and redistribution of silica within the profile. Boettinger and Southard (1991) argued that weathered crystalline silicates from a granitic saprolite are the main source of pedogenic silica for Aridisol pedons in the western Mojave Desert. Reheis et al. (1992) suggested that the silica released by replacement of aluminosilicates may be locally precipitated as amorphous or opaline silica and (or) incorporated into newly formed palygorskite and sepiolite.

Amorphous silica can be precipitated either by evaporative concentration, as the solution becomes increasingly supersaturated, and/or it can be precipitated by a pH change. The buffering effect of sepiolite at pH 8.6 (Martínez-Ramírez et al., 1996), as in the slaking tests, has not been quantified in soil. Since the sepiolite-containing horizons are generally also calcareous, the pH of these soils should be low enough to promote the precipitation of silica in solutions entering these horizons. The rise in pH associated with the hydrolytic exchange of Na^+ as the soils are submerged in water (McBride, 1994, p.92) may be the source of the dissolved silica. This could be compounded by the high water-holding capacity of sepiolite, removing water and thereby creating conditions of silica saturation on a local scale.

1.3.5 Classification

Dorbank (petroduric)

A silcrete was defined as having (an arbitrary) lower limit of 85 wt % SiO_2 by Summerfield (1983b), and was used by Nash and Shaw (1998) to assist in the classification of calcrete-silcrete intergrades in the Kalahari, although they noted the influence of detrital quartz and clay minerals on the value. By this definition, the dorbank has too little SiO_2 (Table 1.4) to be classified a 'silcrete'; this is consistent with the 'silcrete' and 'dorbank' morphological differences reviewed in Section 1.1.1, although both are cemented by silica. Southern African 'silcrete'

does not meet the slaking requirements of dorbank, duripan (Soil Survey Staff, 1999) or petroduric (World Reference Base, 1998) horizons. Since the dorbank horizons are clearly pedogenic (colour, texture, and parent material continuity with surface horizons, Table 1.1), and also meet the requirements of duripan and petroduric horizons (with the exception of the minimum thickness for the cutan KNERS/1), classifying them as one of these seems more appropriate than as ‘silcrete’, despite the presence of the ‘silica-cement’ which corresponds to that inherent in the term ‘sil-crete’.

Table 1.4: XRF analyses of selected duricrusts described in Table 1.1.

	Dorbank			'Sepiocrete'			Sepiolite	
	BULK ^{*1}	<2 μm ^{*2}	<2 μm ^{*3}	<2 μm ^{*4}	BULK ^{*5}	BULK ^{*6}	BULK ^{*1}	'Ideal' ^{*7}
Al₂O₃	7.37	12.2	10.6	3.74	6.87	2.22	2.44	-
CaO	0.21	4.67	2.85	2.55	13.1	13.3	1.46	-
Fe₂O₃	3.73	5.31	5.49	2.27	1.92	1.00	1.61	-
K₂O	1.33	2.20	2.32	2.02	2.32	0.71	0.62	-
MgO	0.04	4.73	4.45	21.9	9.8	14.0	6.35	24.89
MnO	0.04				0.07	0.05	0.01	-
Na₂O	0.06	2.52	1.17	0.59	1.63	1.38	0.16	-
P₂O₅	0.08	0.15	0.11	0.07	0.11	0.19	0.10	-
SiO₂	76.9	56.6	64.6	56.9	54.1	57.0	76.5	55.65
TiO₂	0.47	0.46	0.59	0.16	0.42	0.24	0.18	-
H₂O⁻					2.02	2.40		-
LOI	9.20	11.8	8.61	10.7	4.06	4.37	11.1	19.46
Total	99.4	100.8	100.8	101.0	96.4	96.8	100.5	-
molar Mg/Si				0.57	0.27	0.37	0.12	0.67

*1: Ebenhaeser, 31°35' 50"S, 18°16'45"E, road to Papendorp (Ellis, unpub. data). 2: KNERS/5, milled, Mg-saturated. 3: KV196T/2, crushed, Mg-saturated. 4: SK11/E, crushed, K-saturated. 5: SK11/1. 6: KNERS/4. 7: Stoessel (1988)

'Sepiocrete'

As the morphology and micromorphology shows, the ‘sepiocretes’ are sepiolite-cemented soil horizons (with or without accessory silica). Sepiolitic horizons do not form a diagnostic horizon in the World Reference Base (1998), Soil Taxonomy (Soil Survey Staff, 1999), or the South African system (Soil Classification Working Group, 1991). The ‘sepiocrete’ horizons do not meet the slaking requirements of dorbank/duripan/petroduric horizons. They contain less SiO₂ than typical dorbank (Table 1.4), and too little to be classified a ‘silcrete’ after Summerfield (1983b) and Nash and Shaw (1998). Both silica and sepiolite are present in

the matrix, although the degree to which silica and sepiolite dominate seems to vary even within the same horizon. It seems most probable that both contribute to the structural properties of the horizon. Nash and Shaw (1998) outlined the practical difficulties in classifying calcrete-silcrete intergrades in Botswana. They concluded that while an assessment of the matrix chemistry was the ideal, for practical purposes the end members of the calcrete-silcrete spectrum could be defined by bulk chemical analysis ('silcrete' if more than 85 % SiO_2 and 'calcrete' if more than 50% CaCO_3), and if a duricrust falls between these values, then to examine the micromorphology to identify any evidence of displacement or replacement. They acknowledged, however, the difficulty in classifying material where the material has had a complex evolutionary history, or been almost completely replaced. Thus the terms 'sil-sepiocrete' (for a sepiocrete replaced and now dominated by silica) or 'sepio-silcrete' could be employed in the sense used by Nash and Shaw (1998).

While the '-crete' terminology provides a useful expression of the cemented nature of the horizon, to fit the existing soil classification schemes the terms 'sepiolitic' and 'petrosepiolitic' (in the same sense as 'calcic' and 'petrocalcic') would be appropriate. The terms 'sepiolitic' and 'petrosepiolitic' have the advantage over the '-crete' terminology that they can be more easily be applied as adjectives to other hardpans where sepiolite is significant but not necessarily cementing, such as 'sepiolitic petrocalcic'. This is particularly relevant since sepiolite is closely associated with calcite in Namaqualand soils (M.L. Francis, unpub. data), and is a common mineral in the clay fraction of calcretes (for example Netterberg, 1969; Hay and Wiggins, 1980; Watts, 1980).

The term 'sepiolitic' should be used for horizons which: (a) contain sepiolite in amounts great enough for it to be detected by XRD in the bulk soil; (b) have peds (a fractured surface and not just the cutan) that cling strongly to the wetted tongue; and (c) cause methyl orange to turn from orange to purple-pink over most of a fragmented surface. If the horizon is in addition to the above criteria cemented to such a degree that it will slake neither in acid (so cannot be classified as petrocalcic) nor in alkali (and so cannot be classified as petroduric) then the term 'petrosepiolitic' would be appropriate. The 'sepiolitic' criteria distinguish the 'petrosepiolitic' horizon from a 'silcrete' (of Summerfield, 1983a; Partridge and Maud, 1987), a silica-cemented horizon which does not fit the definition of petroduric.

Sepiolite has an influence on the soil properties, and it is suggested that the term ‘sepiolitic’ be used where the sepiolite content is greater than an accessory phase in the clay fraction. Sepiolite is abundant in coastal Namaqualand soils (Francis et al., 2004) and palygorskite is also present (Singer et al., 1995). Neaman and Singer (2004) outlined the effects of palygorskite, including ‘palycrete’, on soil properties. Sepiolite has a high water holding capacity (Jones and Galan, 1988). When added to lime mortars, this causes a decrease in the rate of the carbonation process by provoking a decrease in the free water content in the porous system of the mortar, which impedes CO₂ dissolution, a rate-controlling step of the carbonation process (Martínez-Ramírez et al., 1995). Further work is needed to establish this effect on soils, it may be similar to the effect of evapotranspiration on calcite precipitation: Netterberg (1969) suggested the decrease in pore water pressure as a result of increased suction pressure will bring about CO₂ loss and favour calcite precipitation. Francis et al. (2007) speculated on the effect this water-holding capacity would have on plants growing in sepiolite-rich soils, and thus its effect on the ecosystem of arid regions. It has a high plasticity (Bain, 1971), which would affect the geotechnical usefulness of the soil.

1.4 Summary and conclusions

1.4.1 Dorbank (petroduric)

The low water permeability (indicated by the amount of time taken for a water drop to penetrate during field tests) of dorbank provides the slow silica-saturated pore water flow rates needed for the shift toward equilibrium and subsequent silica precipitation, and allows the deposition of strongly oriented clay. Illuviation of clay in the dorbank has been a dominant soil forming process: there is a strong orientation of clay parallel to the grains, crescent coatings on the lower part of voids, and in some cases voids are blocked by clay-coated grains. Amorphous material was observed coating some clay grains. There also appears to be a neo-formed Mg-rich smectite in horizon KV196T/3. Although the dry state and red colour of the dorbank profile suggests it is well-drained, a change to a massive structure at this depth is accompanied by an EC maximum. Together with the presence of a sponge spicule, this suggests a periodically water-saturated environment, the composition of which is favourable to Mg smectite clay neoformation.

The high pH of the upper horizons could have increased the solubility and mobility of silica, and the sodic environment have contributed to clay dispersion and rise in pH due to the hydrolytic exchange of Na^+ . Under the low rainfall conditions, the soluble silica will not leach through the profile but accumulate in the subsoil. The abundance of illuviated clay in the pore spaces may have provided a large adsorption area for silica, since the silica is generally (although not exclusively) concentrated on the void side of the clay coatings.

1.4.2 ‘Sepiocrete’

The micromorphology of typical ‘sepiocrete’ is distinctly different from dorbank horizons, the most obvious being the granular microstructure, the micrite-rich matrix, and the lack of crescent clay coatings. It is sometimes difficult to distinguish sepiolite from silica with certainty under the optical microscope, given the low birefringence of sepiolite. Sepiolite appears to form the matrix areas, whereas the silica is localised. The interlocking, subparallel morphology of sepiolite over much of the sample may contribute to the induration.

In contrast to the dorbank samples which slaked in NaOH even if calcareous, neither HCl nor NaOH treatments resulted in slaking of the ‘sepiocrete’ samples. Partial slaking was observed when alkali/acid treatments were alternated. This may suggest that the cement in ‘sepiocrete’ is not solely amorphous silica, or that the presence of sepiolite could have cause a reduction in pH sufficient to reduce the solubility of silica. A weathering profile silcrete also did not slake in concentrated NaOH under the same experimental conditions, which suggests that in addition to sepiolite content, the degree of silica polymerisation and/or impregnation and/or total amount of secondary silica also plays a role in dictating whether slaking of a particular sample will occur. The ‘sepiocrete’ horizons therefore do not meet the slaking requirements of dorbank/duripan/petroduric horizons. They contain less SiO_2 than typical dorbank, and too little to be classified a ‘silcrete’. Both silica and sepiolite are present in the matrix, although the degree to which silica and sepiolite dominate seems to vary even within same horizon. It seems most probable that both sepiolite and silica contribute to the structural properties of the horizon.

The amorphous silica appears in some places to be overlying the sepiolite fibres which suggests that sepiolite precipitated first. In other areas the silica seems to be associated with mineral grains. The timing and precise mechanism of silica precipitation in the ‘sepiocrete’ is difficult to resolve. It seems unlikely that silica precipitation was caused by the initial precipitation of sepiolite depleting the solution in Mg, since Mg is present in excess of the amount of silica required to form sepiolite (using an Mg/Si ratio of 0.67), and thus will not be depleted first during sepiolite precipitation. Etched quartz grains in both ‘sepiocrete’ profiles suggests the local dissolution and redistribution of silica within the profile, perhaps prompted by a (local) rise in pH due to the hydrolytic exchange of Na^+ .

Clay dispersion and migration are not as prominent as in the dorbank horizons, possibly a function of their differing profile chemistry. The pH of sepiolite-bearing horizons is consistent with that for sepiolite formation. The calcic pendants and cappings in the ‘sepiocrete’ from the KNERS profile indicate the mobilisation of calcite, and suggest the profile has a complex evolutionary history. It could be that the ‘sepiocrete’ resulted from the (partial) silicification of what was originally a sepiolite-rich calcic/petrocalcic horizon. In profile SK11 the calcic horizons occur below the sepiolite-rich and ‘sepiocrete’ horizons, suggesting leaching of calcite to the lower part of the profile, but the horizon no longer fits into a “calcrete” category, and can neither be classified as a dorbank/duripan/petroduric, nor a silcrete horizon.

Given the physical properties of sepiolite, and its effect on physical properties of a soil, its presence should be recorded during soil classification. The term ‘sepiolitic’ should be used for horizons which: contain sepiolite in amounts great enough for it to be detected by XRD in the bulk soil, peds (a fractured surface and not just the cutan) cling strongly to the wetted tongue, and methyl orange turns from orange to purple-pink over most of a fragmented surface. If the horizon is in addition to the above criteria cemented to such a degree that it will slake neither in acid (so cannot be classified as petrocalcic) nor in alkali (and so cannot be classified as petroduric) then the term ‘petrosepiolitic’ would be appropriate. The ‘sepiolitic’ criteria distinguish the ‘petrosepiolitic’ horizon from a ‘silcrete’, a silica-cemented horizon which does not fit slaking requirements of a petroduric horizon.

Chapter 2

Soil formation in sediments of the Namaqualand coastal plain

2.1 Introduction

There has been a surge of interest in arid regions, particularly their biodiversity and ecology. Namaqualand itself has been the focus of much research recently, ranging from publications such as Cowling and Pierce (1999) to a Special Issue of the *Journal of Arid Environments*. Although there is eighty or so years of sedimentological and paleontological research that has been conducted in the diamond mining areas along the west coast of southern Africa (Pickford and Senut (2000) and Pether et al. (2000), for example), there is very little information available on the soils. This is becoming increasingly relevant since mining activities in Namaqualand result in large ‘overburden dumps’, formed by the inversion and mixing of the usual regolith profile (commonly tens of metres deep). Soil forming processes have begun anew on the surfaces of these dumps, as previously deep and inaccessible layers of the regolith are now becoming important for land use. This has prompted further studies (including Schmidt, 2002; Mahood, 2003; Blood, 2006; Ndeinoma, 2006), in particular the work of Prinsloo (2005). More details on the effects of the mining processes on the soils and vegetation, and the challenges of the rehabilitation processes are given by Carrick and Krüger (2007).

Information on coastal Namaqualand soils is mostly limited to Land Type Surveys (Land Type Survey Staff, 1987) and unpublished studies done for mining companies, focused on the saline-sodic nature of the soils and the associated rehabilitation difficulties, irrigation reports, and part of a study of Karoo soils by Ellis (1988). An exception is a study by Singer et al. (1995) that detected the fibrous clay minerals sepiolite and palygorskite in the clay fraction. Recently, Francis et al. (2007) summarised the available information and key characteristics of Namaqualand soils, and Chapter 1 described silica- and sepiolite-cemented horizons in Namaqualand.

The aim of this Chapter is to describe and characterise the general soil forming features within a regolith similar to that described by Pether (1994), from the northern part of the Namaqualand coastal plain (Alexander Bay Formation (SACS, 1980)). The mining excavations tens of metres deep down to bedrock have provided an opportunity to examine soil formation in a regolith that has been subaerially exposed in some parts for much of the Neogene.

Conventionally soil pits are dug and described in South Africa to a depth of about 1.5m, below which the importance of a soil for most agricultural purposes diminishes sharply (Soil Classification Working Group, 1991). However, Fey et al. (2002) suggested that the characterisation of the entire regolith before disturbance, assists in understanding the new pedogenic processes forming on the surfaces of mining dumps. Stone and Comerford (1994) reviewed biological activity far below the 1.5m soil depth; and Moody and Graham (1994), in deep sands on a marine terrace in California, argued that there is a zone of active pedogenesis in the basal unit of the regolith just above the bedrock, expressed by illuviation and precipitation of clays, iron oxides and silica. Excavations of the regolith to bedrock during mining on the Namaqualand coastal plain provided many excellent exposures of these processes, both near-surface and deeper in the regolith. Studying the deeper layers of the regolith have helped to distinguish paleosols (Nettleton et al., 2000), which have served as the 'record keepers' of the changing conditions at the soil surface.

2.2 Site description

Sampling was done in two of the mining areas belonging to De Beers Consolidated Mines Ltd - Namaqualand Mines. These are the Buffels Marine Complex (BMC) in the Kleinzee-Port Nolloth area, and the Koingnaas Complex (KNC) further south in the Koingnaas-Hondeklip Bay area (Figure 2.1).

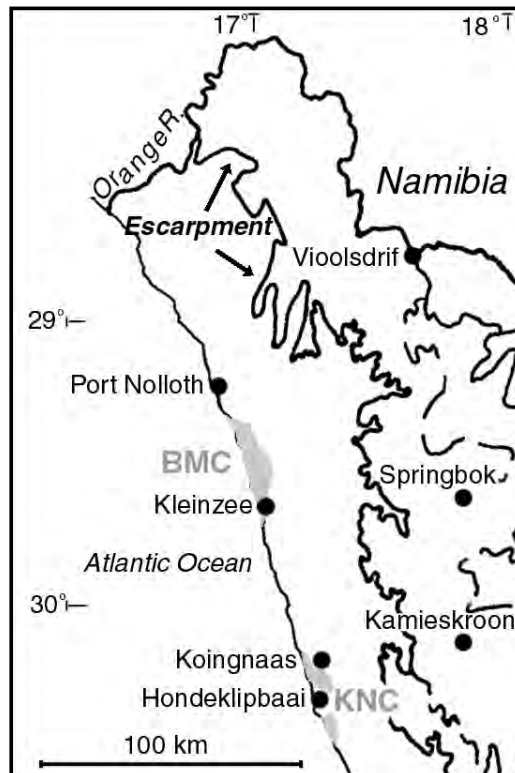


Figure 2.1: Location of field area (grey). BMC: Buffels Marine Complex; KNC: Koingnaas Complex. The escarpment forms the eastern edge of the coastal plain. Modified from Ellis (1988).

2.2.1 Climate

The key influences of climate in soil formation are moisture and temperature. Temperature affects the rate of chemical reactions in the decomposition and synthesis of minerals and in biological processes (White, 1979).

Temperature

In Namaqualand, the prevailing winds are very strong southerly (occasionally gale force), with occasional berg (east) wind conditions, especially during winter. Temperatures increase markedly during berg wind conditions, which may persist for longer than a week. As a result, the average maximum temperature from February to October (late summer to spring) is over 30° C, with April and October experiencing temperatures of 38° C. In contrast, the average maximum temperature from November to January is 25° C (late spring to summer). Minimum temperatures from March to October are around 6° C, with July dropping to 3° C. From November to April the minimum is around 10° C (D.B.C.M., 2000, data collected at Kleinsee, July 1995 to March 1997).

Moisture

White (1979) noted that the effectiveness of moisture in soil forming processes is dependent on i) rainfall (the intensity, duration and seasonal distribution), ii) the evaporation rate from the surface and from within the soil, iii) the topography of the land surface, and iv) the soil and rock mass permeability.

Rainfall

The Namaqualand coastal plain receives less than 150 mm winter rainfall annually, with the figure increasing southwards. Crucially for both plant growth and water movement through the soil, the climate is characterised by highly reliable rainfall when compared to other arid regions with similar mean annual precipitation (Desmet, 2007). It typically arrives as widespread, gentle showers (average rainfall event 6 mm, P. Carrick unpublished data, cited by Desmet (2007)). Drought conditions are rare, and rainfall is higher than average about once every 10 years, causing ephemeral rivers to flow. Flood events occurred in the Buffels River, for example, in 1945, 1961, 1962, 1963, 1976, 1980, 1986, 1996 and 1997 (D.B.C.M., 2000). Coastal fog adds significantly to the total precipitation. It can be observed to extend inland to the rise of the escarpment, occurs frequently along the coastal plain at elevations below the 200 m contour line (Olivier, 2002). Data from the Pilot Fog Study at Kleinsee for the

period July to October 1995 showed that the highest precipitation due to fog occurred during August. The total fog recorded during this period was 1001 mm (D.B.C.M., 2000). Tinely (1985; in D.B.C.M., 2000) estimated that the plants may trap up to 300 mm of fog per annum.

Paleoclimates of the northern Namaqualand region are not that well constrained, but the consensus for the greater area seems to be that it was wetter during the Last Glacial (Van Zinderen Bakker, 1976; Tankard and Rogers, 1978; Parkington et al., 2000).

Evaporation

That evapotranspiration greatly exceeds precipitation in Namaqualand is reflected by a vegetation cover (Sandveld bioregion (Desmet, 2007)) of approximately 60%, as well as the presence of saline pans and ephemeral rivers, and areas with salt efflorescence and crusts at the soil surface. The evaporation rate is of the order of 2 m per year. The evaporation rate is higher than expected for a coastal area due to the wind regime, but is reduced by the regular occurrence of coastal fog (D.B.C.M., 2000).

Topography

The coastal plain is a flat to very gently undulating pediplain truncated by the Great Escarpment (approximately 1500 m a.m.s.l.). There is a small escarpment on the eastern edge of the mining area, with a maximum altitude of 213 m a.m.s.l. There are two rivers in the BMC: the Buffels River with subsurface flow (Heineken, 1981) which forms the southern border of the BMC; and the ephemeral Kwakanaab River, which ends in the Dreyer's Pan area. Dreyer's Pan is one of the large saline pans in the BMC, others are Bloupan, Karaspan, and Soutpan. The ephemeral Swartlintjies River runs through the KNC. The locations of these features are shown in Figure 2.2.

Microrelief

'*Heuweltjies*' (hillocks) occur throughout Namaqualand and along the western

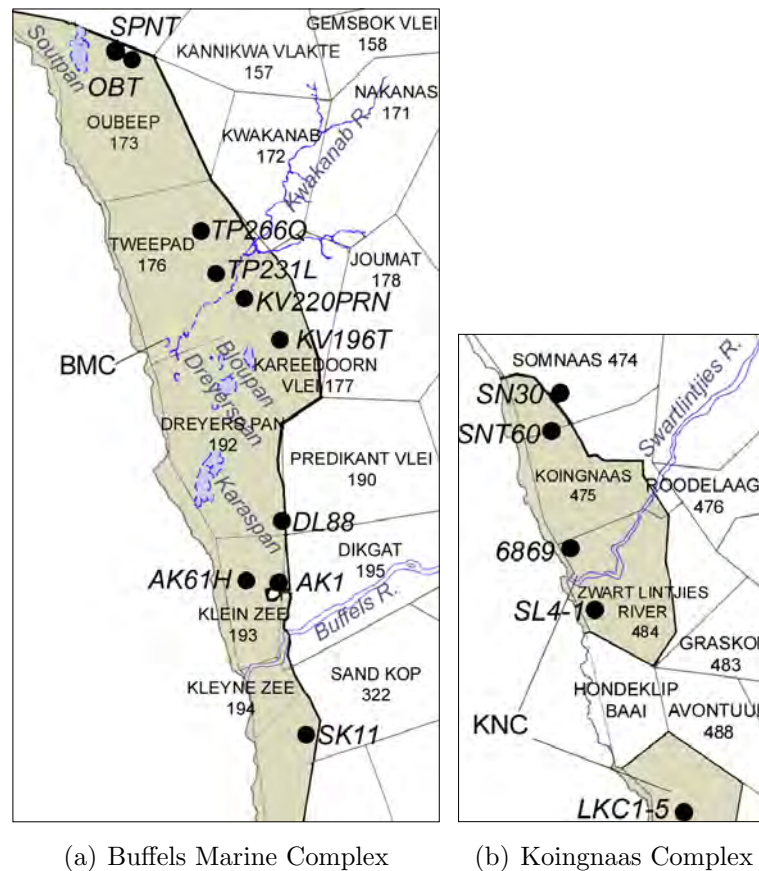


Figure 2.2: Figure 2.1 magnified to show location of sample sites (circles) within Buffels Marine Complex (BMC) and Koingnaas Complex (KNC) at De Beers Namaqualand Mines. Farm boundaries and position of rivers and pans indicated.

and southern Cape coasts (Picker et al., 2007). They are distinguishable in the field and on aerial photographs as circular features (diameter usually 10 - 20 m) showing a different vegetation pattern and a slightly raised (1 - 2.5 m) surface, and they cover most of the field area. They are thought to be termitaria of the harvester termite *Microhodotermes viator* (Moore and Picker, 1991), with debated contribution from mole rats (Lovegrove and Siegfried, 1986; Cox et al., 1987; Lovegrove and Siegfried, 1989; Laurie, 2002; Midgley and Hoffman, 1991) and/or another species of grassland termite in older (30 000 years B.P.) heuweltjies (Midgley et al., 2002) such as *Hodotermes mossambicus* (Moore and Picker, 1991).

Soils within the heuweltjie generally tend to be more alkaline (sodic and calcareous) and enriched with silica (including silica- and calcite-cemented lenses) than intervening soil (Ellis, 2002). This suggests they are drier than the intermound area and is consistent with their raised topography (Francis et al., 2007).

Soil Permeability

Hydrophobicity and crusting at the surface of Namaqualand soils is common. These phenomena affect the soil water balance by enhancing preferential flow (Francis et al., 2007). Soil permeability is also affected by the presence of textural barriers and cemented horizons at depth, strongly influencing subsurface water storage and its provision to plants (Francis et al., 2007).

2.2.2 Regolith

The regolith pertaining to this study comprises successive late Tertiary marine packages, each deposited during sea-level regression (Pether, 1994). Some rest on kaolinized paleochannel sediments, described in detail by Pether (1994), who concluded that they were laid down as a quartzo-feldspathic sediment in a fluvial environment, and subsequently deeply weathered, with extensive alteration of feldspar to kaolinite. These sediments are described in greater detail by Tankard (1966), Tankard (1975), Pether (1994), and Pether et al. (2000). De Villiers and Cadman (2001) favoured an early Tertiary age for the kaolinized paleochannel north of the Swartlintjies River, although it may also contain reworked Cretaceous material (Pether et al., 2000; De Villiers and Cadman, 2001).

The marine packages are arranged *en echelon* down the bedrock gradient, from oldest and highest inland to youngest and lowest at the coast. Each package is named after the elevation of its transgressive maximum as represented in the Hondeklip Bay area (Pether, 1994; Pether et al., 2000). The 90 m package is ca. 18 - 16 Ma, the 50 m package early Pliocene, and the 30 m package not well constrained, but ca. 3.3 Ma or younger (Pether et al., 2000). The 30 m package is transgressed by younger littoral deposits up to about 10 m a.m.s.l. (Pether et al., 2000). The sand fraction is dominated by quartz and feldspar, lesser glauconite and phosphatic shell fragments, and variable amounts of heavy minerals (garnet, magnetite, ilmenite, biotite, sphene, amphibole, epidote, kyanite (rare) and zircon (rare)) (Pether, 1994). The marine packages are capped by recent aeolian deposits. Coastal dunefields originate at the mouth of the rivers and extend inland in a northerly direction. In places, older soil profiles are overlain by aeolian sands. Soil formation has taken place in aeolian, 'sheetwash', and marine-deposited sediments.

2.2.3 Bedrock geology and morphology

The bedrock geology in the vicinity of Kleinzee (Buffels Marine Complex, Figure 2.1) consists of Stinkfontein Formation (Gariep Belt) metasediments, mainly quartzite, phyllite, schist, arkose and minor intercalated volcanics. Amphibolite bands, quartz veins and small pegmatite intrusions are fairly common (Hartnady and Von Veh, 1990; Rogers et al., 1990). Bedrock morphology is characterised by a number of emergent wave-cut terraces (Rogers et al., 1990), on top of which are the marine sediments. The oldest cliff-line is at 95 m a.m.s.l., cut into silcrete-capped, deeply kaolinised bedrock ‘pallid zone’ (Partridge and Maud, 1987).

The Koingnaas Complex (KNC) near Hondeklip Bay (Figure 2.1) consists of Namaqua Basement gneiss and granite-gneiss. The absence of linear terraces in the KNC is attributed to the complex bedrock morphology of the Basement gneiss (Rogers et al., 1990). Palaeochannels have incised the local bedrock, and are filled with kaolinized fluvial sediment (Pether, 1994). Silcrete and the ‘pallid zone’ sediments also occur in the Hondeklip-Koingnaas region. Pether (1994) found the silcretes near Hondeklip Bay to be petrographically and geochemically similar to the high-TiO₂ weathering profile silcretes of Summerfield (1983c), which have been interpreted as markers of the ‘African Surface’ by Partridge and Maud (1987; 2000).

2.3 Methods

Fieldwork took place in February 2002. Fifteen profiles to bedrock were examined and sampled from south of Hondeklip Bay to north of Kleinzee (details of the dorbank (petroduric) profile KV196T are presented in Chapter 1). The sample sites are shown in Figure 2.2. Samples were named according to the mining excavation to which they were closest, the prefix being the farm name. Sample sites were selected to be representative of each terrace and marine package. These are the 50 m and 30 m packages in the Koingnaas area, and the 30 m, 50 m, 65 m and 90 m terraces in the Kleinzee area. Samples (approximately 2 kg) of each horizon were taken from the sidewalls of the mining excavations to bedrock, and from soil pits dug in the undisturbed areas nearby. The soil morphology was described in the field. A 10% solution of HCl was used to test for carbonate, and

30% H_2O_2 for manganese. Colour was described using a Munsell colour chart (Munsell Color Company, 1975). Root content was estimated visually. Horizons falling within 1.5 m of the surface were treated as diagnostic horizons for classification purposes. Those occurring deeper in the profile were described, but treated as non-diagnostic and no consideration given to their position in the profile for classification purposes. Eluvial, bleached horizons occurring in non-diagnostic positions were referred to as ‘gleyed sand’, cemented carbonate horizons were referred to as ‘hardpan carbonate’ when in the diagnostic position, otherwise as ‘calcrete’. Terrain units were described according to the definition in Soil Classification Working Group (1991). Most of the profiles fall into the ‘footslope’ or ‘valley bottom’ units, which in this landscape is the coastal pediplain. Horizons were assigned to either aeolian, upper shoreface or lower shoreface facies parent material. Near-surface aeolian facies were further subdivided where there was a prominent lithological discontinuity. Fluvial material may have been present, but field evidence was not definitive.

Munsell colours were manipulated to arrive at a single value that expressed the redness of each sample for easy comparison. A redness rating (R_r) was selected from Alexander (1985) and Arduino (1985):

$$R_r = (K - H)CV^{-1} \quad (2.1)$$

with K set to 25 (Arduino, 1985), C the Munsell chroma, and V the Munsell value. H is the hue index (Munsell Color Company, 1975) obtained by adding 0 to the number preceding R , 10 to that preceding YR and 20 to that preceding Y in the Munsell colour notation. With K set to 25, all samples redder than 5Y have a redness rating greater than zero.

All samples (i.e. each horizon in every profile) were air-dried, crushed, passed through a 2 mm sieve and weighed. The >2 mm cement was sorted from the >2 mm pebbles and recrushed, to minimise shattering of pebbles/gravel. The <2 mm fraction was used for chemical analyses. The pH (in water) and electrical conductivity (EC) were measured in a 20 g to 50 mL soil-water mixture. Thirty percent H_2O_2 was used to oxidise selected marine sands (6 samples), to check whether alternating colour layers within the unit were a result of oxidation. The uppermost horizon of eleven profiles was selected for organic carbon and nitrogen analysis, milled to a fine powder and analysed in a Eurovector Elemental Anal-

yser. Slaking tests were devised to distinguish silica- from carbonate-cemented hardpan horizons. These tests were based on the WRB (1998) definition of petroduric, petrocalcic and fragic horizons. Each sample was submerged in water, 5M HCl or 6M NaOH and gently heated on a waterbath for four days. Samples which did not slake were then subjected to alternating 5M HCl and 6M NaOH treatments until slaking occurred.

2.4 Results and discussion

Depositional processes on the Namaqualand coastal plain have resulted in the sediment being arranged in horizontal strata.

“The most fundamental and, possibly, the only real difference between soil and other unconsolidated geological material is that, in the case of soils, the materials have been organized by natural, non-depositional processes into horizons.” (van der Eyk et al., 1969, p43)

In some cases the sedimentary features have been completely obscured by pedogenesis, and it was difficult to determine in the field whether the horizontal layers were depositional or pedogenic in origin.

The regolith characteristics are discussed below from the surface to bedrock. A generalized regolith profile is shown in Figure 2.3. This is for a calcareous soil profile. All the horizon sequence permutations and their descriptions are in Table 2.1. The location, composition, cement, and genesis of profiles SK11 (petrosepiolitic) and KV196T (petroduric, dorbank) in the BMC (Figure 2.2) are discussed in Chapter 1. Profile photographs are presented in Appendix A.

Unpublished reports on rehabilitation difficulties at De Beers Namaqualand Mines have noted the highly saline-sodic nature of the base of the soil profiles, compared to the upper horizons and suggested this was caused by the gradual leaching of salts through the regolith over time (Roux and Odendaal, 1992; Scott and Johnston, 1994; Scott et al., 1995). This was mostly based on a studies of the disturbed “overburden dumps” which form a regolith pile that is inverted from its usual horizon sequence (i.e. deepest layers on top). Table 2.1 shows this to be generally true (AK1, AK61H), but also that the individual horizon charac-

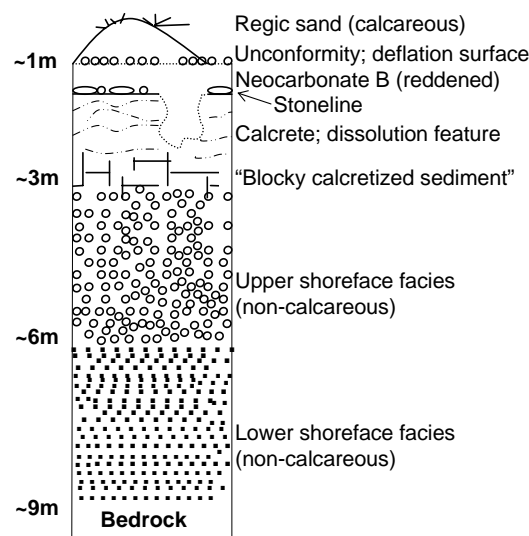


Figure 2.3: Sketch of generalized regolith profile

teristics are more important than absolute depth in determining the EC. The dorbank, calcrete and clay-rich horizons show elevated EC values relative to the horizons above and below. This gives an EC rise, usually around the middle of the profile, where these horizons occur in the profile (KV220PRN, LCK1-5, SN30, SNT60, TP231L, TP266Q).

2.4.1 A horizons

Where the regic sands are less than 500 mm thick and lie over a classifiable buried soil, this soil has been classified. Where the regic sand is more than 0.5 m deep, it has been classified as the Namib soil form (Soil Classification Working Group, 1991).

Soil profiles commonly have a crust on the surface, up to 3 mm thick. The crust appears to consist of an algal mat and deflocculated clay particles cementing the upper part of the A horizon. These were described by Francis et al. (2007). A horizons are darkened by organic matter, which also imparts a strongly hydrophobic character to the horizon, some taking in excess of 20 seconds for a drop of water to penetrate (Table 2.1). Orthic A horizons are present at the surface where there are no regic sands, and are redder and darker than the regic sands, and are generally 0.2 to 0.3 m thick. Some show evidence of a bleaching in the A horizon (DL88, Table 2.1), a feature noted to occur commonly in South African arid soils (Ellis, 1988).

Table 2.1: Profile descriptions (Soil Classification Working Group, 1991). Roman numerals indicate different sedimentary units. Profiles pictured in Appendix A. Abbreviations: ang.-angular; c.-coarse; calc.-calcareous; cont.-continuous; diam.-diameter; disc.-discontinuity; f.-fine; lith.-lithological; med.-medium; mod.-moderate; occ.-occasional; qtz-quartz; pris.-prismatic; sed.-sediment; sec.-seconds; sl.-slight; v.-very; ' - 'not analysed' except for texture and consistency: not applicable.

Depth (m)	Horizon	Facies	Moist-ure	Munsell	Field Texture	>2 mm-Fragments	Structure	Dry	Moist	Wet	Consistency	React HCl	HCl Slaking (5=full)	H ₂ O Cementation	Water absorption	Roots	Transition	Other Features	pH	EC mS/cm
6869: Prieska Form (Orthic A - Neocarbonate B - Hardpan carbonate). KMC, 30 metre package, 41m AMSI (GFS). Terrain unit: foats/lope.																				
/I	0- A1	Regic sand (Orthic A)	Dry	10YR 10/1	Med. sand	Not detected	Apedal	Loose	Loose	Non-sticky	None	-	-	None	1s	Common	Abrupt, smooth, lith. disc.	Common, v. f. macropores	8.6	1.1
/II	0.45- A2	Aeolian deflation	Dry	10YR 10/1	Med. sand	Few, rounded gravel	Apedal	Loose	Loose	Non-sticky	None	-	-	None	1s	Common	Abrupt, smooth, lith. disc.		9.8	-
/III	0.5- II B1	Neocarbonate B	V. sl. moist	10YR 10/1	Med. sand	None	Apedal	Loose	Loose	v. sl. sticky	None	-	-	None	1s	Common	Abrupt, wavy		9.2	-
/IV	0.6- II B2	Neocarbonate B over hardpan carbonate	Moist	10YR 10/1	Loamy sand	Rounded discoid cobbles (stonelike)	Weak c. subang. blocky hard	Sl. firm	Sl. firm	Plastic, sl. sticky	None	-	-	Sl. vesicular, carbonate	2s	Common	Abrupt, wavy, stonelike	C. distinct mottles, 7.5YR 6/8 dry, 10YR 5/6 moist; few clay, carbonate outcans	8.8	8.8
6869: New profile, mining excavation, upper material removed. Ashdam Form (Orthic A - Yellow-brown apedal B - Hardpan carbonate).																				
/I	0- A1	Yellow-brown apedal B	Dry	10YR 10/1	Loamy sand	V. few, c. gravel	Weak to med. c. ang. blocky hard	Loose	Loose	Sl. sticky	None	-	-	None	3s	Few	Abrupt, smooth	Common, v. f. macropores	8.6	1.1
/II	0.32- II C1	Hardpan carbonate	Dry	white	Loamy c. sand	Many, rounded gravel	Mod.-strong ang. blocky v. hard	Loose	Loose	Non-sticky	None	-	-	Mod. laminar-blocky calcite	3s	Not detected	Diffuse, tonguing		9.1	0.45
/III	0.5- II C2	Marine deposit	Dry	7.5YR 7.5/1	C. sand	Many, rounded gravel	Apedal	Loose	Loose	Non-sticky	None	-	-	None	1s	Not detected	Abrupt, smooth		8.1	0.11
6m-9m unit consists of alternate coarser, redder & finer, yellowish-brown layers. A coarser layer (I) is paler & richer in clay (II). Lowest finer olive yellow layer (7) contains thin iron pan ~3mm thick (7a). Numerous vertical termite burrows.																				
/I	6-9 V C3	Marine deposit	Dry	2.5Y 10/1	Med. sand	V. few gravel	Apedal	Loose	Loose	Non-sticky	None	-	-	None	1s	Not detected	Abrupt, smooth	Common, f., prominent black mottles	7.7	0.15
/II	6-9 V C3	Marine deposit + iron pan	Dry	10YR 10/1	Med. sand	Not detected	Apedal	Loose	Loose	Non-sticky	None	-	-	None	1s	Not detected	Abrupt, smooth		8.0	0.52
/III	6-9 V C3	Marine deposit	Dry	5YR 2.5/1	C. sand	Many, c. gravel	Apedal	Loose	Loose	Non-sticky	None	-	-	None	1s	Not detected	Abrupt, smooth		9.2	0.05
/IV	6-9 V C3	Marine deposit	Dry	5YR 4/6	Loamy c. sand	Many, c. gravel	Apedal	Loose	Loose	Non-sticky	None	-	-	None	1s	Not detected	Abrupt, smooth		7.8	0.37
9-18m more homogeneous texture & colour than 6m-9m. Textural layering not associated with prominent colour contrast. Iron pan ~3mm thick (12) runs horizontally between overlying coarse (13) & underlying fine layer (11). Abun. vertical termite burrows (10).																				
/I	9-18 VI C4	Marine deposit	Dry	10YR 10/1	C. sand	Not detected	Apedal	Loose	Loose	v. sl. sticky	None	-	-	None	1s	Not detected	Abrupt, smooth		7.9	0.05
/II	9-18 VI C4	Marine deposit	Dry	10YR 10/1	Med. sand	Not detected	Apedal	Loose	Loose	Non-sticky	None	-	-	None	1s	Not detected	Abrupt, smooth		8.8	0.05
/III	9-18 VI C4	Marine deposit	Dry	10YR 10/1	Med. sand	Not detected	Apedal	Loose	Loose	Non-sticky	None	-	-	None	1s	Not detected	Abrupt, smooth		8.8	0.05
/IV	9-18 VI C4	Marine deposit	Dry	10YR 7.5/1	C. sand	Not detected	Apedal	Loose	Loose	Non-sticky	None	-	-	None	1.5s	Not detected	Abrupt, smooth	Non-calc. shell fragment in iron pan	8.6	0.06
Clay samples not collected in situ. Occ. roots. Two types of channel clay distinguished: coarse channel clay (6869CCa), fine channel clay (6869CCb). There is water dripping out of the clay at approx. 2-3m above the bedrock (~30m deep).																				
/I	18-36 V C5	Gleyed clay (kaolinite)	Wet	5Y 2.5/1	Sandy clay	Not detected	C. ang. blocky	Hard	able	sticky	Plastic, v. sticky	-	-	None	3s	Not detected	Occ. Roots		8.9	0.42
/II	18-36 V C5	Gleyed clay (kaolinite)	Wet	10YR 7/1	Clay	Not detected	C. ang. blocky v. hard	Hard	Firm	Plastic, v. sticky	None	-	-	None	3s	Not detected	Slickensides; adheres to wetted tongue; occ. roots		8.6	0.55
AK1 (Trig): Oakleaf Form (Orthic A - Neocutanic B - Unspecified). Trig beacon near AK1. BMC, 90m terrace, near pallid zone, 118m AMSI (GFS). Terrain unit: crest.																				
/I	0- A1	Orthic A, bio crust	Dry	7.5YR 7.5/1	Loamy sand	Not detected	Loose	Loose	Loose	Sl. plastic, non-sticky	None	-	-	None	6s	Common	Clear, wavy	Biological crust	8.9	1.4
/II	0.05- A2	Orthic A	Dry	7.5YR 7.5/1	Loamy sand	Not detected	Mod. blocky	Loose	Loose	Sl. plastic, non-sticky	None	-	-	None	4s	Common	Clear, wavy		8.4	1.5
/III	0.3- B	Neocarbonate B	Dry	7.5YR 7.5/1	Loamy sand	Not detected	Weak med. blocky	Loose	Loose	Non-sticky	None	-	-	None	3s	Not detected	Abrupt, wavy, to bedrock		8.1	1.9
AK1: Mining excavation, upper material removed. Trawel Form (Orthic A - Neocarbonate B - Dorbank). Terrain unit: crest.																				
/I	0- II B	Neocarbonate B	Obscured	Dry	7.5YR 7.5/1	Loamy sand	Not detected	Soft	Loose	Sl. plastic, sl. sticky	None	-	-	None	3s	Few	Abrupt, smooth		8.9	3.5
/II	0.3- III C1	Calc. dorbank	Obscured	Dry	10YR 7.5/1	Loamy sand	Mod. blocky	Hard-Firm	Loose	Sl. plastic, non-sticky	None	-	-	Mod. carbonate, Si	5s	V. occ. ?	Gradual, smooth	Localised calcareate dissolution; tunnels	8.6	8.9
/III	0.45- III C2	Soft dorbank	Obscured	Dry	7.5YR 5YR	Loamy sand	Laminar	Firm	Firm	Non-sticky	None	-	-	Si, Si	6s	Not detected	Clear, wavy	White spots (gypsum ?)	8.8	4.9
/IV	0.6- III C2	Dorbank	Obscured	Dry	7.5YR 5YR	Loamy sand	Massive	Firm	Firm	Non-sticky	None	-	-	Mod. cont. Si	6s	Not detected	Abrupt, smooth	Tunnels	9.0	4.1
/V	1.2- III C2	Dorbank	Obscured	Dry	7.5YR 7.5/1	Loamy sand	Massive	Firm	Firm	Non-sticky	None	-	-	Mod. cont. Si	8s	Not detected	Clear, wavy	White spots (gypsum?); Mn spots	8.7	4.5
/VI	1.6- III C3	Calc. dorbank	Obscured	Dry	7.5YR 7.5/1	Loamy sand	Massive	Firm	Firm	Non-sticky	None	-	-	Mod. cont. Si, carbonate	8s	Not detected	Clear, wavy	White spots (gypsum?); Mn spots	8.7	6.7
/VII	2-2.3	30cm diam. calc. nest in dorbank	Obscured	10YR 8/2	Loamy sand	Not detected	V. hard v. hard	Firm	Firm	Non-sticky, non-plastic	None	-	-	Strong cont. Si, carbonate	-	Not detected	Clear, wavy	Occ. Mn	8.7	6.7

Table 2.1: Continued.

Depth (m)	Horizon	Facies	Moist-ure	Munsell	Field Texture	>2 mm-Fragments	Structure	Dry Moist	Consistence	Wet	React HCl	HCl NaOH	H ₂ O	Cementation	Water absorption	Roots	Transition	Other Features	pH	EC mS/cm
AK1: New profile below truncated IIB (like AK1/1). Mining excavation, upper material removed. Terrain unit crest.																				
/8	0.3- III C1	Dorbank	Obscured	Dry 7.5YR 7.5YR 6/4 4/4	Med. to f. sand	Not detected	Massive	V. hard V. firm	Non-sticky, non-plastic	None	0	3	-	Cont. Si	10s	Not detected	Abrupt, smooth (darker fissure)		8.1	1.1
/9	0.9- III C1	Dorbank	Obscured	Dry 7.5YR 5YR 5/4 4/4	Med. to f. sand	Few Fe-concretions	Massive	V. hard V. firm	Non-sticky, non-plastic	None	0	3	-	Cont. Si	>10s	Few	Clear, wavy		8.5	1.8
/10	1.5- III C2	Dorbank	Obscured	Dry 7.5YR 7.5YR 6/4 4/4	Med. to f. sand	-	Vesicular	Sl. Fri-able	Non-sticky, non-plastic	Si, loc.	0	1	-	Cont. Si, carbonate	>10s	Few		White spots (gypsum?)	8.7	3.1
/11	1.8- III C3	V. soft dorbank?	Obscured	Dry 10YR 7.5YR 6/6 5/4	Med. to f. sand	-		Sl. Fri-able	Non-sticky, non-plastic	None	-	-	-	Si?	5s	Not detected		Tunnels	7.7	2.3
AK61H: Coege Form (Orthic A - Hardpan carbonate). BMC, 30m terrace, 28m amsl (GPS). Terrain unit: footslope.																				
/4	0- A	Orthic A	Aeolian	Dry 10YR 10YR 6/3 4/3	Med. to f. sand	Not detected	Apedal	Loose	Non-plastic, non-sticky	Mod.	-	-	-	None	>10s (hyd.)	Common	Abrupt, smooth	Biological crust.	8.5	0.45
/1	0.35- II C1	Hardpan carbonate	Obscured	Dry 10YR 10YR 8/1 6/3	Med. to f. sand	-	Laminar-blocky	Loose- v. hard	Non-sticky, non-plastic	Strong	4	0-1	-	Cont. mod. carbonate	3s	Few	Clear smooth	Mn present, well-developed pseudoc-antline	8.6	4.9
/2	1.05- II C3	Blocky calc-realized sediment	Marine	Dry 7.5YR 7.5YR 6/4 5/4	Med. to f. sand	Not detected	Strong c., ang. blocky	Sl. Loose	Non-plastic, non-sticky	Cutan	-	-	-	Discont. carbonate	2s	Not detected	Clear smooth	Carbonate cutans	8.3	6.0
/3	1.55- II C4	Marine deposit	Marine	Dry 10YR 10YR 6/4 5/4	Med. to f. sand	Not detected	Strong, med. blocky	Sl. Fri-able	Non-sticky, non-plastic	None	-	-	-	None	3s	Not detected	Abrupt, wavy, bedrock	Salt efflorescence on sidewall of mine excavation; salty taste	8.0	12
DL88: Augrabies Form (Orthic A - Neocarbonate B). BMC, 65m terrace, 134m amsl (GPS). Terrain unit: midslope.																				
/1	0- AE	Bleached A + biological crust	Aeolian	Dry 7.5YR 7.5YR 5/4 3/4	Loamy sand	V. few, c. gravel	Weak, f. blocky	Loose	Non-sticky, non-plastic	None	-	-	-	None	3s	Common	Diffuse, wavy	Bio. crust; f. droppings; v. narrow tunnels; macropores	8.7	0.22
/2	0.2- B	Neocarbonate B	Aeolian	V. sl. moist 7.5YR 7.5YR 5/4 4/4	Loamy sand	Not detected	Weak, f. blocky	Loose	Non-sticky, non-plastic	Mod.	-	-	-	None	3s	Few	Abrupt	V. narrow tunnels; many macropores; few cutans	8.7	2.1
/3	1.5- C	Dorbank (soft)	Obscured	Dry 7.5YR 7.5YR 6/4 4/4	Loamy sand	Few gravel	Weak, blocky	Fr-able	Non-sticky, non-plastic	None	3-5	5	-	None	10s	Not detected		V. narrow tunnels; many macropores	10.1	0.22
KV220PRN: Mining excavation. Prieske Form (Orthic A - Neocarbonate B - Hardpan carbonate). BMC, 65m terrace, 91m amsl (GPS). Terrain unit: crest.																				
/1	0- A1	Regic sand (Orthic A)	Aeolian	Sl. moist 10YR 10YR 6/4 5/4	Med. sand	Not detected	Apedal	Loose	Non-sticky, non-plastic	Strong	-	-	-	None	1s	Few	Abrupt, smooth, lith. disc.	Aeolian stratification	9.7	0.08
/2	0.18- A2	Regic sand	Aeolian	Sl. moist 10YR 10YR 5/4 4/4	Med. sand	Not detected	Apedal	Loose	Non-sticky, non-plastic	Sl.	-	-	-	None	10s	Few	Abrupt, smooth, lith. disc.	Aeolian stratification; Root tunnels	9.5	0.20
/3	0.4- B1	Neocarbonate B	Aeolian	Sl. moist 10YR 10YR 5/4 3/3	Med. sand	Not detected	Apedal	Loose	Non-sticky, non-plastic	V. sl.	-	-	-	None	30s	Common (old)	Gradual, smooth	Fine droppings, partially decomposed OM; darker	8.8	0.60
/4	0.7- B2	Neocarbonate B	Aeolian	Sl. moist 10YR 10YR 6/4 5/4	Med. sand	V. hard (silica?) nodules	Apedal	Loose	Non-sticky, non-plastic	Strong	-	-	-	None	1s	Few	Abrupt		9.0	0.44
/5	±1.2- B3	Hardpan carbonate	Aeolian	Dry 10YR 10YR 7/3 6/4	Med. sand	Not detected	Laminar	V. hard V. firm	Non-plastic	Strong	5	0-1	-	Discont. mod. carbonate	8s	Not detected	Clear, smooth	Abun. terrestrial bioturbation, calc. tunnels	8.9	3.3
/6	±1.4- B4	Neocarbonate	Aeolian	Dry 10YR 10YR 6/4 5/6	Med. sand	Not detected	Single grain apedal	Loose	Non-sticky, non-plastic	Strong	-	-	-	None	1s	Not detected	Obscured		8.9	1.1
/7	±1.4- B4	Neocarbonate	Aeolian	Dry 10YR 10YR 6/4 4/6	Med. sand	Not detected	Single grain apedal	Loose	Non-sticky, non-plastic	Strong	-	-	-	None	1s	Not detected	Obscured	Abun. terrestrial bioturbation	9.9	0.35
/9	2.3- II B5	Neocarbonate	Obscured	Moist 10YR 10YR 6/4 5/4	Med. sand	Suspended stoneline	Single grain apedal	Loose	Non-sticky, non-plastic	Strong	-	-	-	None	1s	Not detected	Abrupt, smooth stone line (ang.qtz.)	Shall shells; contains non-calc. termite nest (sample #8) with calc. tunnels	9.9	0.19
/10	2.8- III C	Calcrete grading to calc. blocky sed.	Obscured	Dry 10YR 10YR 7/4 6/4	Med. sand	Common stones, conc. upper boundary	Laminar	Hard V. firm	Non-plastic	Strong	-	-	-	Mod. cont. carbonate	4s	Not detected	Clear, smooth	Calc. tunnel	8.5	2.6
/11	3.8- III C2	Marine deposit shoreface	Upper shoreface	Dry 10YR 10YR 5/6 4/6	Med.-c. sand	Not detected	Mod., c., ang. blocky	Soft	Non-plastic, sl. sticky	None	-	-	-	None	1s	Not detected	Abrupt, smooth (erosional)	Tabular cross-bedding; abun. narrow tunnels; U- & vertical calc. burrows	8.1	1.0
/12	5- III C3	Marine deposit shoreface	Upper shoreface	Dry 10YR 10YR 6/4 5/6	Med.-c. sand	Not detected	Mod., c., ang. blocky	Loose- soft	Non-plastic, sl. sticky	None	-	-	-	None	1s	Not detected	Abrupt, wavy, sedimentary	Tabular cross-bedding not as clear. Lower part paler from mixing with /13? Calc. burrow	8.5	0.6
/13	6.2- IV C4	Marine deposit marine	Assumed marine	Dry 5YR 8/1 7/2	Loamy sand	Not detected	Mod., c., ang. blocky	Sl. Fri-able	Non-sticky, non-plastic	None	-	-	-	None	1s	Not detected	Not reached	Mn spots; termite tunnels continue from /12	8.4	1.8
LCK1-s: Mining excavation. Namib Form (Orthic A - Regic sand). KMC, 50 metre package, 30m amsl (GPS). Terrain unit: footslope-valley bottom.																				
/A	0- A	Regic sand (Orthic A)	Aeolian	Dry 10YR 10YR 5/4 3/3	Med. sand	Not detected	Apedal	Loose	Non-sticky, non-plastic	None	-	-	-	None	>10s	Many c.	Clear, smooth	Lots of OM (bank)	6.9	0.21
/B	0.3- B	Regic sand	Aeolian	Dry 10YR 10YR 6/4 5/4	Med. sand	Not detected	Weak, c., ang. blocky	Loose	Non-sticky, non-plastic	None	-	-	-	None	1s	Few c.	Abrupt, smooth	V. occ. burrows	8.9	0.14
/1	1- II B2	Neocutanic B	Obscured	Dry 10YR 10YR 5/6 5/4	Med. sand	Not detected	Weak-mod., c., ang. blocky	Loose	Non-sticky, non-plastic	None	-	-	-	None	1s	Not detected	Clear, smooth		7.3	1.6
/3	1.3- II B3	Neocutanic, luvic	Obscured	Dry 10YR 10YR 5/8 5/6	Med. sand	Not detected	Mod., c., ang. blocky	Sl. Fri-able	Non-sticky, non-plastic	None	-	-	-	None	3s	Not detected	Clear, smooth	Salty taste; few cutans	8.5	3.6

Table 2.1: Continued. *SK11 slaking tests: 2-3 alternating HCl/NaOH

Depth (m)	Horizon	Facies	Moisture	Munsell Dry	Moist	Field Texture	>2 mm-Fragments	Structure	Dry	Moist	Consistency	Wet	React HCl Slaking (5=full)	HCl NaOH H ₂ O Cementation	Water absorption	Roots	Transition	Other Features	pH	EC mS/cm
/4	1.9- III C1	Gleyed sand?	Dry	2.5Y 6/4	2.5Y 5/4	Med. sand	Not detected	Mod., to strong, c., ang.	Soft	Fri-able	Sticky, plastic to v. plastic	None	None	None	2s	Not detected	Abrupt, smooth	Salty taste; few slickensides	6.6	6.6
/5	2.2- IV C2	Sedimentary? Localised	Dry	2.5Y 6/3	10YR 5/4	Med. sand	Not detected	Strong-v. strong	Hard	Sl. firm	Sticky, plastic	None	None	None	2s	Not detected	Abrupt, wavy		6.8	3.1
/6	2.4- V C3	Sedimentary?	Dry	10YR 5/6	10YR 5/4	Med. sand	Not detected	Mod., c., ang. blocky	Sl. hard	Loose	Sticky, plastic	None	None	None	1.5s	Not detected	Diffuse, smooth	Salty taste	6.5	6.0
/7	3.4- VI C4	Marine deposit shoreface	Dry	10YR 5/6	10YR 5/6	C. sand	Many gravel	Weak to mod., c., ang. blocky	Loose	Loose	Non-sticky, non-plastic	None	None	None	1s	Not detected	Inter-bedded	Cross bedding	6.9	1.7
<i>Pale sand (LKC1 5/8), interlayered (wavy, abrupt transitions) with more orange sand (LKC1 5/9).</i>																				
/8	5.4- VII C5	Marine deposit shoreface	Dry	5Y 7/4	5Y 4/4	Med. sand	Not detected	Weak, c., ang. blocky	Loose	Loose	Non-sticky, non-plastic	None	None	None	1s	Not detected	Abrupt, to bedrock		7.1	1.6
/9	5.4- VII C6	Marine deposit shoreface	Dry	2.5Y 6/6	2.5Y 4/4	Med. sand	Not detected	Weak, c., ang. blocky	Loose	Loose	Non-sticky, non-plastic	None	None	None	1s	Not detected	Abrupt, to bedrock		7.7	1.8
OBT: Prieska Form (Orthic A - Neocarbonate B - Hardpan carbonate). BMC, 95m terrace, 99m AMSI (GPS). Terrain unit: crest.																				
/1	0- rs Aeolian deflation surface	Aeolian	Dry	10YR 6/4	10YR 4/3	Med. sand	Few, c. gravel	Apedal	Loose	Loose	Non-sticky, non-plastic	Strong	None	None	10s	None	Abrupt, smooth	Biological crust	8.7	0.02
/2	0.03- A	Orthic A	Dry	10YR 6/3	10YR 4/3	Med. sand	Few gravel	Apedal	Loose	Loose	Non-sticky, non-plastic	Strong	None	None	15s	Many	Gradual, smooth		8.9	0.13
/3	0.25- B	Neocarbonate B	Dry	10YR 6/4	10YR 4/4	Med. sand	Few gravel, carbonate	Weak, f. granular to blocky	Loose	Loose	Non-sticky, non-plastic	Strong	None	None	3s	Not detected	Abrupt, smooth		9.0	0.13
OBT: New profile, mining excavation, upper material removed.																				
/4	0.45- II C1	Hardpan carbonate to calc. blocky sed.	Dry	10YR 6/3	10YR 6/3	Loamy sand	Not detected	Laminar	Hard-v. hard	Sl. firm	Si. firm	Strong	Discont. carbonate	None	3s	Not detected	Clear, tonguing		8.9	0.63
/7	Within II C1	Dissolution or nest?	Dry	7.5YR 5/6	10YR 5/4	Loamy sand	Not detected	Mod., med., ang. blocky	Sl. hard	Loose	V. sticky, si. plastic	Local-ized, si.	None	None	3s	Not detected		Abun. tunnels ~3mm diam. & macropores. Dendritic black material (OM filled tunnels?), no reaction in 30% H ₂ O ₂ (cold)	8.7	2.0
/5	1- II C2	Sedimentary?	Dry	10YR 7/4	10YR 6/4	Loamy sand	Not detected	Strong, c., blocky	Hard-v. hard	Firm-v. firm	Si. firm	Occ.	None	None	3s	Not detected	Not reached	Mn spots on peds; sepiolite cutans	8.7	0.01
/6	1.5- III C3	Sedimentary?	Dry	10YR 6/4	2.5Y 6/4	Loamy sand	Stonelines (sub-ang. qtz, granitic-gneiss, silcrete)	Strong, c., blocky	Sl. hard	Fri-able	Si. sticky, non-to si. plastic	None	None	None	4s	Not detected			9.2	0.18
SK11: Pinedene Form (Orthic A - Yellow-brown apedal B - Signs of Wetness). BMC, 65m terrace, 60m AMSI (GPS). Terrain unit: footslope. Adjacent to mine																				
/A	0- A	Orthic A	Dry	7.5YR 5/5	7.5YR 3/4	Med. f. sand	Not detected	Apedal	Loose	Loose	Non-plastic, non-sticky	None	None	None	4	Many	Abrupt, smooth	Biological crust, OM, occ. droppings	9.1	0.14
/B	0.2- B	Yellow-brown apedal B	Dry	7.5YR 6/6	7.5YR 4/6	Med. to f. sand	Few gravel	Weak, f. blocky	Loose	Loose	Non-plastic, non-sticky	None	None	None	2	Few	Clear, smooth		9.2	0.06
/C	0.6- E	Gleyed sand	Dry	7.5YR 6/4	7.5YR 5/4	Med. sand	Not detected	Apedal	Loose	Loose	Non-plastic, non-sticky	None	None	None	1	Not detected	Abrupt, smooth		9.1	0.08
/D	0.65- B2	Neocutanic	Moist	7.5YR 5/6	7.5YR 4/6	Loamy sand	Not detected	Weak, c., ang. blocky	Sl. hard	Loose	Si. plastic, sticky	None	None	None	3	Few	Abrupt, smooth	Few cutans	8.7	1.3
/E	0.7- II C1	'Sepiocrete'	Obscured									None	2-3	2-3	2-3	Not detected			8.4	0.03
SK11: New profile, upper material removed by mining. Mining excavation																				
/1	0.01- II C1	'Sepiocrete'	Obscured	10YR 7/3	10YR 6/4		Not detected	Laminar calcareate	V. hard	V. firm		Strong	0* 0-1*	Si. carbonate, sepiolite	>20	Not detected	Gradual, wavy	Diffuse Mn coating some peds	8.7	0.04
/6	0.45- II C2	Blocky calcareated sediment	Obscured	10YR 7/4	7.5YR 5/6	Loamy sand	Not detected	Strong, c., blocky to prismatic	Hard-v. hard	Firm-v. firm		V.	-	Discont. carbonate	12	Not detected	Gradual, wavy	Carbonate cutans, Mn spots	9.1	0.02
/3	0.9- II C3	Hardpan carbonate	Dry	10YR 8/3	7.5YR 7/6		Not detected	Laminar	V. hard	Firm-v. firm		Strong	2-3	3	4	Not detected	Clear, wavy	Mn spots on some peds	9.2	0.02
/9	0.9- III C3	Hardpan carbonate	Dry	10YR 8/3	7.5YR 7/6		Not detected	Laminar	V. hard	Firm-v. firm		Strong	3	2-3	2	Not detected	Clear, wavy	Mn spots on some peds	8.8	3.6
/4	1.1- III C4	Neocarbonate	Dry	7.5YR 6/4	7.5YR 5/6	Med. sand	Not detected	Weak, ang. blocky	Loose	Loose	Non-plastic, non-sticky	None	None	None	1	Not detected			8.9	0.04
/4b	1.15- III C5	Neocarbonate	Dry	10YR 7/4	10YR 6/4	Loamy sand	Not detected	Weak., c., blocky	Loose	Loose	Si. plastic, si. sticky	Mod.	-	None	1	Not detected	Clear, wavy, to sample 7		8.7	2.5
/5	0.8- Termitic nest	Termitic nest	Dry	10YR 6/4	10YR 5/6	Loamy sand	Not detected	Mod., c., blocky	Firm	Loose	Si. plastic, si. sticky	Local	-	None	3	Not detected	Diffuse	Carbonate cutans, occ. Mn spots; chert pieces?	8.9	2.6
/7	1.5- IV C6	Sedimentary	Dry	5Y 7/4	10YR 6/3	Sandy loam	Locally abun. gravel	Mod., c., blocky	Firm	Loose	Si. plastic, si. sticky	Local	-	None	3	Not detected	Clear, smooth	Darker yellow-red areas - iron pan?	8.4	6.3
/10	2.2- IV C7	Iron pan	Dry	10YR 6/6	10YR 5/6	C. loamy sand	Abun. gravel	Mod., c., blocky	Firm	Loose	Si. plastic, si. sticky	None	-	None	1	Not detected	Clear, smooth		7.9	2.5

Table 2.1: Continued.

Depth (m)	Horizon	Facies	Moisture	Munsell	Field	>2 mm-Fragments	Structure	Dry	Moist	Consistency	Wet	React HCl	HCl Staking (5=full)	H ₂ O	Cementation	Water absorption	Roots	Transition	Other Features	pH	EC mS/cm
/11	-2.1- IV C7	Sedimentary	Dry	5Y 2.5Y 7/3	Clay loam	Not detected	C., strong blocky	Hard	Friable	V. plastic, v. sticky	Occ.	-	-	-	None	4	Not detected	Abrupt	Occ. Mn spots	8.5	5.4
SK11/8 cut into sample 7 & 11, shape suggestive of a channel. Horizontal white layers continuously cut across it and sample 7.																					
/8	-1.5- Channel or biological? nest?	'Channel' or biological? nest?	Dry	10YR 6/4	C. to f. sand	Suspended gravel layers	Mod., c., blocky	Loose	Loose	Non-plastic, sticky	None	-	-	None	1	Not detected	Abrupt, concave up	Abun. 5mm diam. tunnels		8.2	1.5
/12	2.6- VIII C	Sedimentary	Dry	5Y 5/4	F. sand	Not detected	Mod., c., blocky	SI. firm	Loose	Non-plastic, sticky	None	-	-	None	1	Not detected		Abun. 5mm diam. tunnels w. OM		7.9	3.5
SL4-1: Pinecone Form (Orthic A - Yellow-brown apedal B - Signs of Wetness), KNC, 30 metre package, 46m AMSI (GPS). Terrain unit: footslope.																					
/1	0-0.3 A1	Aeolian	Dry	7.5YR 7.5YR 5/6	Med. sand	Not detected	Apedal	Loose	Loose	Non-sticky, non-plastic	None	-	-	None	1s	Common	Gradual, smooth	V. occ. droppings		8.7	0.04
/2	0.3- B1	Yellow-brown apedal B	Dry	7.5YR 7.5YR 5/6	Med. sand	Not detected	Weak, f., blocky	Loose	Loose	Non-sticky, non-plastic	None	-	-	None	5s	Few	Gradual, sl. tonguing	Few cutans		7.7	0.15
/3	0.5- E	Gleyed sand	Dry	7.5YR 7.5YR 6/4	Med. sand	Not detected	Weak, f., blocky	Loose	Loose	Non-sticky, non-plastic	None	-	-	None	3s	Few	Abrupt smooth			8.4	0.16
/4	0.63- -0.78 B2	Neocutanic	Dry	7.5YR 7.5YR 5/4	Med. sand	Not detected	Mod., c., blocky	SI. hard	Fri-able	V. sl. plastic, sl. sticky	None	-	-	None	3s	V. few	Abrupt smooth	Few cutans		6.7	0.73
SL4-1: New profile, mining excavation, continuous with horizon B2. Upper material removed.																					
/5	0.8- II B3	Slightly Gleyed sand?	Dry	10YR 6/4	Med. sand	Not detected	Mod., c., blocky	SI. hard	Loose- friable	SI. sticky	None	-	-	None	5s	Not detected	Diffuse, wavy	Common macropores, few cutans		7.9	5.6
/6	0.95- III B4	Pedocutanic	Dry	10YR 6/5	Loamy sand	Not detected	Strong, c., blocky to pris.	Firm-able	Fri-able	SI. plastic, sticky	None	-	-	None	3s	Not detected	Diffuse wavy	Few cutans		8.2	4.5
/7	0.97- III B5	Pedocutanic +calcite	Dry	10YR 6/4	Loamy sand	Not detected	Strong, c., blocky to pris.	Hard	V. firm	Mod., c., sticky	Mod.	-	-	None	6s	Not detected	Diffuse wavy	Mn spots; few cutans		8.8	3.6
/8	1.22- III B6	Pedocutanic	Dry	10YR 7/4	Loamy sand	Not detected	Strong, c., blocky to pris.	Hard	SI. firm	Non-plastic, sl. sticky	None	-	-	None	3s	Not detected	Diffuse wavy	Mn spots; few cutans		8.8	4.2
/9	2.45- IV C1	Marine deposit shoreface	Dry	10YR 6/6	Loamy sand	Many gravel	Weak to mod., c., blocky	Loose- soft	Loose	SI. plastic, sl. sticky	None	-	-	None	1s	Not detected	Abrupt, smooth			8.3	4.0
Abundant vertical termite burrows, some extending through the whole of V, into IV, which appear to have been conditils for water movement. Sediment filling them is browner/oranger colour. Burrows look identical to those in 6869.																					
/11	3.05-9 V C2	Marine deposit shoreface	Dry	10YR 7/1	Med. sand	Not detected	Apedal	Loose	Loose	Non-plastic, non-sticky	Mod.	-	-	None	1s	Not detected	Abrupt, smooth to bedrock	Local 'groundwater silcrete'; marine shells		9.2	1.4
SN130: Mining excavation. Preska Form (Orthic A - Neocarbonate B - Hardpan carbonate), KNC, 50 metre package, 66.7m AMSI (GPS). Terrain unit: footslope.																					
/1A	0- A	Regic sand	Dry	10YR 6/3	Med. sand	Few, rounded gravel	Apedal	Loose	Loose	Non-plastic, non-sticky	Mod.	-	-	None	4s	Few	Abrupt, smooth			9.0	0.13
/B	0.3- II B1	Neocarbonate B	Dry	10YR 5/4	Med. sand	Few, rounded gravel	Weak, med., ang. blocky	Loose	Loose	Non-plastic, sl. sticky	Mod.	-	-	None	4s	V. few	Abrupt, smooth to tonguing			9.5	0.17
/2	0.6- III C2	Hardpan carbonate shoreface	Dry	2.5Y 8/1	10YR	Not detected	Laminar	Hard	Firm	Strong	3	2-3	3-4	Cont., carbonate	5s	Not detected	Diffuse, tonguing			8.9	1.0
/3	1.1- III C3	Marine deposit shoreface	Dry	10YR 4/4	C. sand	Many, rounded gravel	Weak, c., ang. blocky	Hard	Fri-able	SI. plastic, sticky	None	-	-	None	3s	Not detected	Clear, smooth			9.3	0.19
/5	±2.2- IV C5	Marine deposit shoreface, rip channel?	Dry	10YR 7/6	Med.-f. sand	Not detected	Strong, c., ang. blocky	Hard	SI. firm	Non-v. sl. plastic, non-sticky	None	-	-	None	2s	Not detected	Abrupt, tonguing to wavy	Occ. Mn spots; occ. tunnels		9.1	0.16
/4	2.1- IV C4	Marine deposit	Dry	2.5Y 7/3	Med.-f. sand	Not detected	Strong, c., ang. blocky	Loose	Loose	Non-plastic, non-sticky	None	-	-	None	1s	Not detected	Abrupt, smooth	V. occ. tunnels; ±8cm diam. tunnel on lower contact		9.0	0.04
/6	±2.5- IV C6	Marine deposit shoreface	Dry	5Y 5/4	Med.-f. sand	Not detected	Strong, c., ang. blocky	Loose	Loose	Non-plastic, non-sticky	Strong	-	-	None	1s	Not detected	Abrupt, to bedrock	Mn spots; marine shells & bed-ding; abun. tunnels; 1m termite tunnels filled with orange sand		9.9	0.09
SN160: Mining excavation. Namib Form (Orthic A - Regic sand), KNC, 50 metre package, 43m AMSI (topo map). Terrain unit: footslope.																					
/1	0- A	Orthic A + Regic sand	Dry	10YR 7/2	Med. sand	2 stonelines (buried deflation surfaces)	Apedal	Loose	Loose	Non-plastic, non-sticky	Mod.	-	-	None	1s	Common	Abrupt, smooth, stoneline	Aeolian stratification		9.7	0.06
/2	1.3- II B1	Neocarbonate B	Dry	10YR 6/3	Med. sand	V. few, rounded, gravel	Apedal	Loose	Loose	Non-plastic, non-sticky	Mod.	-	-	None	1s	Common	Clear, smooth			9.5	0.07
/3	1.5- III B2	Neocarbonate B	Dry	10YR 5/4	Loamy sand	V. few, rounded, gravel	Weak, med., ang. blocky	SI. hard	Loose	SI. plastic, sl. sticky	SI.	-	-	None	1s	Common	Clear, smooth	Few, med., distinct, grey, yellow mottles		9.4	0.31
/4	1.77- III B2	Neocarbonate B	Dry	10YR 5/4	Loamy sand	V. few, rounded, gravel, calcite	Weak, med., ang. blocky	SI. hard	Loose	SI. plastic, sl. sticky	Strong	-	-	None	1s	Common	Clear, smooth			9.0	0.84
/5a	-1.5- IV C1	Hardpan carbonate next to kerst below kerst	Dry	7.5YR 8/2	7.5YR	Not detected	Laminar	Hard-v. firm	Firm-v.	SI. sticky	V.	5	0	-	-	None		Wavy upper boundary shows regular karst features		9.2	0.53
/5b	-1.8- IV C2	Blocky calc. sed. below kerst	Dry	7.5YR 8/2	7.5YR	Not detected	Mod., c., blocky/laminar	Hard-v. firm	Firm-v.	SI. sticky	V.	4-5	5	Cont.	5s	Not detected		Carbonate cutans		8.9	1.1
/5c	1.95- IV C3	Blocky calc. sediment	Dry	7.5YR 8/2	10YR	Not detected	Strong, c., blocky to pris.	Hard-v. firm	Firm	SI. sticky	Strong	-	-	Discont. carbonate	5s	Not detected		Mn spots on pads		8.9	0.94

Table 2.1: Continued.

Depth (m)	Horizon	Facies	Moist-ure	Munsell Dry Moist	Field Texture	>2 mm-Fragments	Structure	Dry Moist	Consistence Moist	Wet	React HCl Slaking (5=full)	HCl NaOH H ₂ O	Cementation	Water absorption	Roots	Transition	Other Features	pH	EC mS/cm
/6	-2.1- IV C4	Obscured	Dry	10YR 7/3	Loamy sand	Not detected	Mod. c. blocky to laminar	Hard	Fr-able	V. sl. sticky, non-plastic	Strong	-	Discont. carbonate	5s	Not detected	Gradual, tonguing	Mn spots on pedis adheres to tongue; sepiolite under calcite cutans	8.8	1.1
/7	-2.3- V C5	Obscured	Dry	2.5Y 7/3	Loamy sand	Few, rounded gravel	Strong c., ang. blocky to columnar	Hard	Firm-frable	SI, plastic, sl. sticky	Only	-	Discont. carbonate	4s	Occ. btw pedis	Gradual, tonguing	Mn spots on carbonate; ped adheres to tongue; sepiolite under calcite cutans	9.1	1.0
/8	Channel into SNT60/7	Local channel?	Dry	10YR 6/3	Loamy sand	Few, rounded gravel	Mod. c., ang. blocky	SI, hard-frable	Loose-frable	SI, plastic, sl. sticky	Only	-	None	3s	Root channels	Gradual, wavy	Mn spots on carbonate; bone filled with f. roots (terrestrial); 8mm diam. tunnel	9.2	0.62
/10	2.8- VI C6	Sedimentary?	Dry	2.5Y 8/2	Loamy sand	Occ. pebble	Mod. c., ang. blocky?	Loose-firm	Loose-firm	SI, plastic, non-sticky	None	-	None	2s	Occ.	Gradual, wavy	Distinct orange mottles; Mn stained small bone/egg shell iron pan; few bones?; Mn staining	9.6	0.24
/11	3.4- VII C7	Sedimentary?	Dry	2.5Y 7/4	Loamy sand	Not detected	Apedal	Loose	Loose	Non-plastic, non-sticky	None	-	None	2s	Not detected	Gradual, wavy		9.3	0.16
/12	3.7- VIII C8	Sedimentary?	Dry	5Y 8/2	Loamy sand	Not detected	Mod. c., blocky to pris.	SI, hard	Loose	Non-plastic, non-sticky	None	-	None	1s	Not detected	Abrupt smooth		9.9	0.33
SPNT: Prieska Form (Orthic A - Neocarbonate B - Hardpan carbonate). BMC, 65m terrace, 57m amsl (GPS). Terrain unit: footslope.																			
/3	0- A1	Regic sand	Dry	10YR 7/2	Med. sand	Not detected	Apedal	Loose	Loose	Non-plastic, non-sticky	Mod.	-	None	3s	Few	Abrupt, smooth	Droppings	9.4	0.09
/1	0.1- A2	Burned Orthic A	Dry	10YR 7/2	Med. sand	V. few gravel	Apedal	Loose	Loose	Non-plastic, non-sticky	Mod.	-	None	10s	Common	Clear, wavy	Lots of organic matter, faecal pellets	9.6	0.10
/2	0.5- II B	Neocarbonate B	Moist	10YR 6/3	Med. sand	V. few gravel	Weak, mod., blocky	Loose	Loose	Non-plastic, non-sticky	Mod.	-	None	3s	Not detected	Abrupt, smooth	Occ. mottles; few cutans	9.6	0.11
SPNT: New profile, mining excavation, upper material removed.																			
/4	0- III C	Hardpan carbonate	Dry	white	Bimodal (1&5mm)	Not detected	Massive	V. hard	V. firm		Strong	4	0	-	Not detected			9.2	0.50
/5	0.3- IV C	Hardpan carbonate	Dry	10YR 8/1	Med. sand	Not detected	Vesicular				Strong	2-5	0	-	Not detected		Dissolution by high salt content (powdery)	9.1	4.6
TP231L: Kinkelbos Form (Orthic A - E - Neocarbonate B). BMC, 50m terrace, 66m amsl (GPS). Terrain unit: crest.																			
/A	0- A	Orthic A	Dry	10YR 6/3	Med. T. sand	Not detected	Apedal to v. ang. blocky	Loose	Loose	Non-plastic, non-sticky	SI, to mod.	-	None	>20s	Many	Clear to gradual, smooth	V. thin biological crust	9.1	0.23
/E	0.3- E	E	Dry	10YR 7/3	Med. sand	Not detected	Apedal to v. weak, med., ang. blocky	Loose	Loose	Non-plastic, non-v. sl. sticky	Strong	-	None	1s	Few	Clear, smooth		9.6	0.12
/B	0.5-? B	Neocarbonate B	Dry	10YR 7/3	Loamy sand	Not detected	Apedal to v. weak, med., ang. blocky	Loose	Loose	Non-plastic, sticky	Strong	-	None	1s	Few	Not reached		9.6	0.11
TP231L: New profile, mining excavation, upper material removed.																			
/1	0- RS	Regic sand	Dry	10YR 6/4	Med. sand	Not detected	Apedal	Loose	Loose	Non-plastic, non-sticky	SI	-	None	>20s	Few	Abrupt, smooth		9.0	0.29
/2	0.6- II B1	Neocarbonate B	Obscured	10YR 5/6	Loamy sand	Not detected	Apedal to weak, c., ang. blocky	Loose	Loose	Non-v. sl. plastic, sl. sticky	Strong	-	None	1s	Few	Abrupt, smooth		9.7	0.35
/3	0.8- III C1	Hardpan carbonate	Dry	7.5YR 8/1	Med. sand	Subrounded qtz gravel	Laminar	V. hard	V. firm		Strong	3-4	0	-	Not detected	Gradual, tonguing	Mh	9.2	1.1
Samples 4 & 5 from same lithology. Sample 4 from upper part and is more intensely bioturbated than Sample 5. This gives strength to the structure. Transition to lower non-bioturbated part is obscured.																			
/4	2- III C2	Marine deposit	Dry	10YR 6/6	Med. sand	Subrounded gravel	Mod. to strong, c., ang. blocky	Loose	Loose	Non-v. sl. plastic, non-sticky	Some	-	None	2s	Not detected	Obscured	Alveolar texture - root activity or burrows?	8.1	1.4
/5	at ±15 III C3	Marine deposit	Dry	10YR 5/6	Med. sand	Subrounded gravel	Strong c., ang. blocky	Loose	Loose	Non-v. sl. plastic, non-sticky	Occ.	-	None	2s	Not detected	Abrupt, to bedrock	Weak bedding/wind erosion?	9.6	0.28
TP266Q: Namib Form (Orthic A - Regic sand). BMC, 95m terrace, 109m amsl. Terrain unit: crest. Mining excavation																			
/5	0- A1	Regic sand	Dry	10YR 6/3	Med. sand	Not detected	Apedal	Loose	Loose	Non-plastic, sticky	Strong	-	None	>10	Common	Abrupt, smooth	Occ. fine droppings	9.1	0.14
/4	1- II B1	Neocarbonate B	Obscured	7.5YR 5/4	Med. sand	Ang. qtz pebbles	Weak c., ang. blocky	Loose	Loose	SI, plastic to plastic, sl. sticky	Strong	-	None	2	V. few	Abrupt, smooth, stoneline (ang. qtz pebbles)		9.9	0.28
/1	1.2- III C1	Hardpan carbonate	Dry	2.5Y 8/1	Med. sand	Not detected	Laminar-blocky	Hard	Frable	Plastic, sticky	Strong	3	1	-	Not detected	Gradual, tonguing	Mn spots	8.3	4.8
/2	1.7- III C2	Neocutanic marine	Dry	10YR 6/6	Med. sand	Not detected	Weak to mod., c., ang. blocky	Loose	Loose	Plastic, sticky	cutans, burrows	-	None	3	Occ. root channels	Abrupt, to bedrock	Mn spots, salty taste, carb. cutans	8.4	2.2

Regic sands are young aeolian dunes, which may be vegetated. In the profiles studied they range in thickness from 0.3 to 3.2 m. They are generally medium sand, single-grain apedal, loose, non-plastic and non-sticky. Most are calcareous. pH in water ranges from 8.7 to 9.8 and EC (in the same 1: 2.5 suspension) is 0.02 to 0.29 mS cm⁻¹ (Table 2.1). Average organic carbon in the surface of regic sands is 0.98 %, and is 1.05 % in orthic A horizons. Average nitrogen is 0.03 % (regic sands), and 0.05 % (orthic A). Humification at the surface of these regic sands is the only visible sign of pedogenesis.

In some cases there is a lithological discontinuity at the base of the regic sand, manifest either as a heavy-mineral enriched layer (such as profile 6869, Table 2.1) or stoneline (such as SNT60, Table 2.1), interpreted to represent a buried aeolian deflation surface. Aeolian deflation processes in the modern interdune surface areas (profile OBT) are evident from heavy-mineral enriched surface sands and gravel-lag deposits with the same particle-size as the buried stonelines.

When compared to profiles with no regic sands, it becomes apparent that the A horizon that developed with the neocutanic or neocarbonate B horizon on which the regic sands lie has been eroded: in areas with no regic sands there is colour continuity between the orthic A horizon and its associated B horizon (profiles AK61H, SK11, SL4-1, SPNT, OBT, TP231L, Table 2.1), whereas there is a marked colour discontinuity between the regic sand and the underlying B horizon (profiles LKC1-5, SN30, SNT60, TP266Q), and in the case of SNT60, also a lithological discontinuity.

Southerly winds prevail along the coastal plain, and are responsible for the formation of coastal dunefields (Harmse and Swanevelder, 1987). The calcareous dunes supply high pH calcareous material to the surface of the soil profile. Continuing burial by young aeolian dunes is evident from regic sands with buried horizons rich in organic matter (KV220PRN/3, and a buried hearth and hand axes and associated rock fragments (Figure 2.4). The age of these dunes is unclear, they form part of a dune corridor north of the Buffels River mouth, and may be analogous to the one north of the Swartlintjies river (Tankard and Rogers, 1978).



Figure 2.4: Archaeological site. Hearth and hand axe (arrowed) buried by regic sands, approximately 1.5m deep. Near AK61H.

2.4.2 B horizons

The most common are neocarbonate B horizons (generally 0.1 to 1.3 m thick), underlain in most cases by hardpan carbonate (Prieska soil form) and less commonly by calcareous dorbank (Trawal soil form). In many cases, there is a stoneline (up to cobble-size) between the hardpan carbonate and the overlying neocarbonate horizon (such as 6869/iv, KV220PRN/9, TP266Q in Table 2.1). The neocarbonate horizons generally have a weak, medium, angular blocky structure; are loose, non- to very slightly plastic and non- to very slightly sticky; and have a medium sand texture. The pH in water is 8.7 to 9.9, and EC (in the same 1 to 2.5 suspension) is 0.04 to 3.5 mS cm⁻¹ (Table 2.1).

Neocutanic and yellow-brown apedal B horizons (0.05 to 0.4 m) are also present, in one case over hardpan carbonate (Ashkam soil form, profile 6869), but more commonly over an eluvial horizon, underlain in turn by another neocutanic horizon with more silt and clay (SK11, SL4-1, Table 2.1). The pH is lower than

the neocarbonate horizons, (7.9 - 9.2) and EC is 0.1 to 2.2 mS cm⁻¹ (Table 2.1). These horizons have a slightly stronger structure than the neocarbonate horizons, and are more sticky and plastic generally. They are loose to friable.

Profile KV196T (furthest inland, Figure 2.2), has a 0.3 m thick red apedal B horizon over a 3 m dorbank horizon (Garies Form). The red apedal B horizon is loose, weak coarse angular blocky, non-plastic and non-sticky, and has a pH in water (1: 2.5 suspension) of 10.1. The EC (of the same suspension) is 0.1 mS cm⁻¹. This profile was discussed in more detail in Chapter 1.

Yaalon (1981) suggested that parent materials of different original carbonate content may be responsible for the final development of either red sands or aeolianites on the KwaZulu-Natal coast. Highly calcareous littoral sands (calcium carbonate content higher than 30 %) become cemented to form the aeolianites, whereas sands containing less than about 25 % CaCO₃ are fixed by vegetation, with soil-forming processes producing clayey red sands. Deposits with a CaCO₃ content close to the threshold values separating the two diagenetic pathways can exhibit both decalcification at the surface and preservation of the CaCO₃ below it (Yaalon, 1981). Pether (1994) noted that the soluble carbonate content of the coastal plain calcretes (acid digestion) is only 3%. The data of Singer et al. (1995) for the same area showed a maximum of 20% CaCO₃ in a calcrete horizon, and most of the A and B horizons had less than 5%. Some profiles like LKC1-5 (Table 2.1) had non-calcareous regic sands. This suggests the relatively low CaCO₃ in the aeolian sands dictates the pedogenic pathway in these deposits, and reddened neocarbonate and neocutanic horizons develop as the aeolian deposits age.

Rubification was used as an index of soil development by Harden (1982) and Bockheim et al. (1992). In the Sonoran desert of Baja California, a progressive development of red pigment in Pliocene to Recent sediments has occurred by *in situ* alteration of iron bearing minerals through an intermediate stage of brown ferric oxide, in areas with a low water table, alkaline groundwater and interstitial oxidising conditions (Walker, 1967; Walker and Honea, 1969; Van Houten, 1973). Soils sampled in this study occur in well drained, oxidised environments. When sorted by their hue, samples fall into the field where goethite is predominant (7.5YR to 2.5YR). The red apedal samples fall into the hematite field (10R to 5YR) (Schwertmann and Taylor, 1989; Schwertmann, 1993).

Age

Sediment supply to the aeolian sand sheet is delivered to the coastline via rivers, washed onto the beaches north of the river mouths, and then blown inland by the predominantly southerly winds (Harmse and Swanevelder, 1987). Dunefields are common on the north side of river mouths on the West Coast, and can be distinguished easily on Google Earth satellite images. Three profiles (6869, SNT60 and SN30) were investigated in the ‘parabolic dunefield’ north of the Swartlintjies River mouth, and one profile (SL4-1) in the older material over which it accreted (Figure 2.5). This ‘parabolic dunefield’ was delineated by Tankard and Rogers (1978, p. 328-330), who proposed that it accreted following movement of the Swartlintjies River mouth sediment source 5 km to the west and 110 m lower

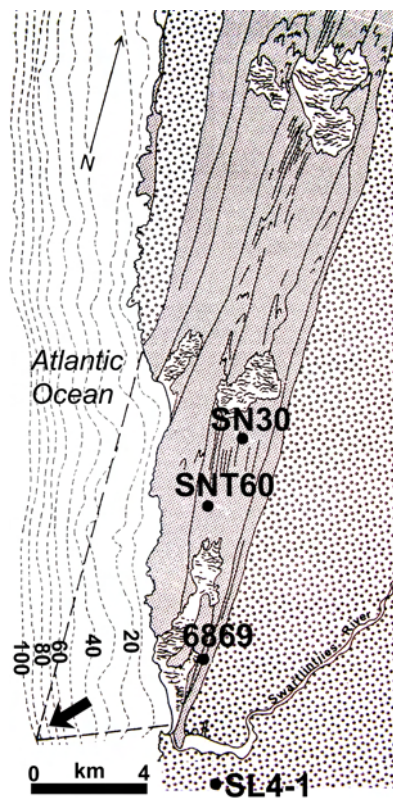


Figure 2.5: Interpretation of dune plume north of Swartlintjies River, from Tankard and Rogers (1978). ‘Vegetated parabolic dune plume’ (grey; SN30, SNT60, 6869) accreted following the movement of the Swartlintjies River mouth sediment-source during Last Glacial (arrowed). It accreted over older ‘degraded parabolic dunes’ (dots; SL4-1). Modern unvegetated barchanoid dunes discontinuously override the plume (clear). Position of profiles SN30, SNT60, 6869 and SL4-1 was determined using their grid co-ordinates on the equivalently-scaled orthophoto sheets 3017AD1, AB21, AA25, AB16, AA20 (1st Edition, 1990).

than present, during the Last Glacial sea-level lowering. Tankard and Rogers (1978) interpreted this ‘parabolic dunefield’ to have formed as barchan dunes which were deposited during the Last Glacial and subsequently vegetated. Modern unvegetated barchanoid dunes override the plume.

Following this interpretation, horizons 6869/i,ii; SNT60/1; and SN30/A which are classified as ‘regic sands’ in Table 2.1 (where the only sign of pedogenesis in the profile is darkening of the upper horizon by organic material), are more specifically the vegetated parabolic dunes that were deposited during the Last Glacial Maximum. Profile SL4-1, occurs within the zone of the older ‘degraded parabolic dunes’ of Tankard and Rogers (1978). Its redder colour and more clay-rich nature compared to the pale regic sands lend support to its greater age.

The colour and lithological discontinuities between the Last Glacial Maximum regic sands and their underlying redder, more clay-rich B horizons horizons (6869/4, SN30/B, SNT60/2, Table 2.1) suggest that their accretion took place after significant pedogenesis had already occurred. The resemblance of these underlying horizons to the B horizons of profile SL4-1 (i.e. the older ‘degraded parabolic dunes’ of Tankard and Rogers (1978)) suggests a pre-Last Glacial Maximum age. This is consistent with the $\delta^{14}\text{C}$ ages of 25 000 to 30 000 years B.P. for calcrete associated with heuweltjies (although further south) in the Clanwilliam and Elands Bay areas (Midgley et al., 2002).

An attempt was made to extend this to the rest of the profiles: the degree of reddening and clay enrichment of profiles AK1/trig, DL88, KV196T, and SK11 (Group Aii in Table 2.2) are of the same magnitude as the pre-Last Glacial Maximum profile SL4-1, and the truncated B horizons (6869/4, SNT60/1 and SN30/A) (Group B). This suggests they are of an equivalent age, and older than profiles OBT, SPNT, TP231L (Group Ai). Together with the data from Midgley et al. (2002), this information shows evidence of pedogenesis from before the Last Glacial for both the northern and southern parts of Namaqualand.

2.4.3 Eluvial horizons

A 0.2 m thick eluvial horizon in the diagnostic position (Soil Classification Working Group, 1991) is present in a calcareous profile TP231L, where it has formed above a neocarbonate B on calcrete (Table 2.1). Bleached horizons also occur

Table 2.2: Redness rating (Arduino, 1985) for each soil profile, calculated from equation 2.1. The higher the redness rating, the redder the soil. /.../ indicates horizon interpreted to be missing or eroded. Abbreviations: db-dorbank; gs-gleyed sand (eluvial); hk-hard carbonate; nc-neocarbonate; ne-neocutanic; ot-orthic; rs-regic sand (may be darkened by organic matter); re-red apedal; rs-regic sand; unsp-unspecified; ye- yellow-brown apedal.

Profile	Soil Form	Horizon Sequence	Redness Rating (dry)
A) A-horizon genetically related to underlying horizons			
i) Low redness rating			
OBT	Prieska Form	ot / nc / hk	3 / 3 / 0
SPNT	Prieska Form	rs / ot / nc / hk	1 / 1 / 3 / 1
TP231L	Kinkelbos Form	ot / E / nc	3 / 2 / 2
ii) High redness rating			
AK1/trig	Oakleaf Form	ot / ne / rock	8 / 6 / ..
DL88	Augrabies Form	ot / nc / unsp	6 / 6 / 5
KV196T	Garies Form	ot / re / db	15 / 12 / 16
SK11	Pinedene Form	ot / ye / gs / ne	8 / 8 / 5 / 9
SL4-1	Pinedene Form	ot / ye / gs / ne	9 / 9 / 5 / 6
B) Regic sands unconformably rest on B-horizon			
6869	Prieska Form	rs / .. / nc / nc / hk	1 / .. / 3 / 6 / 0
LKC1-5	Namib Form	rs / .. / ne	3 / .. / 6
SN30	Prieska Form	rs / .. / nc / hk	3 / .. / 4 / 0
SNT60	Namib Form	rs / .. / nc / hk	1 / .. / 4 / 2
TP266Q	Namib Form	rs / .. / nc / hk	3 / .. / 6 / 0

third in a sequence from the surface, not in a diagnostic position as an E horizon and thus have been classified as ‘gleyed sand’ (‘gs’) according to the definition of the Soil Classification Working Group (1991, p. 243). They are overlain by a B horizon and underlain by an horizon with a much higher clay content and EC (such as SK11 and SL4-1 (Table 2.1). Both SK11 (0.05 m thick) and SL4-1 (0.13 m thick) were non-calcareous. Profile SL4-1 is discussed in greater detail by Francis et al. (2007). The significance of these eluvial horizons for water storage in Namaqualand ecosystems has been discussed by Francis et al. (2007).

Evidence for leaching below the average depth of water storage is often observed in arid-region soils (Buol et al., 1997). Buol et al. (1997) noted that while this is often attributed to a more humid paleoclimate, given the typically erratic nature of the rainfall in arid regions these soil features may simply reflect the rainfall of the extreme, rather than the average, years.

An important point in considering the development of these E horizons is the reliability of the rainfall in coastal Namaqualand: although it is a “arid” region with a high evaporation rate (2 m per year (D.B.C.M., 2000)) and less than 150 mm annual rainfall, the rainfall is reliant and occurs as frequent but low volume winter rainfall events (Desmet, 2007), Namaqualand presently receives

flood events about every 10 years which cause the ephemeral rivers to flow, although drought years do occur (D.B.C.M., 2000).

The example in profile SL4-1 (Table 2.1) occurs in a profile in which vertical tunnels that may be attributed to termites (J. Pether, pers. comm., February 2002) have become conduits for water, extending to bedrock about 12 m deep (Figure 2.6). See Section 2.4.6 for a more detailed discussion of these burrows. The bedrock in this profile shows signs of wetness. This suggests that both lateral and vertical water movement through the regolith is extensive, and occurs along strongly preferential flow paths. Many of the mine excavations have water present, in some profiles water flows out of the deeper parts of the regolith (as in 6869, also with abundant vertical termite burrows (J. Pether, pers. comm., February 2002) which appear to have become conduits for water). The lower part of some B horizons were slightly moist to moist, especially when above a cemented horizon (for example 6869, DL88, KV220PRN, see Table 2.1), which is consistent with the suggestion of Francis et al. (2007) that these act as a barrier to water movement.

Although the Namaqualand coast may have been wetter during the Last Glacial (Van Zinderen Bakker, 1976; Tankard and Rogers, 1978; Parkington et al., 2000), and many profiles are older (Section 2.4.2), Namaqualand presently receives flood events about every 10 years which cause the ephemeral rivers to flow, in addition to reliant but low volume winter rainfall events. Together with the water evident flowing out of the deeper part of the regolith in many profiles, this suggests these subsurface bleached horizons presently function as aquifers during profile wetting, and although some may have existed in a wetter paleoclimate, they continue to be active in the present.

2.4.4 Cemented horizons

Calcite-cemented horizons

Horizons of calcite accumulation are common. The distribution of carbonates can vary from dispersed to highly cemented (calcic to petrocalcic (Soil Survey Staff, 1999); soft carbonate to hardpan carbonate (Soil Classification Working Group, 1991)). In the diagnostic position these horizons were classified as ‘hardpan

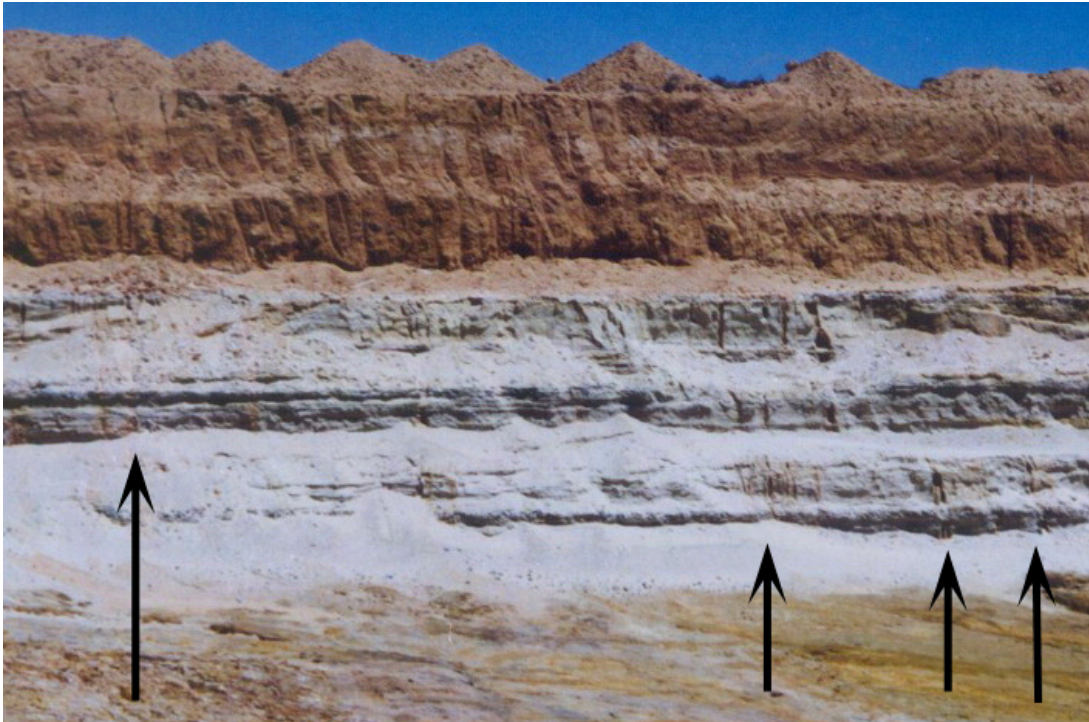


Figure 2.6: Possible vertical termite burrows (arrowed) that have become conduits for preferential flow, extending through upper shoreface (red) and lower shoreface (grey) to bedrock, which shows evidence of wetness (lower right). Mine dumps obscure surface. Benches 3 m high. Profile SL4-1.

carbonate', otherwise as 'calcrete' in Table 2.1. Their thickness ranges from 0.2 m to over 1 m. Petrocalcic horizons slake in acid (Soil Survey Staff, 1999). Some samples classified as hardpan carbonate had areas which slaked in water to a fine sediment (Table 2.1). This is consistent with the observations of Pether (1994) that the soluble carbonate content (acid digestion) is only 3% and the host material is a muddy sand. The average pH in water (1: 2.5 suspension) is 8.3 - 9.6, and EC ranges from 0.02 to 4.93 mS/cm (Table 2.1). Higher salt contents are often associated with dissolution of the horizon (AK1/2, SPNT/5, Table 2.1).

In locations with particularly thick regic sand cover (such as profile KV220PRN (Table 2.1), and the buried hearth site in Figure 2.4) a calcrete horizon is present near the base of the calcareous regic sand (1.2 to 1.4 m deep in profile KV220PRN). This is interpreted to be a modern pedogenic process. In profile KV220PRN, a second calcrete horizon occurs deeper in the profile (2.8 to 3.8 m deep), the upper boundary of which shows dissolution features. The calcrete

lies under a redder neocarbonate horizon, both of which are identical to the calcrete and reddened neocarbonate B horizons found elsewhere (Group B in Table 2.2). This suggests the horizons in Group B are the buried remains of partially eroded paleosols, and that soil forming processes have begun anew in the overlying cover sands, via a process of aggradation as observed by (Knox, 1977) for calcrete profiles near Saldanha Bay.

Silica-cemented horizons

Silica-cemented horizons (dorbank (Soil Classification Working Group, 1991), equivalent to the ‘duripan’ of Soil Taxonomy (Soil Survey Staff, 1999) and ‘petroduric’ of the World Reference Base (1998) are present. These horizons slake in concentrated alkali, or if calcareous, alternating acid and alkali treatments. Horizons that slaked only in concentrated NaOH were interpreted to be silica-cemented and classified as ‘dorbank’. If they effervesced in HCl but slaked only in NaOH, they were classified as ‘calcareous dorbank’.

Their composition, micromorphology and genesis was discussed in more detail in Chapter 1. They can be 3 m and more thick, are generally very hard and very firm, have an average pH in water of 8.5, and an EC (of the same 1: 2.5 suspension) that ranges from 0.02 to 8.9 mS cm⁻¹ (Table 2.1). Horizons with high EC’s show localized dissolution. The dorbank horizons are generally brown (7.5YR 5/4) to yellowish-red (5YR 5/6) when dry and reddish-brown (5YR 4/4) to yellowish-red (5YR 5/6) when moist. The calcareous dorbank horizons are paler than their non-calcareous counterparts. The dorbank horizons in both profile AK1 (Table 2.1) and KV196T (Chapter 1) contain gypsum in cracks and in voids. In KV196T the gypsum was identified by SEM-EDX, also occurs as well crystalline nodules (pictured in Appendix A).

Sepiocrete and sil-sepiocrete intergrades

In this study, samples that effervesced in HCl but slaked only in NaOH were classified as calcareous dorbank. One sample (SK11/1), although locally effervescing vigorously in HCl, only slaked partially after alternating HCl and NaOH treatments. I initially classified it as siliceous calcrete (such as Watts (1980) and Nash and Shaw (1998)), because its colour and macroscopic appearance

are closer to the other calcrete samples than the other dorbank samples, and it occurred above a calcrete. Subsequent SEM studies (Chapter 1) showed that calcite does not play a role in the cement, and that the interlocking of fibres is dominant, suggesting sepiolite contributes to the cement, with localised silica. These ‘sepiocretes’ were discussed in more detail in Chapter 1.

2.4.5 Marine sediments

The marine sediments were broadly divided into an upper shoreface and lower shoreface facies, based on their bedding and particle size characteristics. The upper shoreface facies extends seaward from the low-tide level, comprising the breaker and surf zones. The onshore transport generates three-dimensional, lunate bedforms (megaripples), and larger bedforms. The coarsest sediment in the shallow-marine sequence is concentrated here (Pether, 1994).

The lower shoreface facies is deposited seaward of the breaker zone and its associated larger bedforms. It is subjected to oscillatory wave currents during fair-weather periods. Benthic organisms colonize the less routinely mobile sediment. Erosion and deposition in the lower shoreface take place mainly during and after storms. Hummocky cross-laminated, fine-sandy beds consisting of low angle, undulatory lamination in broad overlapping troughs and low hummocks are recognised as products of storm deposition at lower shoreface to offshore depths. The lower shoreface contains more bioturbated beds and a greater diversity of trace fossils than the upper shoreface (Pether, 1994).

The upper shoreface is on top of the lower shoreface facies on the Namaqualand coastal plain. This is consistent with deposition during sea level regression (Pether, 1994; Pether et al., 2000). Upper shoreface deposits are generally coarser than lower shoreface deposits, and have a redder hue. Vertical burrows filled with coarser sediment also have a slightly redder hue than surrounding sands. The coarser sediment may provide an opportunity for preferential flow, with a greater amount of interstitial space and more oxidation during dry periods. Nearby, iron pans (3 mm thick) in the finer sediment are also testament to the mobilization of iron. Probable hematite halos (comparable to those observed by Walker (1967)) are evident in pale yellow lower shoreface sands (Figure 2.7).



Figure 2.7: Probable hematite ‘haloes’ in lower shoreface sands, approximately 9m deep. Portion of hammer shown is 20cm long.

Upper shoreface sediments

These are generally yellowish-brown when dry (10YR 5/6), medium- to coarse sand with many gravel fragments and a weak- to moderate, coarse, angular-blocky structure. They are generally loose, non-plastic and non-sticky. The average pH in water is 8.35, and EC (of the same 1: 2.5 suspension) is 1.15 mS/cm (range 0.11 to 3.96 mS/cm, Table 2.1). The marine sands are non-calcareous, and often show large-scale bedforms. The upper shoreface ranges from 0.7 to 2 m thick in the profiles studied, but varies depending on the package (Pether, 1994; Pether et al., 2000).

Lower shoreface sediments

These are generally light-grey (10YR 7/1), pale-yellow (5Y 7/4) or light-yellowish-brown (10YR 6/4) when dry. Oxidation of glauconite-rich sediments resulted in some layers becoming a more orange colour (such as in profiles LKC1-5 and SNT60, Table 2.1). This was determined by oxidising green lower shoreface sediments with H_2O_2 , which then became a distinctly more orange colour. The average pH in water of lower shoreface sediments is 8.24, and the average EC (of the same 1: 2.5 suspension) is 0.97 mS/cm (range 0.05 to 2.87 mS/cm, Table 2.1). They are non-plastic and non-sticky, single-grain apedal, loose, non-calcareous medium sand which shows cross-lamination in places, and can contain abundant marine shells. In the profiles studied they are generally 12 m thick, but,

like the upper shoreface facies, the thickness varies depending on the package (Pether, 1994; Pether et al., 2000).

In one place, there appears to be illuviation (or precipitation) of white clay at the base of a much coarser layer within the fine pale sands. This coarser layer is much redder than the over- and underlying pale fine sands. The X-ray diffraction pattern of this coarser layer shows the presence of apatite in addition to smectite, kaolinite and mica. At the base of some profiles there appear to be silica-cemented layers. Some are also calcareous. The silica and Fe-oxide precipitation, and clay illuviation observed in the lower shoreface facies on the Namaqualand coastal plain correspond with Moody and Graham's (1994) observations in deep sands on marine terrace in central California.

Often, the marine deposits rest directly on bedrock. In some profiles the bedrock is highly weathered, deeply kaolinised 'pallid zone' (Partridge and Maud, 1987) on the order of 5 m thickness, which in some cases is associated with silcrete boulders. A silcrete-capping is associated with pallid zones in southern Africa (Partridge and Maud, 1987), these boulders are therefore likely to be remnants of the original silcrete capping. It occurs *in situ* near Kleinzee and Hondeklip Bay. Other profiles rest on kaolinized paleochannel sediments (18 m thick in profile 6869, see Table 2.1). These sediments were described in detail by Pether (1994), who concluded that they were laid down as a quartzo-feldspathic sediment in a fluvial environment, and subsequently deeply weathered, with extensive alteration of feldspar to kaolinite.

2.4.6 Biological activity

Evidence of biological activity is present at all levels in the regolith profile (Table 2.1), from the surface horizons with tunnels a few millimetres in diameter in the A and B horizons of to the deep marine sediments just above bedrock. It is difficult to determine whether burrows in the marine sediments were formed by marine fauna or by burrowing terrestrial organisms. In some cases the burrows have been calcretized, although the surrounding sediment is generally non-calcareous.

Tunnels

Calcrete horizons are extensively tunnelled, the tunnels are approximately 6mm-8mm diameter and a few centimeters long. In some cases the calcrete and deeper marine sediment contains larger tunnels (diameter approximately 10-15 cm). The dorbank horizons often contain 6 mm diameter borings and gypsum-filled voids (tunnels?).

Roots

Klappa (1980) distinguishes rhizoliths from faunal borings and burrows. They are abundant in calcretes and aeolianites of Quaternary age. The calcretized tunnels in sediment below a calcrete horizon in TP231L (Table 2.1) resemble roots and may be rhizoliths. Roots were identifiable in many profiles, up to 2 - 3 m deep (Table 2.1).

Termites

On the Namaqualand coast the heuweltjies are distinguishable on aerial photographs, and in some places may be buried by recent sands. There was also abundant evidence of termite activity in deep profiles. The age of the activity was not always clear, except in places where secondary silica and calcite had clearly replaced the nests or tunnels. A particularly well preserved example of a nest was present in the calcretized sidewall of SK11 approximately 1.7 m deep (Table 2.1; Figure 2.8).

In a mine excavation adjacent to an area with abundant heuweltjies (visible using Google Earth, 29° 30' 45" S, 17° 05' E), a strongly-cemented calcretized nest was present about 2 m deep within a silica cemented, locally calcareous dorbank profile (profile AK1, Table 2.1). It is nearly identical to the fossilised nests presented by Coaton (1981). Silica cementation of the soil surrounding the nest continues from about 30cm from the surface to below the hive (Figure 2.9). Unfortunately AK1 was truncated by mining processes. The clay content of the surface horizon (AK1/1 Table 2.1) suggests it is a B horizon (neocarbonate). This horizon has a redness rating (dry) of 6. This is in line with Group Aii in Table 2.2,



Figure 2.8: Profile SK11 (described in Table 2.1) with termite nest, 1.7 m deep below calcrete.

which suggests a pre-Last Glacial Maximum age for this neocarbonate B horizon. While the underlying dorbank and nest must be older than or contemporaneous with the neocarbonate B horizon, field relationships do not resolve the age of the nest relative to the dorbank. However, given the massive nature and the thickness of the silica cementation in the dorbank overlying the nest, it seems likely that the nest predates the silica cementation. This age is broadly consistent with the $\delta^{14}\text{C}$ ages of 25 000 to 30 000 years B.P. for calcrete associated with heuweltjies (further south) in the Clanwilliam and Elands Bay areas (Midgley et al., 2002), and the $32\,100 \pm 720$ years B.P. for the nearly identical fossilised nests from Clanwilliam presented by Coaton (1981).

As discussed in Section 2.4.3, what appear to be vertical termite burrows (J. Pether, pers. comm., February 2002) are observable for 3 m or more vertically in the marine sediments in sediments up to 12 m deep. They are distinguishable from the surrounding sediment by texture and colour differences (Figure 2.10) and appear in some cases to have acted as conduits for preferential flow from the surface (as in Figure 2.6). Stone and Comerford (1994) note that some African and central Asian desert and dryland termite species extend galleries to remarkable depths to reach free water, citing depths of 10 m to 70 m. As noted in the discussion on eluvial horizons, there were signs of wetness on the bedrock of SL4-1, and water coming out the regolith towards the base of 6869.

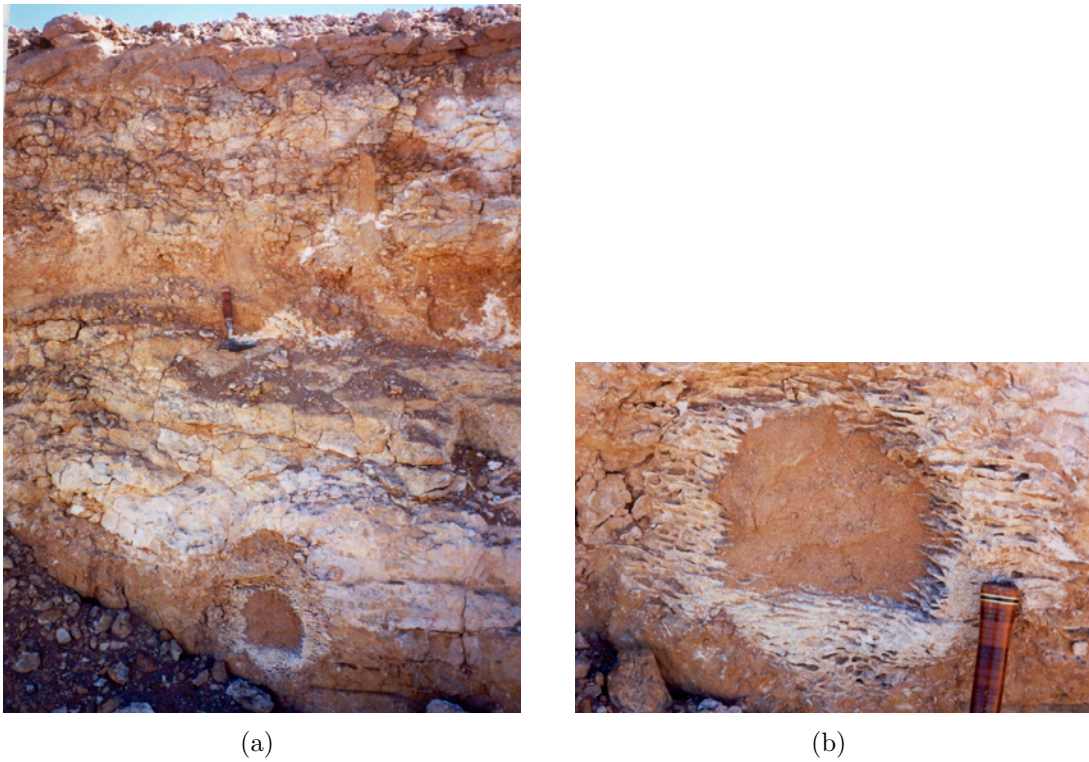


Figure 2.9: Profile AK1 (described in Table 2.1) with strongly-cemented, calcareous hive 2 m deep within dorbank. Hammer 30 cm long.

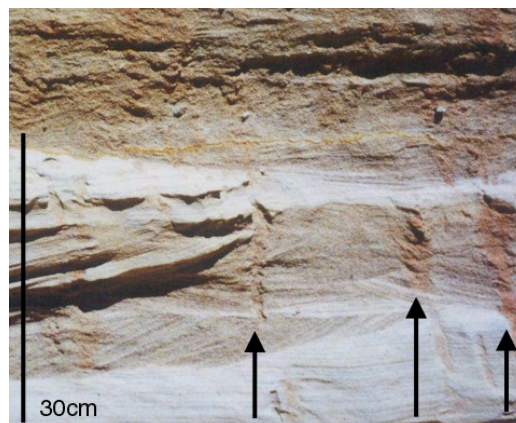


Figure 2.10: Possible vertical termite burrows (arrowed), now conduits for preferential flow in lower shoreface sands.

2.5 Conclusions

Soil formation on the Namaqualand coastal plain seems to be linked to periodic and episodic profile saturation that intrude the background of aridity. That evapotranspiration greatly exceeds precipitation is reflected accumulations of leachable salts such as halite and gypsum, and accumulations of calcite and silica. Soil formation and termite activity is at least as old as the Last Interglacial. E horizons may have formed in a wetter Last Interglacial paleoclimate, but they are still active in the present day. Evidence for this includes moist horizons above cemented barriers and water was observed flowing out of the regolith. This is consistent with the regular winter rainfall, and every 10 year flood events. Seems likely that during the periodic and episodic wet events that the formation of eluvial horizons takes place, and leachable salts are moved through the profile. These features remain metastable in the soil profile during intervening periods of aridity.

The surface soil horizons have generally formed from an aeolian parent material, and seem to follow either a calcareous or non-calcareous pedogenic pathway, perhaps depending on whether the original parent material was calcareous. The non-calcareous pathway leads to more clay-rich, redder apedal horizons that gradually show a stronger structure with depth, and generally rest directly on marine sands via a subtle discontinuity (as observed by Pether (1994)) that suggests pedogenesis continues through the profile into the marine facies. The clays appear to form predominantly in situ, since cutans are not obvious in the field. The lack of cutans may also be a result of the fairly low clay contents to begin with, however, and redistribution of clays within the profile is likely given the water movement through the profile. Further work on the micromorphology of the B horizons would help to confirm this. The calcareous pathway leads to similar clay-rich, redder apedal B horizons, but which differ in that they are calcareous, and rest on a calcrete horizon, often via a stoneline of rounded pebbles. The relatively low CaCO_3 in the aeolian sands dictates the pedogenic pathway in these deposits, and reddened neocarbonate and neocutanic horizons develop as the aeolian deposits age.

Deeper in the profile, there is generally a regular alteration of sedimentary units, such that the upper shoreface facies sediments show a degree of reddening, the lower shoreface sands have remained pale. This seems to be a function of the grain

size, since the upper shoreface materials are coarser due to their higher energy depositional environment, and the redder parts of the lower shoreface are also associated with slightly coarser sands. In some places oxidation of glauconite-rich sediments resulted in some layers becoming a more orange colour.

The Namaqualand coastal plain is well positioned for further work on its regolith, particularly because of the mining excavations which provide excellent exposures of well-defined layers of the regolith down to bedrock. The water-holding capacity of Namaqualand soils is surprising given that they are Aridisols (Francis et al., 2007), and suggests that a case could be made for their endemism (Bockheim, 2005). Some of the features which deserve further study are regular calcrete layers and fossils (marine, terrestrial) which have the potential for dating; the abundance of pedogenic carbonates which could lend themselves to techniques to reveal whether they have played a role in atmospheric CO₂ sequestration (Monger and Gallegos, 2000); evidence of deep/relict termite activity; dunefields overlying buried and truncated soils such as the well characterised Last Glacial dunefield north of the Swartlintjies. The identification and classification of the paleosols in the detail suggested by Nettleton et al. (2000) to reveal subtleties in past soil forming factors, could possibly offer some constraints on the climate conditions under which they formed.

Chapter 3

‘Pseudo-anticlines’ and biogenic features in sepiolite-containing calcrete in Namaqualand

3.1 Introduction

The Namaqualand coastal plain, with its extensive areas of calcrete development, is almost a textbook setting for calcrete development by inorganic processes: it is an area where the evaporation greatly exceeds precipitation; experiences inputs of marine aerosols due to strong onshore winds and the aggradation of calcareous regic sands (Chapter 2) similar to that described by Knox (1977) at Saldanha Bay. It also contains abundant ‘pseudo-anticline’ structures (pictured in (Francis et al., 2007)) which could be attributed to displacive growth of calcite and/or expandable clay minerals (Watts, 1977). There is an abundance of literature on calcrete, with many studies focussing on calcrete micromorphology (Allen, 1985; Monger et al., 1991a; Monger and Adams, 1996, to mention only a few) and it has been reviewed by authors such as Wright and Tucker (1991) and Alonso-Zarza (2003) and references therein. Notable work in southern Africa (Kalahari) includes Netterberg (1969) and Watts (1980), and recently work such as Nash and McLaren (2003).

Biogenic processes, are increasingly being seen as important to calcrete genesis: Phillips et al. (1987) suggested that just as fungal hyphae can stabilize macro-

aggregates in soils, the mineralized filaments may produce permanently stabilized macro-aggregates that provide the locus for further carbonate precipitation, leading to eventual induration. Monger et al. (1991) found that soil microorganisms were involved in calcite precipitation in desert soil near Las Cruces, New Mexico, and that where soil columns were irrigated with Ca-rich solutions, calcite only formed in soils containing soil microorganisms.

Folk (1993) suggested that bacteria and “nannobacteria” (sic) play an important role in catalyzing the precipitation of carbonate minerals. Loisy et al. (1999) noted that the originally organic micro-rods were transformed to calcite via a biomineralization process, which increased the CaCO_3 content of the primary matrix. Diagenetic evolution led to their recrystallization to microsparite, contributing to the hardening of soil layers as the micro- and nanoporosity were progressively filled.

Wright and Tucker (1991) reviewed the formation and characteristics of biotic and abiotic calcretes, and a review of the biogenic process in calcrete development is given by (Goudie, 1996).

This Chapter aims to describe the biogenic contribution to calcrete formation, following Knox's (1977) suggestion that a study of the semi-indurated parts of the profile could bring to light biogenic structures. In calcretes near Saldanha Bay on the west coast of South Africa, Knox (1977) observed that needle fibre calcite (“acicular networks”) and filaments (“tubules”) were associated with the semi-indurated zones in the profile. The strongly indurated zones consisted of cryptocrystalline calcite, and the beta-fabric features were no longer recognizable. This study particularly aimed to distinguish the biogenically acicular calcite from the similar-shaped clay minerals sepiolite and palygorskite using HCl-etching and EDAX analyses, since Singer et al. (1995, p. 65) questioned whether the biogenic calcite fibres described by Knox (1977) in calcretes near Saldanha Bay were indeed calcite, rather than sepiolite/palygorskite fibres. This study also aimed to determine whether the pseudo-anticline structures could be attributed to displacive growth of calcite and/or expandable clay minerals, as speculated by Francis et al. (2007).

3.2 Materials and methods

A subset of samples (calcrete and calcareous nodules) was selected from those described in (Chapter 2). The calcrete samples are SNT60/5A; SPNT/4; OBT/4; TP266Q/1 and calcite nodules (calcite-cemented sand) approximately 3 cm in diameter from neocarbonate B horizons 6869/iii and 6869/iv. The locations and profile descriptions are shown in Chapter 2, Figure 2.2 2 and Table 2.1 respectively. The profiles are pictured in Appendix A.

Namaqualand, particularly the coastal part that was the focus of this study, is a region that experiences an extremely high evaporation rate (about 2 m per year) and less than 150 mm annual winter rainfall, supplemented by regular fog occurrences (Eckardt and Schemenauer, 1998; D.B.C.M., 2000; Olivier, 2002). Crucially for both plant growth and water movement through the soil, the climate is characterised by highly reliable rainfall when compared to other arid regions with similar mean annual precipitation (Desmet, 2007). It typically arrives as widespread, gentle showers (average rainfall event 6 mm, P. Carrick unpublished data, cited by Desmet (2007)). Drought conditions are rare, and rainfall is higher than average about once every 10 years, causing ephemeral rivers to flow. Paleoclimates of the northern Namaqualand region are not that well constrained, but the consensus for the greater area seems to be that it was wetter during the Last Glacial (Van Zinderen Bakker, 1976; Tankard and Rogers, 1978; Parkington et al., 2000). A more detailed summary of the landscape, (paleo)climate and vegetation is given by Desmet (2007) and in Chapters 1 and 2.

Uncoated fragments and thin sections were observed before and after etching in 1M HCl using low vacuum SEM-EDX with a Philips Xl30 ESEM. High vacuum SEM was done on Au-coated fragments using a Leo 1430VP SEM-EDX system. Thin sections for optical microscopy were impregnated with an epoxy resin, and ground without water. For XRD analysis of the carbonates and cutans, an air-dried fragment was ground in an agate pestle and mortar and analysed as a powder. For XRD analysis of the clay fraction, the bulk samples were air-dried, crushed and passed through a 2 mm sieve. To minimize shattering of pebbles/gravel, the >2 mm cement was sorted from the >2 mm pebbles and recrushed. Selected samples were milled and treated with a pH 5 sodium acetate buffer for a short time (following the findings of Vanden Heuvel, 1964) until effervescence ceased, and then concentrated by centrifugation. This was

repeated with fresh solution until there was no more effervescence. The $<2 \mu\text{m}$ fraction was separated by dispersion (shaking briefly by hand, raising the pH to approximately 10 with Na_2CO_3) and settling. The clay suspension was flocculated by the addition of MgCl_2 , after lowering the pH to 5 to 7 with HCl to prevent the precipitation of brucite and/or clay destruction. The clay suspension was then Mg- or K-saturated, concentrated by centrifugation, and sedimented (or smeared, many of the sepiolite-rich samples developed ‘mudcracks’) onto a glass slide. XRD analyses were done using a stepsize of 0.05 degrees and step-time of 40 seconds, using a Bruker D8 Advance Powder Diffractometer with a graphite monochromator, 40 kV and 40 mA. Ethylene glycol was sprayed lightly onto the surface of the Mg-saturated sample slides.

3.3 Results and discussion

3.3.1 Composition

Carbonates

The dominant carbonate mineral in the calcretes is calcite (Figure 3.1). Dolomite appears to be absent. Calcite in the clay fraction shows a very small shift towards magnesian calcite (Figure 3.2). Both SPNT and SNT60/5A have the calcite peak at 0.3023 nm. This yields a 0.037 mole fraction MgCO_3 in the calcite following the calculation $Y = 0.3033 - 0.0271 X$, where Y is the $d(211)$ in nanometres (Doner and Lynn, 1989).

The 0.326 nm peak (well-developed in SPNT/4 and to a lesser extent in SNT60/5a) is somewhat of an enigma. It could be attributed to aragonite (0.327 nm, intensity = 52, JCPDS card 05-0453 from Doner and Lynn, 1989), with the 0.34 nm aragonite peak (intensity = 100) overlapping that of quartz (JCPDS card 05-0490 Drees et al., 1989), but the 0.198 nm (intensity = 65) and other aragonite peaks are absent. The 0.326 nm peak is absent from the clay fraction in both of these samples, although calcite is present (Figure 3.2). If authigenic aragonite were present, it should occur together with calcite in the clay fraction too. Since the material used to determine the nature of the carbonates and to extract the clay fraction were obtained from different pedes, a possibility is that an aragonitic

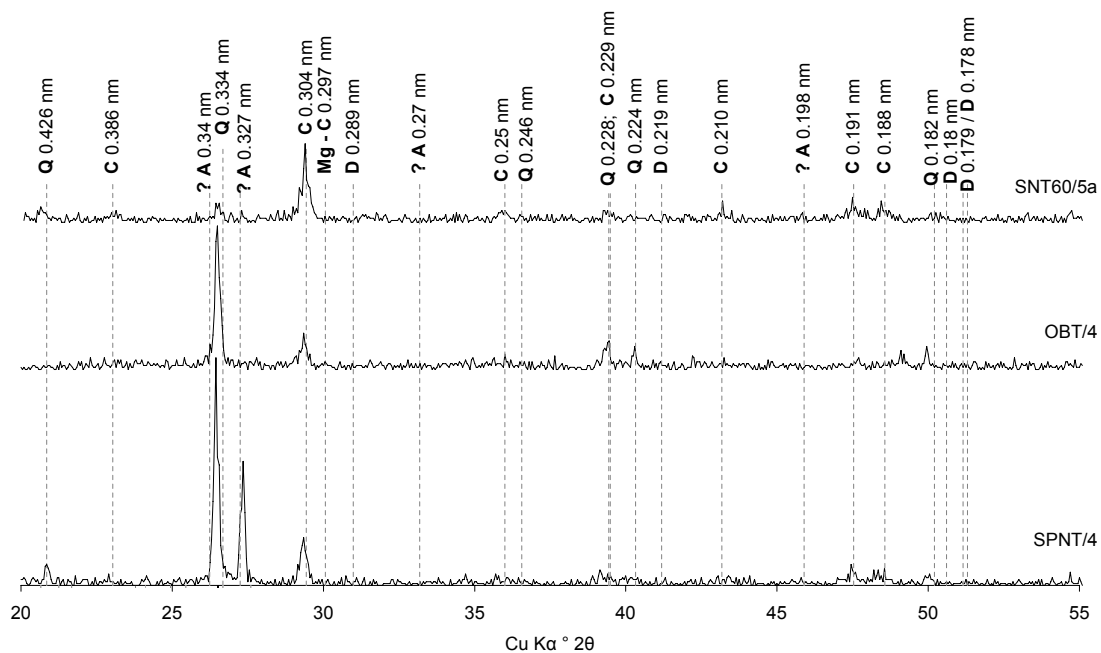


Figure 3.1: Carbonates in calcrete: XRD traces of crushed, bulk samples. Mg-C: Mg-carbonate. Carbonate peaks: Doner & Lynn (1989); quartz: Drees et al. (1989). A: aragonite (JCPDS card 05-0453); C: calcite (JCPDS card 05-0586); D: dolomite (JCPDS card 11-0078); Q: quartz (JCPDS card 05-0490).

shell fragment was present in the ped crushed for bulk XRD analysis, but not the ped from which clays were extracted. Other contenders for the 0.326 nm peak are titanate (0.325 nm, JCPDS card no. 73-2066) and zircon (0.328 nm, JCPDS card no. 83-1379), both present in the heavy mineral fraction of the marine sands (Pether, 1994). A possible reason for their presence in the bulk trace but not the clay fraction, could be that their greater specific gravity caused them to settle faster than the clay particles and so not be extracted with the clay fraction.

Clays

The clay fraction of coastal Namaqualand calcretes is dominated by sepiolite and contains varying amounts of kaolinite, palygorskite and mica (Figure 3.2). Mica is likely to be detrital, given the abundance of it in the lower shoreface facies (see Chapter 2) and that it is a common component of the bedrock in the region.

The decrease of the 1.2 nm peak in TP266Q/1 and the increase of the 1.04 nm peak on heating is consistent with sepiolite (Hayashi et al., 1969). These

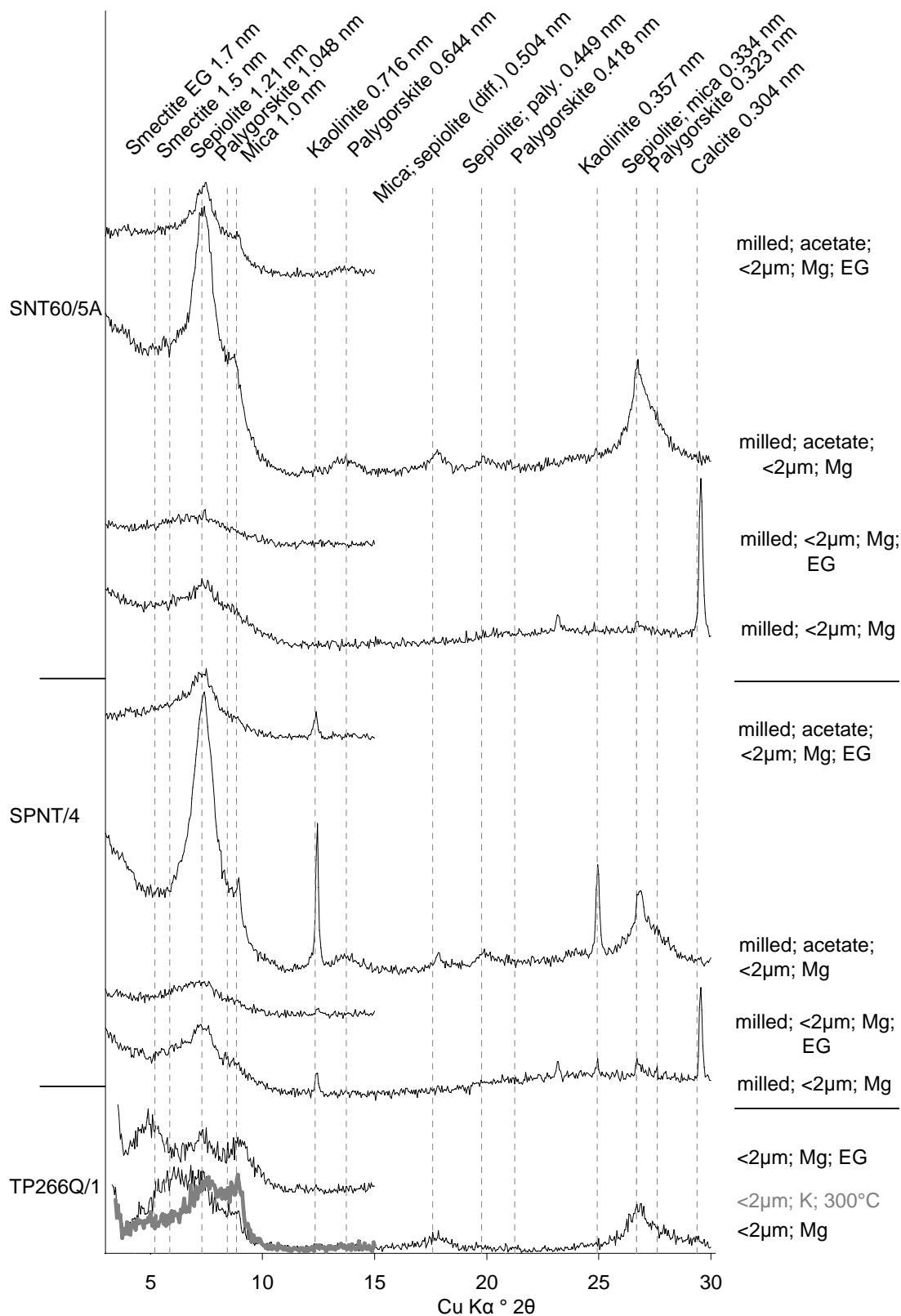


Figure 3.2: XRD traces of the clay fraction from 3 calcretes. Calcite (JCPDS card 05-0586, Doner & Lynn, 1989); kaolinite (Dixon, 1989); mica (Fanning et al., 1989); palygorskite (Bradley, 1940; Christ 1969); sepiolite (Brindley, 1959). Diff.: diffuse; EG: ethylene glycol; paly.: palygorskite.

peak positions overlap with palygorskite and mica, but the heated trace does show a small increase in the 0.94 nm region (Van Scoyoc et al., 1979), suggesting some palygorskite is present even though the 0.644 nm palygorskite peak is absent. This is consistent with the clay mineralogy of other southern African calcretes (Netterberg, 1969; Watts, 1980). Sepiolite and palygorskite are present in Namaqualand soils, with sepiolite dominant in the coastal areas (Singer et al., 1995). Hay and Wiggins (1980) found sepiolite to be the most common clay mineral associated with calcretes in the southwestern USA, and palygorskite was notably absent.

Although the <2 mm samples were milled before acetate treatment to liberate calcite-cemented clays, the clay peaks are substantially enhanced after the acetate treatment (Figure 3.2). The difference is most noticeable with palygorskite, and consistent with Vanden Heuvel's (1964, p. 201) observation that palygorskite showed "greater immobilization" by the calcite aggregates than sepiolite.

Many of the calcretes show sepiolite cutans around the blocky peds, evident in the field by their non-effervescence with HCl and by turning methyl orange pink (Mifsud et al., 1979). An XRD trace of a typical cutan (Figure 3.3) shows sepiolite, quartz and calcite. The sepiolite peak is broad, and it extends into the palygorskite peak zone of 1.048 nm, but the presence of a small amount of palygorskite is suggested by small 0.644 and 0.323 nm peaks.

Watts (1980) noted an inverse relationship between the mol % MgCO_3 in calcite and the sepiolite/palygorskite content, which suggested that these Mg-rich clay minerals were the main Mg-bearing phase in Botswana calcretes. The apparent absence of Mg-calcite and dolomite, and abundance of sepiolite in the calcretes of coastal Namaqualand suggests a similar partitioning has occurred.

3.3.2 Morphology and micromorphology

'Pseudo-anticlines'

Some profiles show 'pseudo-anticline' features (Watts, 1977), pictured in Francis et al. (2007). These may be attributed to both the displacive growth of calcite and expansion of clay minerals (Watts, 1977; Wright and Tucker, 1991). A blocky structure and accommodating planes in calcrete sample TP266Q/1 (Fig-

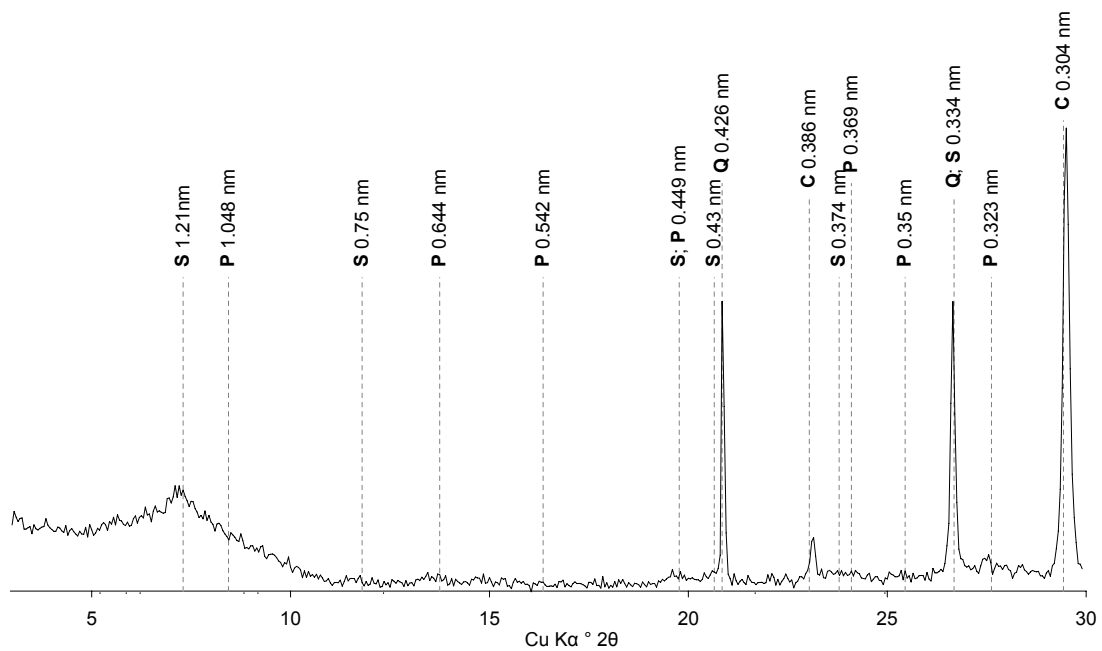
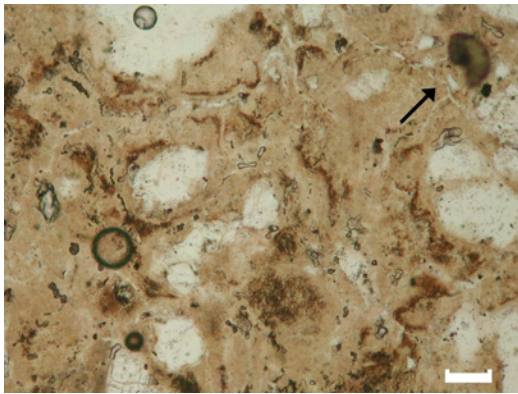


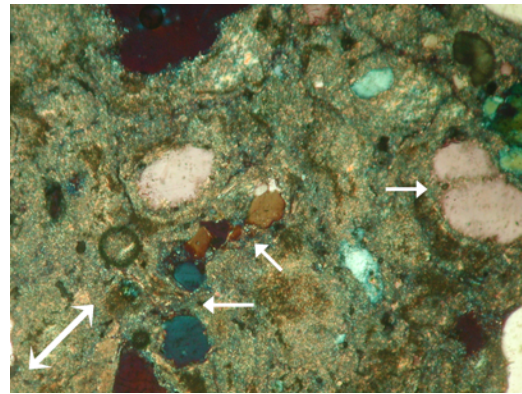
Figure 3.3: XRD trace of sepiolite cutan on calcrite (OBT/4), powdered bulk sample. C: calcite (JCPDS card 05-0586, Doner & Lynn (1989)); P: palygorskite (Bradley, 1940; Christ 1969); S: sepiolite (Brindley, 1959) Q: quartz (JCPDS card 05-0490, Drees et al., 1989).

ures 3.4(a), (b)) suggest shrink/swell behaviour has occurred, and is consistent with presence of smectite in the clay fraction of TP266Q/1 (Figure 3.2), although the ‘diapiric anticlines’ that Watts (1977) attributed to the upward injection of swelling clays were not present. Volumetrically, the displacive calcite appears to be more significant than the shrink/swell behaviour represented by the accommodating planes.

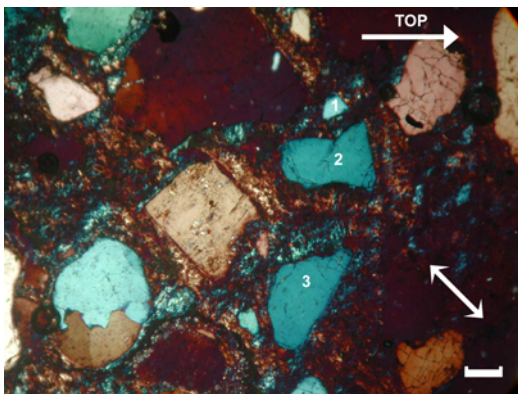
Clay neoformation/illuviation may also contribute to displacement and folding via an increase in volume in a similar manner to displacive calcite, rather than via a shrink/swell mechanism. Clay coatings almost completely fill the intergrain spaces after the calcite is removed, including spaces between a fractured quartz grain (Figure 3.4(c)). This is consistent with Pether’s (1994) observations that the soluble carbonate content (acid digestion) is only 3% and the host material is a muddy sand. The oriented nature of these coatings suggests they are illuvial in origin, although according to Ranson and Bidwell (1990, in Wright and Tucker, 1991), clay coatings in calcareous soils may have formed through stress rather than illuviation.



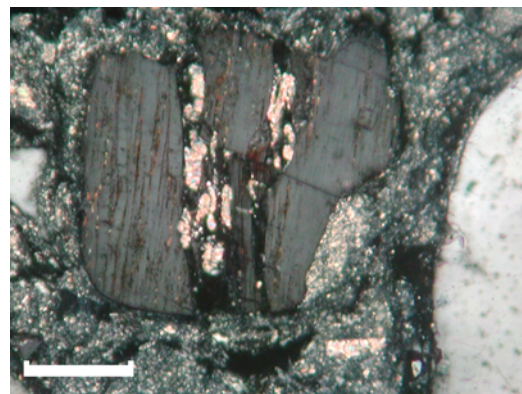
(a) Accommodating planes (arrowed). Scale bar 0.1 mm, ppl.



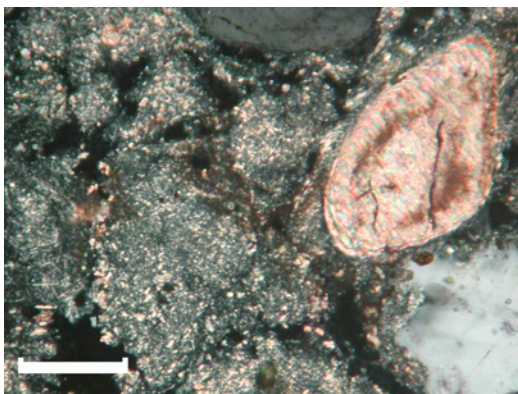
(b) Same as (a). Micrite displacing fractured quartz grains along fractures. Xpl, λ plate, fast direction indicated.



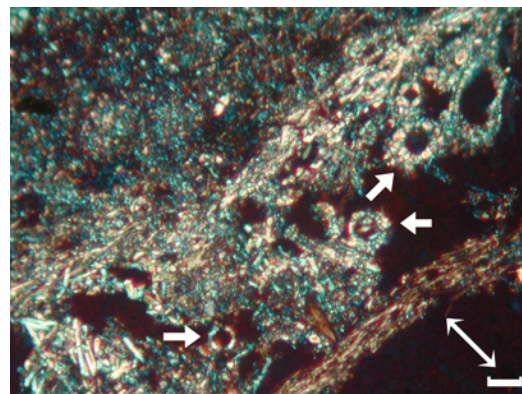
(c) HCl-etched. Orientated clay matrix; fractured quartz grain (1-3). Scale bar 0.1 mm, xpl, λ plate, fast direction indicated.



(d) Calcite displacing feldspar grain along cleavage planes. Scale bar 0.1 mm, xpl.



(e) Calcite replacing ferro-magnesian mineral (pyroxene); embayed quartz grain. Scale bar 0.1 mm, xpl.



(f) Needle fibre calcite and mineralized filaments (arrowed, cross-section) with radial length-fast (?) calcite/oxalate, lining void. xpl, λ plate, fast direction indicated. Scale bar 0.02 mm.

Figure 3.4: Displacive, replacive and needle fibre calcite; clay textures in calcrete TP266Q/1.

Both displacive and replacive calcite are present. Displacive calcite is dominant (Figures 3.4(b), (d)), resulting in a ‘floating fabric’ (Watts, 1978), represented in this sample by a close porphyric c/f-related distribution (Stoops, 2003). As noted by Watts (1978), replacement appears to be of a ferro-magnesian mineral, the shape of which suggests pyroxene (Figure 3.4(e)). Both the embayed quartz grain and the calcite pseudomorph (Figure 3.4(e)) suggest silicate dissolution has also occurred in the profile, although to a lesser extent. Reheis et al. (1992) found that pedogenic calcite both displaced and replaced grains in sediments of the Kyle Canyon alluvial fan, southern Nevada.

In Buczynski and Chafetz’s (1987) model, calcite crystals in the vadose zone precipitate from a supersaturated solution that is not being constantly replenished, forming rapidly at grain contacts as the last fluid dries. This crystallization is too rapid to be accommodated by pressure solution and the interpenetration of quartz grains. Consequently, the ‘rapid’ build-up in stress is released by grain fracturing. This is consistent with much of sample TP266Q/1, with the abundant evidence of grain shattering and the micrite suggesting rapid crystallization. Chadwick and Nettleton (1990, in Wright and Tucker, 1991) attributed displacive fabric features in calcretes to calcite crystals preferentially forming cohesive bonds with other calcite crystals, thereby displacing non-carbonate grains.

Biogenic fabric

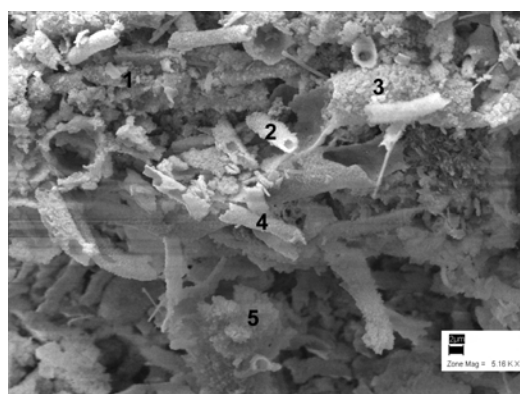
The typical abiotic alpha-fabric features (Wright and Tucker, 1991) dominate the mature calcrete horizon TP266Q/1 (Figure 3.4). Biogenic beta-fabric features (needle fibre calcite, mineralized filaments) are present, but to a lesser degree. They are, however, dominant in calcite-cemented nodules from a calcic B horizon (6869/iii and 6869/iv) above calcrete (Figure 3.5).

Figure 3.4(f) shows the cross-section through mineralized filaments in a void in a mature calcrete horizon (TP266Q/1). They appear to comprise a radially-oriented, length slow mineral with high birefringence, and are closely associated with needle fibre calcite. They are consistent with the morphology of fungal filaments found by Phillips et al. (1987) and Verrecchia et al. (1993). Mineralized filaments dominate the fabric of calcite-cemented nodules from a calcic B horizon above a calcrete (Figure 3.5).

Verrecchia et al. (1993) found that filament coatings were predominantly calcium oxalate. Their analyses showed oxalate to have a C/Ca ratio of about 1, with calcite having a much smaller C/Ca ratio. The C/Ca ratio of filaments in Figure 3.5(a) (analyses 2-4, Figure 3.5(b)) suggests calcium oxalate in the coating, whereas the non-filament matrix (analyses 1 and 5) are micrite. Non-mineralized filaments (Phillips et al., 1987) and nanobacteria (Folk, 1993; Folk, 1999) are also present (Figures 3.5(c), (d)). Verrecchia et al. (1993) attributed the filaments in a calcrete from Israel to fungi, since they occurred in an environment without light, eliminating the involvement of photosynthetic microorganisms like cyanobacteria and algae. This also seems a reasonable assumption to make for the Namaqualand samples. Folk (1993) argued convincingly against modern contamination of the sample, and provided many examples for nanobacteria in calcretes (Folk, 1999).

Needle fibre calcite (Figure 3.5(e), (f)) is present as the MA(2), MAB, and MB rod forms of Verrecchia and Verrecchia (1994), who concluded that MA rods are of biological origin which can be attributed to calcite precipitation in the interior of fungal mycelian bundles, which are then released and redistributed in the soil following the decay of the organic matter. MB rods form after the release of MA rods; their serrated plates are a secondary syntactic growth of CaCO_3 of physico-chemical origin on an MA skeleton. The monocrystalline M micro-rods are much smaller than MA rods (0.5 - 1 μm), and have an ambiguous origin related to either physico-chemical nuclei or calcified bacteria; they are commonly associated with gels or organic material and do not appear to evolve toward larger or more complex morphologies (Verrecchia and Verrecchia, 1994). Loisy et al. (1999) recognised the micro-rods as bacilliform and threadlike bacteria, which mineralize into calcite, forming micro-rod mats and can form clusters and micritic platelets. In Figure 3.5(d) M micro-rods are seen covering needle fibre calcite; this relationship is also present in calcrete in Israel (Verrecchia and Verrecchia, 1994, p. 657) and a calcrete paleosol in France (Loisy et al., 1999, p. 198).

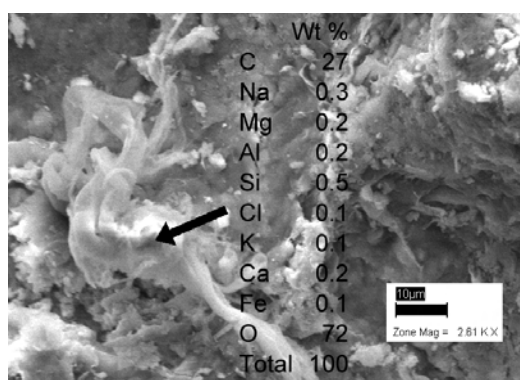
The analysis of the fibrous mat under the nanobacteria (Figure 3.5(d)) suggests that it is not calcite. The morphology of the M micro-rods is very similar to that of the fibrous clay minerals sepiolite and palygorskite, which are abundant in calcretes on the Namaqualand coastal plain (Figures 3.2 to 3.3). The $<1 \mu\text{m}$ clay fraction of this sample is dominated by sepiolite, with less intense palygorskite, smectite, kaolinite and possibly illite (Chapter 4), therefore it seems likely that



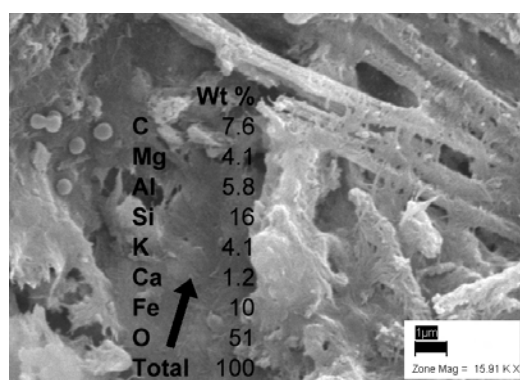
(a) Micrite and Ca-oxalate covered filaments. Scale bar 2 μm . Au-coated.

Wt %	1	2	3	4	4	5
C	14	21	19	19	19	17
Mg			1.4	0.7	0.8	
Ca	34	16	20	22	20	28
O	51	63	60	59	60	55
Total	100	100	100	100	100	100
C/Ca	0.4	1.3	1.0	0.9	1.0	0.6

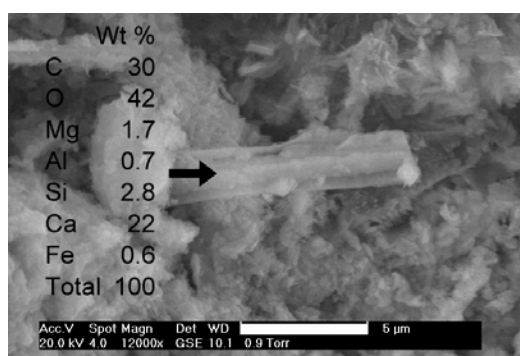
(b) EDAX analyses of areas indicated in (a)



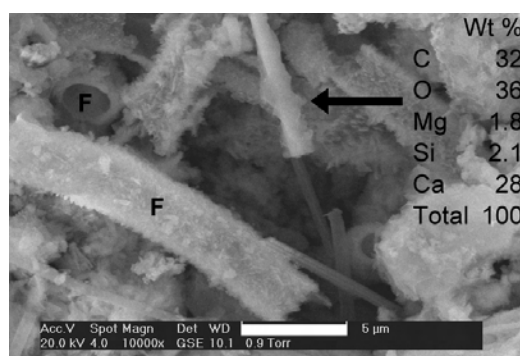
(c) Collapsed, non-mineralized filament. Scale bar 10 μm . Au-coated.



(d) Nannobacteria (left) on fibrous clay mineral mat (analysis arrowed); M micro-rods covering MA needle-fibre calcite (top right). Scale bar 1 μm . Au-coated.



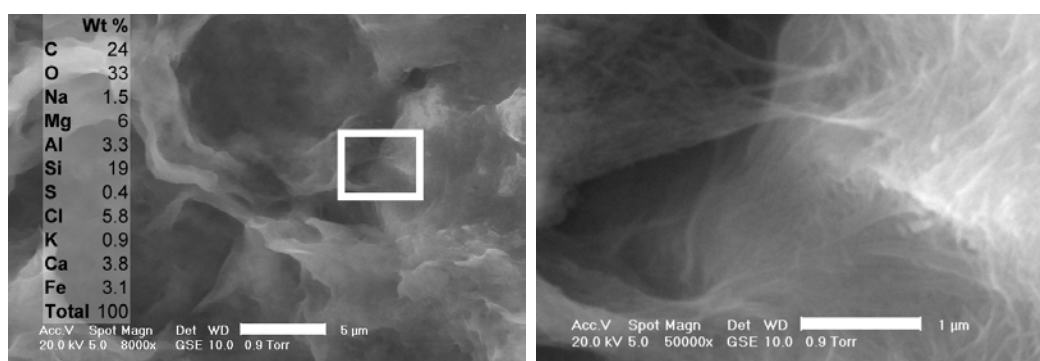
(e) Needle fibre calcite: MAB rod. Scale bar 5 μm . Uncoated.



(f) Mineralized filaments (F); needle fibre calcite: MA rods (MA2 rod (bottom)), MB rod (arrowed). Scale bar 5 μm . Uncoated.

Figure 3.5: SEM images: Biogenic calcite from calcite nodules in 6869/iii and /iv, calcic B above a calcrete. Needle fibre calcite classified according to Verrecchia and Verrecchia (1994, further details in text). Images (a)-(d) collected at University of Stellenbosch, (e), (f) at University of Kwazulu-Natal.

the mat is in fact interwoven (predominantly fibrous) clay minerals. Further evidence for the association of sepiolite/palygorskite with the organic structures is in Figure 3.6. The samples with mineralized filaments and needle fibre calcite from Figure 3.5 were etched in 1M HCl. The micrite, needle fibre calcite and mineralized filaments dissolved (Figure 3.6(a)), and revealed the fibrous clay minerals (Figure 3.6(b)). The composition of the area is consistent with the HCl-etched calcite/oxalate and the clay fraction described above. The large proportion of Mg and Si is consistent with the predominant sepiolite.



(a) Mineralized filament, partially dissolved. (b) Magnification of area indicated in (a).
Scale bar 5 μm . Scale bar 1 μm .

Figure 3.6: 6869/iii, from Figure 3.5 after etching for 15 seconds with 1M HCl.

3.4 Conclusions

The clay fraction of coastal Namaqualand calcretes is dominated by sepiolite, with varying kaolinite, palygorskite and detrital mica contents. The clay fraction is closely associated with calcite: although the <2 mm samples were milled before acetate treatment to liberate calcite-cemented clays, all the clay peaks are substantially enhanced after the acetate treatment. The difference is most noticeable with palygorskite, which is in some cases only detectable after acetate treatment. The apparent absence of Mg-calcite and dolomite, and abundance of sepiolite in the calcretes of coastal Namaqualand suggests that this Mg-rich clay mineral is the main Mg-bearing phase.

Deformation (pseudo-anticlines) in the calcrete appear to result primarily from the displacive effect of calcite crystallization. Although evidence of shrink/swell

behaviour is present in the form of accommodating planes, it does not appear to be as volumetrically significant as displacive calcite. Clay minerals are closely associated with the displacing calcite, suggesting that clay neoformation/illuviation may contribute to displacement and folding, but calcite crystallization seems to be mainly responsible for opening fractures.

Both biotic and abiotic factors contributed to calcrete formation, although abiotic alpha-fabric seems dominant in the mature calcrete horizon, and beta-fabric in calcareous nodules in a calcic B horizon above calcrete.

There is evidence for the association of sepiolite/palygorskite with the organic calcite structures. Since the micromorphology of acicular calcite can sometimes resemble the acicular clay minerals sepiolite or palygorskite, EDAX analyses and HCl-etching is necessary to distinguish the two. In this system, the distinction is made easier by the fact that sepiolite (and to a lesser extent palygorskite) are the main Mg-bearing phases, since the XRD analysis revealed the main carbonate phase in the calcretes is low-Mg calcite.

Chapter 4

Clay mineral occurrences in Aridisols on the west coast of South Africa (Namaqualand)

4.1 Introduction

Namaqualand is an arid region of low agricultural and habitation density, and so information on the soils and their clay mineralogy is sparse in comparison to other areas in South Africa. The Namaqualand coastal plain experiences an extremely high evaporation rate (about 2 m per year) and less than 150 mm annual winter rainfall that is supplemented by regular fog occurrences (Eckardt and Schemenauer, 1998; D.B.C.M., 2000; Olivier, 2002). Namaqualand has recently become the focus of an increasing amount of biodiversity and ecological research (ranging from publications such as Cowling and Pierce, 1999; to a Special Issue of the *Journal of Arid Environments*, 2007). Rehabilitation efforts after the hundred or so years of mining, coupled with the increasing interest in ecology and biodiversity, has prompted a recognition of the soils as a substrate for plant growth and has motivated studies such as those by Prinsloo (2005), Francis et al. (2007) and Chapter 2.

It is this arid climate which has allowed the formation of large amounts of the relatively rare soil clay minerals sepiolite and palygorskite. Singer et al. (1995) studied the mineralogy of Namaqualand soils from the Land Type survey (Land

Type Survey Staff, 1987), and found that palygorskite dominated the soils inland of the escarpment whereas sepiolite was more prominent in the clay fraction of soils from coastal areas due to marine-influenced elevation of magnesium levels. Chapter 1 reported occurrences of ‘sepiocrete’ in Namaqualand, horizons which appear to be cemented by sepiolite. Sepiolite and palygorskite are often reported from arid region soils and are commonly found in calcretes (Vanden Heuvel, 1964; Singer and Norrish, 1974; Yaalon and Wieder, 1976; Elprince et al., 1979; Hay and Wiggins, 1980; Singer and Galan, 1984; Singer, 1989; Blank and Fosberg, 1991; Monger and Daugherty, 1991; Verrecchia and Le Coustumer, 1996; Singer, 2002; Neaman and Singer, 2004; Owliaie et al., 2006), southern African examples of which are described by Netterberg (1969) and Watts (1980). Sepiolite is considered to be rarer in the pedogenic environment than palygorskite (Singer and Galan, 1984; Singer, 1989; Singer, 2002), although Hay and Wiggins (1980) found sepiolite to be the most common clay mineral associated with calcretes in the southwestern USA with palygorskite notably absent.

Kerolite is a hydrated and disordered talc-like mineral ($\text{Mg}_3\text{Si}_4\text{O}_{10}(\text{OH})_2 \cdot n\text{H}_2\text{O}$) with a basal spacing of 0.96 nm, giving a broad diffraction peak at 1.0 nm (Brindley et al., 1977) that is sometimes found with sepiolite and other Mg-rich clay phases. Kerolite and randomly interstratified kerolite-stevensite have been reported to occur with sepiolite (Eberl et al., 1982; Khoury et al., 1982; Hay et al., 1986; Martin De Vidales et al., 1991, among others). Both Stoessell (1988) and L veill  et al. (2002) suggested that the inherent difficulties in its identification (poor crystallinity and XRD peak overlap with other phases) in mixed mineral assemblages means it could be overlooked. In spring-related deposits in the Amboseli Lake Basin on the Kenya-Tanzania border, kerolite appeared often to have had a sepiolite precursor, and may have formed as weathering product during a lowering of pH (Stoessell and Hay, 1978; Hay and Stoessell, 1984). Its stability field is close to that of sepiolite (Stoessell, 1988). Since sepiolite is so abundant in Namaqualand soils, there is a possibility of kerolite occurring too, particularly in the fine clay fraction due to the fine, disordered nature of kerolite (Brindley et al., 1977; Pozo and Casas, 1999). It has not yet been recorded from a pedogenic environment.

The aims of this Chapter were to evaluate the effect of pretreatments on the sepiolite and palygorskite peaks; concentrate kerolite if present; examine the clay mineral associations throughout the profile including the marine parent materi-

als to establish which phases are inherited; and to examine the morphology and modes of occurrence of the fibrous clay minerals in Namaqualand soils, especially for evidence of disintegration or transformation into sheet silicates, since Singer et al. (1995) concluded that the sepiolite and palygorskite in their study were in a state of disintegration or transformation into sheet silicates. This study is relevant to the growing body of literature on sepiolite and palygorskite occurrences, particularly the issue of neof ormation and transformation, that has appeared since the findings of Singer et al. (1995) were published (Torres-Ruíz et al., 1994; Sánchez and Galán, 1995; Lopez-Galindo et al., 1996; Jamoussi et al., 2003; Zaaboub et al., 2005).

4.2 Materials and methods

For analysis of the clay fraction, a subset of 43 samples was selected from those described in Chapter 2. These were selected to be representative of the horizon types encountered. Sampling was done on the Namaqualand coastal plain, in two of the mining areas belonging to De Beers Consolidated Mines Ltd - Namaqualand Mines. These are the Buffels Marine Complex (BMC) in the Kleinzee-Port Nolloth area, and the Koingnaas Complex (KNC) further south in the Koingaas-Hondeklip Bay area. The location of the study area overlaps with the north-western coastal area of the region studied by Singer et al. (1995), an area where they found sepiolite to be dominant. These soils can be classified into the Aridisol and Entisol orders of Soil Taxonomy (Soil Survey Staff, 1999). The clay mineralogy of the dorbank (petroduric) and “sepiocrete” horizons was presented in Chapter 1, and the clay mineralogy of calcretes on the Namaqualand coastal plain was presented in Chapter 3. Profile descriptions and sampling details of the samples used in this Chapter are in Chapter 2. A summary of the landscape, climate and vegetation is in Desmet (2007) and Chapter 2. Profile photographs are presented in Appendix A.

The parent material comprises successive late Tertiary marine packages, each deposited during sea-level regression (Pether, 1994). The marine packages are arranged *en echelon* down the bedrock gradient, from oldest and highest inland to youngest and lowest at the coast. Each package is named after the elevation of its transgressive maximum as represented in the Hondeklip Bay area (Pether,

1994; Pether et al., 2000). The 90 m package is ca. 18 - 16 Ma, the 50 m package early Pliocene, and the 30 m package not well constrained, but ca. 3.3 Ma or younger (Pether et al., 2000). The 30 m package is transgressed by younger littoral deposits up to about 10 m a.m.s.l. (Pether et al., 2000). The sand fraction is dominated by quartz and feldspar, lesser glauconite and phosphatic shell fragments, and variable amounts of heavy minerals (garnet, magnetite, ilmenite, biotite, sphene, amphibole, epidote, kyanite (rare) and zircon (rare)) (Pether, 1994). The marine packages are capped by recent aeolian deposits. Coastal dunefields originate at the mouth of the rivers and extend inland in a northerly direction. In places, older soil profiles are overlain by aeolian sands. Soil formation has taken place in aeolian, 'sheetwash', and marine-deposited sediments.

Some of the marine sediments rest on kaolinized paleochannel sediments, described in detail by Pether (1994), who concluded that they were laid down as a quartzo-feldspathic sediment in a fluvial environment, and subsequently deeply weathered, with extensive alteration of feldspar to kaolinite. These channel sediments are described in greater detail by Tankard (1966), Tankard (1975), Pether (1994), and Pether et al. (2000). De Villiers and Cadman (2001) favoured an early Tertiary age for this channel north of the Swartlintjies River, although it may also contain reworked Cretaceous material (Pether et al., 2000; De Villiers and Cadman, 2001).

Uncoated fragments and thin sections were observed before and after etching in 1M HCl using low vacuum SEM-EDX with a Philips Xl30 ESEM. High vacuum SEM was done on Au-coated fragments using a Leo 1430VP SEM-EDX system. For XRD analysis of the clay fraction, the bulk samples were air-dried, crushed and passed through a 2 mm sieve. To minimize shattering of pebbles/gravel, the >2 mm cement was sorted from the >2 mm pebbles and recrushed. To compare the effect of milling and acetate pretreatments, selected samples were also milled for 5 minutes using a stainless steel ball mill, and then treated with a pH 5 sodium acetate buffer for a short time (following the findings of Vanden Heuvel, 1964) until effervescence ceased, and then concentrated by centrifugation. This was repeated with a fresh pH 5 sodium acetate buffer solution until no further effervescence was observed in the sample. The <2 μm fractions of the (a) sieved, (b) milled, and (c) milled and acetate-treated subsamples were then separated by dispersion (shaking briefly by hand, raising the pH to approximately 10 with

Na₂CO₃) and settling. The 1 to 0.08 μm and $<0.08 \mu\text{m}$ fractions were separated by centrifugation from the $<2 \mu\text{m}$ fraction. The clay suspension was flocculated by addition of MgCl₂ after lowering the pH to 5 to 7 with HCl to prevent the precipitation of brucite and/or clay destruction. The clay suspension was then Mg-, Ca- or K-saturated, concentrated by centrifugation, and sedimented (or smeared, many of the sepiolite-rich samples developed ‘mudcracks’) onto a glass slide. XRD analyses were done with a stepsize of 0.05 degrees and steptime of 40 seconds, using a Bruker D8 Advance Powder Diffractometer with a graphite monochromator, 40 kV and 40 mA. Ethylene glycol was sprayed lightly onto the surface of the Mg-saturated sample slides. After analysis, the ethylene glycollated 1 to 0.08 μm and $<0.08 \mu\text{m}$ samples were allowed to remain under ethylene glycol for 10 weeks, and then re-analysed to allow comparison to the findings of Brindley et al. (1977), Hay et al. (1995) and Léveillé et al. (2002) for kerolite. For samples where glycerol was used, it was by gaseous diffusion. NaN₃ was added to the 1 to 0.08 μm and $<0.08 \mu\text{m}$ suspensions as a bactericide during storage. TEM-EDX analyses of clay fractions were done using a Philips CM120 Biotwin equipped with EDX detector. Total chemical analysis was done on the Mg- and K-saturated clay fractions, using fused glass beads in a Philips 1404 Wavelength Dispersive XRF spectrometer, fitted with a Rh tube.

4.3 Results and discussion

4.3.1 Effect of milling and acetate pretreatments on clay fraction

Milling before separating the clay fraction substantially reduced the sharpness of the peaks. Although the $< 2 \text{ mm}$ samples were milled before acetate treatment in order to liberate calcite-cemented clays, the clay peaks were substantially enhanced after the acetate treatment (Figures 4.1(a), 4.2). This suggests that the clays are aggregated with calcite. The calcite aggregates binding the clays appear to be finer than the size fraction which can be liberated with ball milling, because it is only in the $<0.08 \mu\text{m}$ clay fraction that acetate treatment appeared not to liberate any different clays (compare the $<0.08 \mu\text{m}$ with the 1 to 0.08 μm and $<2 \mu\text{m}$ traces in Figure 4.2).

This was also noted in Chapter 3, where the difference was most noticeable with palygorskite and is consistent with Vanden Heuvel's (1964, p. 201) observation that palygorskite showed "greater immobilization" by the calcite aggregates than sepiolite. The $<0.08 \mu\text{m}$ is the only size fraction where palygorskite could be detected before acetate treatment (Figure 4.2). It may be that palygorskite appeared to be more closely associated (aggregated) with calcite because it is finer than the other clay minerals, and finer than the size fraction that can be liberated by ball milling.

4.3.2 Clay mineral variations in soil profiles

Table 4.1 shows the dominant clay phases in the $<2 \text{ mm}$ fraction for representative soil profiles. The corresponding XRD traces are presented alphabetically in Figures 4.1 to 4.6. Sepiolite occurs across all packages and elevations up to 99 m a.m.s.l., the farthest sampled from the sea (about 30 km). Neither sepiolite nor palygorskite are present in the marine sediments, which contain only smectite, mica, and kaolinite in varying proportions. Although the appearance of sepiolite and palygorskite seems to be limited to subaerially-reworked material, not all aeolian material contains sepiolite/palygorskite (profiles LKC1-5 and SL4-1 in Figures 4.4 and 4.6, for example). It is therefore unlikely that the sepiolite is inherited from either the marine or aeolian parent materials. The appearance of sepiolite and palygorskite are most consistently associated with the presence of calcite in the soil profile. The presence of high angled peaks in 6869/4 and /iv (Figures 4.1(a), (b)) suggests either that some interlayers are present, or that these may be reflections of sepiolite.

Visual evaluation of the peak intensities in Figures 4.1 - 4.6 suggests that sepiolite is more abundant than palygorskite. The relative abundances of sepiolite and palygorskite in Table 4.1 were estimated using the 0.644 nm peak of palygorskite in addition to the 12.1/1.048 nm peak ratio, since the 0.644 nm peak does not overlap with other phases, and its intensity is medium strong (Bradley, 1940), increasing if the sample is oriented (Nathan et al., 1970, in Singer, 1989). However, in a mixture of phases the quantity of sepiolite could be overestimated and that of palygorskite underestimated using peak height or area of the main reflection line, since even in low concentrations sepiolite might show high diffraction intensity (Ouhadi and Yong, 2003). Despite this, the dominance of sepiolite over

Table 4.1: Clay mineral variation down profiles. Abundances were visually estimated from peak sizes: 'xxx' dominant peak; 'x' trace or only in <0.08 μm fraction; '-' not detected. Traces shown in Figures 4.1 to 4.6.

Depth (m)	Horizon †	Facies ‡	Estimated Texture ‡	React HCl	Smectite	1.4 nm	Sepio-lite	Palygor-skite	Mica-illite	Kaolinite	Inter-stratified
6869: Prieska Form (Orthic A - Neocarbonate B - Hardpan carbonate). KNC, 30 m package, 41 m a.m.s.l. (GPS), footslope.											
0-	/i A1	Regic sand (Orthic A)	Aeolian dune	Med. sand	Calc.	No clay					
0.45-	/ii A2	Regic sand	Aeolian deflation	Med. sand	Calc.	No clay					
0.5-	/iii II B1	Neocarbonate B	Aeolian?	Med. sand	Calc.	-	XXX	X	-	X	-
0.6-	/iv II B2	Neocarbonate B	Aeolian?	Lo. sand	Calc.	X	-	XXX	XX	X	X
0.8	over hardpan carbonate										
<i>New profile, mining excavation, upper material removed. Askham Form (Orthic A - Yellow-brown apedal B - Hardpan carbonate).</i>											
?	0.32- /14 III B	Yellow-brown apedal B	Obscured	Lo. sand	<1 μm	X	XXX	X	XX	X	?
0.32-	/15 IV C1	Hardpan carbonate	U. shoreface	Lo. c. sand	Calc.	-----Br.-----	X	X	X	X	-
1-	/16 IV C2	Marine deposit	U. shoreface	C. sand	-						
<i>6m-9m unit consists of alternate coarser, redder & finer, yellower sedimentary layers.</i>											
6-9	/17 V C3	Marine deposit	L. shoreface	Med. sand	-	XXX	-	-	-	X	XX
6-9	/18 V C3	Marine deposit	L. shoreface	C. sand	-	XXX	-	-	-	X	XX
<i>9-18m more homogenous texture & colour than 6m-9m. Textural layering not associated with prominent colour contrast.</i>											
9-18	/13 VI C4	Marine deposit	L. shoreface	C. sand	-						
9-18	/11 VI C4	Marine deposit	L. shoreface	Med. sand	-	XXX	-	-	-	X	X
18-36	/cc V C5	Gleyed clay	Fluvial paleo-	(Sa.) clay	-	-	-	-	-	XXX	-
Water dripping out 2-3m above bedrock. channel											
AK1/TRIG: Oakleaf Form (Orthic A - Neocutanic B - Unspecified). BMC, 90m terrace, 119 m a.m.s.l. (GPS). Terrain unit: crest.											
0-	/1 A1	Orthic A, bio crust	Aeolian	Lo. sand	Calc.	No clay					
0.05-	/2 A2	Orthic A	Aeolian	Lo. sand	-	No clay					
0.3-	/3 B	Neocarbonate B	Aeolian	Lo. sand	Calc.	-----Br.-----	XBr.	-	XXX	X	-
Bedrock from 0.6 m.											
AK61H: Coega Form (Orthic A - Hardpan carbonate). BMC, 30m terrace, 28 m a.m.s.l. (GPS), footslope.											
0-	/4 A	Orthic A	Aeolian	F. sand	Calc.	-----Br.-----				Very little clay in horizon	-
0.35-	/1 II C1	Hardpan carbonate	Obscured		Calc.	XX	XXX	XX	XXX	X	-
1.05-	/2 II C3	Blocky calcretized sed.	Marine		Calc.	cutan					-
1.55-	/3 II C4	Marine deposit	Marine		-						-
Bedrock from 2.1 m.											
LCK1-5: Namib Form (Orthic A - Regic sand). KNC, 50 m package, 30 m a.m.s.l. (GPS), footslope-valley bottom.											
0-	/IA A	Regic sand (Orthic A)	Aeolian	Med. sand	-	Very little clay in horizon			X	-	-
0.3-	/IB B	Regic sand	Aeolian	Med. sand	-	-	-	-	XX	-	-
1-	/1 II B2	Neocutanic B	Obscured	Med. sand	-	XX	-	-	XXX	XX	-
1.3-	/3 II B3	Neocutanic, luvic	Obscured	Med. sand	-						-
1.9-	/4 III C1	Gleyed sand?	Obscured	Med. sand	-						-
2.4-	/6 V C3	Sedimentary?	Obscured	Med. sand	-						-
3.4-	/7 VI C4	Marine deposit	U. shoreface	C. sand	-						-
<i>Pale sand (LKC1-5/8) interlayered with more orange sand (/9).</i>											
5.4-	/8 VII C5	Marine deposit	L. shoreface	Med. sand	-	XXX	-	-	-	-	-
5.4-	/9 VII C6	Marine deposit	L. shoreface	Med. sand	-	XX	-	-	-	-	-
Bedrock from 12 m.											
OBT: Prieska Form (Orthic A - Neocarbonate B - Hardpan carbonate). BMC, 95 m terrace, 99 m a.m.s.l. (GPS), crest.											
0-	/1 rs	Aeolian deflation surface	Aeolian	Med. sand	-						
0.03-	/2 A	Orthic A	Aeolian	Med. sand	-						
0.25-	/3 B	Neocarbonate B	Aeolian	Med. sand	-	-	XX Br.	-	-	-	-
0.45-	/4 II C1	Hardpan carbonate	Obscured		Calc.	-	XXX	X	X	-	-
1-	/5 II C2	Sedimentary?	Obscured	Lo. sand	Occ. calc.						-
Bedrock not reached.											
SL4-1: Pinedene Form (Orthic A - Yellow-brown apedal B - Signs of Wetness). KNC, 30 m package, 46 m a.m.s.l. (GPS), footslope.											
0-0.3	/1 A1	Orthic A	Aeolian	Med. sand	-	-	-	-	XX	X	-
0.3-	/2 B1	Yellow-brown apedal B	Aeolian	Med. sand	-	-	-	-	XXX	X	-
0.5-	/3 E	Gleyed sand	Aeolian	Med. sand	-	-	-	-	XX	X	-
0.63-	/4 B2	Neocutanic	Obscured	Med. sand	-	X	-	-	XXX	XX	-
0.8-	/5 II B3	Slightly gleyed sand?	Obscured	Med. sand	-	-	-	-	XX	X	-
0.95-	/6 III B4	Pedocutanic	Obscured	Lo. sand	-	X	-	-	XXX	XX	-
0.97-	/7 III B5	Pedocutanic	Obscured		Calc.						-
1.22-	/8 III B6	Pedocutanic	Obscured	Lo. sand	-						-
2.45-	/9 IV C1	Marine deposit	U. shoreface	Lo. sand	-						-
3.05-	/11 V C2	Marine deposit	L. shoreface	Med. sand	Calc.						-
Bedrock from 9 m, evidence of wetness.											

† Classified according to the Soil Classification Working Group (1991). Roman numerals indicate different sedimentary units.

‡ Br.-broad; c.-coarse; calc.-calcareous; f.-fine; med.-medium; l.-lower; lo.-loamy; occ.-occasional; sed.- sediment; sl.-slight; u.-upper; v.-very.

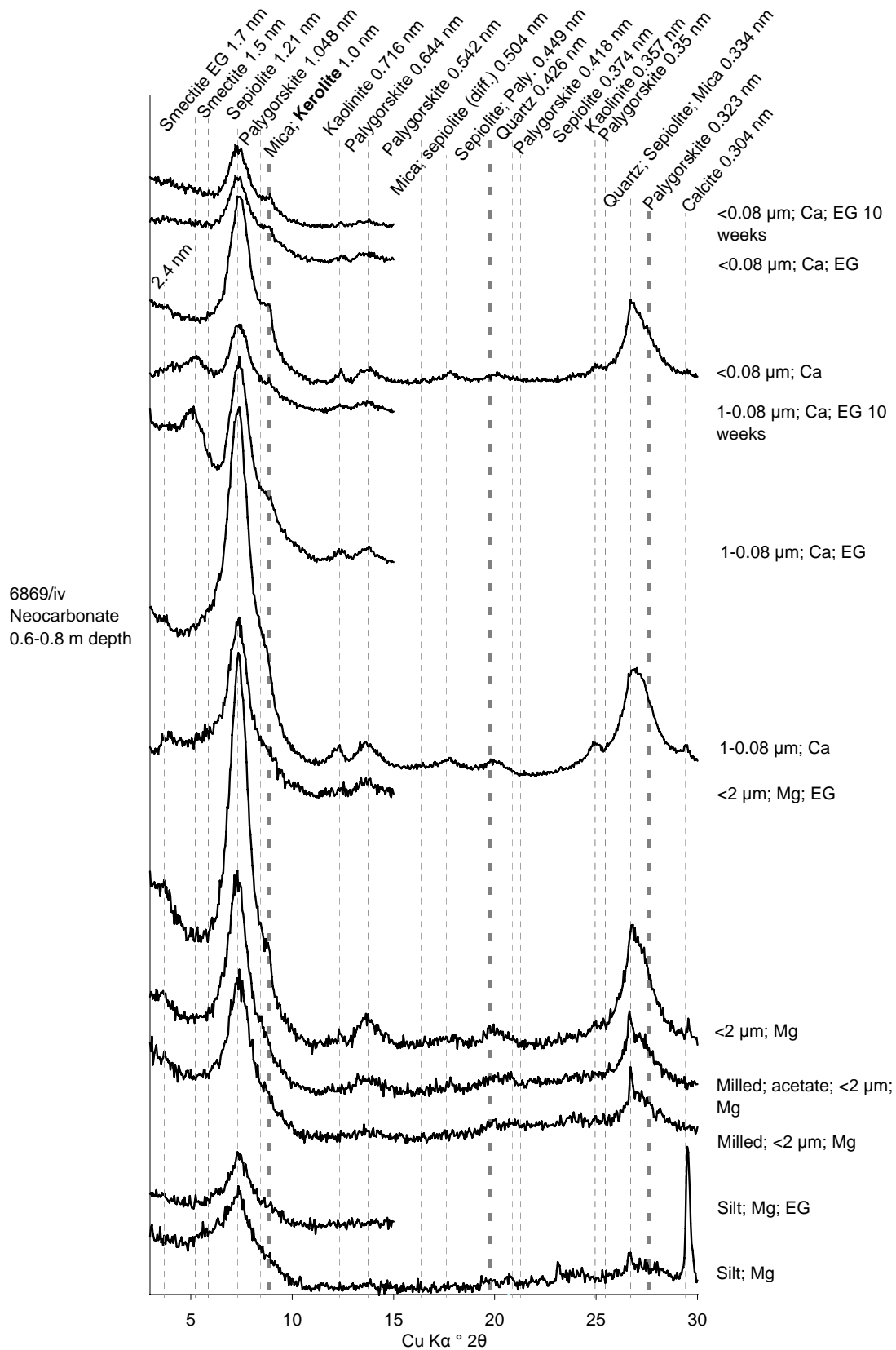


Figure 4.1: (a): XRD traces of clay fraction from profile 6868. Bold lines show kerolite peak positions. Diff.- diffuse; EG: ethylene glycol. 'Milled EG' and 'milled acetate EG' traces identical to '<2 μm EG'.

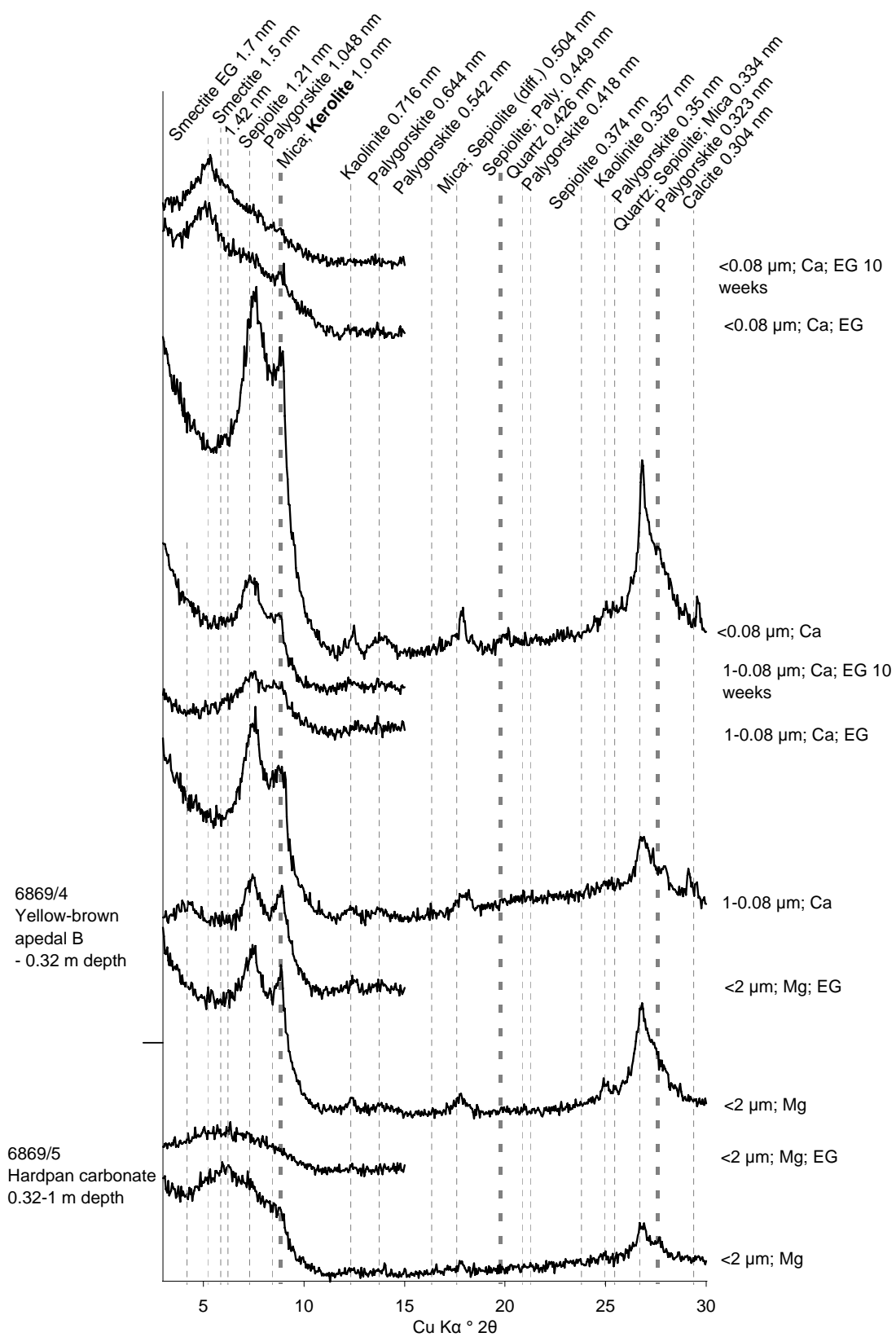


Figure 4.1: (b): Continued - XRD traces of clay fraction from profile 6868.

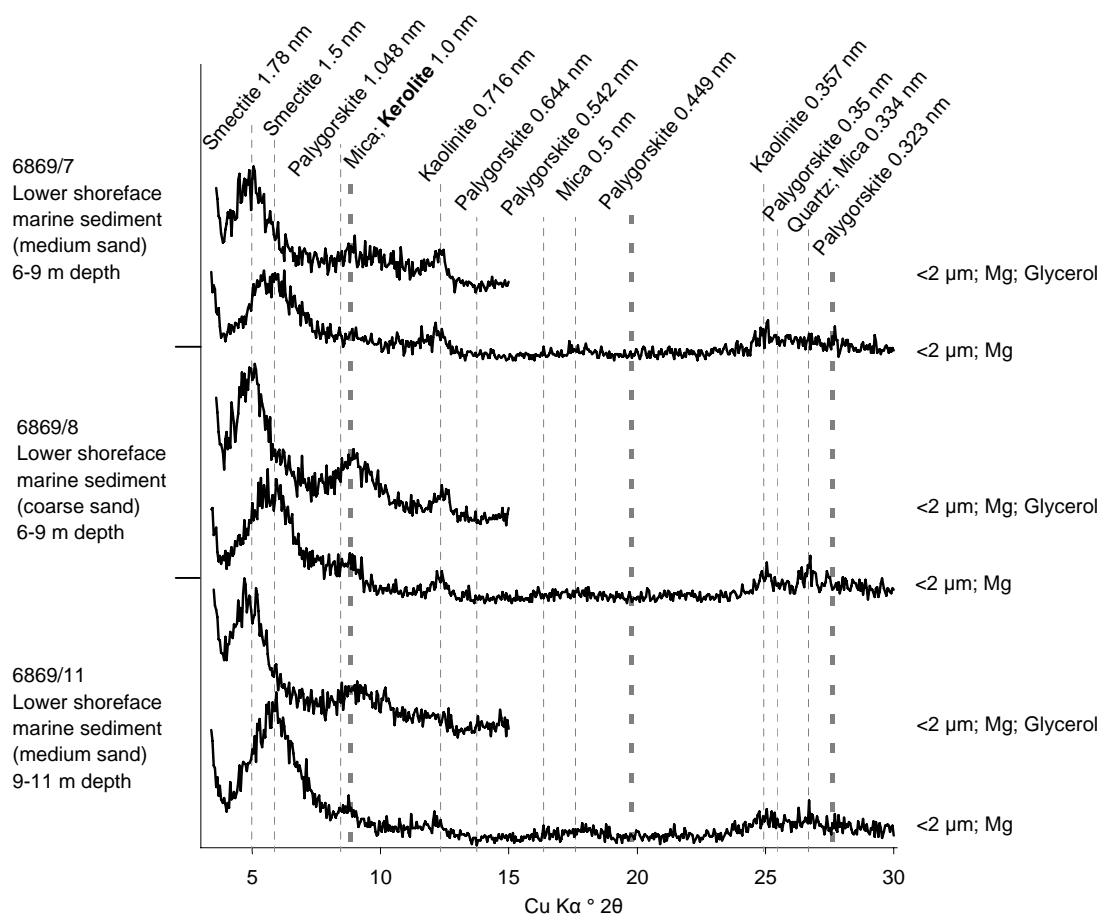


Figure 4.1: (c): Continued - XRD traces of clay fraction from profile 6868.

palygorskite on the coastal plain is consistent with the results of Singer et al. (1995, p. 45), who found that sepiolite-containing soils were concentrated toward the coast, and palygorskite-containing soils farther inland.

The XRD traces from two of the horizons (bulk soil) overlying sepiolite-containing calcretes (AK61H, Figure 4.2; OBT/3, Figure 4.5) and a neocarbonate B horizon over hard rock (AK1/TRIG/3, Figure 4.3) are typified by very broad 1.21 nm and 0.4 to 0.374 nm peaks, suggesting a very fine or poorly crystalline sepiolite phase. TEM analysis of OBT/3 (Figure 4.7(a)) and 6869/iv (Figure 4.10) showed an amorphous phase in addition to crystalline sepiolite and mica. The broad rise in the 0.4 to 0.374 nm region also occurred in traces with a sharper sepiolite peak, such as the calcrete horizon OBT/4. This suggests there is an amorphous silica component in addition to sepiolite in the clay fraction. In AK1/TRIG/3 (Figure 4.7(b)), acicular crystals are apparently developing from an amorphous phase, although well crystallized sepiolite is also present (Figure

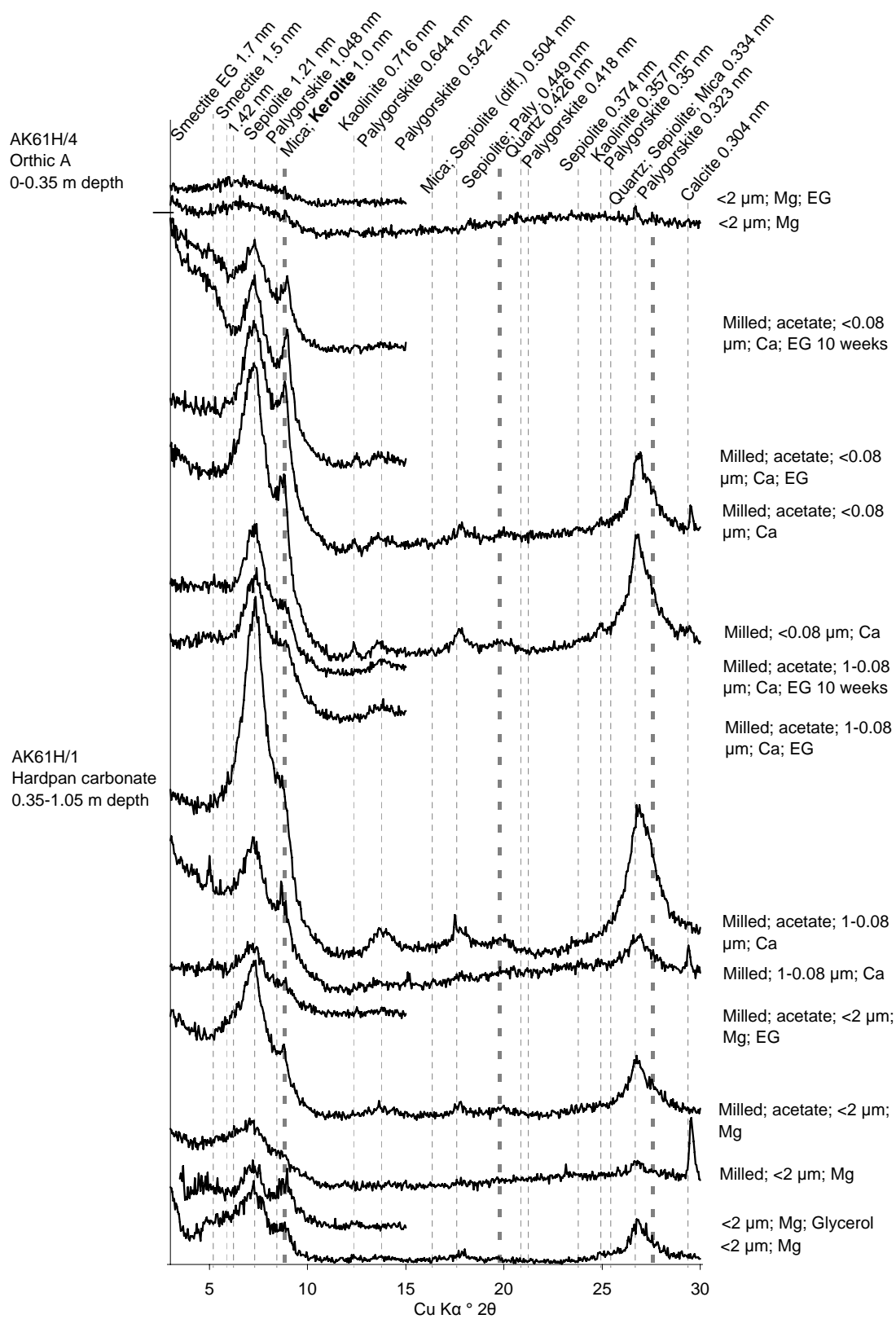


Figure 4.2: XRD traces of clay fraction from profile AK61H. Bold lines show kerolite peak positions. Diff.-diffuse; EG: ethylene glycol. 'Milled EG' traces identical to 'milled acetate EG'.

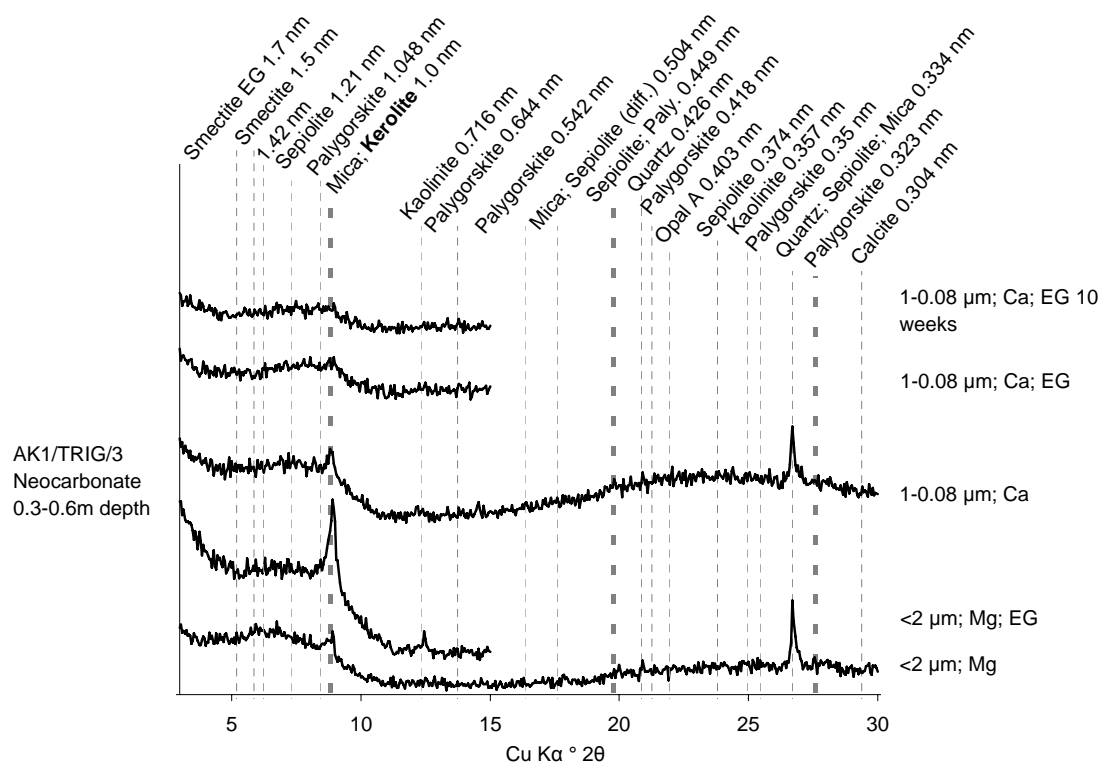


Figure 4.3: XRD traces of clay fraction from profile AK1/TRIG. Bold lines show kerolite peak positions. Diff.-diffuse; EG: ethylene glycol.

4.7(c)). The amorphous silica may be available for sepiolite formation via a process similar to that described by Díaz Torres et al. (1990), in which sepiolite and palygorskite fibres develop from silica gel, or as suggested by Blank and Fosberg (1991), by which sepiolite may form via the addition of Mg to opal.

The hardpan carbonate horizon 6869/5 (Figure 4.1(b)) differs from the other calcrete samples (Figures 4.2, 4.5 and in Chapter 3) in that there is a broad 1.4 nm non-expanding phase dominant and a less dominant 1.21 nm sepiolite peak. Chlorite occurred in the palygorskite-containing soils examined by Singer et al. (1995). Hay and Wiggins (1980), however, found some samples in the southwestern USA that showed a delicate fibrous structure under TEM, but which gave a broad peak from 1.26 to 1.4 nm that was unchanged with ethylene glycol and heating to 300 °C, and only slightly reduced by heating to 500 °C.

There is no discernible trend in mica abundance with depth (Table 4.1). In the Namaqualand soils, the mica is likely to be detrital. Mica is a common component of the bedrock in the region and is also detectable macroscopically in many of the marine deposits, especially the lower shoreface facies. The aeolian deposits are

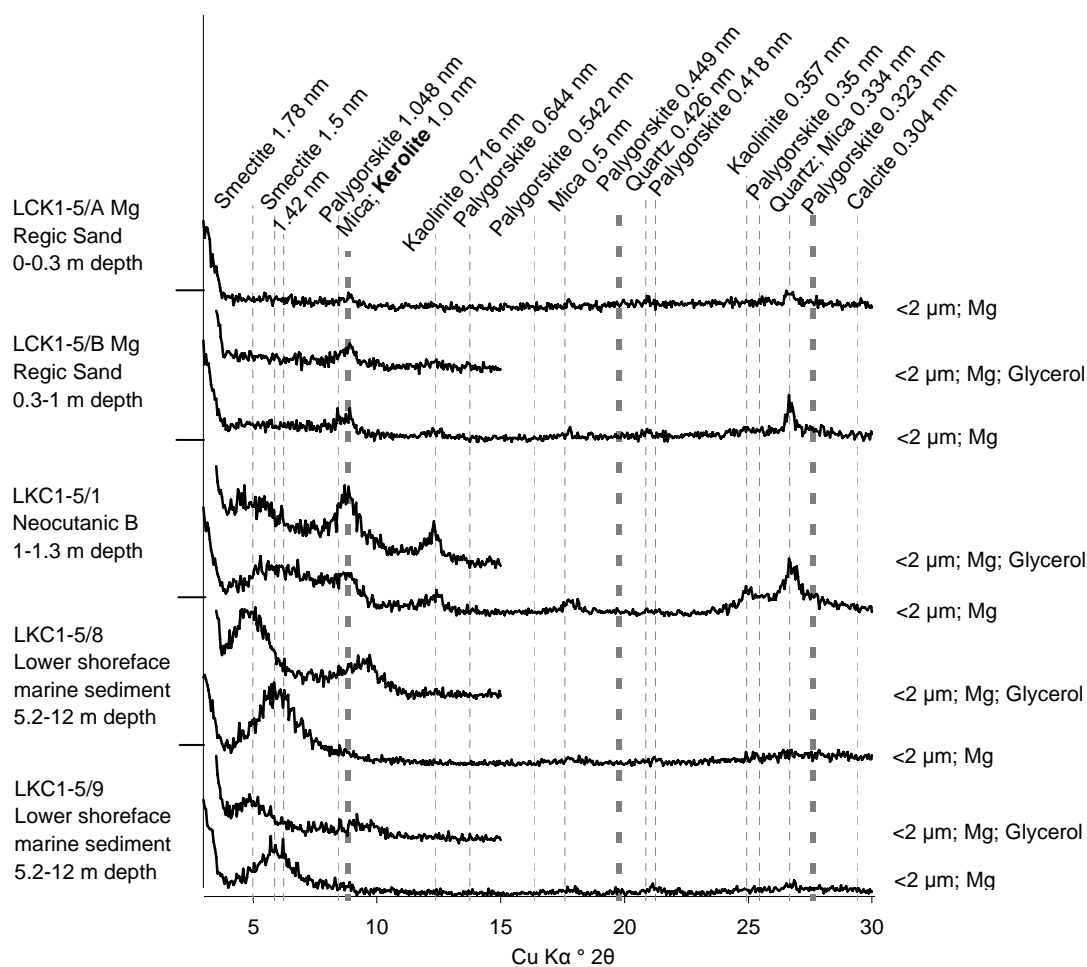


Figure 4.4: XRD traces of clay fraction from profile LKC1-5. Bold lines show kerolite peak positions.

generally derived from the mechanical reworking of this marine material (Tankard and Rogers, 1978; Harmse and Swanevelder, 1987; Pether, 1994). Böhmann et al. (2004) found for soils in the Western Cape (Mediterranean climate) that mica was generally inherited from the parent material, and decreased in proportion to present day mean annual rainfall. Mica neoformation, however, can also take place under 550 mm annual rainfall, provided soils have a pool of exchangeable K and swelling clays as a precursor phase (Böhmann et al., 2004).

Smectite generally increases downwards (Table 4.1) dominating the clay fraction of the marine sands at the base of the profiles. In the case of LKC1-5, a non-calcareous, non-sepiolite/palygorskite bearing profile, it appears to increase at the expense of mica/illite (Figure 4.4).

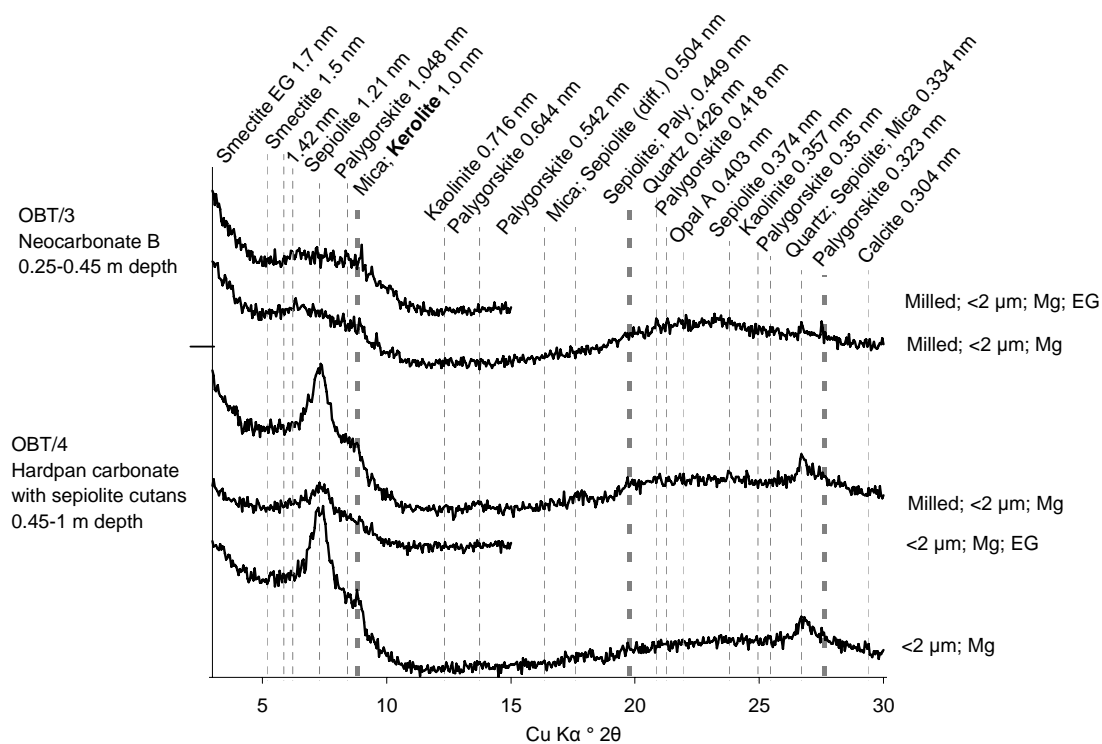


Figure 4.5: XRD traces of clay fraction from profile OBT. Bold lines show kerolite peak positions. Diff.-diffuse; EG: ethylene glycol.

There is a slight increase in the kaolinite content down the profile. The basal parts of the regolith profile are marine sands, which are older than the subaerially reworked upper parts. The basal parts are also wetter, with many profiles having water running out just above or on bedrock. The leaching process in the basal part of the regolith has therefore been more intense than in the upper parts. This is particularly evident in profile 6869, where the lowest part of the profile consists of much older kaolinized fluvial sediments in a bedrock channel underlying the marine sands. Pether (1994) concluded that the channels were laid down as a quartzo-feldspathic sediment in a fluvial environment, and subsequently deeply weathered, with extensive alteration of feldspar to kaolinite. De Villiers and Cadman (2001) favoured an early Tertiary age for this channel north of the Swartlontjies River, although it may also contain reworked Cretaceous material. The overlying marine sediments of profile 6869 are from the 30 m package, the age of which is not well constrained, being estimated at ca. 3.3 Ma or younger (Pether et al., 2000). Böhmann et al. (2004) found for soils in the Western Cape that the transformation of chlorite to kaolinite was the most significant pedogenic

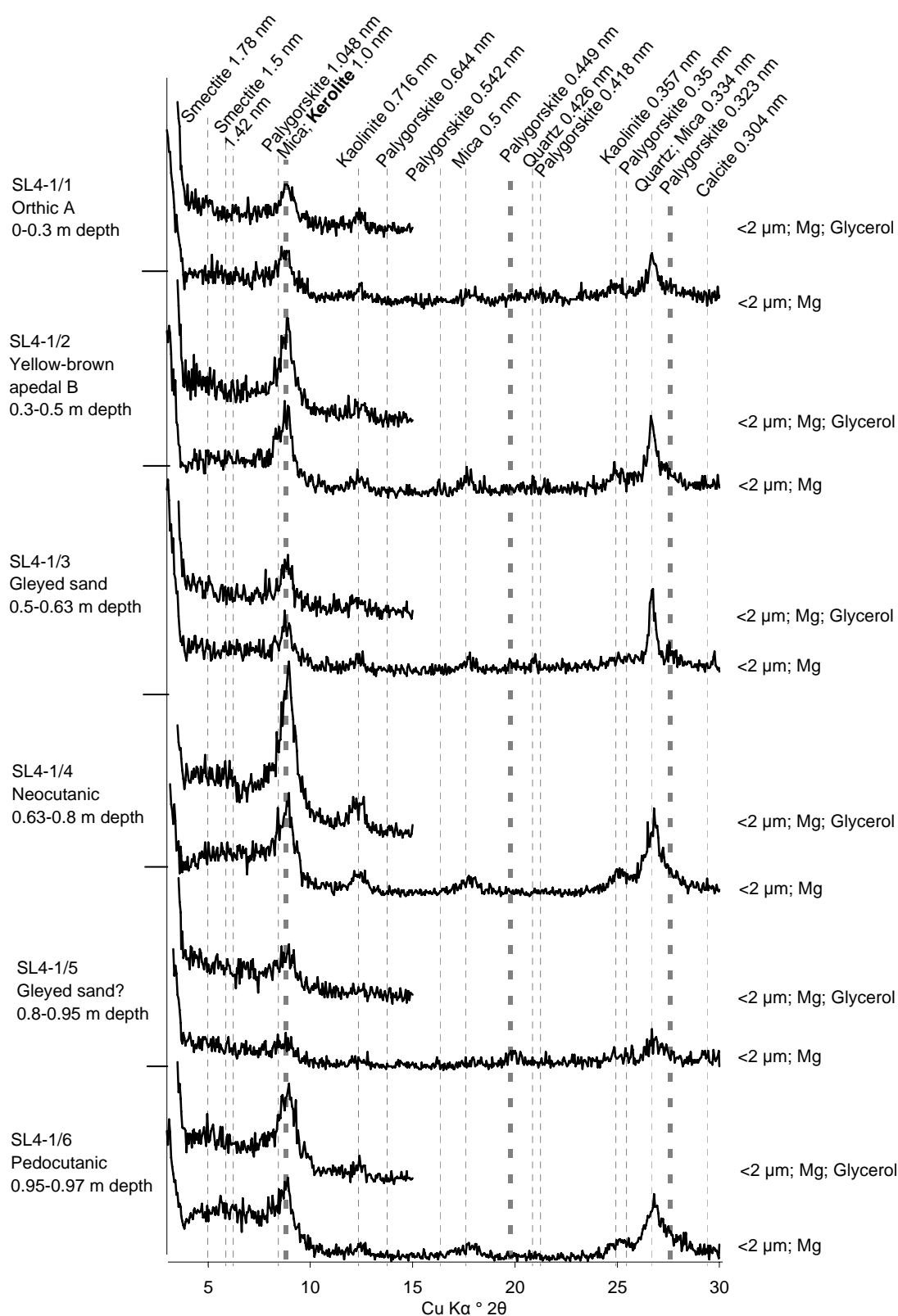
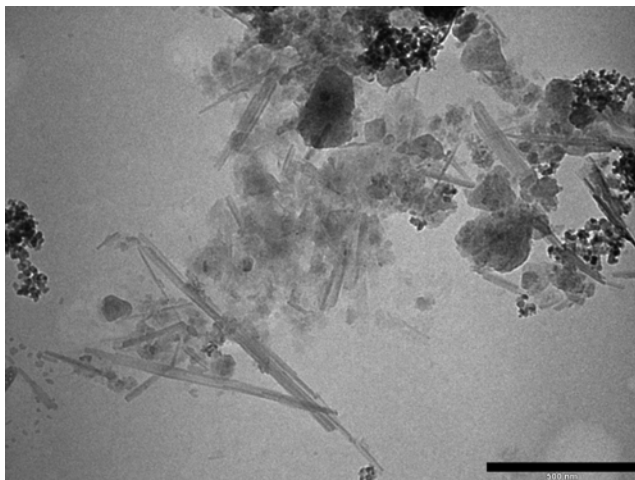
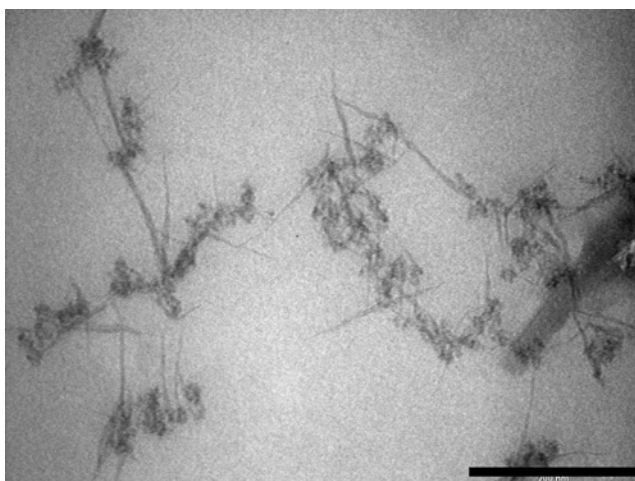


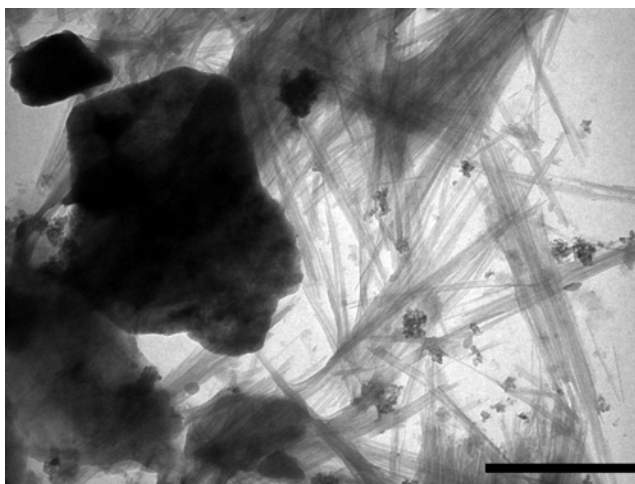
Figure 4.6: XRD traces of clay fraction from profile SL4-1. Bold lines show kerolite peak positions.



(a) $<2 \mu\text{m}$ (milled; acetate-treated) fraction from OBT/3 (Figure 4.5): mica (platy); sepiolite (acicular); amorphous phase (center); aggregated silica(?) spheres. Scale bar 500 nm.



(b) 1 to $0.08 \mu\text{m}$ fraction from AK1/TRIG/3 (Figure 4.3). Scale bar 200 nm.



(c) Same as (b): mica (platy); sepiolite (acicular); aggregated silica (?) spheres. Scale bar 500 nm.

Figure 4.7: TEM images of clay fractions.

process in soils derived from metamorphic rocks, and that the kaolinite content was poorly related to the present day mean annual precipitation, and more likely associated with the chlorite content in the parent rock. Although the soils in the region of the present study on the Namaqualand coast were not derived from metamorphic rock directly, the bedrock underlying the marine deposits on which the soils formed is metamorphic (see references in Chapter 2), and so this theory of kaolinite formation may also apply here.

4.3.3 Kerolite

Kerolite has broad asymmetric XRD peaks at approximately 1.0 and 0.45 nm, and a less intense 0.32 nm peak (Brindley et al., 1977; L veill  et al., 2002). These peaks overlap with other phases present in the samples: the palygorskite 1.048 nm and mica 1.0 nm peaks; the sepiolite 060 and palygorskite 040 peaks at 0.449 nm (Bradley, 1940; Brindley, 1959); and the palygorskite 400 peak at 0.323 (Bradley, 1940) or 0.317 nm (Christ et al., 1969). As a result, all samples with a mix of these phases show peaks in the correct position for kerolite (Figures 4.1(a) and (b), 4.2, 4.3, and 4.5). These patterns show no change in the 1.0 nm peak after ethylene glycol treatment for ten weeks, which is similar to the findings of L veill  et al. (2002), but unlike that of Brindley et al. (1977) and Hay et al. (1995). It may be hypothesized that due to the fine, disordered nature of kerolite (Brindley et al., 1977; Pozo and Casas, 1999), its presence would be better resolved by a study of the fine clay fraction. The concentration of palygorskite in the fine clay fraction, however, means that this was not the case. TEM data were also inconclusive, with both Figures 4.7(a) and (b) (corresponding to the XRD traces of 4.3 4.7(a)), for example, showing poorly crystalline material, although Figures 4.10(a) and (b) do resemble the “colloform aggregates” of Pozo and Casas (1999, p. 402).

4.3.4 Chemical composition of clay fraction

Trends in MgO, Al₂O₃ and SiO₂ (Figure 4.8(a)) show that Namaqualand soil clay fractions lie on a mixing line between sepiolite and mica end-members, with a contribution from smectite. This is consistent with the XRD and TEM results. The soils have a similar chemical composition to the Namaqualand sepiolite-bearing soils studied by Singer et al. (1995).

The influence of mica/illite on the clay fraction chemistry is reflected by the positive correlation between K_2O and Al_2O_3 (Figure 4.8(b)). The trend is also observed in the K-saturated soils where it is displaced to higher K_2O values, and it is very similar to the trend displayed by the data of Singer et al. (1995) for sepiolite-containing soils from nearly the same area. The palygorskite-containing soils of Singer et al. (1995) (from an area more inland of the present study area) are displaced to higher Al_2O_3 values in comparison to both the soils from this study, and the sepiolite-containing soils from their study. This displacement is more pronounced at lower K_2O values, and is consistent with the elevated Al_2O_3 contents of pure palygorskite compared to pure sepiolite (Figure 4.8(b)).

The K_2O content of the Mg-saturated clay fractions ranges from 0.7 to 3.57 %. This is equivalent to 10 to 50 % illite, following the method of Singer et al. (1995) in using 7.1 % K_2O for average illite and assuming that all the K_2O is attributed to mica/illite, since the XRD traces display no prominent feldspar peaks. If, however, the main potassium-bearing phase is mica rather than a relatively K-depleted illite, the maximum calculated mica content is 38 % (using 9.35 % K_2O as the average mica from the mean K_2O content of the mica analyses listed in Figure 4.8).

The present data show a good correlation between Fe_2O_3 and TiO_2 (Figures 4.8(c) and (d)). This can be attributed to the presence of mica in the soils, since the soil clays fall on the mica Fe_2O_3 - TiO_2 trendline (Figure 4.8(d)) and show similar Fe_2O_3/TiO_2 ratios to mica (compare the trendline in Figure 4.8(c) for the sepiolitic and non-sepiolitic soils with the trendline for single mineral micas shown in Figure 4.8(d)). In contrast, pure kerolite, sepiolite, palygorskite (Figure 4.8(c)) and smectite (Figure 4.8(d)) show a poor correlation between Fe_2O_3 and TiO_2 .

The present data suggest the Fe_2O_3 in Namaqualand soils is due to the mica content. This is in contrast to the conclusion of Singer et al. (1995), that Namaqualand sepiolite is a ferric sepiolite. Their conclusion was based on XRF data from whole clay fractions that were CBD-pretreated to remove free iron oxides. Although illite was noted to be present, Singer et al. (1995) did not publish the TiO_2 content of their soils. Also, the interpretation that Fe_2O_3 in Namaqualand soils is due to the mica content is more consistent with the results of Galan and Carretero (1999), who found sepiolite to be a true triocta-

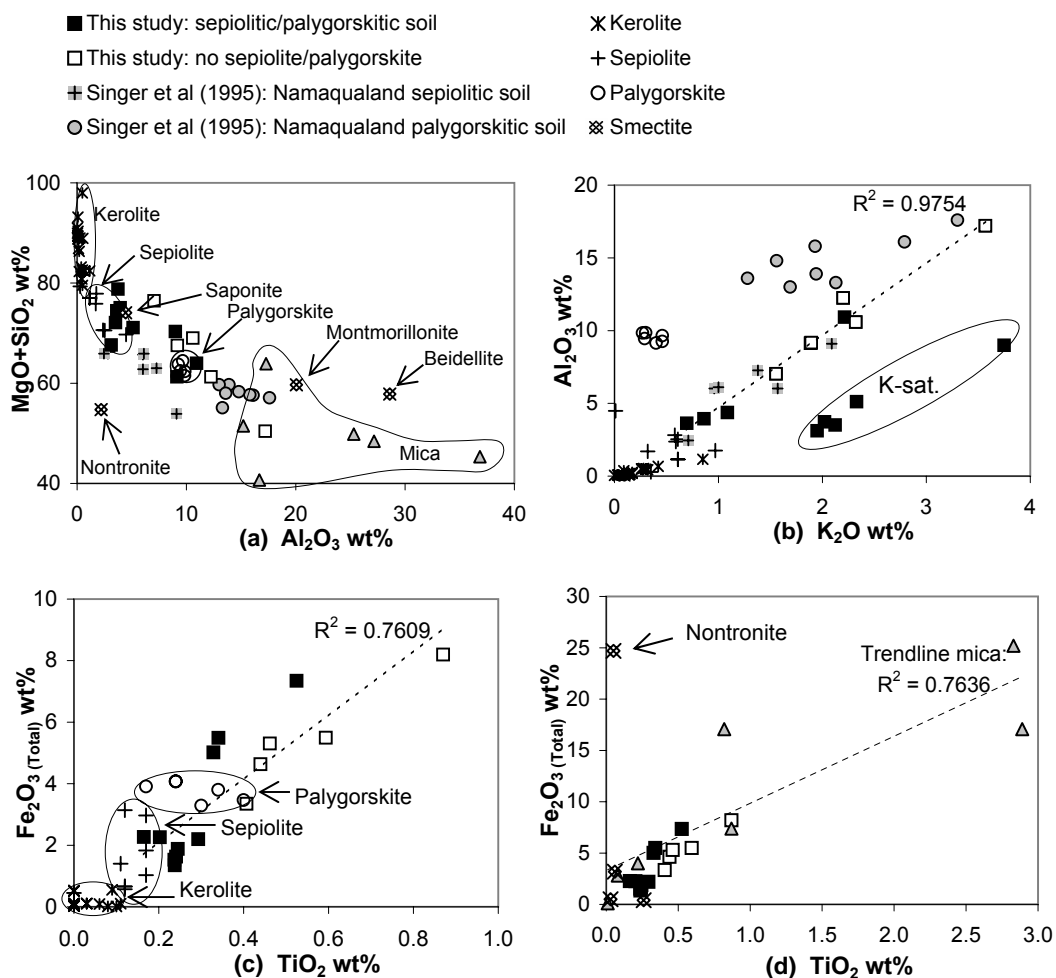


Figure 4.8: Trends in total element composition of Mg- and K-saturated clay fractions from Namaqualand soils compared to pure minerals. (a) to (c): R^2 trendlines based on sepiolitic and non-sepiolitic soils from the present study; (d) R^2 trendline based all the mica data. Note scale differences in (c) and (d), where (c) shows data from this study plotted with kerolite, sepiolite, palygorskite, and (d) plotted with mica and smectite Sepiolite (Stoessell and Hay, 1978; Stoessell, 1988; Singer, 1989), kerolite (Brindley et al., 1977; Stoessell and Hay, 1978; Eberl et al., 1982; Stoessell, 1988; Léveillé et al., 2002), palygorskite (Singer, 1989), and mica and smectite compiled by Deer et al. (1992) - rose muscovite, muscovite, glauconite, phlogopite, biotite, lepidolite, beidellite, saponite, montmorillonite and nontronite.

hedral mineral, very pure (near end-member) with negligible structural substitution and eight octahedral positions filled with magnesium, close to Brauner and Preisinger's (1956) theoretical formula $\text{Si}_{12}\text{Mg}_8\text{O}_{30}(\text{OH})_4(\text{OH}_2)_4 \cdot 8\text{H}_2\text{O}$. Galan and Carretero's (1999) EDX analyses of sepiolite showed no structural Al and Fe, and an octahedral occupancy close to 8. They attributed the presence of some Al, Fe, K or Ca in some of the determinations to minor impurities.

4.3.5 Sepiolite/palygorskite modes of occurrence

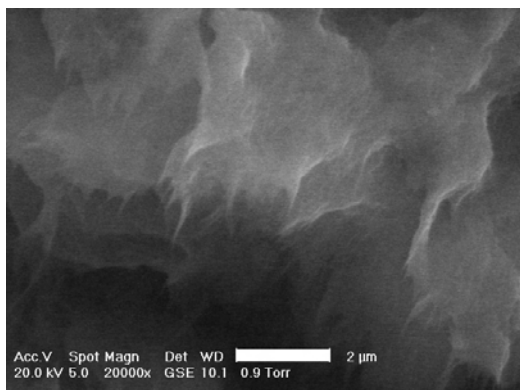
Chapter 3 showed that fibrous clay minerals in Namaqualand calcretes are associated with mineralized filaments and needle fibre calcite, and also occur as frayed mats composed of woven fibres. 'Fraying' is a very common texture in sepiolite/palygorskite occurrences. It is either reported from a sheet that is composed of fibres (Khoury et al., 1982; Jamoussi et al., 2003), or a sheet which appears to be solid (such as Monger and Daugherty, 1991; Pozo and Casas, 1999). Suarez et al. (1994) showed the fraying observed under TEM to be illite particles evolving laterally into palygorskite fibres.

SEM analyses show that much of the sepiolite/palygorskite in this study occurs as fringed sheets (Figure 4.9(a), (b)). These are found coating (rather than evolving from) mica/illite particles (Figures 4.9(c)-(d)), as free-standing mats such as those shown in Chapter 3, and are common on the grain-side of cutans (for example Figures 4.9(e)-(f)).

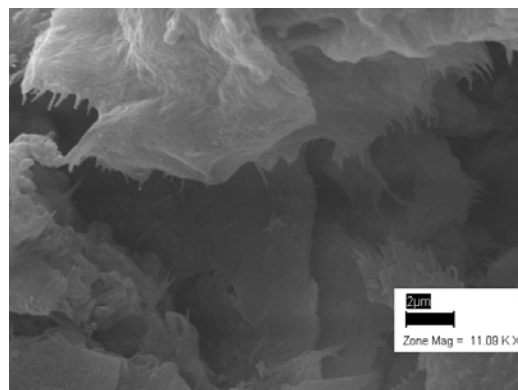
While the textures in Figures 4.9(b)-(f) suggest illuviation of the fibrous clay minerals, another explanation may be that sites such as that immediately adjacent to silicate grains have the highest concentration of silica for their formation. Many examples of etched and embayed silicate grains have been observed in this study. Monger and Daugherty (1991) concluded that silica released from silicate grains by pressure solution during calcite crystallization was required for palygorskite formation in New Mexico aridisols. While Figure 4.9(d) shows distinctly that mica is not evolving laterally to a fibrous mineral, Figure 4.9(a) shows fibres developing from a wavy sheet-like mineral. This resembles the SEM images of mixed-layer kerolite/smectite associated with sepiolite from the Amargosa Desert, Nevada (Eberl et al., 1982, p. 324) and the Amboseli Basin, Tanzania-Kenya (Hay et al., 1995, p. 461).

4.3.6 Palygorskite/sepiolite transformation

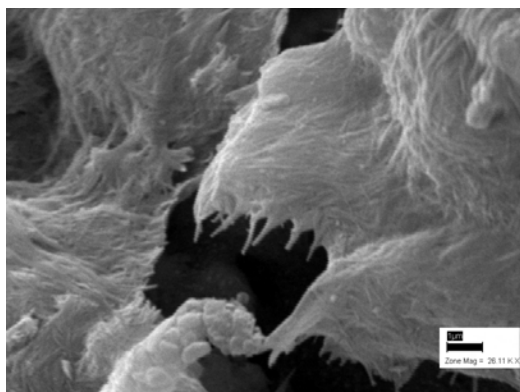
In any discussion of sepiolite or palygorskite, particularly palygorskite and its origins, the issue of transformation to/from a sheet silicate becomes relevant: sepiolite/palygorskite being transformed to smectite (Bigham et al., 1980; Golden et al., 1985), palygorskite fibres developing from an illite (Suarez et al., 1994),



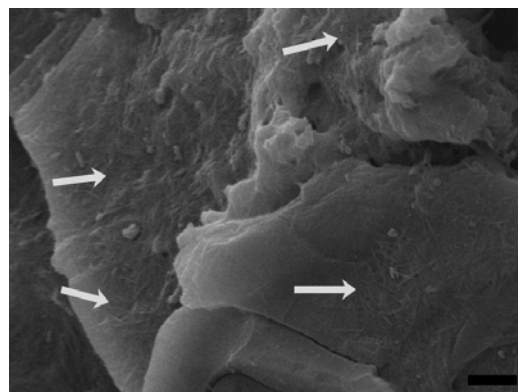
(a) Fringed sheets, etched 15 sec. in 1M HCl. Scale bar 2 μm .



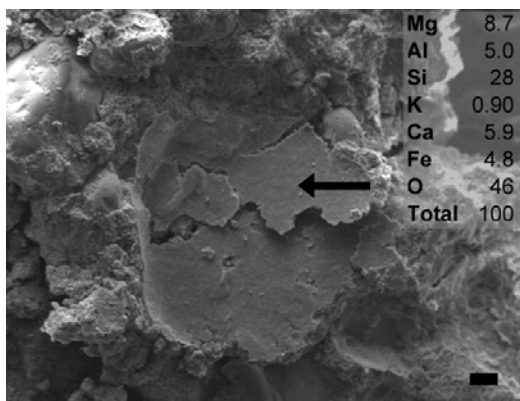
(b) Fringed texture. Scale bar 2 μm .



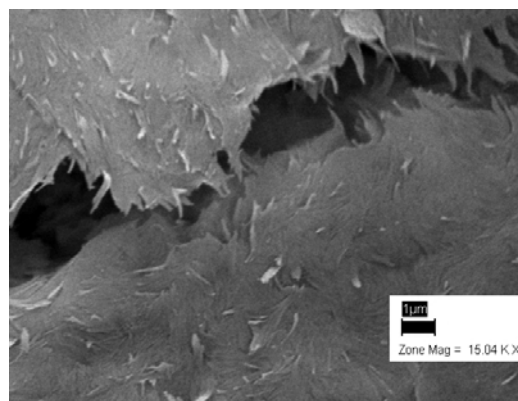
(c) Magnification of (b), showing fibres coating mica grains and fringed texture. Scale bar 1 μm .



(d) Fibres on mica grain (EDX analysis not shown), but no fringing. Scale bar 2 μm .



(e) Sepiolite/palygorskite cutan. Scale bar 100 μm . Fe from sample-holder.



(f) Magnification of cutan in (e). Scale bar 1 μm .

Figure 4.9: SEM images of sepiolite/palygorskite occurrences in calcareous nodules from 6869/iv (XRD traces shown in Figure 4.1(a)).

or no evidence of a solid state smectite-palygorskite transition (Verrecchia and Le Coustumer, 1996; Akbulut and Kadir, 2003). Jones and Galan (1988, p. 654 to 657) reviewed the issue of transformation vs. direct precipitation in sepiolite/palygorskite genesis. Recent studies using trace elements and isotopes favoured a direct precipitation of sepiolite, and a transformation or dissolution-reprecipitation of illite and/or smectite as a mechanism for palygorskite formation (Torres-Ruíz et al., 1994; Sánchez and Galán, 1995; Lopez-Galindo et al., 1996; Jamoussi et al., 2003; Zaaboub et al., 2005).

This study has found no TEM evidence to favour a hypothesis for fibrous mineral degradation to sheet silicates, as was suggested Singer et al. (1995). Figure 4.7(b) shows what seems to be the formation of sepiolite, and Figures 4.7(c), 4.10(a) and 4.10(b) show what seems to be well crystalline sepiolite/palygorskite, the only exception being where a fibre bundle was burned by the electron beam (Figure 4.10(c)). Singer (1989) noted that the variation in morphology of sepiolite and palygorskite crystals under TEM is greater within than between the species, and suggested that may be due to different pretreatments used, or to transport in the case of detrital clays. Owliaie et al. (2006) found three morphological forms of palygorskite in relation to the degree of weathering: i) sheaves or bundles representing the least weathering; ii) “split” bundles and sharp-pointed crystals, some of which may have been transformed to other clay minerals such as smectite; and iii) individual fibres with rounded tips and no sharp edges, indicating maximum weathering.

The TEM images (Figures 4.7 and 4.10) often show sepiolite/palygorskite to occur as flat aggregates giving the appearance of frayed edges, as well as single fibres: they resemble the palygorskite “nanofibres” and “fibre bundles” of Esquivel et al. (2005), the palygorskite textures found by Verrecchia and Le Coustumer (1996) and Khademi and Mermut (1999). None of these authors attributed the textures to transformation into a sheet silicate. The large fibre bundle in Figure 4.10(c) resembles the TEM image of sepiolite precipitated by Siffert and Wey (1962). The fibre bundles are not only evident in the images of the mechanically and chemically treated clay extracts: an in situ fibre bundle in an etched calcareous nodule is shown in Figure 4.10(d).

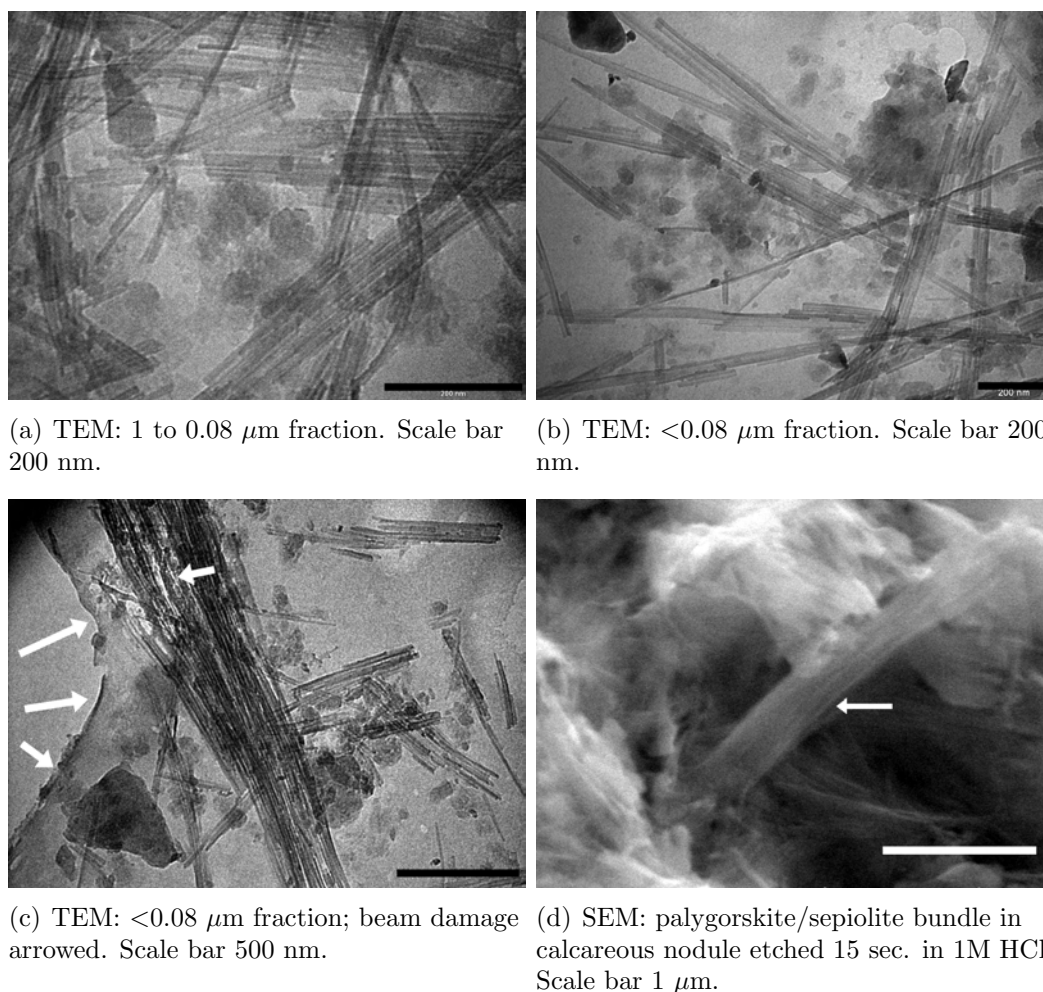


Figure 4.10: TEM images of sepiolite/palygorskite fibres and fibre bundles from 6869/iv (XRD traces shown in Figure 4.1(a)).

4.4 Conclusions

Milling before separating the clay fraction reduced the sharpness of all peaks. Acetate treatment after milling substantially enhanced the clay peaks, which suggests that the clays are aggregated with calcite. The calcite aggregates binding the clays appear to be finer than the size fraction that can be liberated with ball milling, because it is only in the $<0.08 \mu\text{m}$ fraction that acetate treatment appeared not to liberate any further clays.

The $<0.08 \mu\text{m}$ fraction is the only size fraction in which palygorskite could be detected before acetate treatment. It may be that it is finer than the other clay

minerals, and finer than the size fraction which can be liberated with ball milling. Sepiolite was difficult to distinguish from palygorskite in both TEM and SEM images and so this could not be visually confirmed.

Sepiolite is more prominent than palygorskite in the XRD traces. It is unlikely that these fibrous clay minerals are inherited from either the marine or aeolian parent materials, because neither sepiolite nor palygorskite are present in the marine sediments (which contain only smectite, mica, and kaolinite in varying proportions), and although the appearance of sepiolite and palygorskite seems to be limited to subaerially-reworked material, not all aeolian material contains sepiolite/palygorskite. Sepiolite and palygorskite are most consistently associated with the presence of calcite in the soil profile. Sepiolite occurs across all packages and elevations up to 99 m a.m.s.l., the farthest sampled from the sea being about 30 km inland.

There is little trend in mica abundance with depth. In the Namaqualand soils, the mica is likely to be detrital - it is a common component of the bedrock in the region, and also detectable macroscopically in many of the marine deposits, especially the lower shoreface facies. Smectite content generally increases downwards, and dominates the clay fractions of the marine sands at the base of the profiles. In the case of LKC1-5, a non-calcareous, non-sepiolite/palygorskite bearing profile, it appears to increase at the expense of mica/illite. There is a slight increase in the content of kaolinite down the profile. The basal portion of the regolith profile comprises marine sands which are older than the subaerially reworked upper parts. The lower parts are also wetter, with many profiles having water seepage above the bedrock where the leaching process has been more intense and protracted than in the upper parts.

Some SEM images show fibres developing from a wavy sheet-like mineral. These resemble the SEM images of mixed-layer kerolite/smectite associated with sepiolite from the Amargosa Desert (Nevada) and the Amboseli Basin (Tanzania-Kenya). This study was not able to find conclusive evidence for or against the presence of pedogenic kerolite in the clay fraction, although it does not appear to be a dominant phase in the less than 2 μm fraction.

The positive correlation between K_2O and Al_2O_3 is a reflection of the ubiquitous mica in the sediments. The K_2O content of the Mg-saturated clay fractions ranges from 0.7 to 3.57 %, equivalent to 10 to 50 % illite or up to 38 % mica in the clay fractions.

Trends in MgO, Al₂O₃ and SiO₂ show that the soil clay fractions lie on a mixing line between sepiolite and mica end-members, with a contribution from smectite. This is consistent with the XRD and TEM results.

There is a strong correlation between Fe₂O₃ and TiO₂. This can be attributed to the presence of mica in the soils, since the soil clays fall on the mica Fe₂O₃-TiO₂ trendline with similar Fe₂O₃/TiO₂ ratios to mica, rather than a ferric sepiolite.

There was no TEM evidence of fibrous mineral degradation to sheet silicates, nor for the evolution of mica laterally to a fibrous mineral. SEM analyses show that much of the sepiolite/palygorskite occurs as fringed sheets, but higher magnification often reveals these sheets to be composed of fibres. These are found coating (rather than evolving from) mica/illite particles, as free-standing mats, and are common on the grain-side of cutans. Some of these textures suggest illuviation of the fibrous clay minerals, but another explanation may be that sites such as that immediately adjacent to silicate grains have the highest concentration of silica for their formation. One TEM image shows what was interpreted to be acicular crystals developing from an amorphous phase, although well crystalline sepiolite was also present.

Chapter 5

Brine evolution and geochemical barriers: mineral formation in Namaqualand soils

5.1 Introduction

Pedogenic sepiolite dominates the clay fraction of calcareous soils on the Namaqualand coastal plain, sometimes accompanied by palygorskite (Singer et al., 1995, and Chapter 4). The occurrence of sepiolite in soils, especially as a dominant mineral, is generally reported to be rare except for some calcic and petrocalcic horizons. It is more common in arid-region alkaline lake sediments such as in the Tertiary Madrid Basin (Torres-Ruíz et al., 1994; Sánchez and Galán, 1995; Lopez-Galindo et al., 1996) and Tunisian sequences (Jamoussi et al., 2003; Zaaboub et al., 2005). This is an environment which in some cases is difficult to distinguish from the pedogenic (Singer, 1989).

The genesis of both sepiolite and palygorskite requires solutions with high pH, soluble Mg and Si. Palygorskite requires additional Al. Sepiolite requires a slightly higher pH and higher (Mg+Si)/Al than palygorskite (Jones and Galan, 1988, p. 664). This Al for palygorskite formation may be obtained through a pre-existing sheet silicate, possibly through a dissolution-reprecipitation mechanism (Elprince et al., 1979; Galan and Ferrero, 1982; Singer, 1989; Jones and Galan, 1988; Lopez-Galindo et al., 1996). Jones and Galan (1988, p. 663) noted

that the water-accommodating structure of sepiolite is more suited to direct precipitation from solution than that of palygorskite. Some authors, however, have favoured the idea of a neoformation of palygorskite: Singer and Norrish (1974), for example, found no precursor minerals such as smectite, and Monger and Daugherty (1991) favoured neoformation of palygorskite based on its morphology. Recent trace element and isotopic data, however, have tended to show that palygorskite is transformed whereas sepiolite is neoformed. Sánchez and Galán (1995) found that palygorskite was formed by transformation of illite and smectite involving reaction with Mg, and sepiolite was a neoformation product favoured by evaporation of silica- and Mg-bearing waters. Zaaboub et al. (2005) showed that sepiolite would have precipitated directly in lacustrine, playa-lake or sebka environments under alkaline conditions, high Si, high Mg and low Al activity; whereas palygorskite would have formed by transformation of already existing illite and/or smectite type aluminosilicates in solutions in equilibrium with isotopically heavier, and therefore more evaporated, solutions than the sepiolite.

In the pedogenic setting, Bouza et al. (2007) concluded that the association of calcite, fluorite, sepiolite, and possibly opal-CT in Argentinian Aridisols indicated a successive precipitation of these minerals under alkaline conditions during evaporation. Singer and Norrish (1974), considering occurrences of palygorskite in Australian soils, suggested that a soil solution having a similar composition to that of lakes from arid regions where palygorskite typically occurs, would itself constitute a suitable medium for palygorskite formation. Mineral stability diagrams have subsequently been applied to the genesis of sepiolite and palygorskite in soil environments (Singer and Norrish, 1974; Elprince et al., 1979; Fernandez-Marcos et al., 1979; Monger and Daugherty, 1991; Ducloux et al., 1995; Bouza et al., 2007).

Coastal Namaqualand soils experience greater evaporation than precipitation, and exhibit macroscopically many of the typical evaporite minerals (calcite, gypsum, halite). The presence of eluvial and bleached subsurface horizons, and wetness above layers of reduced permeability, suggest the presence of (temporary) subsurface water (Chapter 2 and Francis et al. (2007)). Also, many of the profiles have a calcrete horizon (with abundant sepiolite in the clay fraction, and accessory palygorskite) at the transition from the upper, finer aeolian-deposited sediments, to their underlying coarser upper shoreface marine sedi-

ments (Chapter 2). This fine-coarse transition has been identified by authors such as Yaalon and Wieder (1976), Singer (1989), Singer (2002) and Bouza et al. (2007) as the position at which sepiolite and palygorskite precipitation takes place, due to temporary waterlogging resulting from the accumulation of water at the boundary, until it attains the higher fluid pressure needed to fill the larger pores of the horizon below (Rode, 1969, cited by Yaalon and Wieder (1976)).

The soil mantle in an arid environment is analogous to a closed basin in that it loses more water by evaporation than it loses by hydraulic flow. Although Chapter 2 showed the presence of preferential vertical water movement through the regolith to bedrock, this loss of water through evaporation as the dominant mechanism of mineral formation is evident in the accumulation of evaporite minerals (ranging in the Namaqualand soils from halite and gypsum to calcite and sepiolite). The upward movement of water (vapour) through the soil due to the nocturnal chilling of the surface was demonstrated by (Prinsloo, 2005) and is outlined by Francis et al. (2007). The presence of these evaporite minerals will influence the composition of the soil solution (appropriately simulated through making an extract of a saturated paste) to a degree dependent on both the concentration of the more soluble minerals (e.g. halite) and the solubility of the less soluble minerals (e.g. calcite, sepiolite). This Chapter hypothesized, therefore, that the permeable upper horizons in the Namaqualand soils constitute a shallow ephemeral aquifer, which can be considered the pedogenic analogue of the saline lake environments in which sepiolite typically forms. The chemical evolution of the soil solution and clay mineral genesis could therefore be considered in the same terms as the geochemical evolution of closed-basin brines.

The main objective was to apply the principles of brine evolution, particularly those of the Hardie-Eugster model (Hardie and Eugster, 1970; Eugster and Hardie, 1978; Eugster and Jones, 1979), to sepiolite genesis in arid soils of the Namaqualand coastal plain, assuming that in equilibrated soil solutions the precipitating mineral controls the activity of one of its common ions (Kittrick, 1971). The Hardie-Eugster model was conceptualized for the evolution of closed-basin brines, and has since been applied to a diverse range of environments, from saline soil seeps (Timpson et al., 1986) to coastal pans (Smith and Compton, 2004) and a model of calcrete genesis (Wang et al., 1993).

Evaporite minerals including calcite, gypsum, halite and sepiolite were consid-

ered by Garrels and Mackenzie (1967), Hardie and Eugster (1970) and Eugster and Jones (1979) to precipitate from solution during evaporation and evolution of closed-basin brines. The precipitation of these minerals affects the composition of the remaining brine in a manner determined by the initial ratio of the component ions in the solution. Mineral precipitation was considered to constitute an important chemical divide in the evolving composition of the brine, but it is not the only mechanism which governs chemical fractionation in brines. Other mechanisms of solute depletion include sorption or exchange reactions on active surfaces, degassing, and bacterial reduction (Eugster and Jones, 1979). Conservative solutes, unaffected by such processes, can be used to measure the concentration effects. Depending on the removal mechanisms involved and their relative importance, each solute follows a different evolutionary path. Paths for a specific solute may differ from basin to basin, with the result that solute behaviour can be used to delineate the important processes for a particular basin and aid in unravelling its chemical evolution.

The objective was thus to use the variation in solute composition of equilibrated saturated paste extracts as a means of understanding the pedochemical history of mineral precipitation in Namaqualand soils. The present study was limited to those phases which were observed to be present and have been shown to be neoformed by precipitating from water: gypsum, halite, amorphous silica, calcite, dolomite (to represent Mg-rich calcite, even though no dolomite was detected in the calcretes analysed in Chapter 3), sepiolite and, hypothetically, kerolite, since its environment of formation is very similar to that of sepiolite and it was not possible either to confirm or refute its presence (Chapter 4). The Al-bearing phases that were detected with XRD can all be adequately explained by mineral transformation or dissolution re-precipitation: palygorskite (Jones and Galan, 1988; Sánchez and Galán, 1995; Zaaboub et al., 2005), kaolinite from feldspar weathering (Chapter 2), and smectite from illite/mica (Chapter 4). Although these transformations can only be achieved in a medium of suitable composition (Faure, 1998), for the purposes of this thesis only those phases that are neoformed were considered. Sepiolite was much more prominent on the XRD traces (Chapter 4) than palygorskite.

Soil solution chemistry is used in this Chapter to refine our understanding of the origin of sepiolite, and to contrast this with the genesis of other minerals that formed in the process of evaporation of the soil solution on the Namaqualand

coastal plain. This Chapter focuses particularly on the genesis of sepiolite, because of its relative rarity in the soil environment (although reports of it are increasing) and the uncertainties that sometimes surround its genesis.

5.2 Materials and methods

Fieldwork took place in February 2002. Fourteen soil profiles to bedrock were examined and sampled, from south of Hondeklip Bay to north of Kleinzee, approximately 150 km south of the Orange River on the west coast of South Africa. Samples were taken from the sidewalls of the mining excavations and from soil pits dug in the undisturbed areas nearby (described in Chapter 2). A summary of the landscape, climate and vegetation is given by Desmet (2007) and Chapter 2. Profile photographs are presented in Appendix A. The sepiolite on the Namaqualand coastal plain is clearly pedogenic in origin, since neither sepiolite nor palygorskite are present in the marine sediments (they contain only smectite, mica, and kaolinite in varying proportions), and although the appearance of sepiolite and palygorskite seems to be limited to subaerially-reworked material, not all aeolian material contains sepiolite/palygorskite (Chapter 4). Sepiolite and palygorskite are most consistently associated with the presence of calcite in the soil profile. Sepiolite occurs across all packages and elevations up to 99 m a.m.s.l., the farthest sampled from the sea (about 30 km). Saturated paste extracts were prepared for every sample that was analysed by X-ray diffraction (Chapters 1, 3, 4). The horizon types and their clay mineralogy are described in detail in those Chapters.

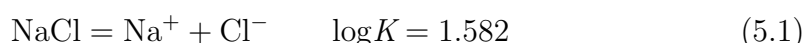
Saturated pastes were prepared with 300g of < 2 mm material, to which water (approximately 100g, depending on the clay content of the soil) was added to form a saturated paste. A subset of samples was duplicated and the saturated pastes allowed to stand for 6 and 60 hours. There was very little difference in composition (and resulting saturation indices) after 24 hours of equilibration and so 24 hours was used for all subsequent samples. Samples were equilibrated at ambient temperatures and open to gas exchange with the atmosphere, and so effectively equilibrated with a $p\text{CO}_2$ of ~ 3.5 atm. The pH of the saturated paste was measured directly. The water from the saturated paste was extracted under vacuum and the following variables analysed: electrical conductivity (EC), using

a calibrated conductivity meter; alkalinity, by potentiometric titration to pH 4.5 with 0.01M HCl; major cations (Ca^{2+} , Mg^{2+} , K^+ , Na^+) by atomic absorption spectroscopy; anions (Cl^- , F^- , NO_2^- , NO_3^- , Br^- , and SO_4^{2-}) by ion chromatography; Si using the blue silicomolybdous acid procedure of Weaver et al. (1968) (described by Hallmark et al., 1982), and P using the ascorbic acid-molybdenum blue method of Murphy and Riley (1962).

Square brackets [] denote ion activities throughout this Chapter. The saturation index (SI) is the $\log(\text{IAP}/K_{\text{eq}})$ for a dissolution reaction (Drever, 1997, p. 25). When the $\text{SI} = 0$, the ion activity product (IAP) = K_{eq} (the solubility product) which implies equilibrium with respect to the phase in question. A negative SI means that the IAP is less than K_{eq} which implies undersaturation of the solution with respect to the phase, and conversely a positive SI implies supersaturation. The saturation index (SI) was used in preference to stability diagrams, because it is a numerical index and allows the variation of mineral stability to be plotted against an independent salinity variable. Stability diagrams also have the disadvantage of requiring assumptions to be made about the activities of accessory solutes.

Speciation and saturation index calculations were performed with the program PHREEQC (Interactive Version 2.8.0.0; Parkhurst and Appelo, 1999), run with the database file *phreeq.dat*. The solubility equations and equilibrium constants in *phreeq.dat* are:

Halite:



Gypsum:



Quartz:



Amorphous silica:



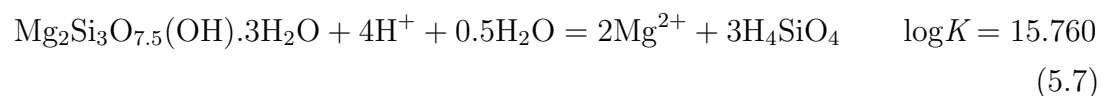
Calcite:



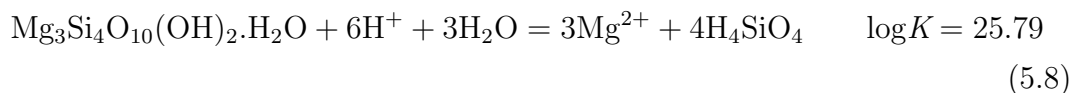
Dolomite:



Sepiolite:



Two equilibrium constants for sepiolite are included in *phreeq.dat*: ‘sepiolite’ which uses $\log K = 15.760$ from Stoessell (1988), and ‘sepiolite (d)’ which uses $\log K = 18.78$ from Wollast et al. (1968). The former was used in this Chapter because it was calculated from samples equilibrated for nearly 10 years at 25° C and 1 atm and is in good agreement with that extrapolated by Christ et al. (1973) from higher temperatures. The $\log K$ determined by Wollast et al. (1968) was for a poorly crystalline, non-equilibrated sample (Christ et al., 1973; Stoessell, 1988). Kerolite was added to the *phreeq.dat* database file using the $\log K$ from Stoessell (1988):



PHREEQC is a computer program written in the C programming language that is designed to perform a wide variety of low-temperature aqueous geochemical calculations (Parkhurst and Appelo, 1999) with capabilities for speciation and saturation-index calculations. PHREEQC uses ion-association and Debye Hückel expressions to account for the non-ideality of aqueous solutions. This type of aqueous model is adequate at low ionic strength but may break down at higher ionic strengths (in the range of seawater and above) (Parkhurst and Appelo, 1999). The authors of PHREEQC attempted to extend the range of applicability of the aqueous model through the use of ionic strength terms in the Debye Hückel expressions. These terms were fit for the major ions using chloride mean-salt activity-coefficient data. Thus in sodium chloride dominated solutions (as with the saturated paste extracts from Namaqualand Coastal Plain, see Section 5.3, Table 5.1) the model may be reliable at higher ionic strengths. For high ionic

strength waters, the specific interaction approach to thermodynamic properties of aqueous solutions should be used (Pitzer, 1973; Pitzer, 1979; Harvie and Weare, 1980; Harvie et al., 1984), but this approach is not incorporated in PHREEQC 2.8.0.0 (Parkhurst and Appelo, 1999). PHREEQC Version 2.12 uses the Pitzer activity coefficient model and so replaces PHRQPITZ (Plummer et al., 1988) for brine speciation calculations, using the *pitzer.dat* database. However, at the time of writing the *pitzer.dat* database included for download with PHREEQC Version 2.13.2 is of limited usefulness to soil applications since the database contains no data for silica and pedogenic clay minerals. The database file *phreeq.dat* consequently remains the most suitable for this system.

5.3 Results and discussion

Seawater has an ionic strength of 0.67 according to the PHREEQC calculation of the seawater data from Nordstrom et al. (1979) (included with the PHREEQC distribution as Example 1 of the Help File). The speciation calculations showed the ionic strength of the samples to be in range of 0.004 to 0.76, with most of the samples falling well below the concentration of seawater (Figure 5.1). Given the discussion in Section 5.2, it suggests that PHREEQC is an adequate tool with which to perform speciation calculations in these soils.

Watts (1980) noted an inverse relationship between the mol % MgCO_3 in calcite and the sepiolite/palygorskite content, which suggested that these Mg-rich clay minerals are the main Mg-bearing phase in Botswana calcretes. The apparent absence of Mg-calcite and dolomite, and abundance of sepiolite in the calcretes of coastal Namaqualand suggests that a similar partitioning has occurred (Chapter 3) and so it has been assumed in this Chapter that sepiolite controls the Mg levels in the saturated paste extracts.

The saturated paste extract data (Table 5.1) were divided into sepiolitic and non-sepiolitic categories based on XRD findings (Chapters 1, 3, 4) and then PHREEQC (Parkhurst and Appelo, 1999) was used to calculate the ion activities and mineral saturation indices. A few samples showed detectable Br^- , NO_3^- , F^- and NO_2^- , but these could not be accurately determined because the high salinity of the samples required a large dilution, resulting in the less abundant ions being diluted to below the detection limit of ion chromatography.

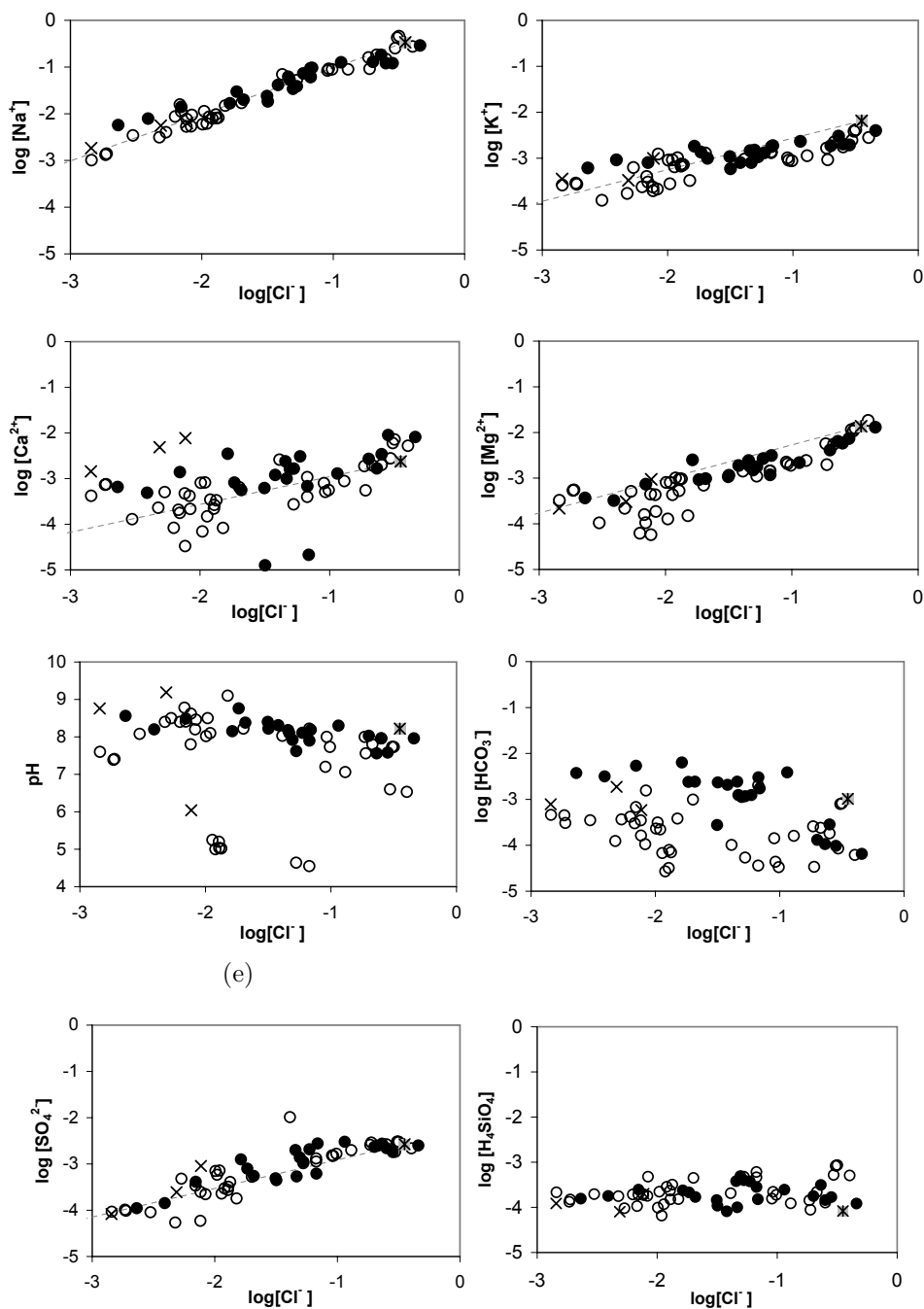


Figure 5.1: Variation of ion activities with Cl^- in saturated paste extracts. Solid circles represent soils with sepiolite (some with accessory palygorskite) in the clay fraction; open circles represent no detectable sepiolite or palygorskite; \times - no clay present. Na-Cl represents the conservative slope. Grey square with * is seawater from Nordstrom et al. (1979) which is included in the PHREEQC User Manual (Parkhurst and Appelo, 1999) as Example 1. Dashed line: seawater composition projected back to zero.

Table 5.1: Composition of saturated paste extracts.

Sample	Depth m	Horizon	Classification †	pH	EC mS/cm	Alkalinity ‡	Na ⁺	K ⁺	Mg ²⁺	Ca ²⁺	Cl ⁻	SO ₄ ²⁻	mmol/L			SAR ¶
													P	S	Si	
6869/i	0-	A1	Regic sand (Orthic A)	8.95	0.380	2.09	1.91	0.321	0.584	1.16	1.50	0.220	0.008	0.207	2	
6869/ii	0.45-	A2	Regic sand	9.19	1.00	2.80	6.18	0.366	1.04	1.24	5.41	0.822	n.a.	0.214	6	
6869/iii	0.5-	II B1	Neocarbonate B	8.31	5.83	2.96	50.9	1.01	8.43	5.60	47.7	-	n.a.	0.185	19	
6869/iv	0.6-0.8	II B2	Neocarbonate B	8.10	7.19	1.74	67.1	1.03	8.98	5.07	59.4	3.71	n.a.	0.212	25	
6869/v	0.32-	IV C1	Hardpan carbonate	8.52	4.70	3.52	30.5	0.837	6.09	7.80	39.2	3.58	n.a.	0.56	12	
6869/vi	1-	IV C2	Marine deposit	8.02	1.09	0.213	5.93	0.249	1.32	1.35	8.85	0.205	0.018	0.422	5	
6869/vii	6-9	V C3	Marine deposit	8.38	0.690	0.150	3.39	0.185	0.601	0.636	5.16	0.162	n.a.	0.382	4	
6869/viii	9-18	VI C4	Marine deposit	8.39	0.496	0.203	3.52	0.115	0.252	0.286	3.28	0.262	0.151	0.427	7	
AK11/10	1.5-	III C2	Dorbank	7.56	27.1	0.180	252	4.54	48.7	13.6	342	39.4	0.015	0.624	45	
AK11/6	1.6-	III C3	Dorbank	7.96	48.0	0.150	396	6.29	98.2	69.6	715	56.0	0.008	0.227	43	
AK61H/4	0-	A	Orthic A	8.15	3.19	9.24	20.6	2.28	12.8	18.2	20.3	9.11	n.a.	0.51	5	
AK61H/1	0.35-	II C1	Hardpan carbonate	7.96	19.7	0.500	167	3.02	43.1	26.9	370	30.1	0.008	0.275	28	
KV196T/1	±1-	B2	Red apedal B	9.27	0.779	6.62	5.67	0.815	0.114	0.165	2.66	0.656	n.a.	0.71	15	
KV196T/2	1.3-	C1	Dorbank	8.00	7.81	2.25	100	1.53	14.0	9.51	79.9	11.5	n.a.	1.44	29	
KV196T/3	1.45-	C2	Dorbank	7.79	18.9	0.583	174	1.92	39.7	24.5	223	27.8	0.013	0.668	31	
KV196T/4	1.6-	C3	Dorbank	7.99	37.9	1.78	429	4.41	88.1	0.874	418	78.6	n.a.	0.29	64	
KV196T/5	1.8-	C4	Hardpan carbonate	8.22	7.24	2.24	51.0	2.24	14.8	60.0	44.7	78.2	n.a.	0.75	8	
KV196T/7	? - 3.5	C6	Soft dorbank	8.22	8.96	3.05	123	1.85	8.45	6.56	89.6	10.7	n.a.	1.30	45	
KV196T/8	±3.5-	C7	Dorbank	8.03	10.9	0.160	96.0	1.39	14.3	25.4	56.0	91.0	0.007	0.425	22	
KV196T/9	±4.5-	C8	Dorbank	7.73	37.6	1.64	588	6.08	84.2	52.7	478	68.3	n.a.	1.48	71	
LKC1-5/A	0-	A	Regic sand (Orthic A)	5.99	1.51	0.76	7.26	1.13	3.20	4.76	7.82	3.76	0.114	0.326	4	
LKC1-5/B	0.3-	B	Regic sand	8.21	1.34	0.375	6.09	0.931	2.50	2.50	10.0	2.52	0.018	0.185	4	
LKC1-5/1	1-	II B2	Neocutanic B	7.11	12.7	0.268	119	1.51	15.4	5.69	160	16.7	0.010	0.279	37	
LKC1-5/3	1.3-	II B3	Neocutanic, luvic	7.94	24.4	0.375	219	2.59	44.7	16.1	351	36.8	0.009	0.265	40	
LKC1-5/9	5.4--12	VII C6	Marine deposit	7.76	11.9	0.060	119	1.22	12.1	3.38	129	13.2	0.008	0.335	43	
OB1/5	1-	II C2	Sedimentary?	8.18	6.32	3.71	80.2	1.93	14.6	14.6	59.7	16.7	n.a.	0.81	21	
SK11/A	0-	A	Orthic A	8.49	1.43	7.26	16.3	0.939	2.94	5.77	8.17	1.93	n.a.	0.55	8	
SK11/B	0.2-	B	Yellow-brown apedal B	8.56	0.603	4.62	6.34	0.683	1.20	2.21	2.57	0.39	n.a.	0.35	5	
SK11/C	0.6-	E	Gleyed sand	8.20	0.721	3.71	8.81	1.03	1.05	1.61	4.37	0.50	n.a.	0.39	8	
SK11/D	0.65-	B2	Neocutanic	7.90	9.42	4.13	77.6	2.33	6.20	3.70	87.6	4.28	n.a.	0.60	35	
SK11/6	0.45-	II C2	Blocky calcitized sediment	8.30	20.2	6.40	171	3.30	16.0	9.88	161	30.5	n.a.	0.52	48	
SK11/9	0.9-1.1	III C3	Hardpan carbonate	8.03	18.6	0.230	177	2.73	29.9	20.7	290	28.9	0.503	1.260	35	
SK11/5	0.8-1.5	III C3	Termite nest	8.19	10.9	2.63	128	2.58	20.9	0.146	93.2	24.3	n.a.	0.32	39	
SL4-1/1	0-0.3	A1	Orthic A	7.47	0.475	0.440	1.34	0.294	1.31	1.76	1.87	0.313	0.011	0.346	1	
SL4-1/2	0.3-	B1	Yellow-brown apedal B	5.03	1.67	0.058	9.19	0.949	3.36	1.09	14.6	1.38	0.023	0.527	6	
SL4-1/3	0.5-	E	Gleyed sand	5.23	1.59	0.057	10.3	0.749	1.60	0.615	13.7	0.923	0.009	0.368	10	
SL4-1/4	0.63-	B2	Neocutanic	4.60	7.54	0.023	72.0	1.57	6.67	1.81	77.3	7.16	n.a.	0.980	35	
SL4-1/5	0.8-	II B3	Gleyed sand?	6.57	36.1	0.143	365	4.11	111	33.5	538	42.2	0.008	0.922	43	
SL4-1/6	0.95-	III B4	Pedocutanic	7.80	25.1	0.430	253	3.38	41.0	15.5	314	34.5	0.011	0.436	48	
SNT60/5	~1.5-2.3	IV C1	Hardpan carbonate	8.76	2.81	3.63	35.7	1.66	4.18	3.78	22.3	4.16	na	0.50	18	
SNT60/6			Local channel?	8.38	3.35	3.18	23.6	1.19	4.04	2.37	24.8	2.66	na	0.38	13	
SNT60/7	~2.3-2.8	V C5	Blocky calc. sediment	8.40	3.63	0.345	28.7	1.31	4.51	2.66	38.1	2.55	0.008	0.332	15	
SNT60/10	2.8-	VI C6	Sedimentary?	8.46	1.52	0.563	12.7	0.327	0.394	0.412	9.83	1.58	0.011	0.453	20	
SNT60/11	3.4-	VII C7	Sedimentary?	8.51	1.15	0.307	9.06	0.240	0.179	0.174	7.70	0.770	0.008	0.417	22	
SNT60/12	3.7-	VIII C8	Sedimentary?	8.94	2.06	0.540	17.4	0.413	0.513	0.480	12.5	0.660	0.008	0.319	25	
TP231/4	2-	III C2	Marine deposit	8.11	8.08	1.95	95.6	1.77	16.7	19.5	79.1	19.1	n.a.	0.79	22	
TP266Q/1	1.2-1.7	III C1	Hardpan carbonate	7.58	25.2	0.180	167	2.94	53.8	71.7	424	30.5	0.008	0.392	21	

† Classified according to the Soil Classification Working Group (1991). Roman numerals indicate different sedimentary units.

‡ Alkalinity: $\text{CO}_3^{2-} + \text{HCO}_3^-$, since CO_3^{2-} was only detected in LK1-5/B and SNT60/10 and $\leq 0.01 \text{ mmol}_c/\text{L}$.

§ N.a. - not analysed. Since P was very low and together with F made no difference to the saturation index calculations it was not measured in all samples.

¶ SAR=sodium adsorption ratio: $\text{Na}/\sqrt{(\text{Ca} + \text{Mg})/2}$.

Soluble Al was not measured since it was assumed to be low at the pH range encountered, and the Al-bearing phases that were detected with XRD could all be adequately explained by mineral transformation or dissolution re-precipitation (see Section 5.1). The phosphate and fluoride were very minor and made no difference to the saturation index calculations. The system was therefore simplified to the components Na^+ , K^+ , Ca^{2+} , Mg^{2+} , Si, pH, Cl^- , SO_4^{2-} , and HCO_3^- .

Most of the soils for which there was a positive sepiolite identification (1.2 nm XRD peak, Chapters 1, 3, 4) showed a positive sepiolite saturation index (Figure 5.2), suggesting that the saturated paste extracts were in equilibrium with sepiolite. This is in direct contrast to the findings of Singer et al. (1995), which were that sepiolitic and palygorskitic soils in the same region were undersaturated with respect to both these phases when using a 1:1 soil-water solution. Their interpretation, therefore, that these minerals were pedogenically formed in the past and are currently in a state of alteration towards mixed layer or smectite clay due to a reduction in alkalinity and/or Mg supply induced by climatic shifts during the Late Pleistocene and Holocene, therefore requires revision. Following Kittrick's (1971, p. 453) suggestion that "where the soil solution has had appreciable contact with precipitating minerals, it is likely to be in equilibrium with them", the data from the current study showing sepiolite equilibrium in sepiolitic soils suggest that sepiolite can be considered a 'precipitating mineral' and thus forming in the present day. Furthermore, in Chapter 4 there was no TEM evidence to favour a hypothesis for fibrous mineral degradation to sheet silicates.

5.3.1 Chloride as a proxy for evaporative concentration

Chloride is a reliable measure of the degree of evaporative concentration up to halite saturation because chloride is usually conserved over the widest concentration range since anion exchange is minor and Cl^- remains in solution until halite reaches saturation (Eugster and Jones, 1979). Eugster and Jones (1979) explained that this does not mean the solute is not involved in the formation of efflorescent crusts (which were observed in some profiles in this study, see Chapter 2), but that it will be redissolved quantitatively by subsequent runoff. Halite remains undersaturated at all concentrations in the saturated paste extracts (Figure 5.2), confirming the suitability of Cl^- being used as a proxy for evaporative concentration in this system.

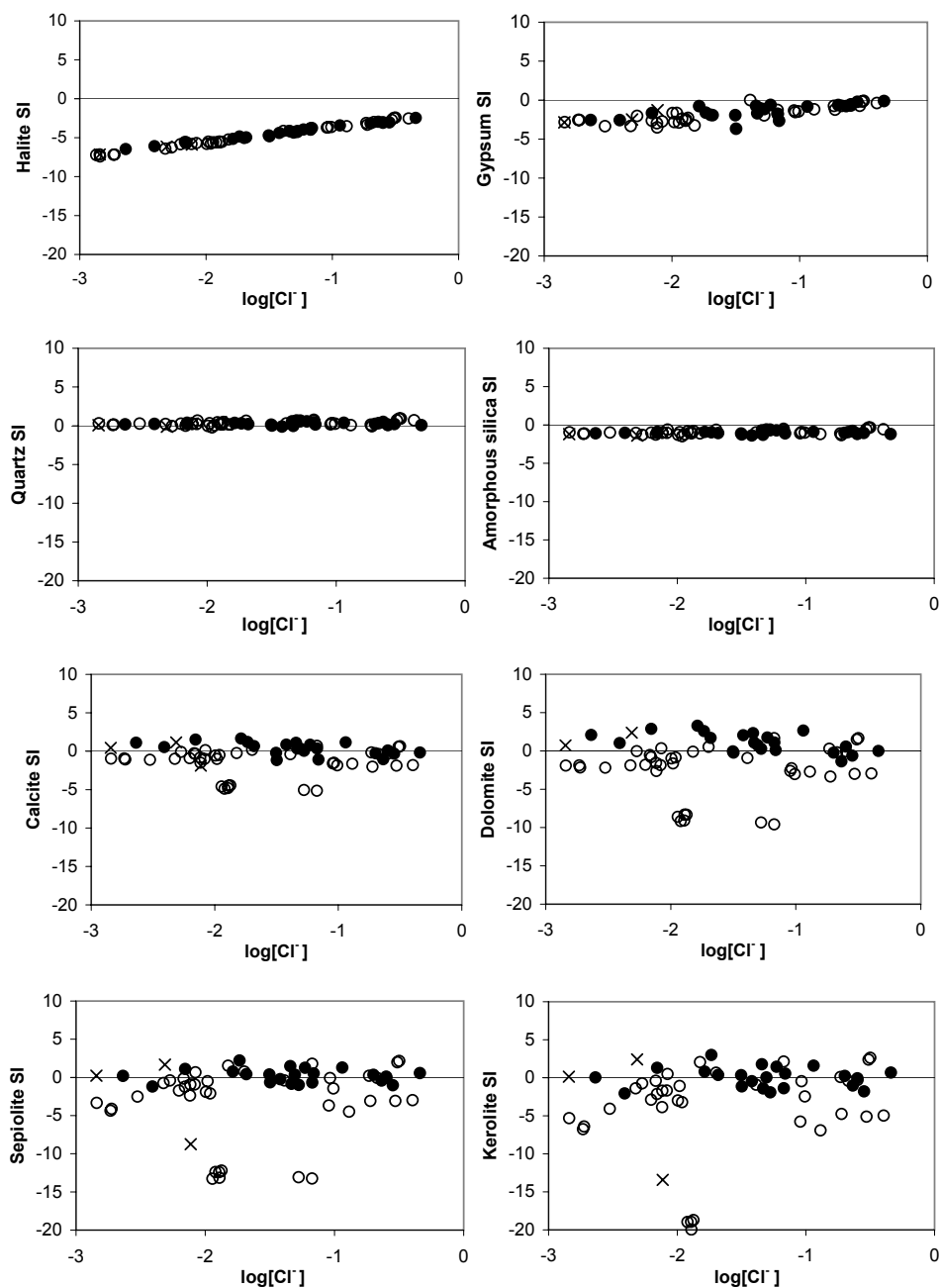


Figure 5.2: Variation of mineral saturation indices (SI) with Cl^- activity in saturated paste extracts. $\text{SI} > 0$ indicates supersaturation, $\text{SI} < 0$ undersaturation, and $\text{SI} = 0$ equilibrium with respect to a phase. Symbols as for Figure 5.1.

The variation in activity of all the ions with Cl^- is consistent with a seawater dilution line (Figure 5.1). The ions K^+ , Ca^{2+} and Mg^{2+} increase with increasing evaporation but at a slope less than that for the conservative solutes Na^+ and Cl^- (Figure 5.1). According to Eugster and Jones (1979), this is typical for removal mechanisms such as mineral precipitation, sorption, or degassing, which operate over the full range of evaporative concentration so that an essentially linear relationship results, but with a slope less than that for conservative solutes. Sulfate increases until $\log[\text{Cl}^-]$ reaches -1 and then levels off (Figure 5.1) as gypsum reaches saturation (Figure 5.2: gypsum SI vs $\log[\text{Cl}^-]$).

H_4SiO_4 activity remains unchanged for all levels of evaporation (Figure 5.1). This is consistent with the behaviour of an uncharged solute which has reached saturation with respect to the corresponding solid phase (Eugster and Jones, 1979). In the Namaqualand soil system the most likely neoformed minerals controlling the H_4SiO_4 solubility are sepiolite and amorphous silica/quartz. Many of the sepiolite-containing samples show an amorphous silica component in their XRD trace (Chapter 4), and silica-cemented horizons are common (Chapter 1), ranging from silcrete to petroduric (WRB, 1998). There are many examples of etched quartz grains suggesting remobilisation of silica. Figure 5.2: sepiolite SI vs $\log[\text{Cl}^-]$ shows that the sepiolite-bearing soils are saturated or supersaturated with respect to sepiolite through the entire concentration range. All the soils analysed are close to saturation with respect to both quartz and amorphous silica (Figure 5.2: quartz and amorphous silica SI vs $\log[\text{Cl}^-]$).

Both quartz and amorphous silica saturation indices are independent of pH (Figure 5.3) and directly dependent on silica concentration (Figure 5.4). This is because the solubility of both quartz and amorphous silica is expressed only in terms of one aqueous species, H_4SiO_4 (equations 5.3 and 5.4). As a result, in the amorphous silica and quartz SI vs $\log[\text{H}_4\text{SiO}_4]$ plots (Figure 5.4), the SI reaches zero where $\log[\text{H}_4\text{SiO}_4]$ is equal to the $\log K$ used to calculate the saturation index of the respective phases, in this case -2.710 for amorphous silica and -3.980 for quartz. In the H_4SiO_4 vs Cl^- activity plot, however, (Figure 5.1), the X- and Y-axes were calculated from independent variables. Therefore, in the Namaqualand coastal plain soils the best explanation for the unchanged H_4SiO_4 activity for all levels of evaporation (Figure 5.1) is that it is consistent with the behaviour of an uncharged solute which has reached saturation with respect to the corresponding solid phase (Eugster and Jones, 1979), i.e. quartz, amorphous silica and/or sepiolite.

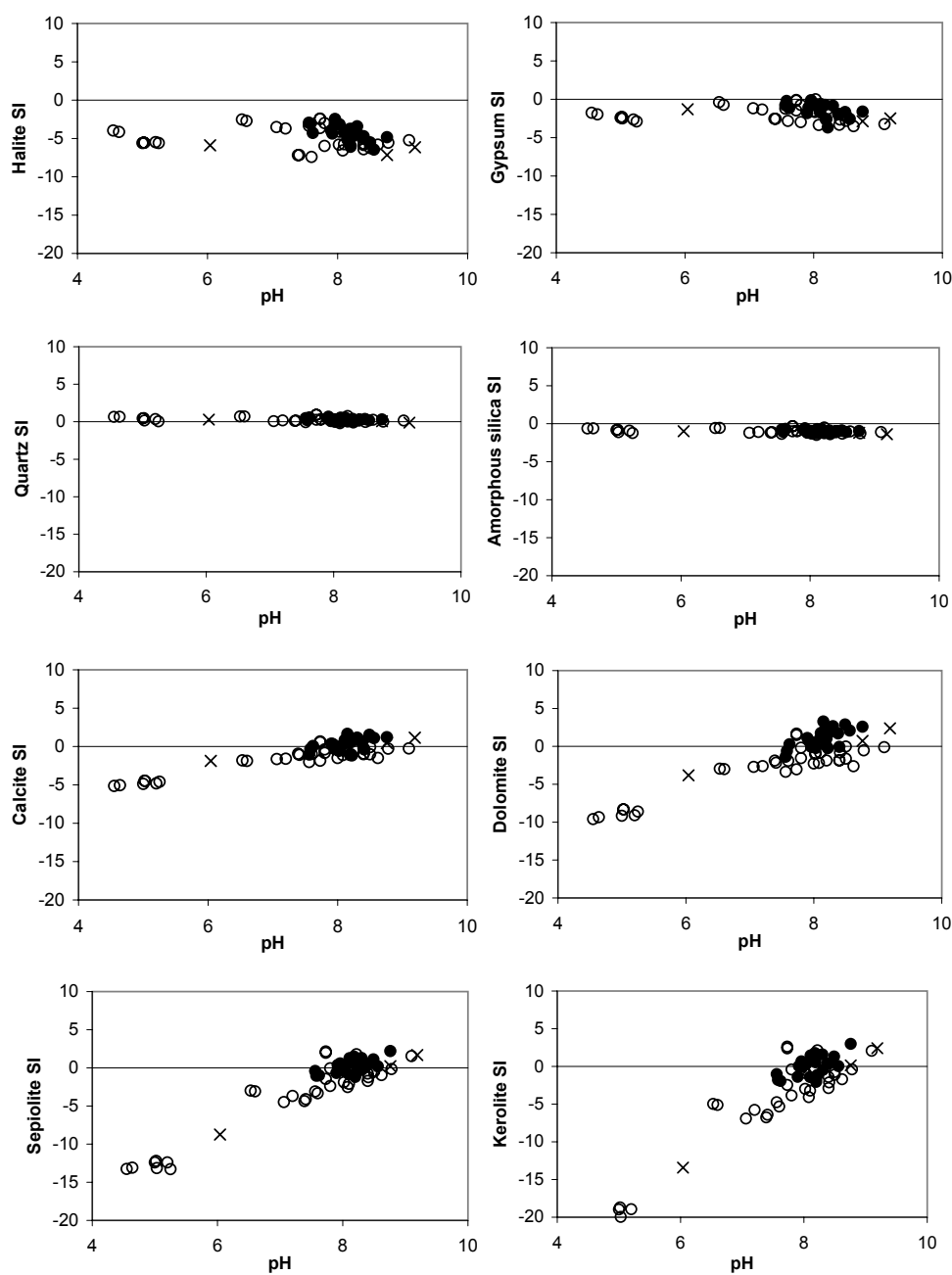


Figure 5.3: Variation of mineral saturation indices (SI) with pH; saturated paste extracts. $SI > 0$ indicates supersaturation, $SI < 0$ undersaturation, and $SI = 0$ equilibrium with respect the phase in question. Symbols as for Figure 5.1.

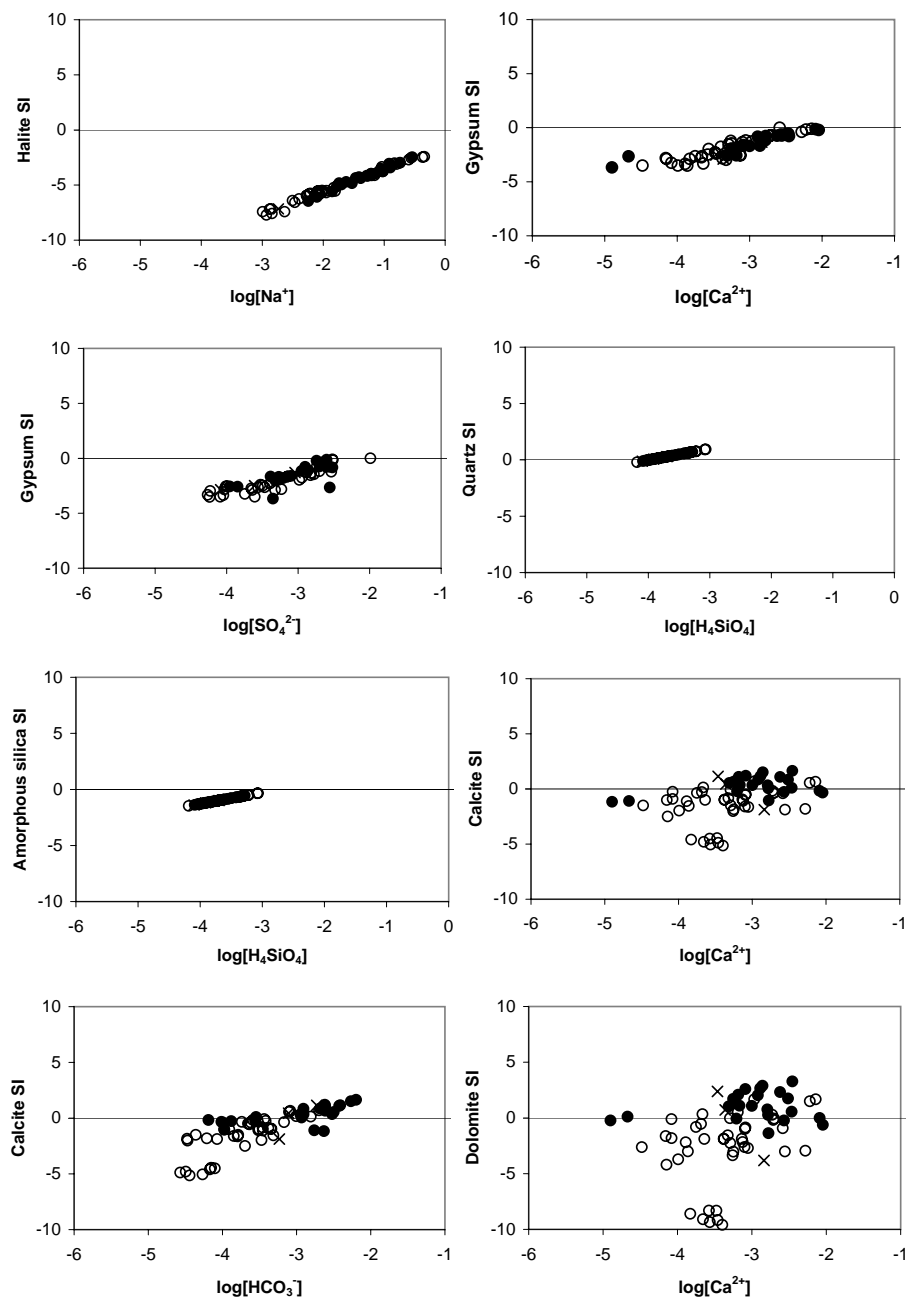


Figure 5.4: Variation of mineral saturation indices (SI) with activity of component ion; saturated paste extracts. $SI > 0$ indicates supersaturation, $SI < 0$ undersaturation, and $SI = 0$ equilibrium with respect to a phase. Symbols as for Figure 5.1.

Alkalinity was only present as bicarbonate. The HCO_3^- activity vs Cl^- activity plot (Figure 5.1) most effectively distinguishes the sepiolitic vs non-sepiolitic soils, with the sepiolitic soils generally having higher HCO_3^- activities consistent with observations that only the calcareous soils are sepiolitic. The HCO_3^- activity of both the sepiolitic and non-sepiolitic soils decreases slightly with increasing Cl^- . The decrease in HCO_3^- activity coupled with a simultaneous increase in Ca^{2+} is consistent with calcite precipitation at the first ‘chemical divide’ in the Hardie-Eugster model of brine evolution (Hardie and Eugster, 1970; Eugster and Hardie, 1978; Eugster and Jones, 1979). All the Namaqualand soils are close to saturation with respect to calcite (Figure 5.2: calcite SI vs $\log[\text{Cl}^-]$).

Calcite, usually the first mineral to precipitate on evaporative concentration, represents a critical branching point in the evolutionary path of the evaporating water (Eugster and Jones, 1979). The path then taken by the solution depends on whether the calcium concentration in equivalents is greater or less than the carbonate alkalinity in equivalents, that is, whether $2m_{\text{Ca}^{2+}}$ is greater or less than $(m_{\text{HCO}_3^-} + 2m_{\text{CO}_3^{2-}})$ where m is molal units (Drever, 1997, p. 330). This is because two conditions must be fulfilled simultaneously during the equilibrium precipitation of calcite: 1) the ion activity product $[\text{Ca}^{2+}][\text{CO}_3^{2-}]$ must remain constant, and 2) Ca^{2+} and CO_3^{2-} are removed in solution in equal molar proportion (Eugster and Jones, 1979). Condition 1 specifies that the concentrations of Ca^{2+} and CO_3^{2-} must vary antithetically, whereas condition 2 requires that the $\text{Ca}^{2+}/\text{CO}_3^{2-}$ molar ratio will change unless it was precisely one at the outset (Eugster and Jones, 1979). The net effect is that waters in which HCO_3^- is dominant over Ca^{2+} initially will become enriched in HCO_3^- and depleted in Ca^{2+} , and vice versa (Eugster and Jones, 1979).

In these coastal Namaqualand soil solutions it appears that calcite precipitation results in a solution in which the Ca^{2+} increases and HCO_3^- decreases (Figure 5.1). According to the conditions outlined above, this is because the initial $\text{Ca}^{2+}/\text{HCO}_3^-$ ratio is greater than one. Given the proximity of the sea (maximum sampling distance 30 km from coast) and strong onshore winds, these soils would be expected to reflect maritime ionic ratios. $\text{Ca}^{2+}/\text{HCO}_3^-$ ratio is greater than one for seawater, according to the data from Nordstrom et al. (1979) (plotted in Figure 5.1): the molality of Ca^{2+} in seawater is $9.504\text{e-}03$, and of HCO_3^- is $1.514\text{e-}03$. CO_3^{2-} is negligible in comparison at $3.821\text{e-}052$. This is consistent with trends in Figure 5.1 and suggests that initial maritime ratios control the

evaporative evolution of the soil solution by providing an initial $\text{Ca}^{2+}/\text{HCO}_3^-$ ratio greater than one.

5.3.2 Marine-influenced initial ratios and subsequent evaporation trends

The increasing Mg with increasing Cl activity (evaporation) (Figure 5.1), is in contrast to that which is expected to occur, given that sepiolite is expected to precipitate with increasing evaporation, as was shown in the classic model of Garrels and Mackenzie (1967). Since both sepiolitic and non sepiolitic soils show the increasing Mg with Cl trend, it cannot be attributed to an increase in actual sepiolite content.

The Ca-HCO_3^- -Cl trend is also opposite to that of Garrels and Mackenzie (1967). It was established in Section 5.3.1 that the increasing Ca and decreasing HCO_3^- with Cl trend is a result of evaporating a solution with a $\text{Ca}^{2+}/\text{HCO}_3^-$ ratio greater than one, and that the initial ratio is marine-influenced. Singer et al. (1995) considered sea-spray enriched precipitation as one source of Mg for sepiolite precipitation. The saturated paste extracts have similar Mg/Cl ratios to seawater (Figure 5.1). It can be hypothesized that the trend of increasing (rather than decreasing) Mg with Cl may also be marine-influenced.

Mg-Cl trends from a variety of literature sources are tabulated in Table 5.2. Only Mg-silicates and Ca-Mg carbonates were included in the table because the focus was on the marine-influenced increasing Mg-Cl and Ca-HCO_3^- -Cl trends. Where the original authors' data were not in mmolc/L, it was replotted in these units and on a log-log scale for comparison with data from the present study. Theoretical evaporation trends for two soil solutions in the present study were also included: one from a non-calcareous, non-sepiolitic horizon and the other from a calcareous, sepiolitic horizon. Both horizons are otherwise similar in terms of their environments of formation (clay-enriched sand over a barrier, see Chapter 2).

Table 5.2 shows that the maritime and continental areas show distinctly opposite trends. The marine-influenced areas, as in this study, generally show a trend of decreasing pH, increasing Ca and increasing Mg with increasing evaporation. This can be explained by their initial solute proportions $\text{Ca} > \text{HCO}_3^-$,

$Mg > HCO_3^-$, $Mg > Si$ and $Mg > Ca$, consistent with the ‘chemical divides’ of the Hardie-Eugster model of brine evolution (Hardie and Eugster, 1970; Eugster and Hardie, 1978; Eugster and Jones, 1979). In contrast, continental areas such as that studied by Garrels and Mackenzie (1967) show decreasing Ca, decreasing Mg and increasing HCO_3^- with evaporation, due to their initial solute proportions $Ca < HCO_3^-$, $Mg < HCO_3^-$, $Mg < Si$ and $Ca > Mg$ (Table 5.2). The trends do not depend on such factors as the maximum concentration or ionic strength, scale, using Cl as the concentration factor, modelling the evaporation from a single sample or plotting all the samples against Cl for a system.

According to the Hardie-Eugster scheme presented in Drever (1997, p. 331), sepiolite precipitation affects the Mg/HCO_3^- ratio. Where Mg was present in excess initially, it is the HCO_3^- that is depleted (as Table 5.2 shows to have occurred in maritime areas). Where the HCO_3^- is present in excess initially, it is the Mg that is depleted - as in the model by Garrels and Mackenzie (1967) and other continental areas (Table 5.2). This maritime-continental model is simplistic in that factors other than the marine influence could affect initial Mg ratios, such as the parent soil or rock type, which have not been accounted for in the compilation of the data in Table 5.2. The data collected in Table 5.2 serves to show, however, that the changes in ionic ratios in the saturated paste extracts are consistent with other marine-influenced surface waters, and differ antithetically to surface waters where the maritime influence is absent. The data by Banks et al. (2004) is an exception to the maritime-continental evolution trends, but they are from a cold arid environment, in contrast to the other continental locations in Table 5.2. Additionally, they are from a diversity of hydrological, geological and topographical environments which were sparsely sampled, and the immature highland groundwaters are dominated by Ca, Mg and HCO_3^- ions resulting from carbonate and silicate weathering reactions (Banks et al., 2004).

The maritime influence on the $Mg-Ca-HCO_3^-$ ratio in coastal areas is also indicated by the different composition of fog water collected at the coast compared to fog water collected further inland. The west coast fog, which can be observed to extend inland to the rise of the escarpment, occurs frequently along the coastal plain at elevations below the 200 m contour line (Olivier, 2002). Data from Eckardt and Schemenauer (1998) showed that fog collected at Gobabeb (Desert Ecological Research Unit) in Namibia, 60 km from the coast, had an average composition showing $Ca > HCO_3^- > Mg$, after rinsing to remove previously built-up

aerosols. These aerosols had a much higher Mg content than the fog. In contrast, fog collected in the same study from “the gravel plain near the coastal town of Swakopmund” had a composition showing $\text{Mg} > \text{Ca} > \text{HCO}_3^-$, a considerably more maritime signature according to the data in Table 5.2. This suggests that fog deposition nearer the coast is accompanied by a greater proportion of marine aerosols than fog which has travelled further inland. Further evidence of the elevated Mg from marine aerosols in coastal fog is found in the work of Olivier (2002), who found $\text{Mg} > \text{Ca} > \text{HCO}_3^-$ in a windblown sea-salt contaminated fog collector at Cape Columbine on the West Coast of South Africa. After washing down the collector screens prior to collecting the second sample, a more accurate reflection of the fog water composition was obtained: $\text{HCO}_3^- > \text{Ca} > \text{Mg}$.

5.3.3 pH control of sepiolite equilibrium

Although sepiolitic soils are more abundant on the higher side of the Mg-Cl trend (Figure 5.1), the degree of evaporative concentration shown by the saturated paste extracts does not distinguish the sepiolitic from non-sepiolitic soils (Figure 5.2). In contrast to halite and gypsum, which clearly approach saturation as the Cl^- activity increases, the phases sepiolite, calcite, dolomite and kerolite are consistently close to saturation for all levels of Cl^- activity (Figure 5.2).

On first consideration, this appears to be a problem related to the kinetics of precipitating a complicated Mg-silicate such as sepiolite, compared to a relatively simple salt like gypsum or halite. However, unlike evaporating water bodies that may be supersaturated with respect to a phase for which the kinetics of precipitation may be slower than the rate of evaporation, the solutions used in the present study are from equilibrated saturated paste extracts. The likelihood of equilibration with respect to sepiolite is indicated by the fact that the samples in which sepiolite was detected in the clay fraction have extracts that are close to saturation with respect to sepiolite. In the equilibrated saturated paste extracts it would therefore be expected that higher Mg levels would be correlated with a higher soil sepiolite content.

Of all the species plotted against the chloride activity in Figure 5.1, it is the HCO_3^- activity that most obviously distinguishes the sepiolitic- from non-sepiolitic soils. This is reflected in the saturation index trends with pH: rather than increas-

ing with increasing chloride activity, the saturation indices of sepiolite, calcite, dolomite and kerolite are controlled by increasing pH (Figure 5.3). In contrast, gypsum and halite, the two minerals which do show increasing saturation with increasing chloride activity, display no change in saturation with pH.

Furthermore, halite and gypsum saturation are equally controlled by the concentration of each of their component ions in solution, but this is not the case for calcite, dolomite, sepiolite and kerolite (Figures 5.4 and 5.5). Sepiolite and kerolite saturation are independent of Mg^{2+} and H_4SiO_4 activities and depend only on H^+ activity at the magnesium and silica levels measured on the Namaqualand coastal plain. This is consistent with the work of Deocampo (2005) concerning the stabilities of sepiolite and kerolite during evaporation in waters of Tanzania. Deocampo (2005) noted that "...no simple evaporatively-controlled trend is apparent. In fact, pH variability is responsible for most of the observed change in saturation state...". As with sepiolite and kerolite, saturation with respect to calcite and dolomite in Namaqualand soils is dependent neither on Ca^{2+} nor the Mg^{2+} activity, but only the HCO_3^- activity over all concentrations of these elements encountered in the soils studied.

The pH-dependence of the sepiolite and kerolite saturation indices is to be expected, since the H^+ term is present in their solubility equations (equations 5.7 and 5.8, Section 5.2). The H^+ term is absent in halite and gypsum solubility equations (equations 5.1 and 5.2). Although the solubility equations of calcite and dolomite do not contain an H^+ term (equations 5.5 and 5.6), the pH dependence of calcite and dolomite is due to the PHREEQC speciation equation $CO_3^{2-} + H^+ = HCO_3^-$, $\log K = 10.329$, which uses the pH and HCO_3^- concentrations input by the user to calculate the CO_3^{2-} concentration which is then used in the solubility equations of calcite and dolomite (equations 5.5 and 5.6).

The implication for sepiolite genesis on the Namaqualand coastal plain is that sepiolite precipitation is more likely to be triggered when a solution encounters a pH barrier than by the concentration of ions through evaporation, since even the lowest Mg-Si levels are almost sufficient for sepiolite saturation (Figures 5.1, 5.2). This is similar in principle to the 'geochemical barriers' discussed by Sauer and Stahr (2004), and implies that lateral subsurface flow with no evaporative concentration along its route could result in sepiolite precipitation. In Namaqualand, there is evidence of lateral subsurface water movement in the

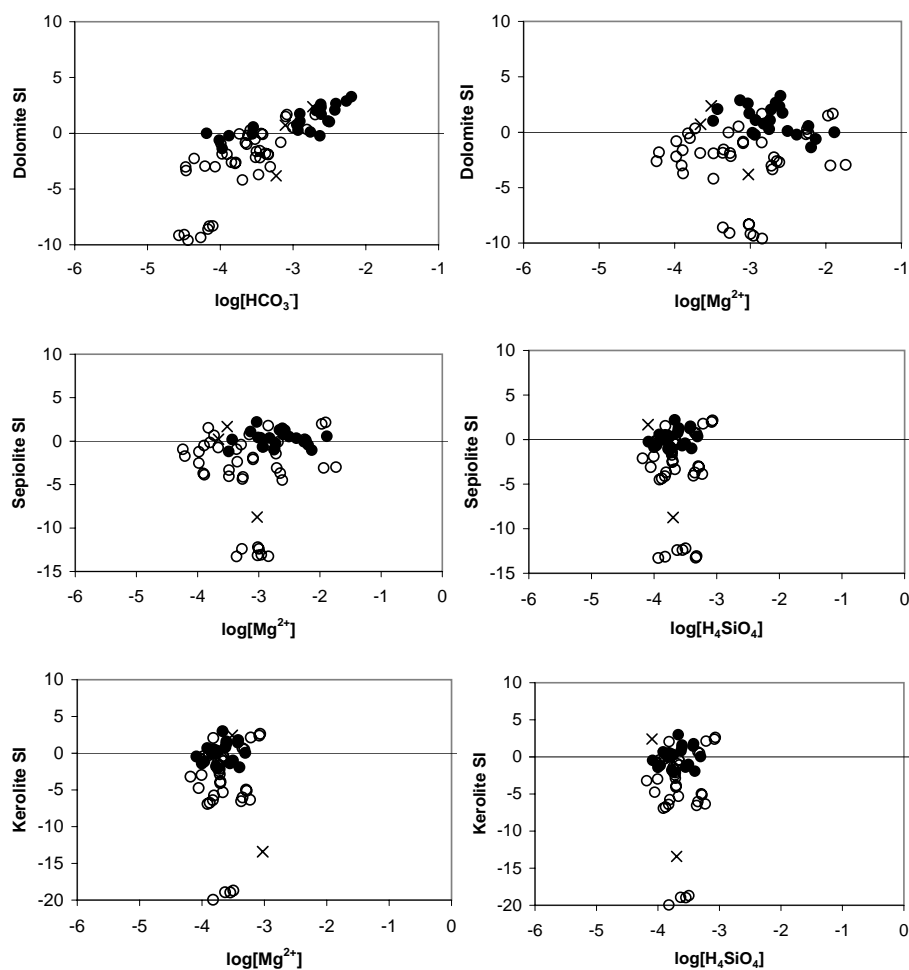


Figure 5.5: Continued from Figure 5.4 - Variation of mineral saturation indices (SI) with activity of component ion; saturated paste extracts. $SI > 0$ indicates supersaturation, $SI < 0$ undersaturation, and $SI = 0$ equilibrium with respect to a phase. Symbols as for Figure 5.1.

form of extensive, prominent E horizons (described in Francis et al. (2007) and Chapter 2). Evidence of pH control of sepiolite is that sepiolite is only associated with calcareous horizons (Table 5.1 and Chapter 4) suggesting that the carbonate buffers the pH at a sufficiently high level for sepiolite to precipitate. An additional mechanism of pH control on the Namaqualand coastal plain may be changing pCO_2 . Loss of CO_2 has been cited as a factor in calcite precipitation (Netterberg, 1969; Watts, 1980; Goudie, 1983; Wright and Tucker, 1991; Rodas et al., 1994, for example).

PHREEQC was used to calculate mineral saturation indices with the pCO_2 set at values ranging from -1 to -5. This was achieved by setting the log partial pressure

for $\text{CO}_2(\text{g})$ (equivalent to the target saturation index) from -1 to -5 in successive simulations in the EQUILIBRIUM_PHASES datablock of PHREEQC and using the default initial amount of 10 moles $\text{CO}_2(\text{g})$. None of the mineral phases were allowed to precipitate when they reached equilibrium so that the variation in saturation indices was only due to changing pCO_2 and not changing ion ratios due to removal from solution during mineral precipitation. The results in Figure 5.6 confirm the pCO_2/pH dependence of calcite (and dolomite), and show that both sepiolite and kerolite saturation are even more dependent on the pH/pCO_2 than calcite. Figure 5.6 shows that increasing pCO_2 causes a decreasing pH in the soil solution, with a resulting undersaturation in the pH-dependent phases kerolite, sepiolite, dolomite and calcite. Neither gypsum nor amorphous silica are affected. This is consistent with Jones and Galan (1988), who noted (p. 664) that both sepiolite and palygorskite require a low sediment-water pCO_2 , and is identical to the trend of decreasing kerolite and sepiolite saturation indices with increasing pCO_2 found by Deocampo (2005) for waters in Tanzania.

Palygorskite is not well confined on the diagram in Figure 5.6, as it contains Fe and Al terms that were not analysed in this study. Instead, PHREEQC was specified to calculate Al from equilibrium with K-mica, and Fe from equilibrium with goethite from the *phreeq.dat* database distributed with the program (Parkhurst and Appelo, 1999). The palygorskite dissolution reaction and log K were obtained from Singer and Norrish (1974). The undersaturated position of this mineral relative to sepiolite, however, is consistent with the XRD finding that palygorskite is a much less prominent constituent than sepiolite.

The data in Figure 5.6 suggest that if the soil solution became equilibrated at a higher than atmospheric pCO_2 (as is typical in the soil environment) and was subsequently exposed to a lower pCO_2 , equilibrium with sepiolite would be approached more rapidly than with calcite. One of the mechanisms for kerolite precipitation in caves in Hawaii proposed by L evill e et al. (2000) involves CO_2 -degassing.

5.3.4 Coastal sepiolite and inland palygorskite in Namaqualand

Singer et al. (1995) studied the mineralogy of Namaqualand soils from the Land Type Survey (Land Type Survey Staff, 1987). They found that palygorskite

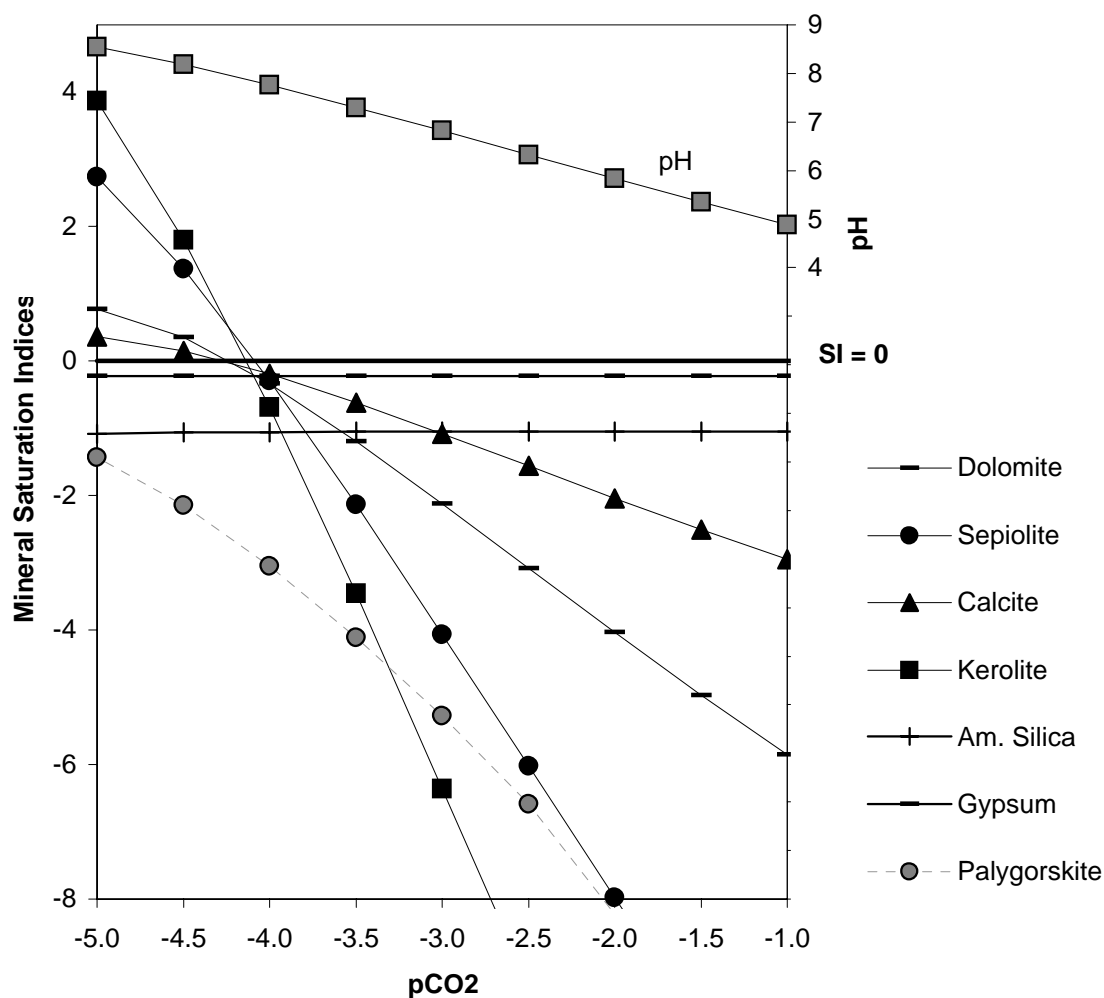


Figure 5.6: Variations in saturation indices with $p\text{CO}_2$ in the saturated paste extract of calcrete TP266Q/1. Palygorskite is poorly constrained. Equilibrated at atmospheric $p\text{CO}_2$ (-3.5), PHREEQC calculated a $p\text{CO}_2$ of -3.7 from the alkalinity input data.

dominated the soils inland of the escarpment whereas sepiolite dominated the clay fraction of soils from the lower-lying, coastal areas. Singer et al. (1995) suggested a dissolution-precipitation mechanism for the formation of palygorskite, and an additional marine Mg source for sepiolite formation. This is consistent with Chapters 1, 3, and 4, which reported that sepiolite is more prominent than palygorskite in the XRD traces from Namaqualand coastal plain soils. The marine-influenced elevated Mg is a likely explanation for sepiolite-dominance at the coast, and palygorskite-dominance inland. Sepiolite is favoured to form in an environment with a higher $(\text{Mg}+\text{Si})/\text{Al}$ ratio than palygorskite (Jones and Galan, 1988). The Mg concentration in the Texas High Plains appears to

have determined whether sepiolite-dolomite or palygorskite-calcite were formed (McDaniel et al., 1992).

In Section 5.3.2 it was established that the coastal areas had elevated Mg compositions relative to continental areas, which resulted in an increasing Mg trend with evaporation during the precipitation of sepiolite according to the Hardie-Eugster scheme since $Mg > HCO_3^-$ initially. Figures 5.1, 5.2 and 5.5 suggest that even nearly the lowest Mg^{2+} and H_4SiO_4 activity is sufficient for sepiolite saturation on the Namaqualand coastal plain, given an appropriate environmental pH. The result is that after sepiolite precipitation is initiated (by an geochemical pH barrier, see section 5.3.3), Mg levels will rise causing the increasing (Mg+Si)/Al ratio to continue to favour sepiolite precipitation. This suggests that once sepiolite has begun to precipitate, the subsequent salinity with its accompanying Mg increase makes substantial palygorskite formation unlikely to follow.

The sequence of formation of accessory amounts of palygorskite relative to sepiolite on the Namaqualand coastal plain remains speculative. Jones and Galan (1988, p. 664) noted that in lacustrine closed basins or marginal continental basins transitional to the marine, the occurrence of palygorskite appears to indicate brackish water and the presence of sepiolite reflects salinity increases. Zaaboub et al. (2005), however, showed that sepiolite would have precipitated directly in lacustrine, playa-lake or sebka environments under alkaline conditions, high Si and Mg and low Al activity, and arid to semiarid climate, whereas palygorskite would have formed by transformation of already existing illite and/or smectite type aluminosilicates in solutions in equilibrium with isotopically heavier and, therefore, more evaporated solutions than the sepiolite.

5.3.5 Summary of mineral genesis on the Namaqualand coastal plain

The results presented in this Chapter allow the following general summary to be made of secondary mineral formation in the study area.

Halite and gypsum

Halite and gypsum approach saturation as the concentration of their component ions in solution increases. Halite remains undersaturated at all sodium and chloride concentrations in the saturated paste extracts. At higher chloride concentrations, gypsum reaches saturation, and begins to remove sulfate from solution.

Calcite

All the soils are close to saturation with respect to calcite. The HCO_3^- activity decreases slightly with increasing Cl^- . The decrease in HCO_3^- activity coupled with a simultaneous increase in Ca^{2+} is consistent with calcite precipitation at the first ‘chemical divide’ in the Hardie-Eugster model of brine evolution, and consistent with the maritime $\text{Ca}^{2+} > \text{HCO}_3^-$ initial ratio.

Calcite remains consistently close to saturation for all levels of Cl^- activity (Figure 5.2). The calcite saturation index is not dependent on the Ca^{2+} activity, only on the HCO_3^- activity and pH for the range of concentrations encountered for these parameters.

Sepiolite-palygorskite

Although the sepiolitic soils are more abundant on the higher side of the Mg-Cl trend, the degree of evaporative concentration (as reflected by Cl concentration) in the saturated paste extracts does not distinguish sepiolitic from non-sepiolitic soils. Even the lowest Mg^{2+} and H_4SiO_4 activity is sufficient for sepiolite saturation given an appropriate environmental pH. Sepiolite remains consistently close to saturation for all levels of Cl^- activity. The sepiolite saturation index is independent of Mg^{2+} and H_4SiO_4 and depends only on the H^+ activity at the magnesium and silica levels measured.

The HCO_3^- activity vs Cl^- activity plot most effectively distinguishes the sepiolitic vs non-sepiolitic soils, with the sepiolitic soils generally having higher HCO_3^- activities. This is reflected in the saturation index trends with pH: rather than increasing with increasing chloride activity, the saturation indices of sepiolite is

controlled by increasing pH. Evidence of pH control on sepiolite precipitation is that sepiolite is only associated with calcareous horizons suggesting that the carbonate buffers the pH at a sufficiently high level for sepiolite to precipitate. An additional mechanism of pH control on the Namaqualand coastal plain may be changing $p\text{CO}_2$, similar in principle to the loss of CO_2 that has been cited as a factor in calcite precipitation. Sepiolite precipitation is therefore more likely to be triggered when a solution encounters a pH barrier than by the concentration of ions as a result of evaporation, since even the lowest Mg-Si levels are almost sufficient for sepiolite saturation.

The marine-influenced high Mg level coupled with the Hardie-Eugster model of brine evolution provides an explanation for sepiolite dominance at the coast, and palygorskite dominance inland. Coastal areas, unlike continental areas, have $\text{Mg} > \text{HCO}_3^-$ initially, which results in an increasing Mg trend with evaporation during the precipitation of sepiolite according to the Hardie-Eugster scheme. Even the lowest Mg^{2+} and H_4SiO_4 activity is sufficient for sepiolite saturation on the Namaqualand coastal plain, given an appropriate environmental pH. The result is that after sepiolite precipitation is initiated by a geochemical pH barrier, Mg levels will rise causing the increasing (Mg+Si)/Al ratio to continue to favour sepiolite precipitation. This suggests that once sepiolite has begun to precipitate, the subsequent salinity with its accompanying Mg increase makes substantial palygorskite formation unlikely to follow.

Most of the soils for which there was a positive sepiolite identification showed a positive sepiolite saturation index, suggesting that the saturated paste extracts were in equilibrium with sepiolite. This is in direct contrast to the findings of Singer et al. (1995), which were that sepiolitic and palygorskitic soils in the same region were undersaturated with respect to both these phases when using a 1:1 soil-water solution. Their interpretation, therefore, that that these minerals were formed pedogenically in the past, but are in a state of alteration towards a mixed layer or smectite clay as a consequence of a reduction in alkalinity and/or Mg supply induced by climatic shifts during the Late Pleistocene and Holocene requires revision. The data showing sepiolite equilibrium in sepiolitic soils suggest that sepiolite can be considered a 'precipitating mineral' and thus as forming in the present day. Furthermore, in Chapter 4 there was no TEM evidence to favour a hypothesis for fibrous mineral degradation to sheet silicates.

Silica

In the Namaqualand soil system the most likely minerals controlling the H_4SiO_4 solubility are sepiolite and amorphous silica/quartz. H_4SiO_4 activity remains unchanged for all levels of evaporation, consistent with the behaviour of an uncharged solute which has reached saturation with respect to the corresponding solid phase.

pH variation and its potential to affect the genesis of calcic, sepiolitic and duric soils

The data in Figure 5.6 suggest that decreasing the pH by 0.5 units decreases the calcite saturation index by 0.45 units and the sepiolite saturation index by 1.9 units, while leaving the amorphous silica saturation index unchanged. The effect of a pH change on the sepiolite saturation index is therefore > 4 times that of the effect on calcite. The effect of pH fluctuations on calcite and silica solubilities is important in the genesis of calcrete-silcrete intergrades in the Kalahari, Botswana (Nash and Shaw, 1998; Kampunzu et al., 2007). The data in Figure 5.6 show that pH affects the solubility of sepiolite even more than it does calcite. Since sepiolite is often a significant part of arid region soils where calcite and amorphous silica are common, the mineral solubility-pH relationships may assist in explaining the relationships between calcic, sepiolitic and duric soils and their intergrades.

5.4 Conclusions

PHREEQC is an adequate tool with which to perform speciation calculations for Na-Cl dominated soils of the Namaqualand Coastal Plain system, since the ionic strength of the samples falls in the range of 0.004 to 0.76, with most of the samples being well below the concentration of seawater. The variation in activity of all the ions with Cl^- is consistent with a seawater dilution line.

The equilibrated saturated paste extracts were ranked in order of their Cl^- content as a proxy for degree of evaporative concentration in the field. The data trends when all the “closed system” saturated pastes were considered together are consistent with the predictions of the Hardie-Eugster model for closed-system

evaporating brines, as well as with experimental and simulated evaporations of solutions with similar initial ratios as the saturated paste extracts. The Hardie-Eugster model of brine evolution in closed basin brines can therefore be applied generally to the soil system in Namaqualand.

The Namaqualand coastal plain, like other maritime areas, generally shows a trend of decreasing pH, increasing Ca and increasing Mg with increasing evaporation. This can be explained by their marine-influenced initial ratios and is consistent with the 'chemical divides' of the Hardie-Eugster model of brine evolution. K^+ , Ca^{2+} and Mg^{2+} increase with increasing evaporation but at a slope less than that for the conservative solutes Na^+ and Cl^- , and suggests removal mechanisms such as mineral precipitation, sorption, or degassing which operate over the full range of evaporative concentration.

Considering the formation of minerals in the arid soil environment in the same terms as the geochemical evolution of brines has helped to refine the model of mineral formation on the Namaqualand coastal plain. Halite remains undersaturated at all concentrations in the saturated paste extracts. At higher concentrations, gypsum reaches saturation, and sulfate is removed from solution. H_4SiO_4 activity remains unchanged for all levels of evaporation or pH. Calcite remains close to saturation, and is only dependent on the HCO_3^- activity and pH for the range of Cl^- activity encountered. Most of the soils for which there is a positive sepiolite identification show a positive sepiolite saturation index. The sepiolite saturation index is independent of Mg^{2+} and H_4SiO_4 and only increases with increasing pH. Sepiolite precipitation is therefore more likely to be triggered when a solution encounters a pH barrier than by the concentration of ions by evaporation. Evidence of the pH control on sepiolite saturation is that sepiolite is commonly associated with calcareous horizons. The effect of a pH change on the sepiolite saturation index is much greater than its effect on calcite.

The marine-influenced high Mg level coupled with the Hardie-Eugster model of brine evolution offers an explanation for sepiolite-dominance at the coast, and palygorskite-dominance inland. Coastal areas, unlike continental areas, have $Mg > HCO_3^-$ initially, which results in an increasing Mg trend with evaporation during the precipitation of sepiolite according to the Hardie-Eugster scheme. The result is that after sepiolite precipitation is initiated by a geochemical pH-barrier, Mg levels will rise causing the increasing $(Mg+Si)/Al$ ratio to continue

to favour sepiolite precipitation. This suggests that once sepiolite has begun to precipitate, the subsequent salinity with its accompanying Mg increase makes substantial palygorskite formation unlikely to follow.

Chapter 6

Micromorphology, mineralogy and genesis of soils associated with a Namaqualand ‘heuweltjie’

6.1 Introduction

‘Heuweltjies’ (Afrikaans for small hills) occur throughout Namaqualand and along the western and southern Cape coasts (Picker et al., 2007). They are thought to be termitaria of the harvester termite *Microhodotermes viator* (Moore and Picker, 1991), with a debated contribution from mole rats (Lovegrove and Siegfried, 1986; Cox et al., 1987; Lovegrove and Siegfried, 1989; Laurie, 2002; Midgley and Hoffman, 1991) and other animals (Milton and Dean, 1990). Midgley et al. (2002) obtained $\delta^{14}\text{C}$ ages of 25 000 to 30 000 years B.P. for calcrete associated with heuweltjies in the Clanwilliam and Elands Bay areas, similar the $32\,100 \pm 720$ years B.P. for the nearly identical fossilised nests from Clanwilliam presented by Coaton (1981).

Heuweltjies are distinguishable in the field as circular features (diameter usually 10 to 20 m) showing a different vegetation pattern and a slightly raised (1 to 2.5 m) surface, presenting what Laurie (2002) referred to as an “ostrich leather” texture on aerial photographs. When using Google Earth (<http://earth.google.com/>) to observe the study area, between Papendorp and Strandfontein, the heuweltjies become discernable as green circular features at an eye altitude of 2 to 5 km.

They represent zones of denser vegetation because of the nutrient cycling into the heuweltjie (Midgley and Musil, 1990; Midgley and Hoffman, 1991) and higher base status of on-mound compared to off-mound soils (Ellis, 2002). A good example of heuweltjie-modified soils influencing vegetation patterns is evident at the location 31° 44' 10" S, 18° 14' 20" E, just north of Strandfontein and a little south of the heuweltjie in the present study, where the greener vegetation pattern of heuweltjies in this region has persisted through subsequent ploughing and cropping. Similar examples can be seen throughout their zone of occurrence along the western and southern Cape coasts.

Ellis (2002) noted that there seems to be a direct relationship between hardpan occurrence and termite activity: where the rainfall is at its lowest, termite activity is presently relict and mounds are characterized by a central petrocalcic to petroduric hardpan, and a petroduric over petrocalcic horizon towards the outer edge and in the surrounding inter-mound areas. In the higher rainfall zone (250 to 450 mm) the general tendency is that limited termite activity is present though only in the centre of most mounds but absent on certain, apparently the oldest, mounds. Where termites are still active, the areas of activity have hypocalcic to hypercalcic horizons with petroduric or petrocalcic horizons on the perimeter of the mound, even when no hardpans occur in surrounding soils. With increasing rainfall, age and relict termite activity, a broken hardpan and/or more base-rich soil material is found on the mounds. In these latter cases the soils of the inter-mound areas have moderate to low base status without any of the above-mentioned hardpans.

Since the publication of the work by Ellis (2002), it was noticed that the fibrous clay minerals sepiolite and/or palygorskite are commonly associated with the calcrete in the heuweltjies. Palygorskite tends to occur more in heuweltjies in inland areas, consistent with the sepiolite-palygorskite distribution in Namaqualand (Singer et al. (1995) and Chapter 5). Sepiolite and palygorskite are often reported from arid region soils and are commonly found in calcretes (Vanden Heuvel, 1964; Singer and Norrish, 1974; Yaalon and Wieder, 1976; Elprince et al., 1979; Hay and Wiggins, 1980; Watts, 1980; Singer and Galan, 1984; Singer, 1989; Blank and Fosberg, 1991; Monger and Daugherty, 1991; Verrecchia and Le Coustumer, 1996; Singer, 2002; Neaman and Singer, 2004; Owliaie et al., 2006). The hardpan horizon of the heuweltjie commonly grades from a petrocalcic in the centre through a 'sepiolitic'/'petrosepiolitic' horizon (as defined in Chapter 1),

to the petroduric horizon on the edges. In the heuweltjie soils, the petrocalic horizon is commonly 'sepiolitic' as defined by Chapter 1. Usually there are abundant sepiolite cutans (up to a few millimetres thick) around the nodules of calcrete. These cutans are generally white, non-calcareous, adhere strongly to the wetted tongue and react with methyl orange to change it from orange to pink/purple, indicating sepiolite (Mifsud et al., 1979). Personal observations showed that both pure calcite, and calcrete in which sepiolite is only detectable when the clay fraction is concentrated and examined by XRD, react negatively to the methyl orange test (Chapter 1). In contrast, most of the calcrete in the centre of the heuweltjies react positively to the methyl orange test, suggesting substantial concentrations of sepiolite. In an area like Worcester, for example, these horizons are only associated with the heuweltjies and are not present in the inter-heuweltjie areas.

Heuweltjies are sometimes described as Mima-like mounds (for example Cox et al., 1987; Lovegrove and Siegfried, 1986; Milton and Dean, 1990; Lovegrove and Siegfried, 1989). Horwath and Johnson (2006), (2007) summarised the characteristics of Mima and Mima-like mounds. Horwath and Johnson (2006) noted that the term 'Mima mound' comes from Mima Prairie, a tract in the Puget Sound lowlands south of Olympia, Washington. Mima-like mounds elsewhere, although they may bear resemblances to the type locality, differ in height, diameter, texture, internal composition and structure, and in the elevations at which they occur. Numerous theories for the origins of Mima-mounds have been proposed (Washburn, 1988; Reider et al., 1996; Horwath and Johnson, 2006, and references therein). These can be grouped into five main genetic categories: erosional, depositional, fossorial (burrowing) animals (usually rodents), periglacial, and seismic origins (Horwath and Johnson, 2006). The heuweltjie soils show some similarities to Mima(-like) mounds, particularly their raised surfaces, silica and/or calcium carbonate hardpans and clay-accumulation horizons (Spackman and Munn, 1984; Hobsan and Dahlgren, 1998), as well as their organic matter (nitrogen) enrichment (Midgley and Musil, 1990; Litaor et al., 1996; Hobsan and Dahlgren, 1998). They differ in that the clay mineralogy of the Mima(-like) mounds does not contain sepiolite or palygorskite, only smectite, kaolinite (Hobsan and Dahlgren, 1998) and illite (Spackman and Munn, 1984), and we have not observed in heuweltjies the plug or central pipe that was noted in Mima-like mounds by Spackman and Munn (1984) and Reider et al. (1996).

Most of the previous heuweltjie work has focused on biogenic aspects, such as their spacing, origin and age, but even though the heuweltjie is in fact a soil feature there have been few published studies done on the soil forming processes within the heuweltjie (Van der Merwe, 1940; Slabber, 1945; Ten Cate, 1966; Burgers, 1975; Ellis et al., 2001; Ellis, 2002). There has been some work done on the soil properties (such as Watson, 1962) and micromorphology of termite mounds (for example Stoops, 1964; Mermut et al., 1984; Lobry de Bruyn and Conacher, 1990), but these did not include heuweltjies. We therefore aimed to use soil micromorphology and the principles of brine evolution from Chapter 5 to help explain the soil formation within the heuweltjie, particularly the relationship between the petrocalcic, '(petro)sepiolitic' (Chapter 1) and petroduric horizons, and to refine Ellis' (2002) model of hardpan formation in heuweltjies in the light of the new data. Since this is the first published account of thin section descriptions through a heuweltjie, the detailed descriptions, photographs and terminology that were used are included in full to allow for easier comparison in future studies.

6.2 Materials and methods

Heuweltjies were sampled from Papendorp–Strandfontein (1 heuweltjie), Stellenbosch (1 heuweltjie), Oudtshoorn (1 heuweltjie), and Worcester (2 heuweltjies). The locations are shown in Figure 6.1.

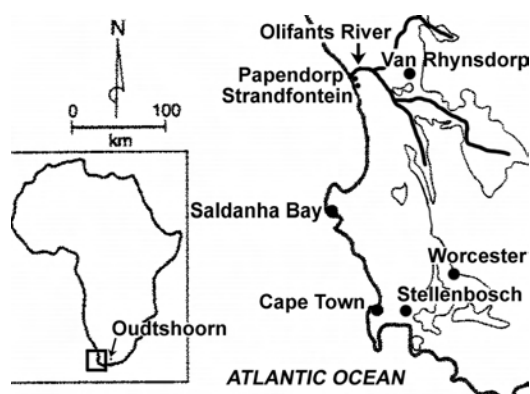


Figure 6.1: Location of Papendorp–Strandfontein, Stellenbosch, Oudtshoorn, and Worcester, where heuweltjies were sampled for this study. Modified from Pether et al. (2000).

Seven samples of the calcrete horizons and the associated sepiolite/palygorskite cutans were sampled in the Oudtshoorn and Worcester heuweltjies to confirm the presence of palygorskite and/or sepiolite, after field tests with methyl orange were positive for sepiolite (methyl orange shows a purple-pink colour, Mifsud et al., 1979). Bulk samples were ground with an agate pestle and mortar with distilled water and sedimented onto glass slides for XRD analysis (machine setup as for the Papendorp heuweltjie detailed below).

The main focus of this study was the Papendorp heuweltjie. It is located at 31° 42' 32" S, 18° 13' 32" E, elevation 60 m a.m.s.l., on the south side of the Olifant's River mouth, on a road-cut along the R362 between the towns of Papendorp and Strandfontein (Figure 6.1), on an undulating coastal plain, sea-facing (west) in natural (grazed) veld. Mean annual rainfall for the Papendorp/Strandfontein area is < 150 mm. Samples were taken of the hardpan horizons and their overlying loose horizons through a cross-section of the heuweltjie from the centre to the edge (Figure 6.2).

Approximately 2 kg bulk sample was taken of each horizon of the Papendorp heuweltjie, as well undisturbed, vertically orientated material for the preparation of thin sections. Section dimensions are given in Section 6.3.4 (Table 6.2). Thin sections for optical microscopy from the Papendorp heuweltjie were impregnated with a polyester resin and ground without water, and left uncovered on one side to allow for etching and SEM-EDX work. Fine grained calcite was identified by effervescence in 1M HCl under the optical microscope. Calcite was distinguished from calcium oxalate by its insolubility in 2M acetic acid, since both calcium carbonate and calcium phosphate are soluble (Post, 1985). Slaking tests were based on the WRB (1998) definition of petroduric, petrocalcic and fragic horizons. An intact fragment a few centimetres in diameter was submerged in water, 5M HCl or 6M NaOH and gently heated on a waterbath for four days. Uncoated fragments and thin sections were observed before and after etching in 1M HCl using low vacuum SEM-EDX with a Philips Xl30 ESEM. High vacuum SEM was done on Au-coated fragments using a Leo 1430VP SEM-EDX system. For XRD analysis of the clay fraction, the bulk samples were air-dried, crushed and passed through a 2 mm sieve. The <2 μm fraction was separated from the bulk samples by dispersion (shaking briefly by hand, raising the pH to approximately 10 with Na_2CO_3) and settling. The clay suspension was flocculated by addition of MgCl_2 after lowering the pH to 5 to 7 with HCl to prevent the precipitation of brucite

and/or clay destruction. The clay suspension was then Mg-saturated, concentrated by centrifugation, and sedimented (or smeared, many of the sepiolite-rich samples developed ‘mudcracks’) onto a glass slide. XRD analyses were done with a stepsize of 0.05 degrees and steptime of 40 seconds, using a Bruker DD8 Advance Powder Diffractometer with a graphite monochromator, 40 kV and 40 mA. Ethylene glycol was sprayed lightly onto the surface of the Mg-saturated sample slides. TEM-EDAX analyses were performed on the clay fractions using a Philips CM120 Biotwin equipped with EDAX detector.

Thin sections were made through exit towers and frass from the surface of an active heuweltjie in Stellenbosch, to assist in the recognition of the fossil termite features in the Papendorp heuweltjie. The excrement samples were collected loose and randomly oriented on the section (3 x sections, 20 x 40 mm diameter; thickness 30 μm). Two 2 termite exit towers were sampled (approximately 10

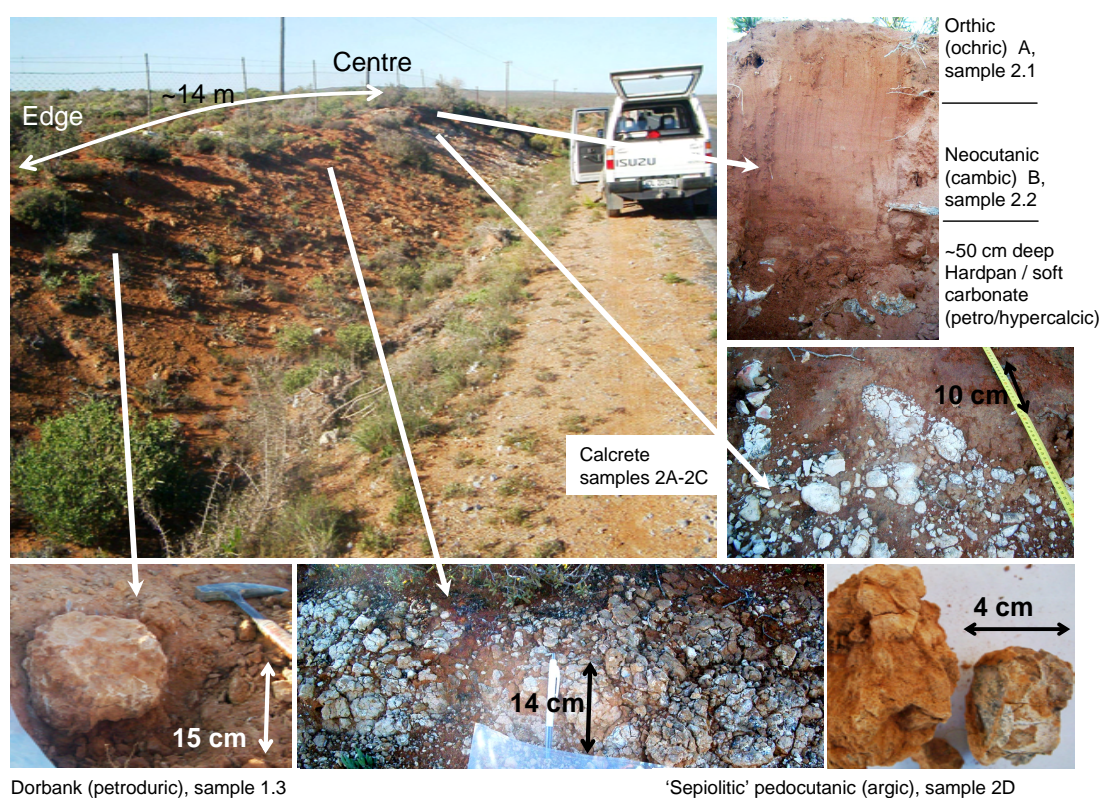


Figure 6.2: Photographs of sample locations within heuweltjie. White cutans in the calcrete and sepiolitic’ pedocutanic (argic) horizons react positively with methyl orange in the field, suggesting sepiolite.

cm high, diameter 8 to 10 mm), both of which were orientated in cross-section on the thin section (20 x 40 mm diameter; thickness 30 μm). Thin sections were impregnated with an epoxy resin under vacuum and ground without water. The Stellenbosch heuweltjie is located on the south side of Papegaaiberg (Stellenbosch) above the graveyard in a pine plantation. Parent material is non-calcareous, yellow-brown apedal soil formed on granite. Mean annual rainfall for the Stellenbosch area is >650 mm.

6.3 Results and discussion

6.3.1 Profile descriptions

The heuweltjie (pictured in Figure 6.2 with the sample locations) is typical of those in the arid western parts of South Africa described by Ellis (2002). Termite activity is presently low, increasing after rainfall. It has a petrocalcic horizon in the centre of the mound and a petroduric horizon at the edges. Between the two is a ‘sepiolitic’ argic horizon. The landscape is otherwise free of calcrete.

Profile descriptions through a cross-section of the heuweltjie are given in Table 6.1. The calcrete horizon is ‘sepiolitic’ (as defined by Chapter 1), similar to heuweltjies from widely spread localities such as the Knersvlakte, Oudtshoorn and Worcester (Figure 6.3). It contains sepiolite cutans that are generally white, non-calcareous, adhere strongly to the wetted tongue and react with methyl orange to change it from orange to pink/purple (Mifsud et al., 1979). Towards the centre of the heuweltjie the calcrete is more laminar, and then grades outwards and downwards into a more nodular texture. The sepiolite cutans are much more abundant on the nodular peds. Between the petrocalcic at the centre and the dorbank (petroduric) at the edge of the heuweltjie is a hard but friable horizon that is composed of brown non-calcareous nodular, clay-rich peds that are covered by white sepiolite cutans and sepiolite coating cracks in the peds (Figure 6.2). Based on these cutans I classified this pedocutanic (argic) horizon (sample 2D) as ‘sepiolitic’ (Chapter 1). The cutans are not present in the dorbank at the edge of the heuweltjie (Figure 6.2).

Table 6.1: Profile descriptions from Papendorp heuveltjie, pictured in Figure 6.2 (Section 6.2). Blank fields: *not detected*, except slaking tests *not tested*. Abbreviations: cont.-continuous; mod.-moderate; qtz -quartz; s -seconds; sl.-slight; v.-very.

Sample Depth Name	Diagnostic Horizon †	pH saturated paste	Munsell		Coarse Frag.	Structure	Dry	Consistency		Effervescence HCl	Methyl Orange	Slake (0=no, 5=full)	Cementation	Water Absorption	Roots	Transition	Other Features	
			Dry	Moist				Moist	Wet									
Profile "2": Centre of heuveltjie: Gamoeop Form (Orthic A - Neocutanic B - Hardpan carbonate).																		
2.1	0-0.2 m	Orthic (ochric) A; bleached; crust	7.6	Sl. moist	5YR 4/4	5YR 4/6	Sand	Few sepiolite; single-clay; grain shale	Loose	Loose	Non-plastic, non-sticky	None	No reaction	None	3s	Common	Abrupt, smooth	Tunnel ~3 cm diameter, few macropores
2.2	0.2-0.55 m	Neocutanic (cambic) B	6.9	Sl. moist	5YR 5/4	5YR 4/6	Sand	Few sepiolite; single-grain qtz	Loose	Loose	Non-plastic, non-sticky	None	No reaction	None	1s	Few	Abrupt, wavy to tonguing	Few macropores
2A	0.55 m - 1 m	Soft carbonate (hyper-)calic	8.3	Dry	5YR 8/2	5YR 7/3	5YR	Nodular	Hard	Friable	Sl. plastic, sl. sticky	5	Cont. sl. calcite	3s	Few	Not reached	White sepiolitic cutans	
C horizon grades laterally in sequence 2A-2B-2C-2D towards edge of heuveltjie																		
2B (2 m from 2A)								Massive	Hard	Hard-	Sl. plastic, Friable sl. sticky	4	2	-	Few	Not reached	Tunnels ~3 mm wide, 3 cm long; white sepiolitic cutans	
2C (3.2 m from 2A)	1 m	Soft carbonate (hyper-)calic		Dry	5YR 8/2	5YR 8/3	5YR	Nodular	Hard	Friable	Sl. plastic, sl. sticky	4	5	4	Few	Not reached	Few cracks; white sepiolitic cutans	
2D (7.5 m from 2A)	1 m	'Sepiolitic' pedocutanic (argic)		Dry	7.5YR 4/2	7.5YR 4/4	7.5YR	Medium blocky	Hard	Friable	Sl. plastic, sl. sticky	2-3	4	4	Few	Not reached	Tunnels ~3 mm wide, 3cm long; abund. cracks; white sepiolitic cutans	
Profile "1": Edge of heuveltjie ~8 m from 2D: Oudshoorn Form (Orthic A - Neocutanic B - Dorbank)																		
1.1	0-0.04 m	Orthic (ochric) A; bleached; crust	8.7	Sl. moist	5YR 4.5/6	5YR 3/4	Sand	Mod. qtz gravel, shale	Loose	Loose	Non-plastic, non-sticky	V. sl.	No reaction	None	3s	Common	Abrupt, smooth	Few macropores
1.2	0.04-0.15 m	Neocutanic (cambic) B	8.5	Sl. moist	5YR 4.5/6	5YR 4/6	Sand	V. few qtz	Loose	Loose	Non-plastic, v. sl. sticky	None	No reaction	None	1s	Few	Abrupt, smooth	Few macropores
1.3	0.15 m - 1 m	Dorbank (petroduric)	9.1	Dry	7.5YR 5/6	7.5YR 3.5/4	7.5YR	Massive	Very hard	Firm		0	3-4	-	None	5s	Not reached	Few fine cracks

† Classified according to the Soil Classification Working Group (1991), in brackets is the WRB (1988) equivalent.

‡ Changes to purple in the presence of sepiolite or Mg-smectite (Mifsud et al., 1979).

§ Water from dropper spreads instantly away along very fine cracks (dendritic pattern).

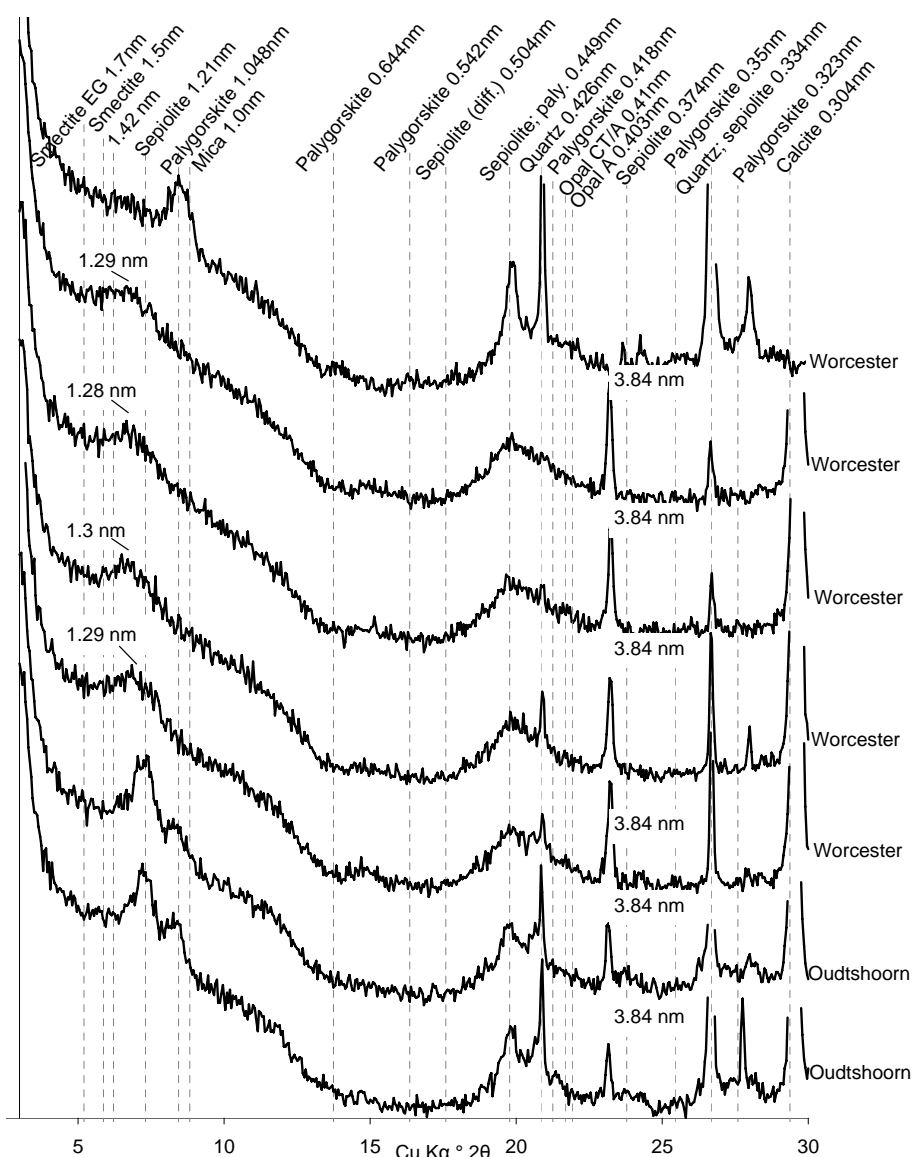


Figure 6.3: XRD traces of white palygorskite/sepiolite cutans and associated calcrite from the centre of heuweltjies from Worcester and Oudtshoorn. Bulk samples ground with agate pestle and mortar and sedimented onto glass slides. Diff.: diffuse; paly.: palygorskite. Quartz and calcite peaks cropped.

6.3.2 Clay mineralogy

Calcrete in centre of heuweltjie: samples 2A, 2B, 2C

XRD analyses of the clay fraction (Figure 6.4), shows a strong 1.28 or 1.33 nm peak for the calcrete (samples 2A to 2C) in the centre of the heuweltjie. Hay and Wiggins (1980) found a 1.26 nm peak for sepiolite in some calcretes of the

southwestern United States. SEM images of a calcrete fragment from sample 2A showed a fibrous clay mineral resembling sepiolite or palygorskite (Figure 6.13(f)). Sepiolite is associated with ‘non-heuweltjie’ calcrete from Namaqualand (Chapters 3, 4) and other southern African calcretes (Netterberg, 1969; Watts, 1980). Palygorskite was not evident in the heuweltjie calcrete, consistent with previous findings for the Namaqualand coastal region (Singer et al. (1995) and Chapters 1, 3, 4). With the exception of mica, the peaks of the overlying neocutanic (cambic) B horizon are not as well defined.

‘Sepiolitic’ pedocutanic (argic) 7.5 m from centre of heuweltjie: sample 2D

The clay mineralogy of this sample 2D is less clear: it adhered to the wetted tongue, but the darker colour (Table 6.1) meant that the methyl orange test was only clear on the white, non-effervescent cutans (Figure 6.2), where it turned purple suggesting sepiolite. It did not show as clear a sepiolite peak as the calcrete samples 2A to 2C in the centre of the heuweltjie, and the ‘sepiocrete’ described in Chapter 1. Figure 6.4 shows the major clay peak of 2D to be broader than in the calcrete samples 2A to 2C, and centred around 1.4 to 1.5 nm. The 1.28 nm peak became more apparent on glycolation. Hay and Wiggins (1980) also found a broad 1.26 to 1.4 nm peak for clay minerals in sepiolite-rich calcretes of the southwestern United States. TEM images (Figure 6.5) of the clay fraction from sample 2D showed acicular minerals to be present, confirming the presence of sepiolite and possibly palygorskite. Acicular minerals were not the dominant morphology over the entire prepared TEM grid, however.

Dorbank (petroduric) at edge of heuweltjie

The rise in the background of the dorbank trace at around 0.4 nm (6.4) is consistent with the silica cement suggested by full slaking only in NaOH (Table 6.1). The dorbank horizon (sample 1.3) and the overlying neocutanic (cambic) B horizon (sample 1.2) show poorly defined clay peaks. These broad clay peaks were also observed in some dorbank horizons from other parts of Namaqualand (Chapter 1), and could be a function of disordered siliceous coatings masking the clay minerals in dorbank horizons (Flach et al., 1969; Blank and Fosberg, 1991).

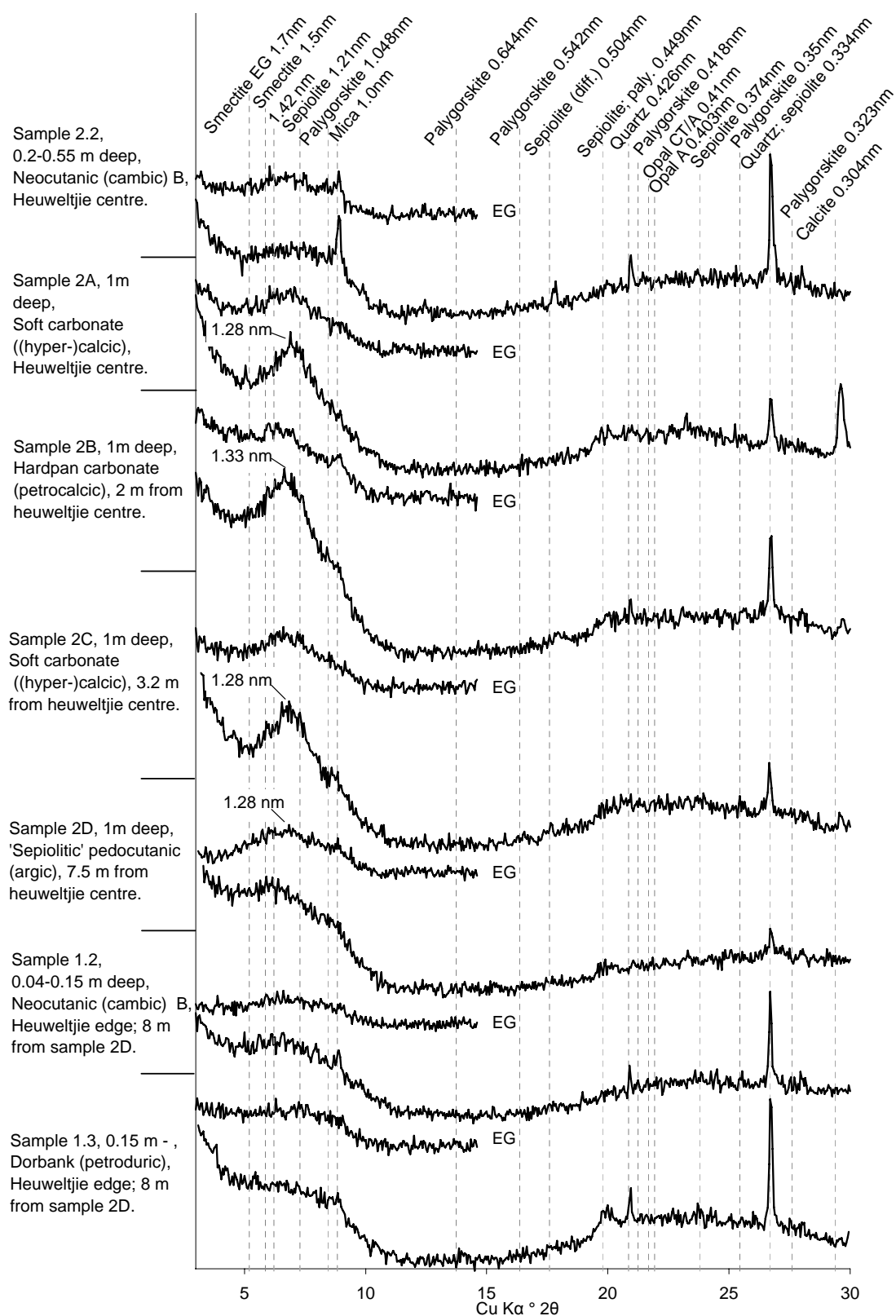


Figure 6.4: XRD traces of Mg-saturated, $<2 \mu\text{m}$ fraction from milled samples from Papendorp heuweltjie. Diff.: diffuse; EG: ethylene glycol; paly.: palygorskite.

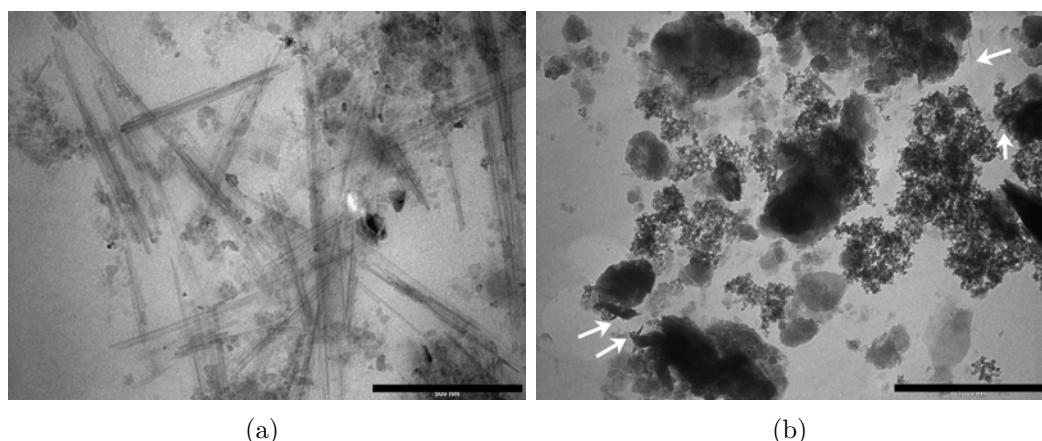


Figure 6.5: TEM image of the same clay fractions from the XRD traces in Figure 6.4. (a) Fibrous clay in $< 0.08 \mu\text{m}$ fraction from 'sepiolitic' pedocutanic (argic) sample 2D. Scale bar 500 nm. (b) $< 2 \mu\text{m}$ fraction from dorbank (petroduric) sample 1.3, fibrous minerals possibly developing from mica (arrowed). Scale bar $1 \mu\text{m}$. EDAX analysis showed the large platy crystals to have a biotite composition.

In one instance (Figure 6.5(b)) the morphology suggests the development of fibrous clay minerals from a mica-like structure, similar to the palygorskite fibres observed developing from an illite by Suarez et al. (1994).

6.3.3 Micromorphology of excrement and exit towers: Stellenbosch heuweltjie

In addition to examining thin sections through the heuweltjie near Papendorp, material was sampled from the surface of an active, non-calcareous heuweltjie in Stellenbosch, to assist in the recognition of the fossil termite features in the Papendorp heuweltjie. Thin sections of loose, fresh termite excrement and a cross-section through a termite exit tower (approximately 10 cm high and 1 cm diameter) are pictured in Figures 6.6 to 6.7.

The excrement samples were collected loose and randomly oriented on the section. They are non-calcareous ellipsoids (0.8 x 0.4 mm) or spherical (0.3 to 0.4 mm diameter). Each has a massive microstructure, a $c/f_{5\mu\text{m}}$ ratio of 1:20, which is considerably finer than any of the samples from the heuweltjie near Papendorp (Table 6.2), and an open porphyric c/f -related distribution. The

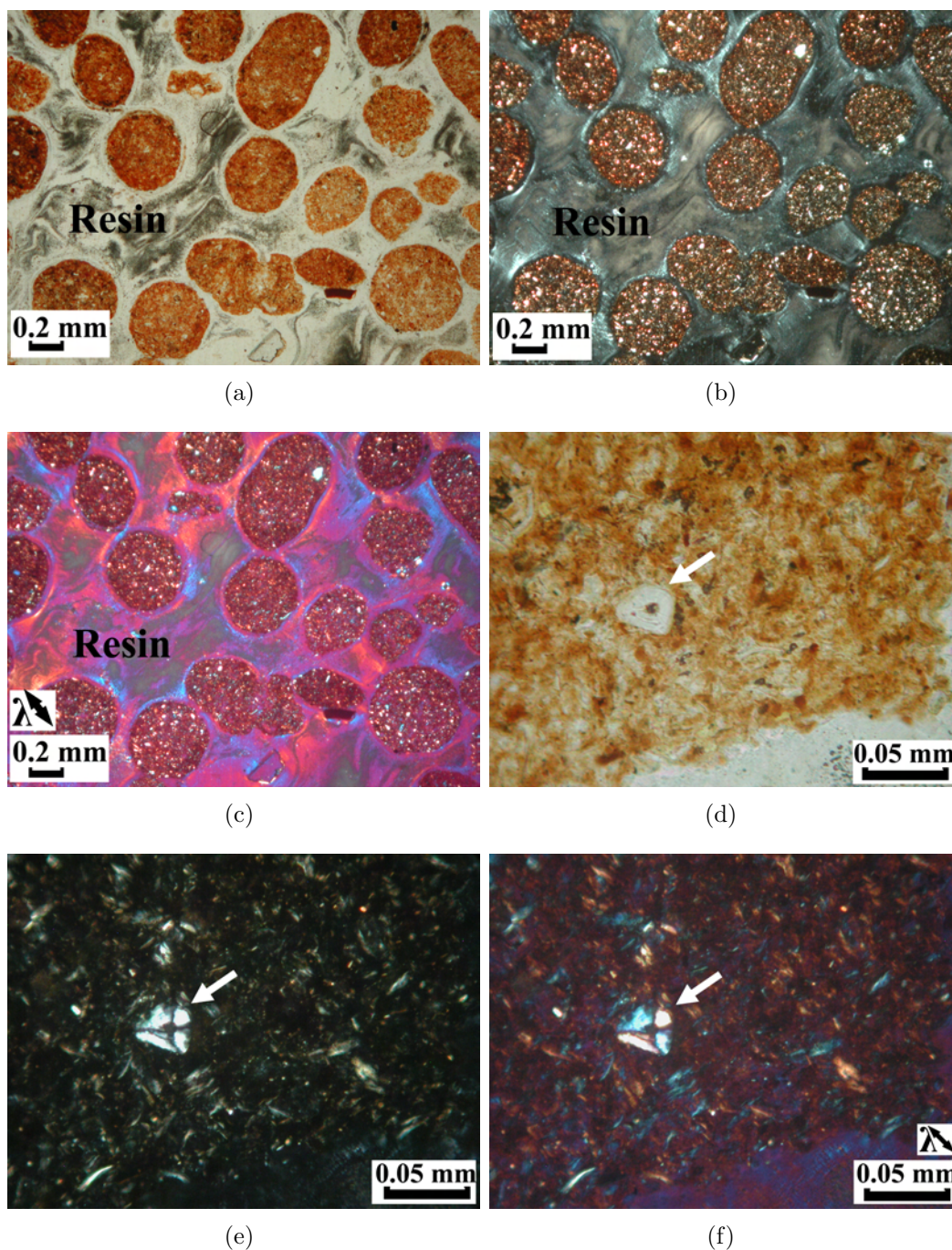


Figure 6.6: Photomicrographs of termite excrement composed of very fine quartz and organic matter from the surface of an active, non-calcareous heuweltjie from Papegaaiberg (Stellenbosch). (a)–ppl, (b)–xpl, (c)– λ -plate, fast-direction NW-SE: termite excrement (collected loose, random orientation) set in resin. (d)–ppl, (e)–xpl, (f)– λ -plate, fast-direction NW-SE: magnification of (a)–(c) showing spherulite with pseudo-negative interference figure in termite excrement. Note the perpendicular arrangement of acicular grains in (e) and (f).

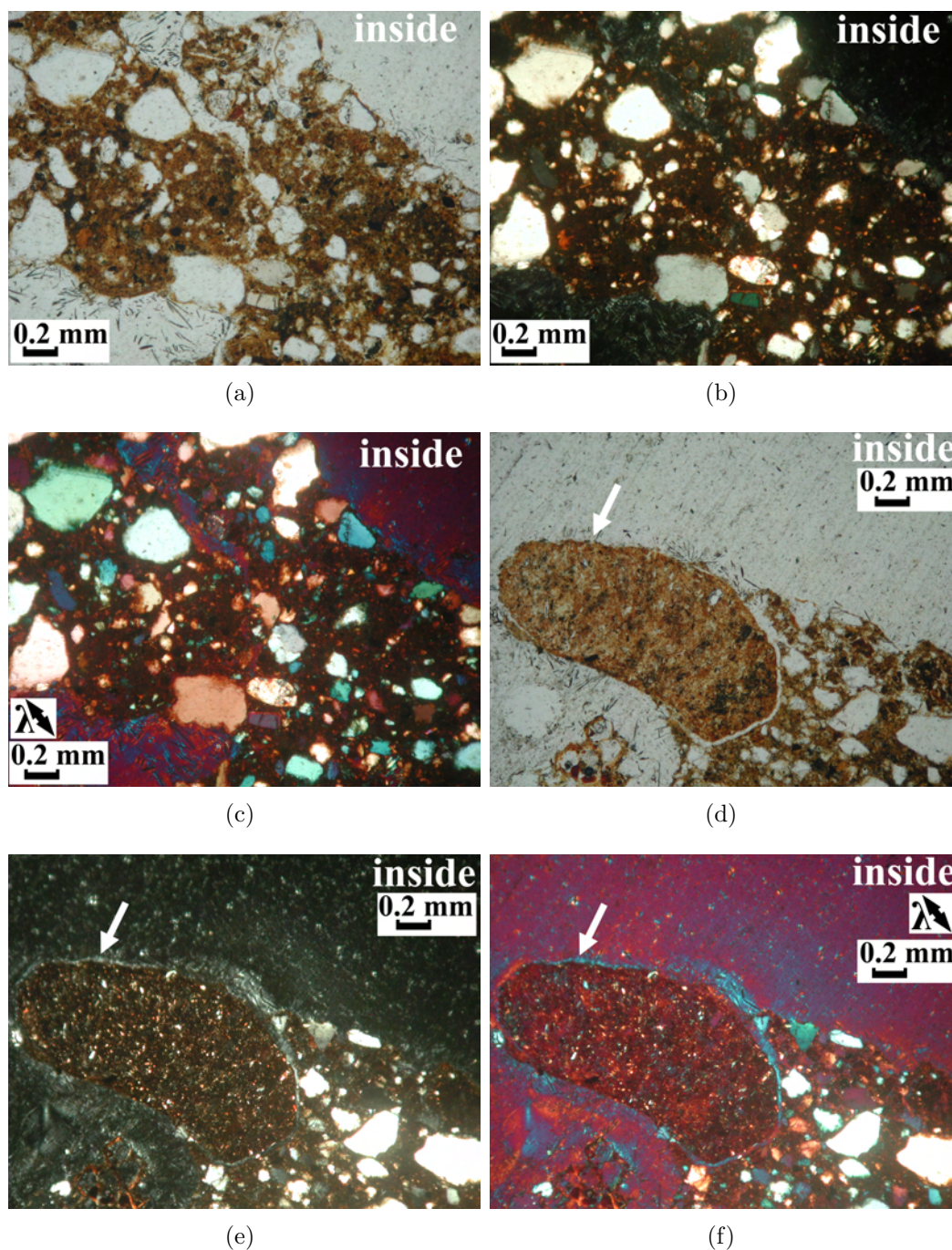


Figure 6.7: Photomicrographs of cross-section through termite exit towers, composed of subrounded quartz particles in a clay-organic matrix. Collected on the surface of an active heuweltjie on Papegaaiberg (Stellenbosch). Inward side of exit towers indicated. Termite excrement pellet (arrowed) within wall of exit tower. (a)–ppl, (b)–xpl, (c)– λ -plate, fast-direction NW-SE, (d)–ppl, (e)–xpl, (f)– λ -plate, fast-direction NW-SE.

coarse material mostly comprises $< 30 \mu\text{m}$, angular, acicular-prolate fragments likely to be quartz. There are occasional 4 mm spheroidal quartz particles. The micromass appears to be an organic-clay mixture, and has an undifferentiated to stipple-speckled b-fabric. The excrement contains spherulites 8 to 15 μm diameter, non-effervescent with cold 10% HCl, with pseudo-negative uniaxial interference colours (Figure 6.6).

The termite exit towers (Figure 6.7) have a 6 to 7 mm internal diameter. The wall is 3 to 5 mm thick and has a massive microstructure. They contain considerably more coarse material ($c/f_{5\mu\text{m}}$ ratio 3:1 and a close porphyric c/f -related distribution). The coarse material comprises angular, predominantly spheroidal quartz fragments 0.3 mm to 20 μm diameter. There is no apparent change in composition (clay, organic material) on either inner- or outer wall surfaces. They are non-calcareous. The micromass appears to be organic matter- clay mixture with an undifferentiated b-fabric. They resemble the material shown by Jungerius et al. (1999, p. 355). The wall includes one ellipsoid excrement (0.85 x 0.3 mm), identical to the material in the excrement sample. The only spherulite (with pseudo-negative uniaxial interference colours) observed in both of the towers sectioned occurred within this excrement.

The spherulites are similar to the spherulites in herbivore dung described by Canti (1998). According to Canti (1997), spherulites in herbivore dung are 5-15 μm diameter, compared to the 8 to 15 μm diameter for those observed in the Stellenbosch heuweltjie frass (Figure 6.6). The spherulites did not effervesce in cold 10% HCl. No reaction with HCl was observed by Brochier et al. (1992) either. However, Canti (1997) noted that the gas bubbles (but usually only one per spherulite) were clearly evolved, appearing almost immediately on wetting, and so could only be observed by allowing a front of HCl to advance onto dry spherulites in the field of view at high power magnification. This method was employed in this study but produced no effervescence.

6.3.4 Micromorphology of the heuweltjie at Papendorp

Full thin sections descriptions through a cross-section of the Papendorp heuweltjie are presented in Table 6.2, with the corresponding pedofeatures pictured in Figures 6.13 to 6.23. These are the first micromorphological data presented for South African heuweltjie soils.

Table 6.2: Thin section descriptions of samples from Table 6.1. Abbreviations: c/f: coarse/fine; diam.: diameter; incl.: including; max.: maximum; occ.: occasional; OIL: oblique incident light; PPL: plane polarised light; XPL: cross polarised light.

Heuveltjie centre; Orthic (Ochric) A (sample 2.1, 20 cm deep).	
Vertical section; size 40 x 100 mm; thickness 30 - 40 μm . See Figure 6.8(a).	
Micro-structure:	Bimodal ped size distribution: 1) peds 2 to 3 cm diam.: moderately separated subangular blocky to subrounded microstructure; 20% of section; 2) highly separated subrounded spheroidal crumb microstructure. Interped areas (40% voids) not as densely packed as peds.
Groundmass	
c/f limit:	5 μm
c/f ratio:	9:1
c/f-related distribution:	Coarse monic to fine chitonic (better expressed in OIL, grains coated by amorphous Fe-oxides incl. hematite (red in OIL)).
Coarse Material:	Mostly subrounded-subangular quartz, coated with fine hematite (red OIL). Bimodal size distribution: 0.4–0.8 mm diam. (15%) and 0.05–0.1 mm (70% in peds; 30% between). Also orthopyroxene, garnet, zircon, opaques (metallic lustre in OIL). Some altered organic material.
Micromass:	Very little fine material. Mostly amorphous Fe-oxides, incl. hematite (red in OIL). Some amorphous organic material, in one case linearly concentrated along the top of a ped. Undifferentiated b-fabric.
Pedofeatures: Nodules	
	Few moderately impregnated Fe (hydr)oxides.
Coatings	
	Sand and silt particles coated with red (OIL) Fe oxides.
Channels	
	Some vertical channels which may have originated from water movement, and channels around peds.
Heuveltjie centre; hardpan carbonate (petrocalcic) sample 2A.	
3 x vertical sections; size 40 x 55 mm; thickness 30–35 μm . See Figures 6.8–6.11.	
Micro-structure:	Weak to moderately separated granular microstructure dominant. Granules ('peloids'; 'ooids') 0.3–0.03 mm diam. Channels, chambers (together 10%). Some (5%) thin planar voids (0.6 mm x 3 cm), some of which contain fine roots in handspecimen and define larger scale moderately separated subangular blocky microstructure (2 cm diam. peds).
Groundmass	
c/f limit:	5 μm
c/f ratio:	1:8
c/f-related distribution:	Double-spaced to open porphyric, chitonic.
Coarse Material:	Mostly subrounded-subangular very fractured quartz. Max. diam. 0.5 mm, common 0.4 mm, and also 0.04 mm diam. Opaques, generally rounded, garnet, orthopyroxene, occ. zircon, and also mica(?). Tissue residue.
Micromass:	Micrite interspersed with clay. PPL: Yellow to brown, speckled. XPL: crystallitic b-fabric dominant (micrite), also granostriated (clay; micrite).
<i>continued...</i>	

Table continued from previous page

Pedofeatures: Nodules

- i) Clay-quartz compound fragments (Figures 6.8(e)-(h)): rounded, generally spherical 1 cm to 0.7 mm diam. clay aggregates, distinguishable also in handspecimen. Less calcite than matrix, darker in PPL, more Fe (hydr)oxides, and have a granostriated b-fabric; not crystallitic like matrix. These clay nodules contain quartz grains (coated with oriented clay coatings) and cross-cutting micrite veins. The entire nodule often has a micrite hypocoating (banded, speckled).
- ii) Limpid yellow clay nodules (1 to 0.04 mm) (Figures 6.9, 6.10(a)-(e), 6.11): subangular, very low 1st order interference colours, often concentric-striated b-fabric, also cross-striated. Some coated with micrite hypocoatings giving the appearance of an 'oid' (Figure 6.9(a)), larger ones have Mn(?), and Fe accumulations. Some have concentric dark rings and core, possibly oxides. Some nodules have an internal radial and concentric orientation (Figure 6.10(c)). The limpid cores often show pseudo-negative uniaxial interference figures, and one seems to be overgrown from the centre by micrite (Figures 6.10(d)-(e)).
- iii) Micrite nodules (granules, resembling 'peloids') Figure 6.9, likely mixed with clay, 0.35 mm diam. One shows a pseudo-positive interference figure, some seem to be combined radial/concentric orientation, but generally the orientation not clear, possible due to the small size of the particles. These seem related to ii) above, it may be that the section does not pass through the core.
- iv) Opaque Localised moderate to strongly impregnated Fe (hydr)oxide nodules (dark in PPL, yellowish-green in OIL), and accessory dendritic and dispersed Mn oxides (10% section, effervesces in cold H₂O₂).

Coatings

- i) Quartz and orthopyroxene grains coated with red (in OIL) Fe (hydr)oxides (as in sample 2.2) (Figures 6.8(c)-(f), 6.9(a)) many of which are in turn coated by micrite (mixed with clay) hypocoatings ('oids'), and some by acicular calcite (radial orientation). The micrite hypocoatings are spherical, even when coating an elongate grain (Figure 6.8(e)). In some cases grain is coated by a limpid orange oriented (length-slow grain-parallel and perpendicular) clay coating (Figures 6.10(h)-(j)), which can in turn be coated by a micrite hypocoating. Sometimes fibro-radial orientation can be discerned.
- ii) Limpid clay nodules coated with micrite ('oids'), but not coated with hematite as the quartz and orthopyroxene grains (as in i) above). Instead there is generally a dark boundary (oxides?) between the nodule and the micrite coating (Figures 6.9, 6.10(d), (e), 6.11). Sometimes fibro-radial orientation can be discerned. Quite common is pseudo-negative limpid core zoning out to pseudo-positive micrite (Figure 6.9(c)), and in one case a second generation of micrite causes the 'oid' to zone back to pseudo-negative (Figure 6.10(e)).
- iii) Vughs coated by micrite.
- iv) Some micrite (+clay) seems to form laminar coatings of larger clay aggregates, resembles pendants but not restricted to the lower part (Figures 6.8(e)-(h)).

Channels

- i) Filled with limpid yellowish clay with cross-striated b-fabric, some channels are mixed with micrite and have a crystallitic b-fabric.
- ii) Coated by dark amorphous organic matter (Figures 6.8(b)-(d)). Some are continuously filled with more loosely packed matrix material, possibly ellipsoid mineralo-organic excrements, some contain tissue residue.

Phytoliths

- i) 0.6 x <0.1 mm with some square cells (0.1 x 0.05 mm) which are colourless in PPL, have 4th order green/pink interference colours, and are composed of calcite not Ca-oxalate (dissolve in 2N acetic acid) (Figures 6.10(f)-(g)). Covered by matrix micrite in some places.
- ii) Silica phytolith (isotropic).

continued...

Table continued from previous page

Excrement

Ellipsoidal, dark, speckled, 0.02 mm diam. (Figures 6.8(c)-(d))

HCl etching:

Limpid yellow clay nodules become clearer, orientation easier to see. They appear to be oriented clay. b-Fabric is concentric striated. Quartz fractures show less relief (Figure 6.11).

2m from heuweltjie centre; hardpan carbonate (petrocalcic) sample 2B. 3 x vertical sections; size 40 x 55 mm; thickness 30–35 μm . See Figures 6.14–6.17.

Micro-structure: Weakly separated granular microstructure. Granules ('peloids'; 'ooids') 0.3 - 0.03 mm diam.

Groundmass

c/f limit: 5 μm

c/f ratio: 1:8

c/f-related distribution: Double-spaced to open porphyric; chitonic.

Coarse Material: Mostly subrounded-subangular very fractured quartz, 0.5 - 0.04 mm diam., commonly 0.4 mm. Opaques, generally rounded, garnet, cpx, occ. zircon.

Micromass: Micrite (less abundant than 2A) interspersed with clay and oxides. PPL: Yellow to brown, speckled, with Fe (hydr)oxides (dark PPL, yellowish-green OIL), and accessory dendritic or dispersed Mn oxides (effervesces cold H_2O_2) in 40% section - more abundant than 2A. XPL: speckled b-fabric dominant, also granostriated.

Pedofeatures: Nodules

i) Clay-quartz compound fragments (Figures 6.14): Rounded, generally spherical 0.7 mm diam. clay aggregates, distinguishable also in handspecimen. Very similar to the matrix, but have less calcite, and have a grano-circular-striated b-fabric, not crystallitic. They contain quartz grains (coated as the matrix), (granostriated) clay, opaque material, and what appears to be altered organic remains. One clay aggregate (Figure 6.17(b)–(d)) has low birefringence (sepiolite?) and contains quartz grains and needles. The clay forms spherical coatings on the angular quartz grains and needles that are aggregated to form the nodule.

ii) Opaque Localised moderate to strongly impregnated Fe (hydr)oxide nodules (dark in PPL, yellowish-green in OIL), and accessory dendritic or dispersed Mn oxides (effervesces cold H_2O_2) in 40% section - more abundant than 2A. The nodules appear to have less calcite than the matrix, some have cross-cutting micrite veins.

iii) Limpid yellowish clay nodules (300 - 70 μm) (Figures 6.15, 6.16): subangular to rounded, with a cross-striated b-fabric and very low (first order) interference colours, occasionally will show pseudo-negative uniaxial interference colours, may zone outwards to pseudo-positive (commonly in the micrite coating); sometimes fibro-radial orientation can be discerned. Some have concentric dark narrow rings which may be oxides, or a dark core.

iv) Micrite nodules (granules, resembling 'peloids') (e.g. Figure 6.15) likely mixed with clay, 0.35 mm diam. One shows a pseudo-positive interference figure, some seem to be combined radial/concentric, but generally the orientation not clear, possible due to the small size of the particles.

v) Digitate calcite nodule 0.2 mm diam.

Coatings

i) Quartz and orthopyroxene grains coated by red (OIL) Fe (hydr)oxides (as in samples 2.2, 2A), in turn coated by micrite (mixed with clay) and sepiolite (Figure 6.15).

ii) Limpid clay nodules occasionally coated with hematite and/or other oxides (Figure 6.16), but most commonly only by micrite.

iii) Some micrite and sepiolite coating larger clay aggregates (Figures 6.14, 6.17(b)–(d)), micrite coating is thicker around the angular parts of the nodule to give a spherical ooid-like structure.

continued...

Table continued from previous page

Altered grains

Generally elongated, 3 x 0.6 mm, speckled orange-brown, have a circular striated b-fabric (Figure 6.16).

Pendents and cappings

Large scale (cm's) micrite laminations (mixed with clay(?)) (for example Figures 6.17(e)-(f)).

Excrement

Rounded, 0.05 mm diam., ellipsoidal, dark, micritic, appears to be contained in plant tissue residue (Figure 6.17(a)). A lot of tissue residue seems altered to micrite, and is associated with more clay rich fragments.

Channels

i) Filled with limp yellowish clay with cross-striated b-fabric and very low interference colours (sepiolite), some channels are mixed with micrite and have a crystallitic b-fabric.

3.2 m from heuweltjie centre; hardpan carbonate (petrocalcic) sample 2C. 3 x vertical sections; size 40 x 25 mm; thickness 30–35 μm . See Figures 6.18–6.19.

Micro-structure: Weakly separated granular to massive microstructure. Granules ('peloids'; 'ooids') 0.3 - 0.03 mm diam.

Groundmass

c/f limit: 5 μm

c/f ratio: 1:8

c/f-related distribution: Double-spaced to open porphyric; chitonic.

Coarse Material: Mostly subrounded-subangular very fractured quartz. 0.5–0.04 mm diam., commonly 0.4 mm. Opaques, generally rounded, garnet, orthopyroxene, occ. zircon.

Micromass: Micrite interspersed with clay. PPL: Yellow to brown, speckled. XPL: speckled b-fabric dominant, also granostriated.

Pedofeatures: Nodules

i) Clay-quartz compound fragments (Figures 6.18(a), (b)): Rounded, generally spherical (also angular) 0.7 mm diameter clay aggregates, distinguishable also in handspecimen. Very similar to matrix, but have less calcite. Micrite veins cross cutting, and micrite hypocoatings (banded, speckled). They are darker in PPL, contain more Fe (hydr)oxides than the matrix, and have a granostriated b-fabric, not crystallitic. They contain quartz grains (Fe-, clay coated), (granostriated) clay, and opaque material.

ii) Limpid yellow clay nodules (Figures 6.19(a)–(c)): subangular (300 - 70 μm) which have a cross-striated b-fabric and low first order interference colours, occasionally show pseudo-negative uniaxial interference figures, and may be coated with micrite and acicular calcite (radial orientation). Some have concentric dark narrow rings, which could be oxides and is suggestive of multistage growth. One has a light-coloured core (quartz?) (Figure (d)), in contrast to the dark cores usually observed in samples 2A–2B.

Coatings

i) Quartz and orthopyroxene particles coated with red (OIL) Fe (hydr)oxides (as in samples 2.2, 2A, 2B), in turn coated by acicular calcite (radial orientation, Figures 6.19(f), (h), easier to see than in samples 2A-B), and also by grain-parallel oriented clay that is revealed on etching in HCl (Figures 6.19(g), (i)).

ii) Limpid yellow clay nodules have oxide coatings, covered by radially oriented calcite (Figures 6.19(a), 6.19(d)).

Channels; excrement

Filled with 0.05 mm diam. spheres ('peloids'), which appear to be excrement and have the same b-fabric (speckled, micrite) as matrix (Figures 6.18(e), (f)). Matrix and excrement both dissolved during HCl-etching. Some channels have chambers and most have fine, dark (hypo)coatings that appear to be organic matter.

continued...

Table continued from previous page

Pendants

Large scale (cm's) micrite laminations (Figures 6.18(a)–(d)).

HCl etching:

Figures 6.19(d)–(i) Limpid yellow clay nodules (spherulites and concentric nodules) become clearer, orientation easier to see, and concentric dark rings are less prominent. Appear to be clay with low interference colours. Fractures in silicate grains show less relief. Micrite matrix ('peloids') dissolved.

7.5 m from heuweltjie centre; 'sepiolitic' pedocutanic (argic) (sample 2D). 2 x vertical sections; size 20 x 15 mm; thickness 20 to 25 μm . See Figures 6.20, 6.21, 6.22.

Micro-structure: Weakly separated vughy to massive microstructure.

Groundmass

c/f limit: 5 μm

c/f ratio: 1:2

c/f-related: Single-spaced porphyric; chitonic.

distribution:

Coarse: Mostly subrounded to subangular very fractured quartz. 0.5 to 0.04 mm diam., commonly 0.4 mm. Opaques, generally rounded, occ. zircon, feldspar.

Micromass: PPL: Pale yellow-brown, mostly limpid clay (and silica?). XPL: Grano- and circular striated b-fabric.

Pedofeatures: Nodules

i) Clay-quartz compound fragments: Angular compound fragments comprising either 1) quartz grains and clay nodules with granostriated b-fabric (caused by oriented clay coatings) set in a darker, more speckled matrix than the surrounding matrix, and the entire fragment is coated with clay oriented parallel to the edges. Along one side of one fragment there is a zone of clay with very low interference colours, consisting of interwoven domains of oppositely oriented fibres (perpendicular and parallel to the nodule) which appear to be sepiolite (Figure 6.21), or 2) comprising quartz grains set in a *fibrous matrix* (Figure 6.22) that is consistent with sepiolite.

Coatings

Quartz particles coated with red (OIL) Fe (hydr)oxides (as in samples 2.2, 2A to C), which is in turn coated by oriented clay coatings (Figure 6.20). Clay nodules not coated with hematite.

Heuweltjie edge (8 m from 2D); dorbank (petroduric), sample 1.3. 1 x vertical section; size 45 x 90 mm; thickness 35 to 40 μm . See Figure 6.23.

Micro-structure: Vughy microstructure

Groundmass

c/f limit: 5 μm

c/f ratio: 2:1

c/f-related: Chito-gefuric to close porphyric.

distribution:

Coarse: Mostly subrounded-subangular very fractured quartz grains 0.4 to 0.03 mm diam. coated with fine hematite (red in OIL). Some larger grains have embayments (0.02 mm) filled with hematite (Figure 6.23(a)). Occ. orthopyroxene, garnet, opaques, zircon.

Micromass: Silica and clay and Fe oxides. PPL: Orange-brown, mostly speckled. XPL: Granostriated b-fabric.

Pedofeatures: Nodules:

i) Spherulites, some of which show pseudo-negative uniaxial interference figures, some appear to have an isotropic core. Others show concentric banding.

continued...

Table continued from previous page

ii) Aggregates (Figures 6.23(a)–(c)) containing quartz grains with red Fe coatings, cemented by silica (mixed with clay and Fe to give a limpid orange colour). The aggregates contain more interstitial silica and fewer quartz grains than the matrix.

Coatings:

i) Quartz particles coated with red (OIL) Fe (hydr)oxides (as in 2.2, 2A to D). Some larger grains have embayments (0.02 mm) filled with hematite (Figures 6.23(a), (g) to (f)).

ii) Laminated (in places) orange-brown, generally limpid, compound clay and silica coating a) spherical, rounded peds 0.5 to 1 cm diam., b) an elongated channel(?) 3 x 0.5 cm, and c) large irregular (5 cm) peds. In one instance the amorphous silica is clearly on the outer part (Figure 6.23(d) to (f)).

iii) Silica and Fe-stained clay compound coatings around channels and vughs. The silica is in places transparent in PPL but in other places seems to be coloured by iron and mixed with clay. In some cases the silica is clear, and occurs on the void-side of the coating (6.23(g) to (h)). In one case it can be discerned as edge-parallel length-slow (Figure 6.23(i)).

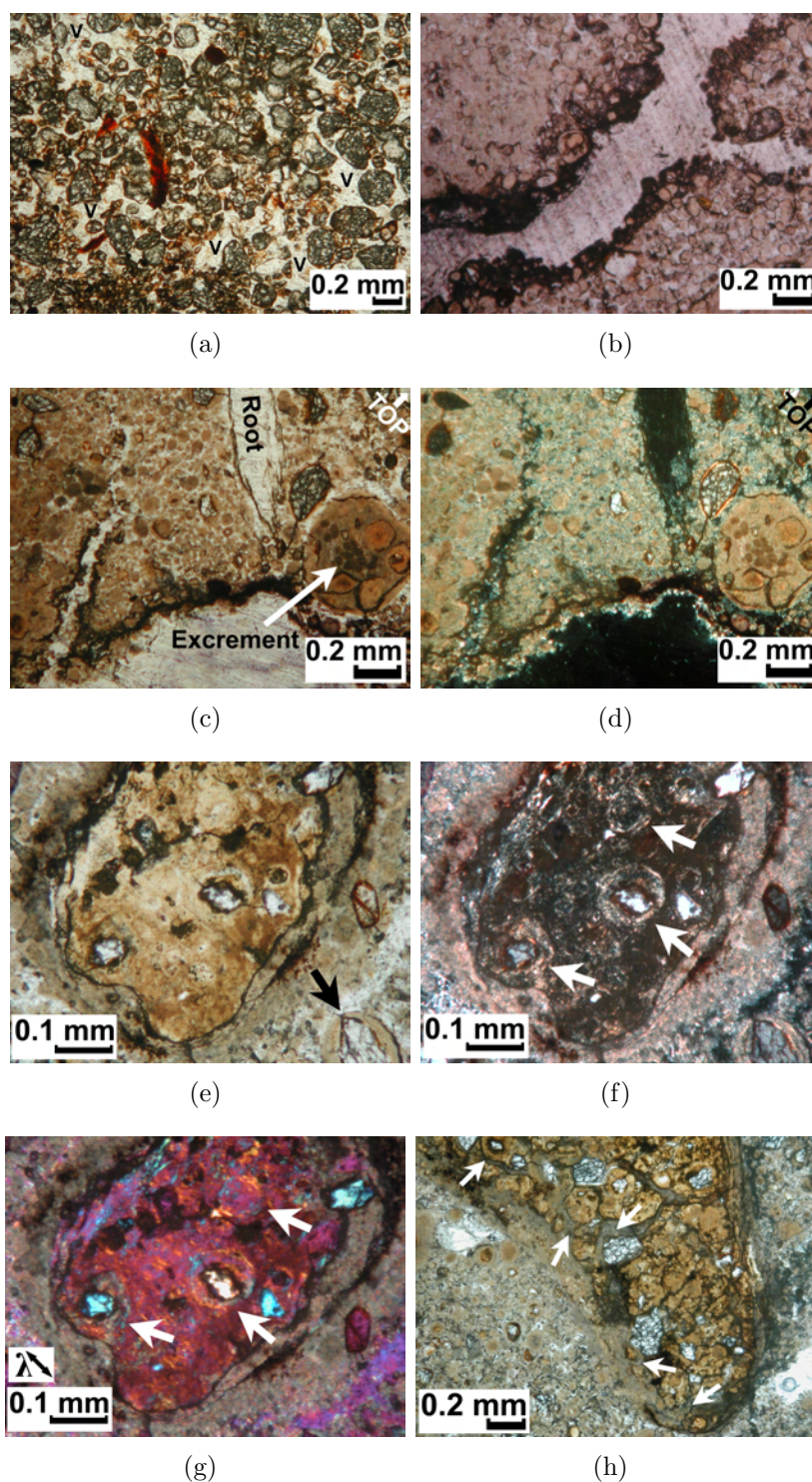


Figure 6.8: Photomicrographs from centre of heuweltjie. Way-up is top of page. (a) Orthic A horizon (sample 2.1, 20 cm deep), v: void, ppl. (b)-(g) Calcrete (sample 2A) underlying sample 2.2. (b) Tunnel lined with organic matter, ppl. (c) Chamber and tunnel lined with organic matter; excrement in nodule; quartz grain coated with red Fe, ppl. (d) xpl. (e)-ppl, (f)-xpl, (g)- λ -plate, fast-direction NW-SE: clay nodule with micrite hypocoting, internal ooid-like structures form granostriated b-fabric. Note thinning of micrite coating around an angular hematite-coated quartz grain to form spherical ooid (arrowed in (e).) (h) Clay nodule fractured by micrite, ppl.

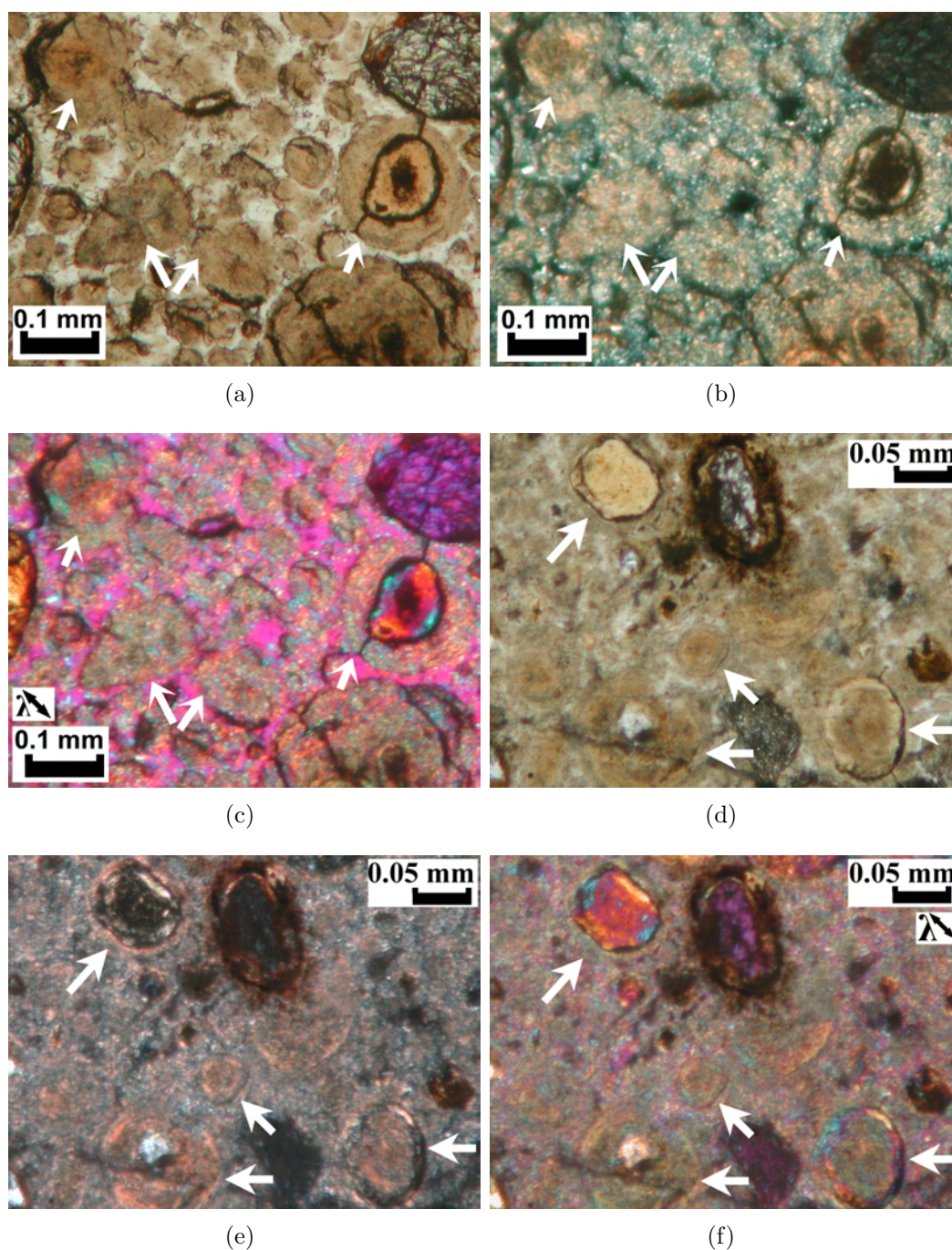


Figure 6.9: Photomicrographs from calcrite (2A) in the centre of heuweltjie. Way-up is top of page. (a)–ppl, (b)–xpl, (c)– λ -plate, fast-direction NW-SE: oriented granules (arrowed top-left), unoriented granules/‘peloids’ (arrowed centre), limpid oriented core with an oriented micrite coating (arrowed right); quartz grains coated with red Fe. (d)–ppl, (e)–xpl, (f)– λ -plate, fast-direction NW-SE: limpid oriented nodule with thin unoriented micrite coating (arrowed top), oriented micrite nodule (arrowed centre), quartz grain with oriented micrite coating (arrowed bottom-left), oriented limpid nodule undergoing “micritization” from the centre (arrowed bottom-right).

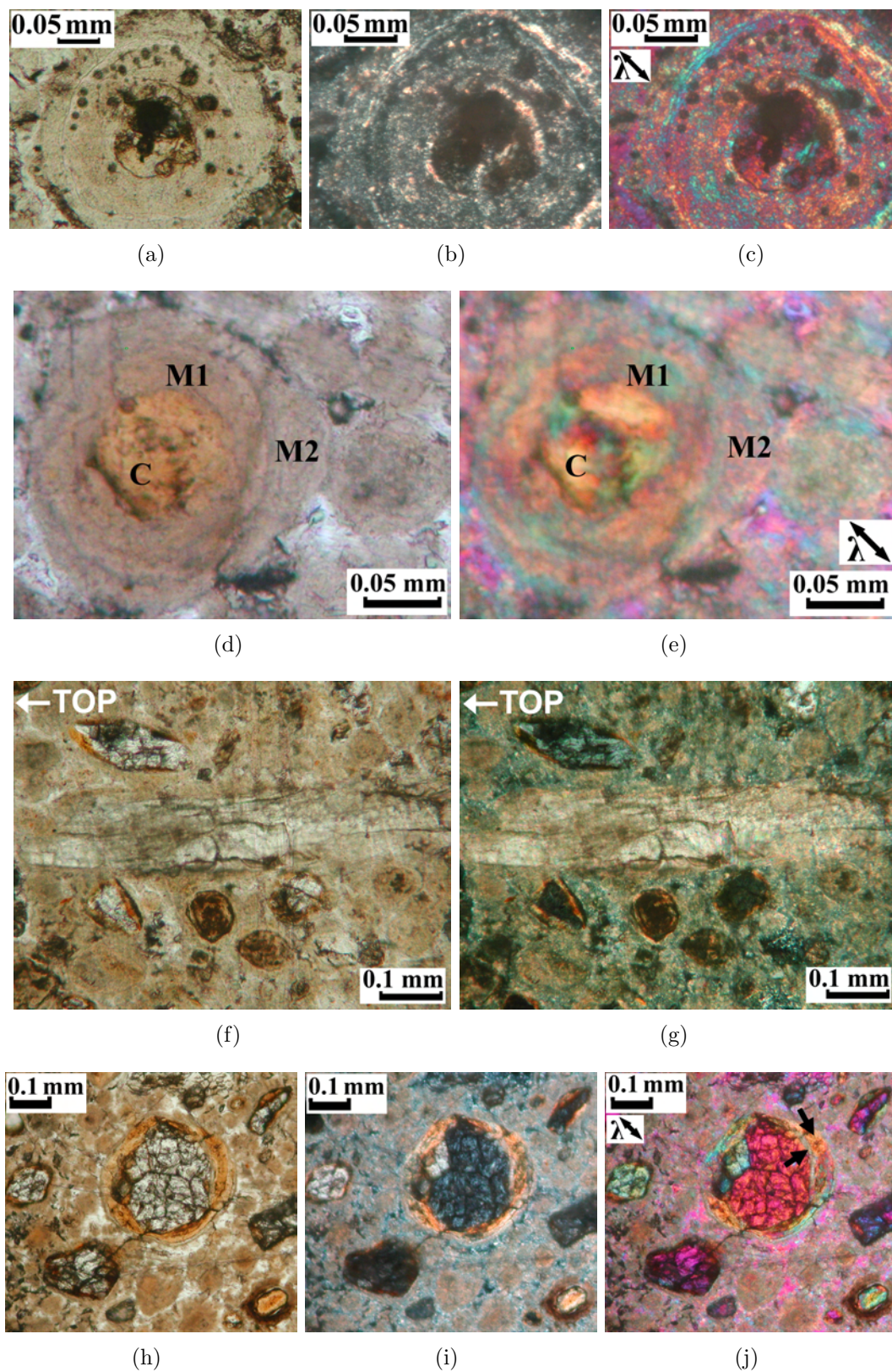


Figure 6.10: Photomicrographs from calcrite (2A) in centre of heuweltjie. Way-up is top of page. (a)–ppl, (b)–xpl, (c)– λ -plate, fast-direction NW-SE: radial and concentric orientation in layers of nodule.(d)–ppl, (e)– λ -plate, fast-direction NW-SE: limpid pseudo-negative core (C) surrounded by pseudo-positive (M1) and pseudo-negative (M2) micrite.(f)–ppl, (g)–xpl: calcite (which dissolved in 2N acetic acid) phytolith.(h)–ppl, (i)–xpl, (j)– λ -plate, fast-direction NW-SE: Fe, clay coatings: note perpendicular orientations.

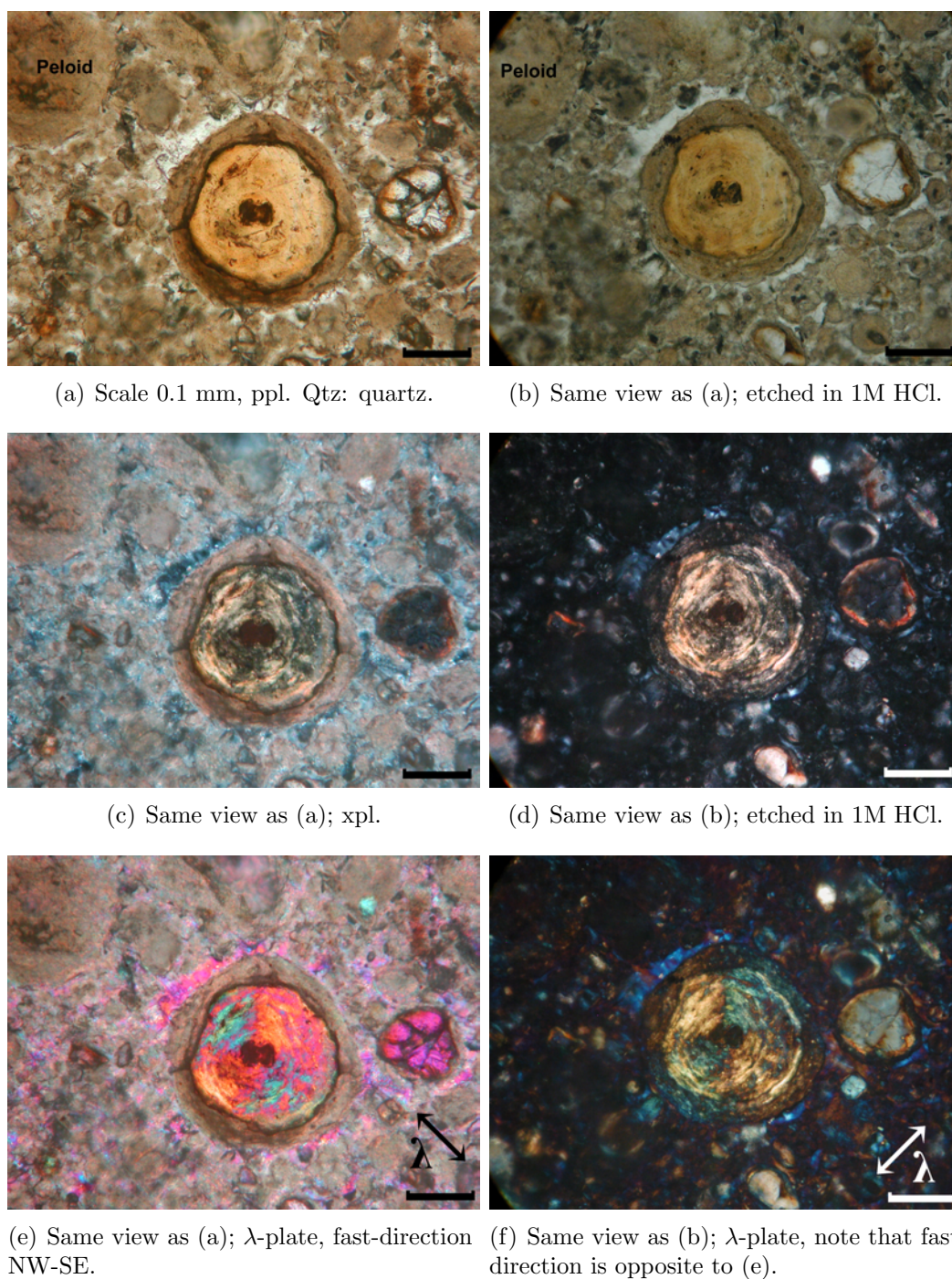
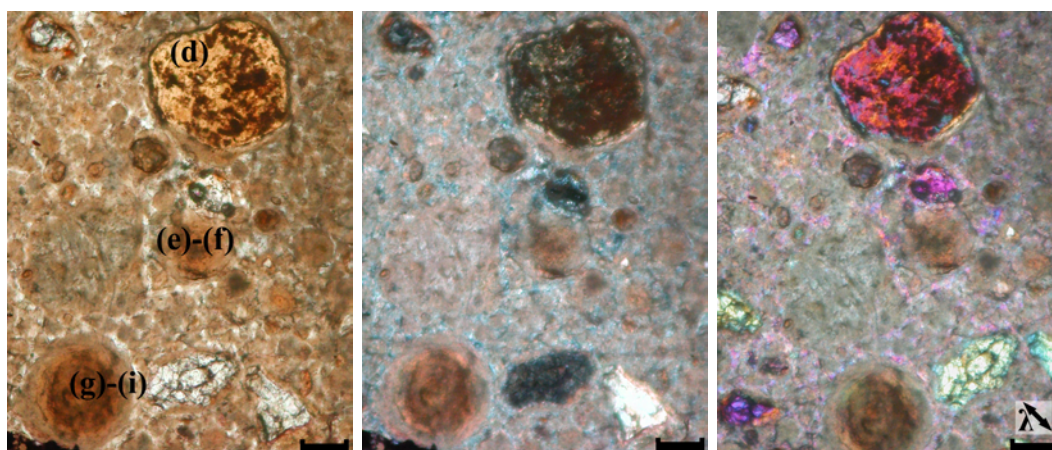


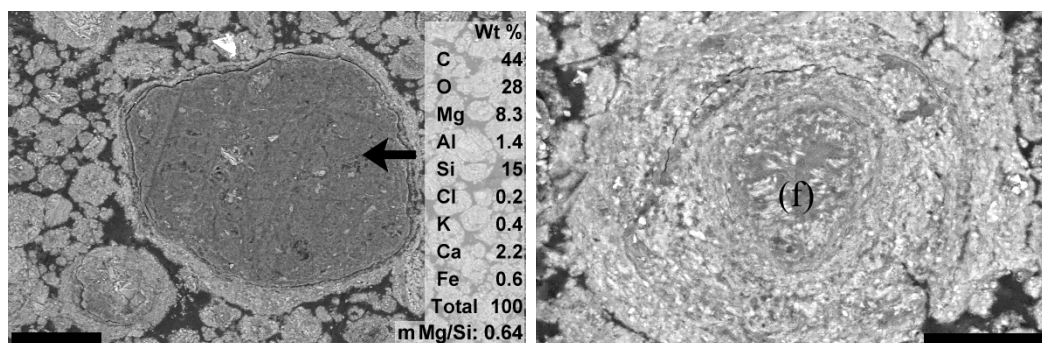
Figure 6.11: Photomicrographs: HCl etching of peloids and a coated limpid nodule with pseudo-negative uniaxial interference figure (sample 2A, calcrete in centre of heuweltjie). Way-up is top of page.



(a) Scale 0.1 mm, ppl, magnified in (d) to (i).

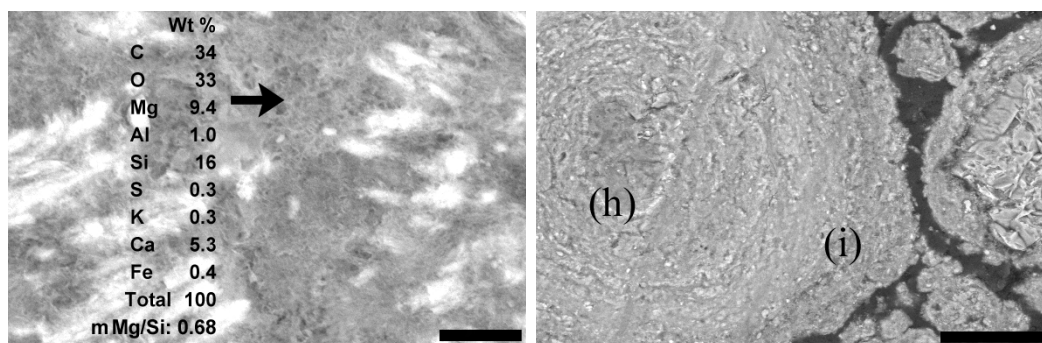
(b) Same as (a), xpl.

(c) Same as (a), λ -plate, fast-direction NW-SE.



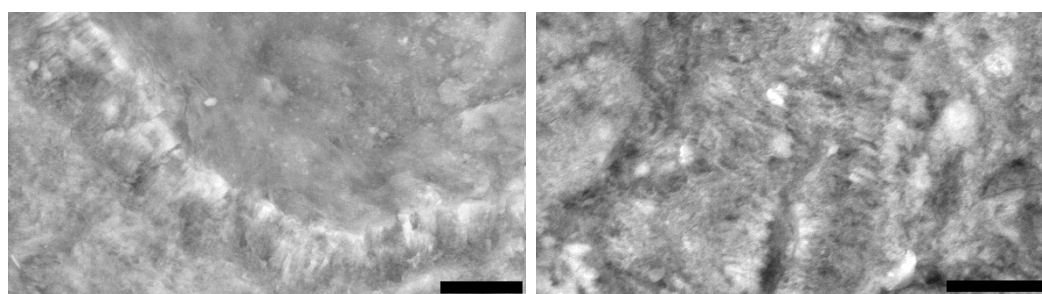
(d) Magnification of (a), scale bar 100 μm .

(e) Magnification of (a), scale bar 50 μm .



(f) Magnification of (e), sepiolite (grey mesh), radial calcite (white). Scale 5 μm .

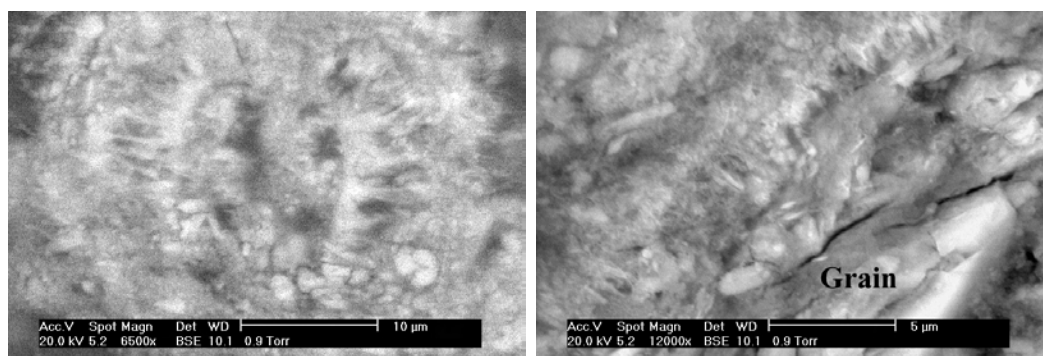
(g) Magnification of (a), scale bar 50 μm .



(h) Magnification of (g), radial orientation of needle fibres. Scale 5 μm .

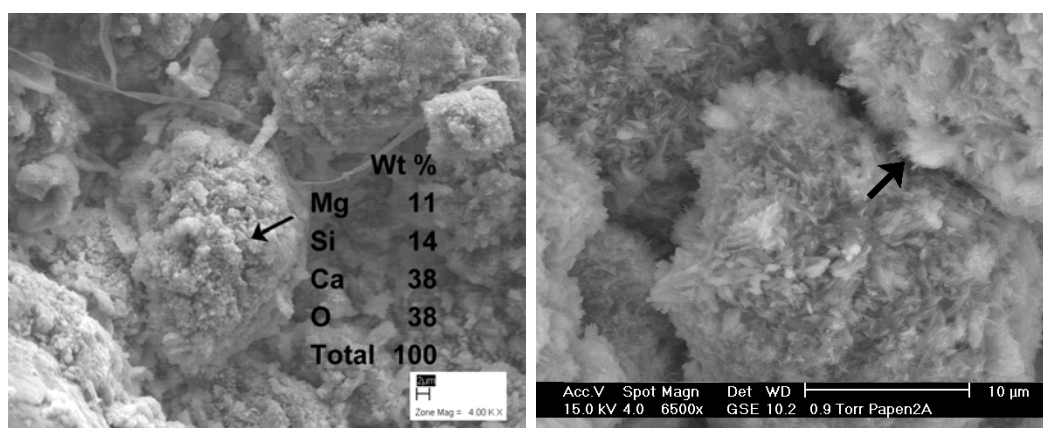
(i) Magnification of (g), radial orientation of needle fibres. Scale 5 μm .

Figure 6.12: Photomicrographs and corresponding ESEM images from calcrite (2A) in centre of heuweltjie. Calcite is white; grey colours are lower atomic numbers such as Mg or Si. Way-up is to the right.



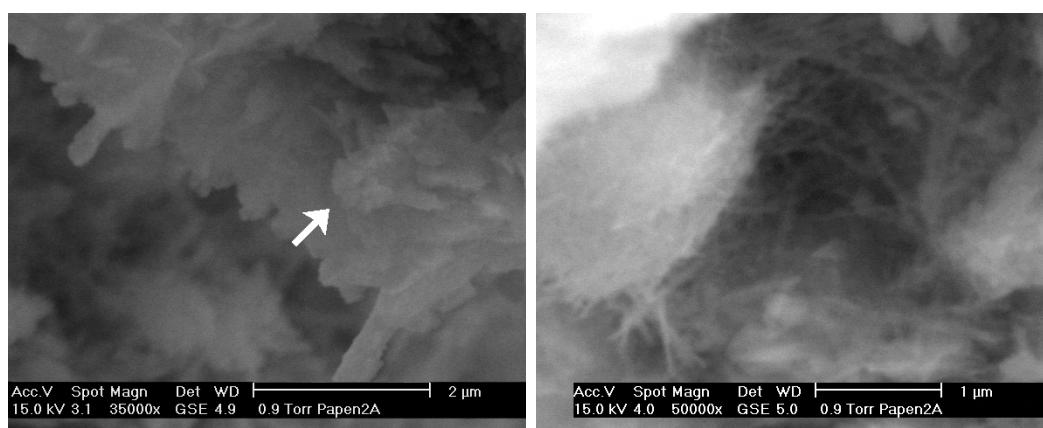
(a) 'Ooid' composed of radial acicular calcite. EDAX suggests sepiolite present in lesser amounts. Scale 10 μm .

(b) Radial, acicular calcite coating silicate grain. EDAX suggests sepiolite present in lesser amounts. Scale 5 μm .



(c) Fragment: micrite nodules (ooids), note hollow centres, and fungal filament. Scale 2 μm .

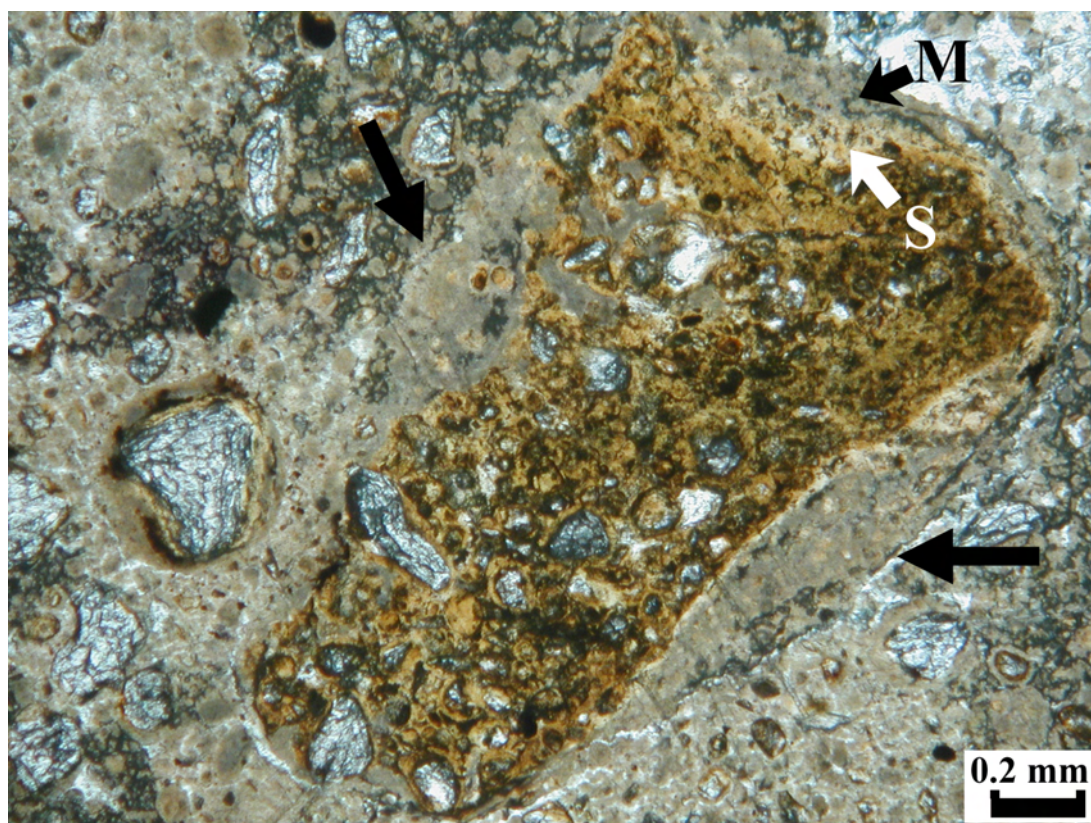
(d) Fragment showing radial orientation of acicular calcite in nodules. Area magnified in (e) arrowed. Scale 10 μm .



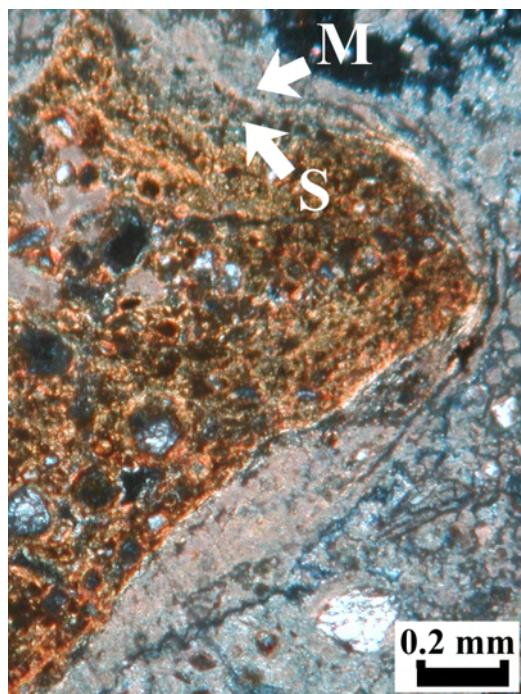
(e) Magnification of (d), MB rod arrowed (after Verrecchia and Verrecchia (1994)). Scale 2 μm .

(f) Sepiolite fibres in the same fragment. Scale 2 μm .

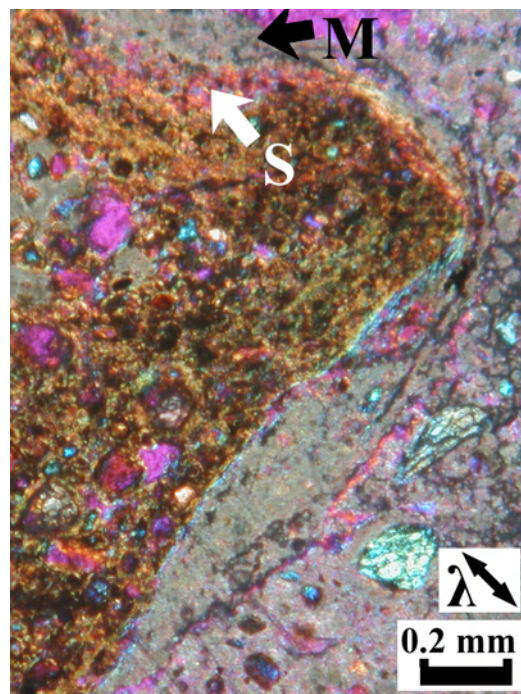
Figure 6.13: ESEM images of fragments and thin sections from calcrete (2A) in centre of heuweltjie.



(a)

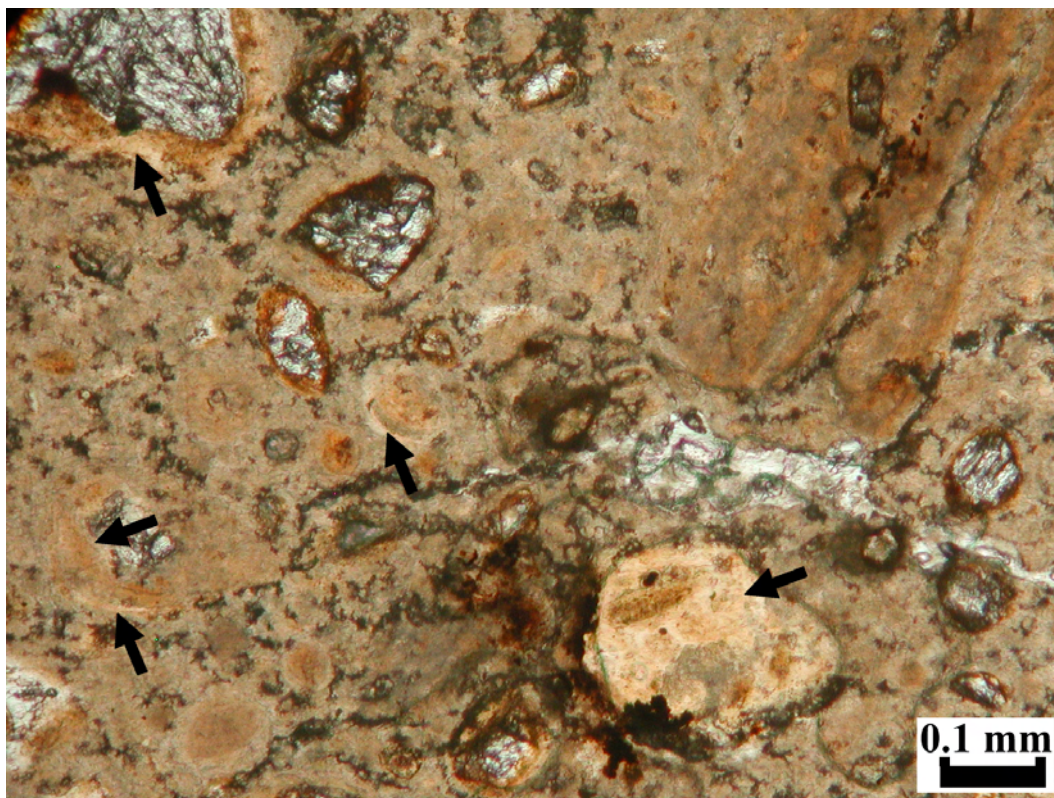


(b)

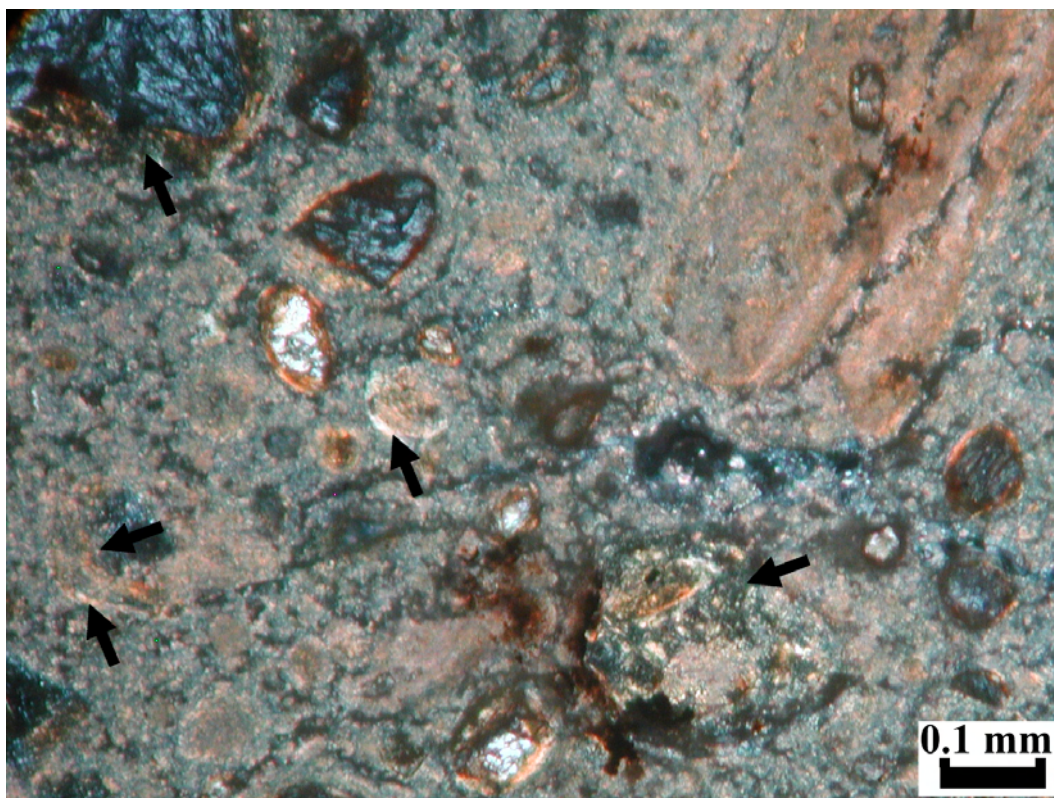


(c)

Figure 6.14: Photomicrographs from calcrete (2B), 2 m from centre of heuweltjie. Way-up is top of page. (a)–ppl, (b)–xpl, (c)– λ -plate, fast-direction NW-SE: quartz-clay aggregate with sepiolite (S) coating covered by micrite (M) coating. Note thickening of micrite coating to give spherical ooid-like structure (arrowed in (a)). This pattern is also present around the quartz grain on the left. Dispersed opaques in nodule and matrix are Mn and Fe (hydr)oxides.

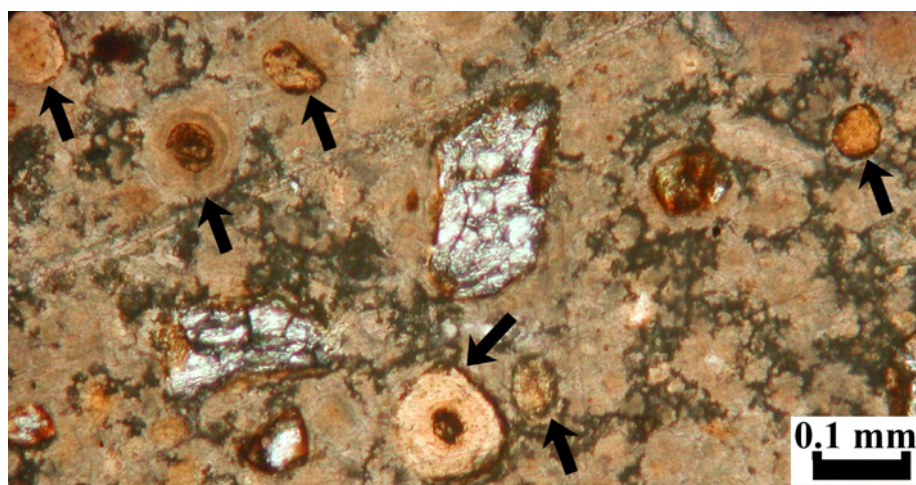


(a)

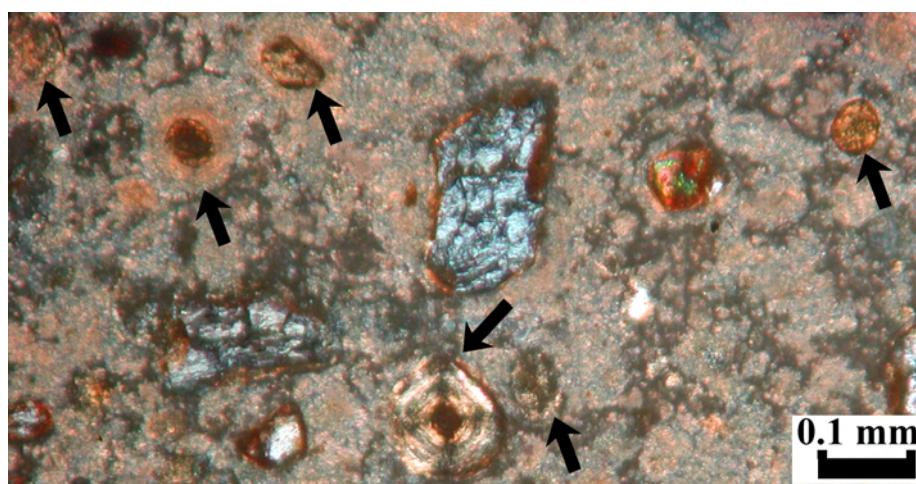


(b)

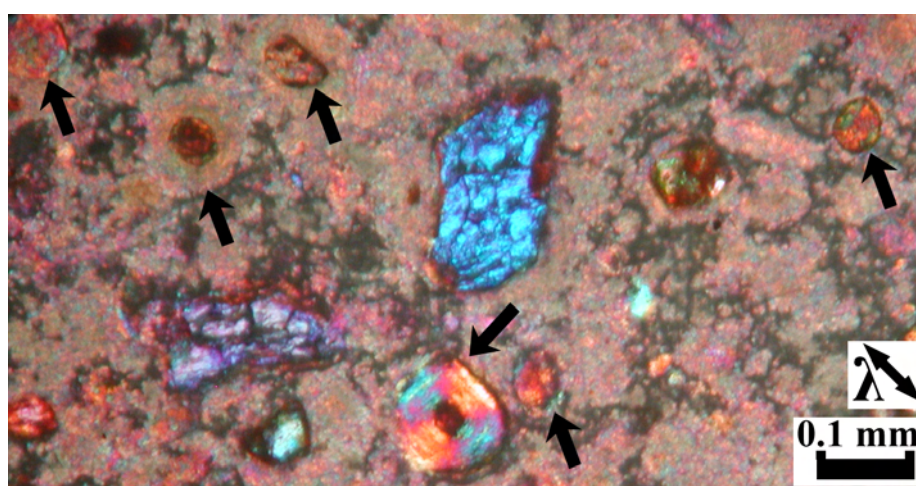
Figure 6.15: Continued - photomicrographs from calcrete (2B), 2 m from centre of heuweltjie. Way-up is top of page. (a)-ppl, (b)-xpl: sepiolite nodule and layered calcite-sepiolite grain coatings in a micrite-clay matrix.



(a)



(b)



(c)

Figure 6.16: Continued - photomicrographs from calcrete (2B), 2 m from centre of heuweltjie. Way-up is top of page. (a)–ppl, (b)–xpl, (c)– λ -plate, fast-direction NW-SE: limpid clay nodules (pseudo-negative and unoriented), with oriented (pseudo-positive) micrite coatings.

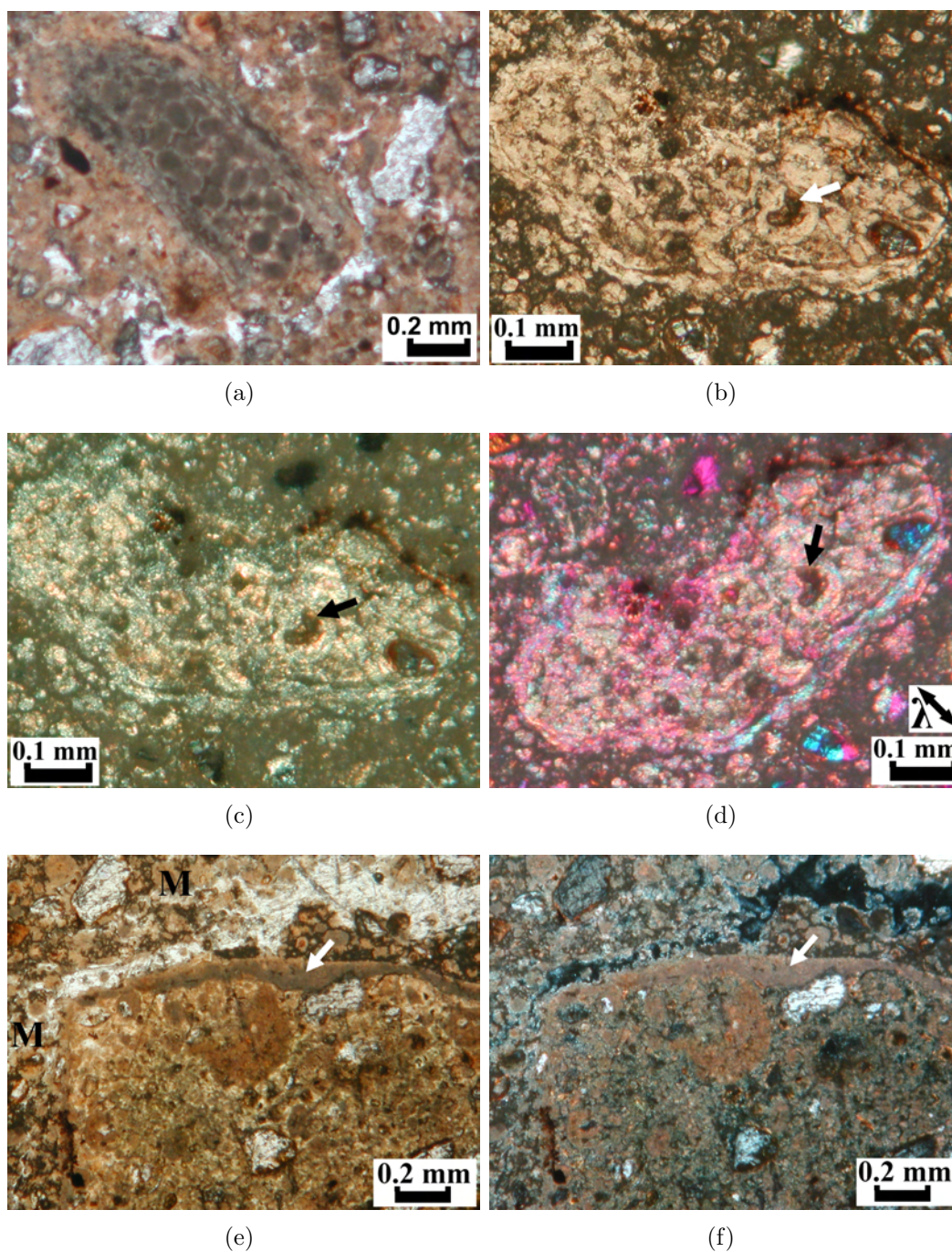


Figure 6.17: Continued - photomicrographs from calcrite (2B), 2 m from centre of heuveltjie. Way-up is top of page. (a)–ppl: calcified, excrement-filled organ residue. (b)–ppl, (c)–xpl, (d)– λ -plate, fast-direction NW-SE: sepiolite clay-quartz nodule containing organ residue (needle, arrowed) in oxide-rich matrix. Quartz grains coated by red Fe oxides. Needle and grain above it are coated by clay, giving the appearance of spherical ‘ooids’. Lower part of the nodule shows grain-parallel clay orientation. (e)–ppl, (f)–xpl: micrite capping ped (arrowed), in a more oxide-rich matrix (m).

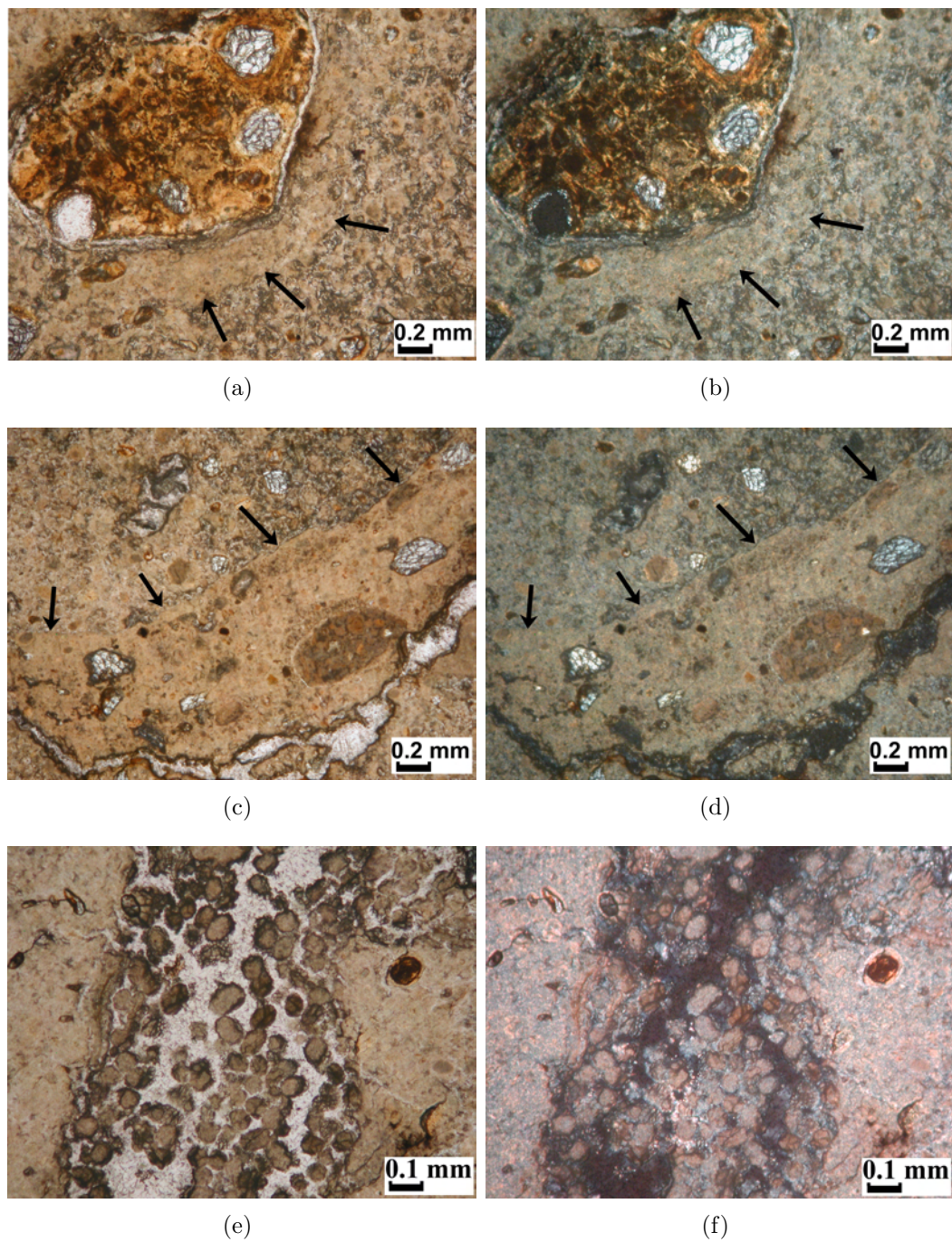


Figure 6.18: Photomicrographs from calcrete (2C), 3.2 m from centre of heuweltjie. Way-up is top of page. (a)–ppl, (b)–xpl: calcite pendent below clay-quartz compound fragment. (c)–ppl, (d)–xpl: calcite pendent associated with an organic matter-lined tunnel. (e)–ppl, (f)–xpl: micrite-containing excrement in tunnel.

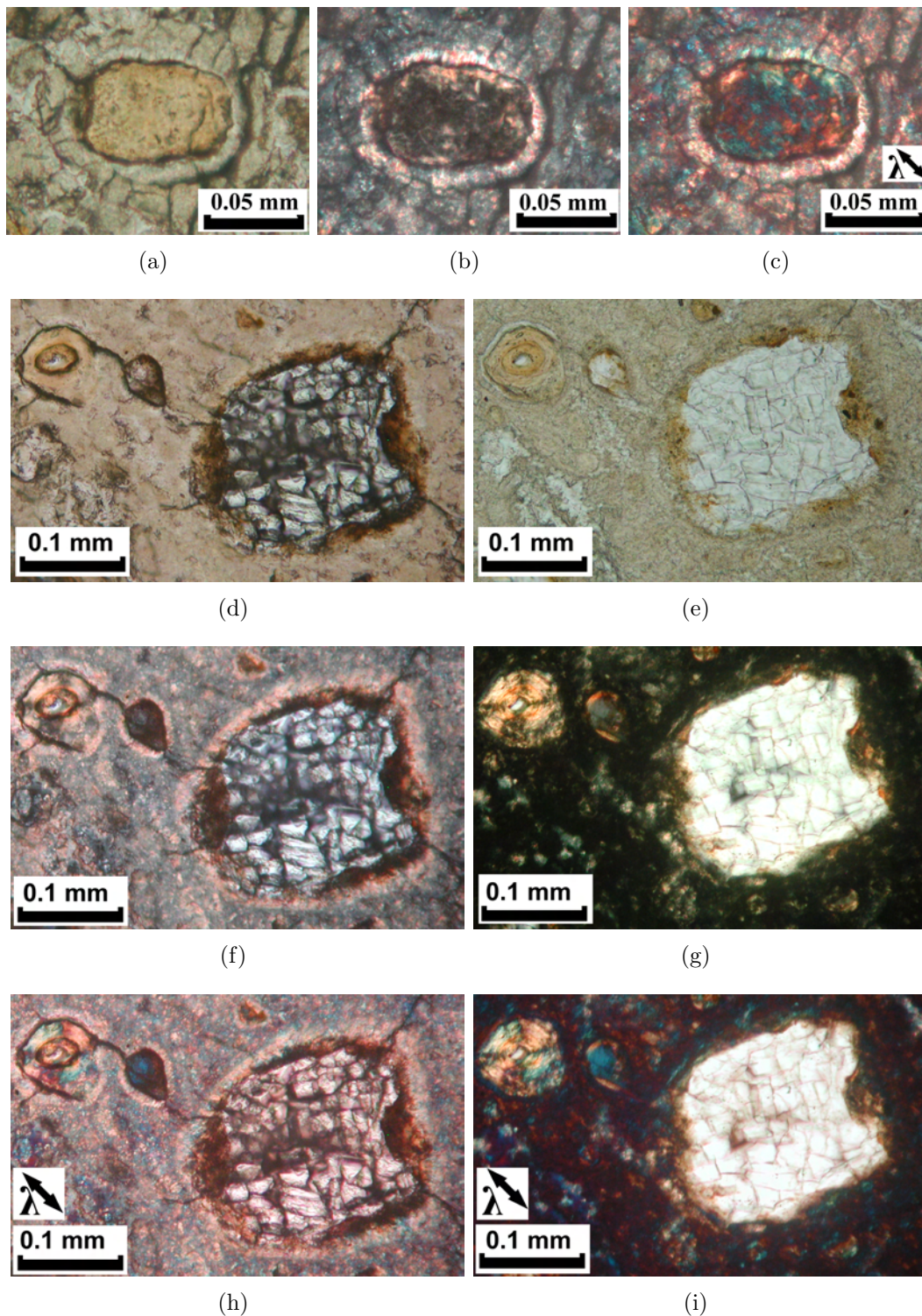


Figure 6.19: Continued - photomicrographs from calcrete (2C), 3.2 m from centre of heuweltjie. Way-up is top of page. (a)–ppl, (b)–xpl, (c)– λ -plate, fast-direction NW-SE: fibro-radial calcite coating a limpid clay nodule. (d)–ppl, (e)–ppl, HCl-etched, (f)–xpl, (g)–xpl, HCl-etched, (h)– λ -plate, fast-direction NW-SE, (i)– λ -plate, HCl-etched: fibro-radial calcite and grain-parallel clay coating a quartz grain; 2-generations of clay oriented around quartz fragment forming an ooid-like structure with a pseudo-negative interference figure.

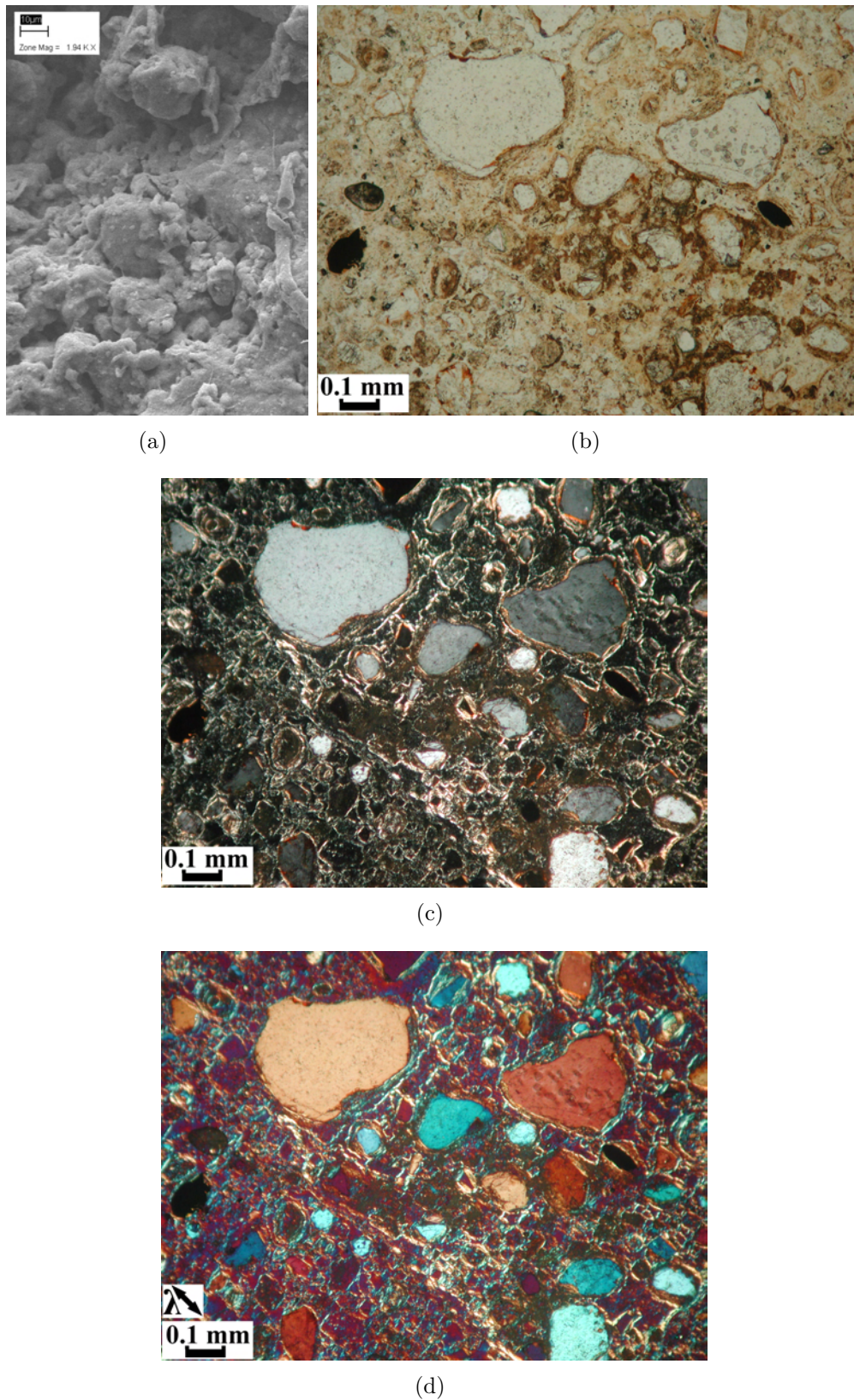


Figure 6.20: Non-calcareous 'sepiolitic' pedocutanic (argic) (2D), 7.5 m from centre of heuveltjie. (a) SEM image of fragment, showing smooth coatings of grains. Scale 10 μm . (b)–ppl, (c)–xpl, (d)– λ -plate, fast-direction NW-SE, way-up is top of page: photomicrographs of grain-parallel, aligned clay and dominating granostriated b-fabric. Section is thinner than 2A to 2C.

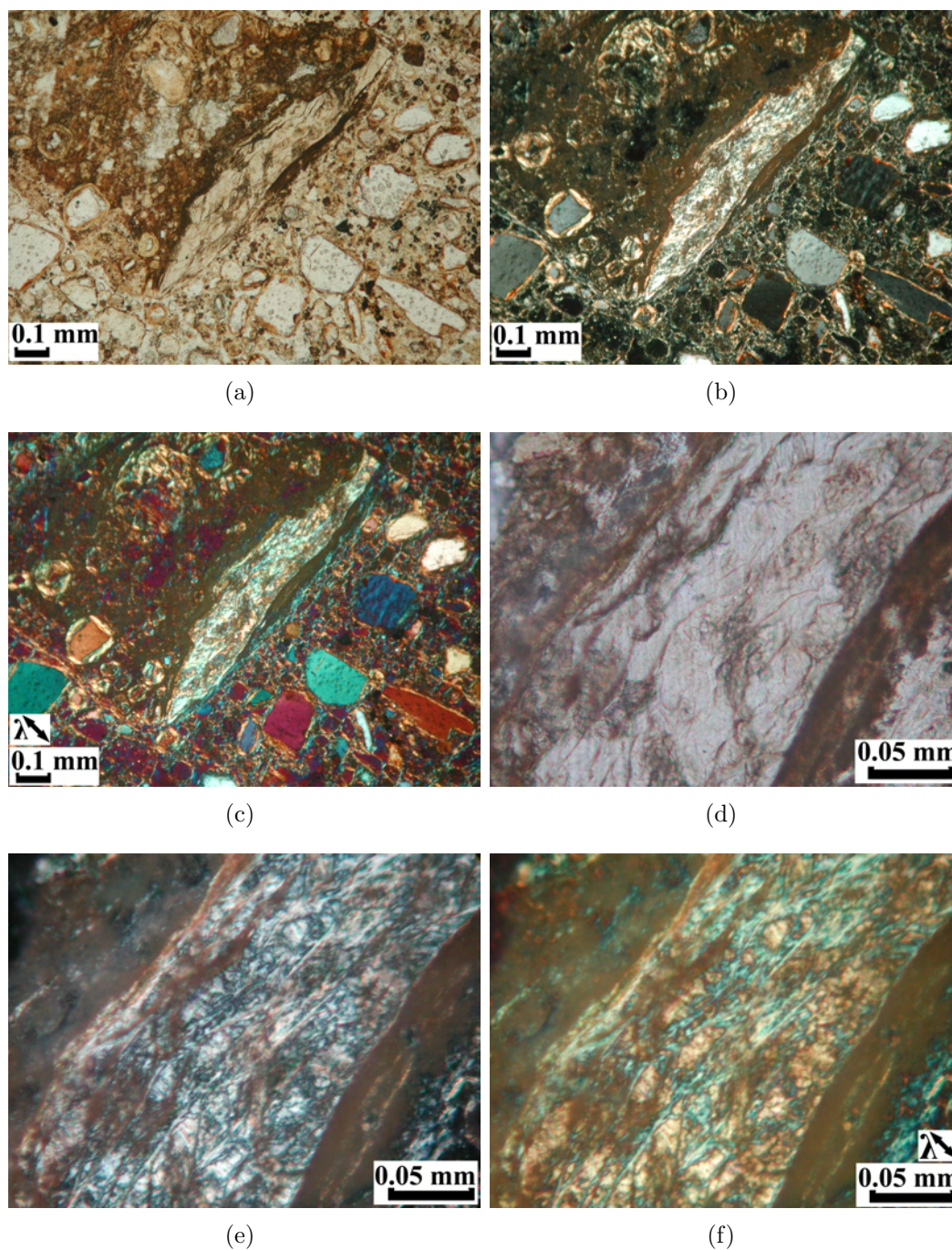


Figure 6.21: Continued - photomicrographs of non-calcareous ‘sepiolitic’ pedocutanic (argic) (2D), 7.5 m from centre of heuweltjie. Way-up is top of page. (a)–ppl, (b)–xpl, (c)– λ -plate, fast-direction NW-SE: clay capping on a (rotated) quartz-clay aggregate. (d)–ppl, (e)–xpl, (f)– λ -plate, fast-direction NW-SE: magnification of clay capping showing interwoven fibre domains.

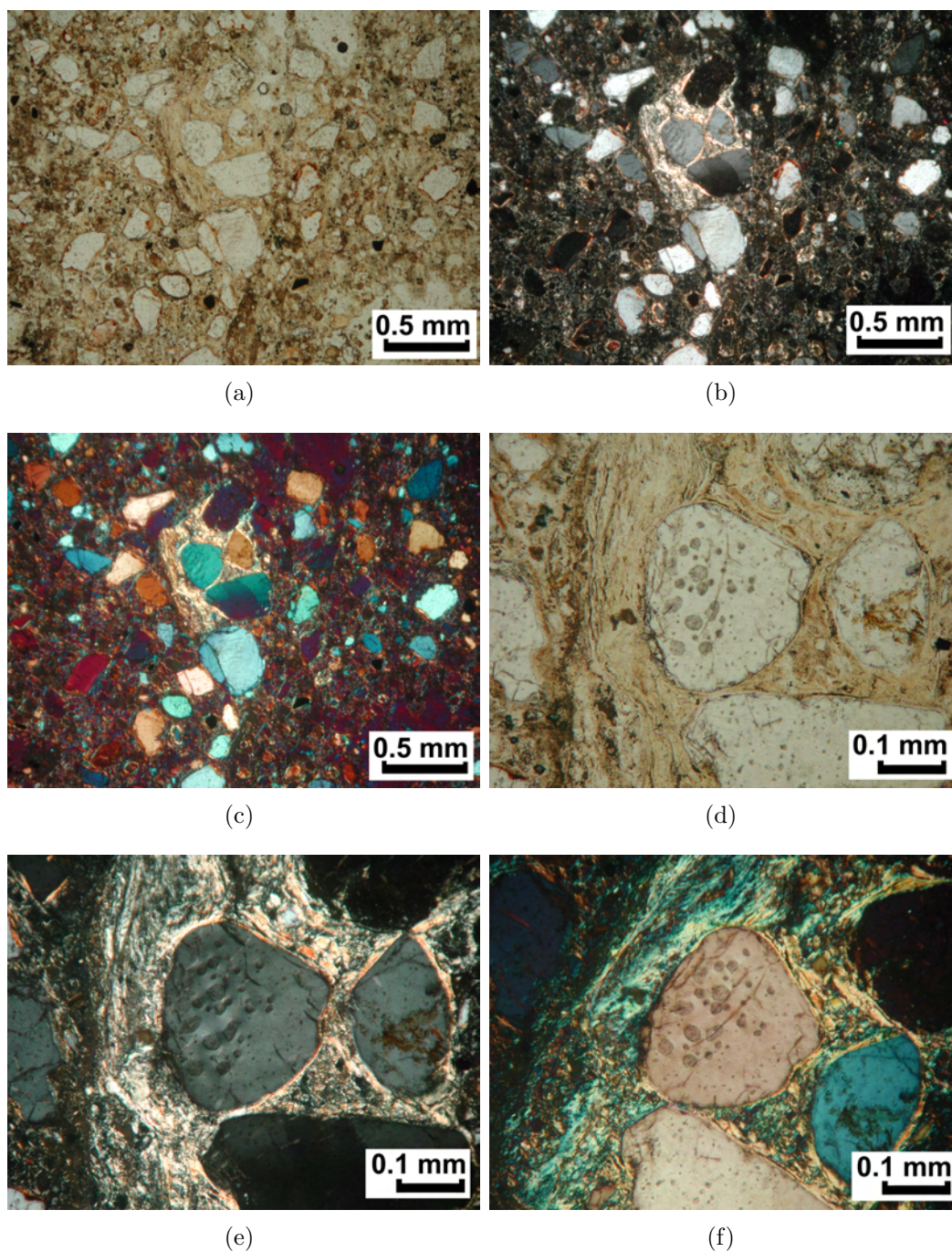


Figure 6.22: Continued - photomicrographs of non-calcareous 'sepiolitic' pedocutanic (argic) (2D), 7.5 m from centre of heuweltjie. Way-up is top of page. (a)–ppl, (b)–xpl, (c)– λ -plate, fast-direction NW-SE: Aggregate with sepiolite matrix. (d)–ppl, (e)–xpl, (f)– λ -plate, fast-direction NW-SE: magnification of fibrous sepiolite matrix showing fibre domains.

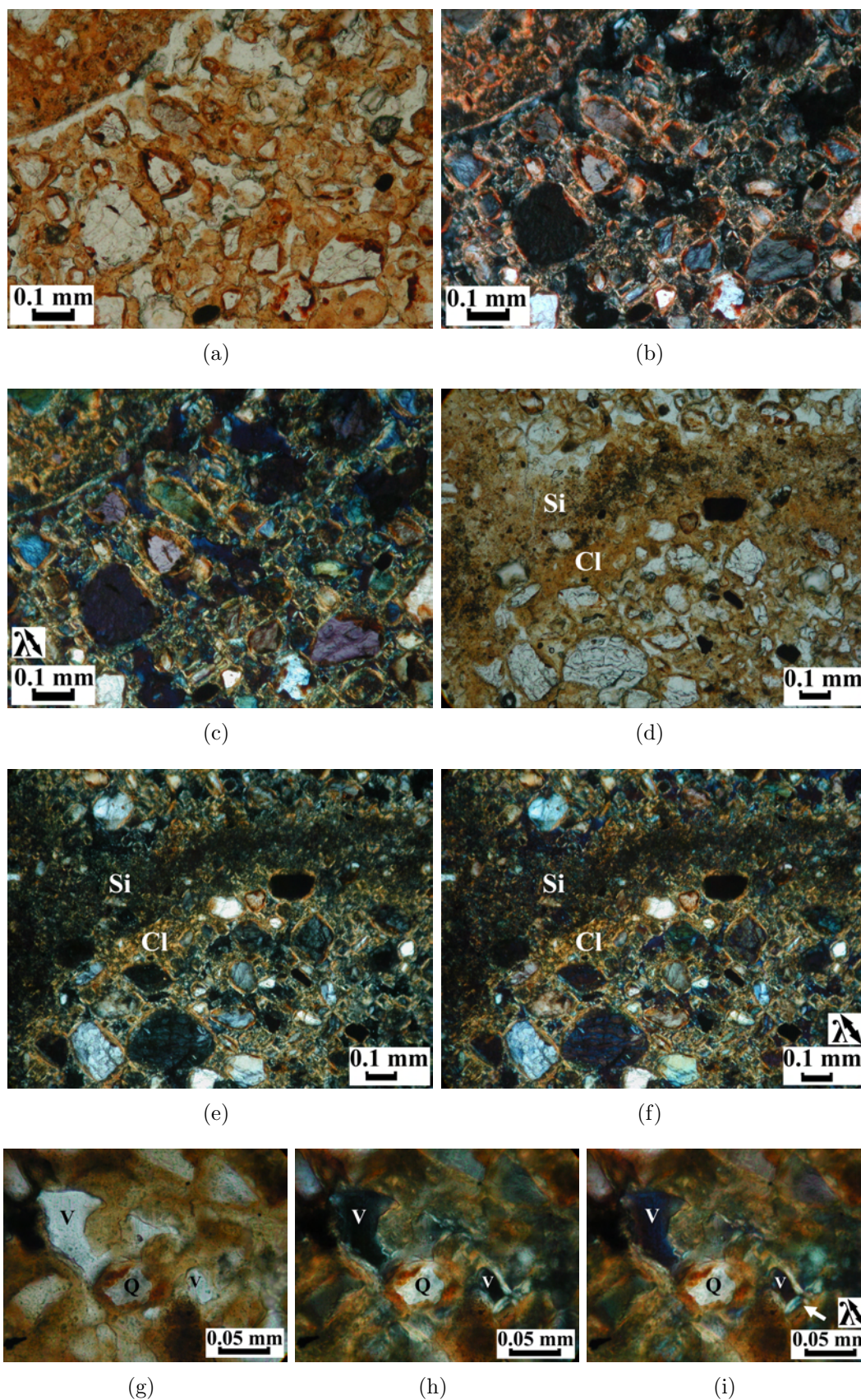


Figure 6.23: Photomicrographs of non-calcareous dorbank (petroduric, sample 1.3), 8 m from sample 2D. Way-up is top of page. (a)–ppl, (b)–xpl, (c)– λ -plate, fast-direction NW–SE: aggregate (top-left) in granostriated matrix of Fe-coated quartz grains cemented by limpid-orange silica mixed with clay and Fe. (d)–ppl, (e)–xpl, (f)– λ -plate, fast-direction NW–SE: silica-rich (Si) over clay-rich (Cl) capping on ped. Voids in ped contain silica. (g)–ppl, (h)–xpl, (i)– λ -plate, fast-direction NW–SE: Fe coating quartz grain (Q); silica (length-slow arrowed in (i)) lining voids (v).

Biological activity

Evidence of biological activity could only be found in the calcrete in the centre of the heuweltjie (samples 2A to 2C). Neither the ‘sepiolitic’ pedocutanic (argic; sample 2D) halfway to the edge, nor the dorbank (petroduric; sample 1.3) at the edge exhibited such evidence. This is consistent with observations that the centre of the heuweltjie is where the termite activity is concentrated. Tunnels and chambers were lined with organic matter (Figures 6.8(b) to (d); 6.18(c) to (d)). The dark ellipsoid (0.8×0.4 mm) just above the tunnel in Figures 6.18(c) to (d) and in the ped in Figures 6.17(e) to (f) appear to be termite excrement, based on the morphology of the termite excrement from the active heuweltjie in Stellenbosch (Figures 6.6 to 6.7). Smaller excrement particles in the form of 0.1 to 0.05 mm diameter calcareous spheres are also abundant: in one case within what appears to be termite excrement (Figures 6.8(c) to (d)); in calcified plant organ residue (Figures 6.17(a)); and in a tunnel (Figures 6.18(e) to (f)). Plant remains are present, some of which appear to be fresh (such as Figure 6.8(c) to (d)), some that seem to be needles that have been coated in clay (Figure 6.17(b) to (d)), and some (most commonly) that appear to have been calcified (Figures 6.17(a), 6.10(f) to (g)). Highly birefringent phytoliths such as that pictured in Figures 6.10(f) to (g) are composed of calcite and not calcium oxalate, since they dissolved completely in 2N acetic acid. Rectangular silica phytoliths (isotropic) are also present.

Horizon over calcrete in the heuweltjie centre

The horizon is non-calcareous and has very little clay (Figure 6.8(a)). Interped areas and some voids surrounding the peds have much less of the fine (50 to 100 μm) material. Some of the coarser (0.4 to 0.8 mm) material seems wedged in vertically elongated voids (planes, ped margins, channels). The bleached A horizon (Table 6.1) is also consistent with clay dispersion and leaching (Ellis, 1988; Francis et al., 2007). The lack of clay and presence of hematite coatings suggest a well-drained environment, and is consistent with its lower-pH and the tonguing nature of the transition to hardpan carbonate (petrocalcic) horizon below (Table 6.1).

Calcrete in the heuweltjie centre

The calcrete contains much fewer sand grains (10-20% vs 60% for the overlying orthic (ochric) A horizon), and virtually no void space (compare Figure 6.8(a) with Figure 6.15, for example). The calcite is mostly micrite, possibly a result of the high clay content of the matrix (Wieder and Yaalon, 1974, 1982, in Wright and Tucker 1991). Hay and Reeder (1978) also noted that porosity appeared to control the micrite distribution for ooids formed by replacement of clay coatings.

Calcic pendants and cappings (Figures 6.17(e) to (f), 6.18(a) to (d)) suggest remobilisation of calcite, consistent with the more acidic, well-drained overlying horizons and tonguing transition to the calcrete. This tonguing transition on the heuweltjie crest resembles the karstic processes that operated on the anticline crests in folded Miocene limestones in the Madrid Basin (Sanz, 1996, in Alonso-Zarza, 2003).

Calcareous ooids and peloids

The terms ‘peloid’ and ‘oid’ are applied descriptively to carbonate sedimentary rocks, usually marine limestones. They were not used in Stoops’ (2003) soil micromorphological description scheme; they are included instead in the concepts of ‘granular microstructure’ and micrite ‘(hypo)coatings’. Boggs (1995, p. 199) defined ‘oid’ as a general name for coated carbonate grains (0.02 to 2 mm in size) containing a nucleus (commonly a shell fragment, pellet or quartz grain) surrounded by thin coatings of fine calcite or aragonite. Most ooids display an internal structure consisting of concentric layers, but some show a radial structure.

Boggs (1995, p. 201) defined ‘peloid’ as a nongenetic term for carbonate grains composed of micro- or cryptocrystalline calcite/aragonite that do not display distinctive internal structures, which are generally smaller than ooids (0.03 to 0.1 mm). Peloids may be: 1) Fecal pellets, the most common kind of peloid, produced by organisms that ingest calcium carbonate muds and generally contain enough organic matter to make them appear dark or opaque. 2) Formed by the micritization of small ooids or rounded skeletal fragments, due to boring activities of certain organisms (boring algae) which convert the original grains into a nearly uniform homogeneous mass of micrite. 3) Very small, well rounded intraclasts formed by reworking of semiconsolidated mud or mud aggregates (Boggs, 1995).

Peloids and ooids are not restricted to limestones of marine origin. Wright and Tucker (1991) noted that these are a very common feature of many calcretes. Siesser (1973) referred to them as ‘diagenetic ooids/intraclasts’ to distinguish them from their marine counterparts, and noted that Quaternary calcretes contain the only known ooids/intraclasts in any South African Cretaceous or Cenozoic rocks. Ooids and peloids have also been recorded from pedogenic calcretes in northern Tanzania (Hay and Reeder, 1978); in the southwestern United States (Hay and Wiggins, 1980); Tarragona, northeastern Spain (Calvet and Julia, 1983); calcretes developed in the Old Red Sandstone of Scotland (Wright et al., 1993); the Kalahari valley (Nash and McLaren, 2003); and calcretes containing bee nests on the Eastern Canary islands (Alonso-Zarza and Silva, 2002).

The granular microstructure that is most strongly developed in the center of the heuweltjie (Table 6.2) comprises 0.3 to 0.03 mm diameter granules that resemble ‘peloids’, and abundant micrite-coated grains that resemble ‘ooids’ (for example, Figures 6.9, 6.10(a) to (e), 6.11). They were not observed in a calcrete described in Chapter 3, which is a ‘non-heuweltjie’ calcrete farther north on the Namaqualand coastal plain near Kleinzee. Pellets have been described in soils associated with termites by Stoops (1964) and Mermut et al. (1984).

The ooids in the Papendorp heuweltjie often have a core of limpid yellowish clay/silica with low birefringence, usually rimmed with a dark layer under the micrite (Figures 6.9(a) to (c); 6.10(d) to (e), 6.11; 6.16). Less common is a nucleus of Fe-coated quartz grains (top of Figures 6.8(c) to (d); bottom-right of Figures 6.8(e) to (f); bottom-left of Figures 6.9(d) to (f)). In some cases the core seems to be hollow (Figures 6.13(a), (c)). In most cases the coatings are composed of radially oriented acicular calcite, which also commonly forms thin coatings on much larger detrital grains (Figures 6.13(a), (b), (d), 6.19), similar in principle to the ‘pseudo-ooids’ of Hay and Reeder (1978). In many cases the radial acicular calcite is contained within concentric envelopes, to form successive layers of differently-oriented and/or oppositely-elongated calcite (Figures 6.10(a) to (e), 6.12(e) to (i)). Etching in HCl to remove a radial calcite coating on a detrital grain revealed a concentrically-oriented, length-slow coating that appears to be clay (Figures 6.19(d) to (i)).

According to Siesser (1973), the formation of diagenetically formed ooids and intraclasts in South African coastal calcretes takes place as rain water percolates

through an unlithified calcareous sand deposit, dissolving carbonate along its downward path. This carbonate-laden water is eventually checked in its descent and drawn upward somewhat by capillary action. Evaporation and soil suction in the uppermost zones of the sediment body cause precipitation of a concentric coating of carbonate mud around individual grains (incipient ooids) or composites of grains (incipient intraclasts). As this dissolution-precipitation cycle is repeated, the micritic coatings thicken and locally push grains apart.

Davies et al. (1978) found that ooids synthesised in quiet-water conditions had a radial orientation of carbonate crystals (as observed in the heuweltjie), whereas the ooids that formed in agitated conditions has a prevalently tangential orientation due to the grain collisions which inhibited any crystal growth other than tangential. The most important parameters in quiet-water ooid formation were high molecular weight organic components, the presence of Mg in addition to Ca, the presence of carboxylic groups (for example solutions containing humic acids), and a capacity to participate in hydrophobic/hydrophilic interactions. These parameters were critical to membrane formation, and it was the formation of the hydrophilic high molecular-weight membranes that was important in the formation of ooids. These membranes formed concentric shells which acted as growth surfaces for carbonate, and also induced periodicity in carbonate precipitation. There is much literature on the possible mechanisms involved in the formation of rounded calcite aggregates, spheres, spherulites and peloids, dealing particularly with the question of whether biotic or abiotic processes were the cause (for example, Tracy et al., 1998a; Tracy et al., 1998b; González-Muñoz et al., 2000; Raz et al., 2000; Braissant et al., 2003; Bosak et al., 2004; Fernández-Díaz et al., 2006). The mechanism proposed by Davies et al. (1978) for the formation of quiet-water ooids is the best explanation for the formation of ooids in the heuweltjie soils, in view of the number of parallels between the quiet-water ooid-forming processes described by Davies et al. (1978) and conditions in the calcrete of the Papendorp heuweltjie. The heuweltjie ooids are closely associated or cored with sepiolite (Figures 6.4, 6.12(e) to (f), 6.13(f)) with its strongly hydrophilic character (Alvarez, 1984), and its high Mg content. The induced periodicity in carbonate precipitation described by Davies et al. (1978) explains the successive acicular layers seen in the ooids, particularly the successive sepiolite (hydrophilic and therefore a precipitational substrate) and micrite/acicular calcite layers in the coatings (Figures 6.10(a) to (e), 6.12(g) to (i), 6.15 (arrowed), 6.16 (arrowed middle)).

Further support for the hydrophilic/hydrophobic membrane theory of Davies et al. (1978) is that the organic material in the Namaqualand soils impart a strongly hydrophobic character (Francis et al. (2007) and Chapter 2). In the Papendorp heuweltjie, it took longer for a drop of water to penetrate the sandy non-cemented A horizon than the cemented subsurface horizons (Table 6.1). The ooids in this heuweltjie are also closely associated with organic/biogenic material: fungal filaments (Figure 6.13(c)) and biogenic calcite (MA and MB rods of Verrecchia and Verrecchia (1994), Figure 6.13(e)). Alonso-Zarza and Silva (2002) noted organic material and organic films associated with ooids formed in calcrete containing bee nests in the Canary Islands. They concluded this favoured the precipitation of calcite and the adhesion of clays (mostly palygorskite).

Limpid nodules

Pseudo-negative uniaxial ‘spherulites’

Somewhat of an enigma are limpid yellow nodules 300 to 70 μm in diameter, with pseudo-negative uniaxial interference figures, usually with a dark round- or dumbbell-shaped core, and a dark rim between them and the matrix calcite (Figures 6.9(a) to (c), 6.11, 6.16). Canti (1997) defined spherulites as “crystal aggregations with an approximately circular outline and a permanent cross of extinction in crossed polarized light”. Although the samples do show a permanent uniaxial extinction cross under crossed-polars, they do not show the same neo-formed radial crystallitic texture that characterises calcite spherulites commonly observed on laminar calcretes (for example Verrecchia et al., 1995; Mees, 1999).

Canti (1998) acknowledged this problem while defining fecal spherulites: since true spherulitic crystallization consists essentially of constrained dendritic growth from the spherulite centre, all spherulites *sensu stricto* are radial. However, if that was taken as part of a definition, petrographers and micromorphologists would be unable to classify spherical bodies with an extinction cross because of the impossibility of determining the often microcrystalline layout purely morphologically. Canti (1998) therefore used the term “spherulite” to describe all objects displaying the basic extinction cross. The limpid yellow nodules with pseudo-negative uniaxial interference figures pictured in Figures 6.9(a) to (c), 6.11, 6.16 superficially resemble the fecal spherulites found in herbivore dung

(Canti, 1997; Canti, 1998) and in fresh termite frass (Figure 6.6, described in Section 6.3.3). They are similar in their pseudo-negative interference figures, dark core and lack of effervesce in cold 10% HCl, but differ in being considerably larger than the 5 to 15 μm calcite spherulites that commonly occur in herbivore dung (Canti, 1997). Seong-Joo and Golubic (1999) noted similar dumbbell-shaped, dark centres in 30 to 500 μm spherulites formed in silicified stromatolites (carbonates) in China, and noted (p. 194) that the texture is reminiscent of that produced by the process of diagenetic granularization or condensation of organic matter as discussed by Knoll et al. (1988). This is consistent with the termite activity which concentrates organic matter in heuweltjies. In addition, some process akin to the ‘granularization or condensation of organic matter’ may also occur in the termite gut, producing a dark core like those seen in the termite fecal spherulites (section 6.3.3 and Figure 6.6).

Possible Other Morphological Forms

The limpid yellow nodules with pseudo-negative uniaxial interference figures pictured in Figures 6.9(a) to (c), 6.11, 6.16 appear to be the same material that also forms (a) the limpid nodules with a cross-striated b-fabric and low first order interference colours (top, Figures 6.9(d) to (f), Figures 6.19(a) to (c)). This material also appears to form (b) unoriented coatings (interpreted as sepiolite in Figures 6.14, 6.15) juxtaposed with micrite. Sometimes it appears to form (c) oriented coatings around grains (Figures 6.10(h) to (j)), some of which seem to have formed in more than one stage (Figures 6.19(d) to (i), left).

Some of the nodules seem to have undergone ‘micritization’ which gives them a highly birefringent crystallitic b-fabric in the centre and which ESEM shows to be acicular calcite and micrite (Figures 6.9(d) to (f), 6.12, top-left of Figure 6.16).

It is unclear whether they are the same material as the ‘clay-quartz compound fragments’ in Table 6.2, which occur in the ‘sepiolitic’ pedocutanic (argic) sample 2D as well as the calcrete horizons 2A to 2C. The ‘clay-quartz compound fragments’ are somewhat darker in PPL but have a matrix that is strongly granostriated, and the granostriations are commonly oriented in a ‘pseudo-negative uniaxial’ pattern (Figures 6.8(e) to (g), 6.14, 6.17(b) to (d), 6.18(a) to (b)). In the ‘sepiolitic’ pedocutanic (argic) horizon (sample 2D) it appears to form the fibrous capping as well as the coatings (Figures 6.21, 6.22).

Composition

The nodules do not react with cold 10% HCl. After etching the thin section in HCl, most of the matrix micrite is removed, and the spherulites show much clearer pseudo-negative uniaxial interference figures (Figures 6.11, 6.19(d) to (i)). This suggests that while some may have been ‘micritized’, they are not primarily composed of calcite. Their low Ca, high Mg, and high Si contents (SEM-EDAX analysis such as in Figure 6.12) coupled with their low birefringence argue against them being composed of chalcedony or other carbonate minerals which have a tendency to form “true” spherulites (aragonite, dolomite and vaterite, for example). Also, in the Papendorp heuweltjie samples, the limpid yellow nodules are always pseudo-uniaxial negative under crossed-polars, whereas the calcite coatings are generally oriented pseudo-positive (Figures 6.9(a) to (c), top-left; compare to the pseudo-negative limpid nodule coated by a pseudo-positive micrite coating on the right), but Figures 6.10(d) to (e) show the variability.

In addition to the 1.2 nm sepiolite peak in the calcrete samples 2A to 2C, they and the silica-cemented dorbank sample 1.3 all show a broad rise in the background at around 0.4 nm (Figure 6.4), consistent with amorphous silica (Drees et al., 1989). However, the fibrous nature (particularly Figure 6.12(f) and its accompanying EDAX analyses) suggests that they are composed of sepiolite rather than (amorphous) silica. The EDAX analyses in Figure 6.12(d) and 6.12(f) have molar Mg/Si ratios of 0.64 to 0.68, consistent with the molar Mg/Si of 0.667 for sepiolite (Stoessell, 1988). Also, where orientation can be discerned it seems to be concentric rather than radial (Figure 6.11), suggesting it is a length-slow mineral like sepiolite (Phillips and Griffen, 1981). Summerfield (1983b, Plate 3.1(h)) noted that length-fast chalcedony occurs predominantly as spherulites with pseudo-uniaxial extinction crosses in southern African silcretes. Summerfield (1983a), however, noted that length-slow chalcedony formed in the presence of Mg^{2+} and SO_4^{4-} by replacement (rather than void-fill) in carbonate and evaporite host materials. ‘Spherulites’ with pseudo-negative uniaxial interference figures were also present in a dorbank horizon overlying a ‘sepiocrete’ (‘petrosepiolitic’) horizon in the Knersvlakte (Chapter 1, Figure 1.9).

Although the low birefringence of the nodules is consistent with the other evidence for sepiolite rather than (amorphous) silica, silica (opal-CT) has been reported to show weak anisotropy in soils. In Figure 6.23(h), for example, the

anisotropic void coating was interpreted as silica. Broadly similar pedofeatures (although in a massive rather than oriented form) were noted in Sardinia, Italy in >2.7 Ma buried paleosols (Usai and Dalrymple, 2003). They suggested that the “milky pedofeatures” as they were termed, were made of different phases of silica such as inorganic opal-A, opal-C and opal-CT, but mainly composed of opal-C. They noted that slight and local birefringence in colourless white-milky pedofeatures had been previously described for opal-CT by Drees et al. (1989). Although silica was the main constituent of the “milky pedofeatures” (reaching 67% of the total weight), the remaining constituents were around 25% Al_2O_3 , 5% MgO, 2 to 4.6% Fe_2O_3 and 2% CaO, which they attributed either to impurities chemisorbed to silica (Drees et al., 1989) or to analytical inaccuracy. Gutiérrez-Castorena et al. (2006) described weak anisotropy in opaline coatings on channels and fissures in the strongly alkaline sediments of the former Texcoco Lake (Mexico City). They suggested that the weak anisotropism could be related to an initial crystallisation of the opal-A to opal-CT (anisotropic domains), or to the presence of fine clay particles oriented according to the flow direction of the colloids (parallel anisotropic streaks).

A possible explanation for these limpid nodules may be a process similar to the pseudomorphic replacement of sepiolite by opal in deposits in the Madrid Basin, Spain (Bustillo and Bustillo, 2000; Bustillo and Alonso-Zarza, 2007). The Madrid Basin typically consists of carbonates, high magnesium clays and opaline cherts. Bustillo and Alonso-Zarza (2007) suggested that the preferential silicification of the sepiolite deposits is due to the fibrous structure and high absorption capacity of sepiolite, which helped to retain interstitial fluids, and the fact that sepiolite and opal are stable under relatively similar geochemical conditions. Bustillo and Alonso-Zarza (2007) proposed that the replacement of sepiolite by opal took place via an initial silicification, which resulted in an atypical, porous opal. In thin section this showed striated birefringence, as a consequence of the sepiolite fibrous structure. When the silicification progressed the fibres became joined and cemented together to form blades, resulting in a compact structure in which the inherited striated birefringence could still be observed. In a later phase, compact and isotropic opal may have formed due to the loss of the inherited sepiolite structure. In some cases, noted Bustillo and Alonso-Zarza (2007), it is difficult to distinguish Mg clay fibres from their imprints on the opal.

‘Sepiolitic’ pedocutanic (argic) midway to edge of heuweltjie (sample 2D)

The clay mineralogy of non-calcareous (Table 6.1) sample 2D is somewhat of an enigma (see discussion in Section 6.3.2). It appears that the cutans are sepiolite, and the matrix is dominated by a 1.4 to 1.5 nm non-expanding mineral. The micromorphology is consistent with this interpretation: the quartz grains coated by strongly oriented clay with low first-order interference colours which appears to be illuvial in origin. This clay is distinct from the interwoven fibre domains of the clay forming cappings and the matrix of nodules (Figure 6.20 to 6.22).

The origin of fibrous coating on the side of the clay nodule in 2D (Figure 6.21) is unclear. It may be part of a crust that has been buried by bioturbation, since the clay aggregate fragment to which it is attached seems discordant with the surrounding material, or it may be a sepiolite cutan, many of which are evident in the field (Figure 6.2). In Figure 6.22 it appears to form the matrix of a nodule that is discordant with the rest of the matrix. The interwoven, length-slow fibres with low birefringence occur in domains similar to those described by Stahr et al. (2000) for a palygorskite-cemented hardpan in Portugal. While the illuviation of clay in the matrix is indicated by the strongly oriented grain coatings, the interwoven nature of most of the sepiolite occurrences suggest that the sepiolite is neoformed. Singer and Norrish (1974) noted neoformed palygorskite cutans in otherwise palygorskite-free soils in Australia. Sample 2D was therefore classified as a ‘sepiolitic’ (Chapter 1) pedocutanic (Soil Classification Working Group, 1991) or argic (WRB, 1998) horizon.

Sample 2D differs from the calcrete samples 2A to 2C only by its lack of calcification. It contains the same quartz-clay aggregates, the same clay coatings oriented so strongly that it gives the appearance of a pseudo-negative interference figure, and the same limp yellow clay nodules, some of which show pseudo-negative uniaxial interference figures. There are no signs of calcite leaching (pendants) in 2D. This suggests that the calcrete horizons 2A to 2C formed via the calcification of a pedocutanic (argic) horizon similar to 2D.

Dorbank (petroduric) at heuweltjie edge; sample 1.3

This dorbank is similar to others in southern Africa (see, for example, Chapter 1). There is a strong grano-, poro- and circular striated pattern to the matrix (Figures 6.23(a) to (c)), suggesting the illuviation of clay and silica has been a prominent process in the horizons formation.

The quartz grains are coated with hematite, as in the overlying neocutanic (cambic) B horizon, the calcrete and the sepiolitic pedocutanic (argic) horizons of the heuweltjie. The matrix does not show the same red colour, and appears to be composed of amorphous Fe (hydr)oxides mixed with amorphous silica and clay. The clay- and/or Fe-enriched coatings appear to have formed before the silica coatings: in one instance, the silica is concentrated on the outside of clay capping a ped (Figures 6.23(d) to (f)), and also silica is generally (but not exclusively) concentrated on the void side of the clay coatings (Figures 6.23(g) to (i)), similar to that described by Litchfield and Mabbutt (1962) for red-brown hardpans in Western Australia. These observations are consistent with Summerfield (1983b, p. 80), who noted that slow movement of silica-saturated pore waters is required for the shift towards supersaturation and subsequent precipitation to take place, and that silica will only precipitate where the presence of other constituents does not favour the formation of other silicates. This may explain the location of the silica on the outer (void) sides of the clay and Fe-oxides (Figures 6.23(d) to (i)).

The aggregate in the top-left corner of Figures 6.23(a) to (c) contains silica nodules but their orientation is obscured by Fe. In one case the silica coating a void was discerned to be length-slow (Figure 6.23(i)). Neither limpid clay nodules nor 'spherulites' seem to be present, unlike the calcrete samples 2A to 2C and 'sepiolitic' pedocutanic (argic) sample 2D. This horizon seems to be formed by silicification of an horizon similar to the overlying neocutanic (cambic) B horizon, similar to Figure 6.8(a).

While the calcrete horizons 2A to 2C appear to have formed via the calcification of a pedocutanic (argic) horizon similar to 2D, the dorbank at the edge of the heuweltjie does not. It does not contain the 'clay-quartz compound fragments' which occur in both the calcrete and the 'sepiolitic' pedocutanic (argic) 2D, and has a closer resemblance to the overlying neocutanic (cambic) horizon than the pedocutanic (argic) horizon in which the calcrete formed.

6.3.5 Heuweltjie formation

Organic matter as a source of ions for calcrete formation

The calcrete occurs only in the centre of the heuweltjie mounds, a feature which is common in many heuweltjie landscapes such as the Worcester-Robertson area. The concentration of calcite in termite mounds in otherwise calcite-free soils has been noted before: Watson (1962), for example, noted calcareous soil below a non-active termite mound in otherwise calcite-free ferrallitic soils in what is now Zimbabwe. Monger and Gallegos (2000, p. 278 to 280) suggested that termites could be mining carbonate from depth, obtaining the calcite from the plants they consumed, and/or biomineralising calcite internally. Ellis (2002) proposed that the petrocalcic horizon at the centre of the mound formed as the concentration of plant material by termite activity led to the build-up of bases (especially Ca) and silica in the heuweltjies over time. This is consistent with the nutrient cycling into heuweltjie soils noted by authors such as Midgley and Hoffman (1991) and Midgley and Musil (1990). The heuweltjie at Papendorp shows abundant micromorphological evidence of the accumulation of organic matter (plant remains and calcite phytoliths, tunnels lined with organic matter, see Section 6.3.4) that is associated only with the calcrete in the centre of the heuweltjie (samples 2A to 2C). Evidence of organic matter accumulation is absent from both ‘sepiolitic’ pedocutanic (argic) sample 2D and dorbank sample 1.3 on the periphery. The presence of many calcite phytoliths (which dissolved completely in 2N acetic acid) in the calcrete further argues for the plant matter–calcite association.

Data from Midgley and Musil (1990) showed that foliar Ca for plants associated with heuweltjies in the Worcester-Robertson valley ranges from 853.29 mmol/kg (3.42%) for on-mound *Ruschia caroli* to 256.48 mmol/kg (1.03%) for off-mound *Euphorbia burmannii*. This is higher than the 0.67 to 1.14% foliar Ca and 0.83 to 1.36% stem Ca in *Brunia albiflora* found by Poole (1999) in the Western Cape coastal zone (Rooi Els, Kleinmond, Grabouw). It is even twice that of *Cornus florida*, the calcium “pump” known for its high foliar Ca levels, which has 1.73% foliar Ca (data from Jenkins et al., 2007; published in Holzmueller et al., 2007).

This calcite mineralisation in the centre of heuweltjies in an otherwise non-calcareous landscape bears some resemblance to the calcite mineralisation in Iroko trees (*Milicia excelsa*) and surrounding soil in the Ivory Coast and Cameroon

(Braissant et al., 2004; Cailleau et al., 2005, and references therein). These trees contain significant calcium carbonate accumulations within their tissues and are associated with calcium carbonate in their surrounding soils, even though they grow on non-calcareous orthox soils which normally have a pH of 4.3 to 6.0. Braissant et al. (2004) and Cailleau et al. (2005) showed that the calcium carbonate mineralisation in the trees and their surrounding soils is caused by soil bacteria, which oxidise the Ca oxalate that is present in the living tissues of *M. excelsa*, the wood-rot fungi, decaying wood and their surrounding soils.

Braissant et al. (2002) studied the growth of bacteria in a medium containing potassium oxalate. They used *Ralstonia eutropha* (syn: *Alcaligenes eutrophus*) and *Xanthobacter autotrophicus*, which are ubiquitous and most easily found in oxalate-rich litters such as those associated with *Oxalis*, *Rumex*, *Rheum* and *Eucalyptus* (Braissant et al., 2002). Much of the plant material available to the foraging termites in Namaqualand is enriched in oxalate (A. Milewski, pers. comm., 2007), for example ‘vygies’ (*Mesembryanthemum* spp.), *Oxalis* spp and *Rumex* spp (VetPath Veterinary Pathologists, 2004). Braissant et al. (2002) found that the growth of *R. eutropha* and *X. autotrophicus* showed a rapid consumption of oxalate associated with a continuous increase in pH. The final pH after 7 days of incubation was >9.5 , from an initial pH of 7, and consistent with the theoretical pH of 9.55 ± 0.05 after total oxalate consumption (Braissant et al., 2002).

Castanier et al. (1999, p. 20) noted that “carbonate precipitation always appears to be the response of heterotrophic bacterial communities to enrichment of the environment in organic matter”. Given the high nitrogen content as a result of the accumulation of organic matter by termites and its subsequent degradation (Midgley and Musil, 1990), the passive carbonatogenesis induced by several metabolic pathways of the nitrogen cycle described by Castanier et al. (1999) may also be relevant to calcite genesis within the heuweltjie. These induce production of carbonate and bicarbonate ions, and as a metabolic end-product, ammonia, which induces pH increase (Castanier et al., 1999).

Source of ions for sepiolite/palygorskite formation

Chapter 5 showed that most of the measured Mg and Si levels on the Namaqualand coastal plain were sufficient for sepiolite saturation given an appropriate environmental pH, and concluded that sepiolite precipitation is more likely to be triggered when a solution encounters a pH barrier (such as a calcic horizon) than by the concentration of ions by evaporation. This suggests that after the calcite has precipitated in the centre of the heuweltjie, it buffers the pH sufficiently high allowing for the precipitation of sepiolite.

In addition to the coastal proximity of the Papendorp heuweltjie causing high soil Mg levels (Chapter 5), data from Midgley and Musil (1990) showed that foliar Mg is high in plants associated with heuweltjies in the Worcester-Robertson valley: the foliar Mg ranges from 888.52 mmol/kg (2.16%) for on-mound *Ruschia caroli* to 259.98 mmol/kg (0.63%) for off-mound *Euphorbia burmannii*. It seems likely therefore that termite concentration of plant material, in addition to raising the Ca-levels, also raises the Mg levels to allow for sepiolite (and palygorskite) precipitation within heuweltjies.

Leaching and redistribution of ions within the heuweltjie: zoning of sepiolite and dorbank (petroduric)

Ellis (2002) observed that in areas of lower rainfall, CaCO_3 is leached to a shallow depth to form the (petro)calcic horizon at the centre of heuweltjie mounds where termite activities have ceased. Pendants in the calcrete sample 2C confirm the remobilisation of calcite within the calcrete horizon (see section 6.3.4). Spackman and Munn (1984) used differential leaching to explain why the upper parts of a profile in a mima-like mound in Wyoming contained more Ca^{2+} , and the lower parts more Mg^{2+} and Na^+ .

The gradual zoning outward from sepiolitic-calcite in the centre through (petro)-sepiolitic to silica-cement at the edges of heuweltjies (Figure 6.24) is very similar to the calcite-palygorskite sequence developed in an alluvial fan sequence in Spain (Rodas et al., 1994). Rodas et al. (1994) observed calcretes (with palygorskite in the clay fraction) in the proximal part of the alluvial fan, and non-calcareous 'palycrete' where palygorskite formed the cementing agent in the distal parts. Silicification was associated with both calcrete and 'palycrete' in the alluvial fan

sediments, but was interpreted by Rodas et al. (1994) to be superimposed on previous duricrust levels.

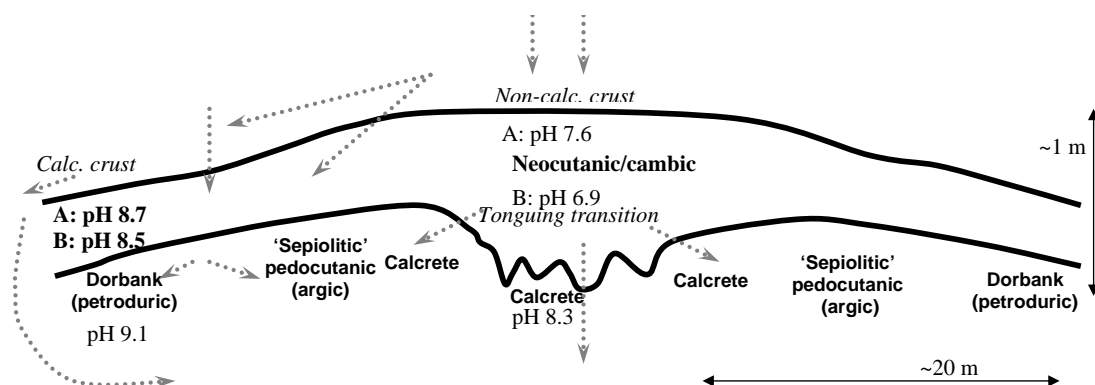


Figure 6.24: Distribution of minerals and inferred water movement (dashed arrows) through the Papendorp heuweltjie. See text for explanation. Calc.- calcareous. Modified from (Ellis, 2002).

In heuweltjies, Ellis (2002) noted that the highest silica mobility occurred in the well-drained cambic and calcic horizons, and that calcic horizons, with their higher pH, had the highest water-soluble silica concentration. Ellis (2002) suggested that because the calcic horizon usually occurs near the centre of the heuweltjie, this is likely to be the zone where most of the silica, together with that in the cambic horizon, is generated after a rain event. The silica then moves vertically and horizontally (Figure 6.24) to the depth where the petroduric horizon is located (Ellis, 2002). The position of the silica-cemented horizons on the edge of the heuweltjie is consistent with Ellis and Lambrechts's (1994) observations that the extensive dorbank horizons in southern Africa usually occur on level to slightly sloping land, and mainly on footslopes.

Rodas et al. (1994) suggested that the calcretes (with palygorskite in the clay fraction) in the proximal part of the alluvial fan, and non-calcareous 'palycrete' formed during the movement of alkaline phreatic waters through the fan, as the precipitation of calcite in the proximal part of the fan shifted the composition of the water to a lower Ca/Mg-ratio and lower CO_3^{2-} in the distal parts. This is similar in principle to the effect mineral precipitation has on the evolving composition of an evaporating brine (for example Hardie and Eugster, 1970; Eugster and Hardie, 1978; Eugster and Jones, 1979). Chapter 5 concluded that the pre-

precipitation of calcite and sepiolite on the Namaqualand coastal plain resulted in increasing Ca and Mg and decreasing HCO_3^- trends with evaporation, due to the initial $\text{Mg}^{2+} > \text{HCO}_3^-$ and $\text{Ca}^{2+} > \text{HCO}_3^-$ ratios according to the Hardie-Eugster scheme. The movement of the Mg-Si enriched water downslope, coupled with the decrease in HCO_3^- and increase in Mg^{2+} due to sepiolite precipitation, allows for the precipitation of the ‘sepiolitic’ zone on the outer side of the calcrete.

The presence of Fe, Al and Mg in silica-rich solutions reduces the solubility of silica, but it tends to cause clay authigenesis or the formation of other silicates rather than the precipitation of pure silica (Summerfield, 1983b, p. 79). This is consistent with conditions within the heuweltjie, where the enrichment of cations such as Ca and Mg in the heuweltjie centre caused by termite foraging results in calcite and clay authigenesis near the centre, leaving the precipitation of silica to occur on the periphery.

6.4 Conclusions

Biological activity was only evident in the calcrete in the centre of the heuweltjie (samples 2A to 2C), and neither in the ‘sepiolitic’ pedocutanic (argic; sample 2D) halfway to the edge, nor the dorbank (petroduric; sample 1.3) at the edge. This is consistent observations that the centre of the heuweltjie is where the termite activity is concentrated.

The pedogenesis of the hardpans in the heuweltjie is proposed to be as follows: enrichment of cations such as Ca and Mg in the heuweltjie centre caused by termite foraging results in calcite and clay authigenesis in the centre of the heuweltjie, leaving the precipitation of silica to occur on the periphery. The decaying organic matter concentrated in the centre of the mound by the termites is sufficient to supply the components for calcite precipitation in the centre of the heuweltjie. Following calcite precipitation, the pH is suitable for sepiolite precipitation. The movement of the Mg-Si enriched water downslope, coupled with the predicted decrease in HCO_3^- and increase in Mg^{2+} due to sepiolite precipitation, allows for the precipitation of the ‘sepiolitic’ zone on the outer side of the calcrete, and extend beyond the calcrete in some heuweltjies.

Further work to confirm the extent to which the (a) passive bacterial precipitation

of calcium carbonate in the nitrogen cycle and (b) the bacterial decomposition of plant oxalates are likely to contribute to the formation of calcic horizons in the heuweltjie. Oxalates are particularly common in Namaqualand plant species and so this avenue of research may be a fundamental link in the organic matter-calcite relationship in heuweltjies.

General summary of findings and recommendations for further work

Although some 'sepiocrete' horizons superficially resemble silica-cemented horizons in their hardness, they are different to both dorbank/duripan/petroduric and silcrete horizons. The 'sepiocrete' horizons do not meet the slaking requirements of dorbank/duripan/petroduric horizons. They contain less total SiO₂ than either a typical dorbank, or a 'silcrete'. Sepiolite appears to form the matrix areas, whereas the silica is localised. The interlocking, subparallel morphology of sepiolite may contribute to the induration, although the degree to which silica and sepiolite dominate seems to vary even within the same horizon. It seems most probable that both sepiolite and silica contribute to the structural properties of the horizon. The timing and precise mechanism of silica precipitation in the 'sepiocrete' is difficult to resolve. It seems unlikely that silica precipitation was caused by the initial precipitation of sepiolite depleting the solution in Mg, since XRF analysis of the clay fractions showed Mg is present in excess of the amount of silica required to form sepiolite. This is consistent with other data from the Namaqualand coastal plain that show Mg levels to be high, possibly as a result of the marine influence. Etched quartz grains in both 'sepiocrete' profiles suggests the localised dissolution and redistribution of silica. Evidence of calcite mobilisation indicates a complex evolutionary history. It could be that the 'sepiocrete' resulted from the (partial) silicification of what was originally a sepiolite-rich calcic/petrocalcic horizon, but the horizon no longer contains enough calcite to be classified as a petrocalcic.

While the '-crete' terminology provides a useful expression of the cemented nature of the horizon, to fit the existing soil classification schemes the terms 'sepiolitic' and 'petrosepiolitic' (in the same sense as 'calcic' and 'petrocalcic') would be more appropriate. The terms 'sepiolitic' and 'petrosepiolitic' have the advantage over the '-crete' terminology that they can be more easily be applied as adjectives to other hardpans where sepiolite is significant but not necessarily cementing, such as 'sepiolitic petrocalcic'. This is particularly relevant since sepiolite is closely associated with calcite in Namaqualand soils, and is a common mineral in the clay fraction of calcretes.

The term 'sepiolitic' is appropriate for horizons which contain sepiolite in amounts great enough for it to be detected by XRD in the bulk soil, peds (a fractured surface and not just the cutan) cling strongly to the wetted tongue, and methyl orange turns from orange to purple-pink over most of a fragmented surface. If the horizon is in addition to the above criteria cemented to such a degree that it will slake neither in acid (so cannot be classified as petrocalcic) nor in alkali (and so cannot be classified as petroduric) then the term 'petrosepiolitic' would be appropriate. The 'sepiolitic' criteria distinguish the 'petrosepiolitic' horizon from a 'silcrete', a silica-cemented horizon which does not fit slaking requirements of a petroduric horizon.

Sepiolite has a high water holding capacity. Its high plasticity affects the geotechnical usefulness of the soil, but many effects of large quantities of sepiolite in a soil still need to be quantified. The high water-holding capacity would directly affect the water-availability to plants growing in sepiolite-rich soils, which in turn affects the ecosystem of arid regions. It also indirectly causes a decrease in the rate of the carbonation process in lime mortars, as a decrease in the free water content in the porous system of the mortar impedes CO_2 dissolution, which is a rate-controlling step of the carbonation process. This effect on soils may be similar to the effect of evapotranspiration and CO_2 loss on calcite precipitation. The usefulness of a soil survey, therefore, would be increased by indicating the presence of large quantities of sepiolite in a soil using the terms 'sepiolitic' or 'petrosepiolitic'. When sepiolite is present in sufficient quantity, the bulk soil adheres to the wetted tongue, and methyl orange turns from orange to purple-pink. In combination, the field tests can be quite diagnostic, and only a few samples need to be verified by XRD.

Although the volume of literature on calcrete is now very large, there is very little detailed information on the Namaqualand coastal plain calcretes. Their examination formed only a part of the larger Namaqualand soils investigation, and so there is still a lot of detail that is unresolved. This includes the micromorphological aspects of sepiolite/palygorskite occurrences in calcrete, particularly their relationship to other clay minerals, calcite, and biogenic features; as well as a full comparison to "heuweltjie calcrete". This study has, however, resolved two main points: i) Deformation (pseudo-anticlines) in the calcrete appear to result primarily from the displacive effect of calcite crystallization. Although evidence of shrink/swell behaviour is present, this does not appear to be as volumetrically significant as displacive calcite. Clay minerals are closely associated with the displacing calcite, suggesting that clay neof ormation/illuviation may contribute to displacement and folding, but calcite crystallization seems to be mainly responsible for opening fractures. ii) Both biotic and abiotic factors contributed to calcrete formation. Abiotic alpha-fabric seems dominant in mature calcrete horizons, whereas biogenic beta-fabric is dominant in calcareous nodules in a calcic B horizon above calcrete.

This study confirmed the prominence of pedogenic sepiolite in the clay fraction of calcareous coastal plain soils. The $<0.08 \mu\text{m}$ fraction was the only size fraction where palygorskite could be detected before acetate treatment. There was no conclusive evidence for or against the presence of kerolite in the clay fraction. There was no TEM evidence of fibrous mineral degradation to sheet silicates, nor for the evolution of mica laterally to a fibrous mineral. SEM analyses show that much of the sepiolite/palygorskite occurred as fringed sheets, but higher magnification often revealed these sheets to be composed of fibres. These are found coating (rather than evolving from) mica/illite particles, as free-standing mats, and were common on the grain-side of cutans. One TEM image revealed what appeared to be acicular crystals developing from an amorphous phase, although well crystalline sepiolite was also present. The abundance of sepiolite in the calcic soils of the coastal plain (in some horizons it comprises nearly 100% of the clay fraction) makes it ideal for further work on the formation of sepiolite.

The sepiolite and calcite saturation indices are only dependent on pH, for the Mg, Si and pH ranges that were encountered on the Namaqualand coastal plain. In contrast, amorphous silica remained saturated regardless of the pH or concentration. Sepiolite precipitation is therefore more likely to be triggered when

a solution encounters a pH barrier than by the concentration of ions by evaporation. Evidence of the pH control on sepiolite saturation is that sepiolite is commonly associated with calcareous horizons. The effect of a pH change on the solubility of sepiolite is even greater than its effect on calcite solubility. Since sepiolite is often a significant part of arid region soils where calcite and amorphous silica are common, the mineral solubility-pH relationships may assist in explaining the relationships between calcic, sepiolitic and duric soils and their intergrades.

The marine-influenced high Mg coupled with the Hardie-Eugster model of brine evolution provides an explanation for sepiolite-dominance at the coast, and palygorskite-dominance inland. Coastal areas, unlike continental areas, have $Mg > HCO_3^-$ initially, which results in an increasing Mg trend with evaporation during the precipitation of sepiolite according to the Hardie-Eugster scheme. The result is that after sepiolite precipitation is initiated by an geochemical pH barrier, Mg levels will rise causing the increasing (Mg+Si)/Al ratio to continue to favour sepiolite precipitation. This suggests that once sepiolite has begun to precipitate, the subsequent salinity, with its accompanying Mg increase, makes substantial palygorskite formation unlikely to follow. Most of the soils for which there was a positive sepiolite identification showed a positive sepiolite saturation index, suggesting that the saturated paste extracts were in equilibrium with sepiolite. This is a direct contrast to previous findings for Namaqualand, and previously published interpretations relating to the alteration/disintegration of sepiolite and palygorskite therefore require revision. The data from the present study showing sepiolite equilibrium in sepiolitic soils suggest that sepiolite can be considered a 'precipitating mineral', and so forming in the present day.

This study developed a model for the formation of the calcrete, '(petro)sepiolitic', and petroduric horizons of heuweltjies. Enrichment of cations such as Ca and Mg in the heuweltjie centre caused by termite foraging results in calcite and sepiolite authigenesis. The decaying organic matter concentrated in the centre of the mound by the termites is sufficient to supply the components for calcite precipitation in the centre of the heuweltjie. Following calcite precipitation, the pH is suitable for sepiolite precipitation. The movement of the Mg-Si enriched water downslope, coupled with the decrease in HCO_3^- and increase in Mg^{2+} due to sepiolite precipitation, allows for the precipitation of the 'sepiolitic' zone on the outer side of the calcrete and extend beyond the calcrete in some heuweltjies,

leaving the precipitation of silica to occur on the periphery. The following mechanisms are likely to contribute to the formation of calcic horizons in the heuweltjie but are as yet untested: passive bacterial precipitation of calcium carbonate in the nitrogen cycle; and the bacterial decomposition of plant oxalates. Oxalates are particularly common in Namaqualand plant species and so this avenue of research may be a fundamental link in the organic matter-calcite relationship in heuweltjies.

The Namaqualand coastal plain is well positioned for further work on its regolith, particularly because of the mining excavations which provide excellent exposures of well-defined layers of the regolith down to bedrock. Some of the features which deserve further study are regular calcrete layers and fossils (marine, terrestrial) which have the potential for dating; the abundance of pedogenic carbonates lend themselves to techniques that could reveal whether they played a role in atmospheric CO₂ sequestration; evidence of deep/relict termite activity; dunefields overlying buried and truncated soils such as the Last Glacial dunefield north of the Swartlintjies. Soil formation and termite activity is at least as old as the Last Interglacial, and the identification and classification of the paleosols in greater detail may reveal subtleties in past soil forming factors and possibly offer some constraints on the climatic conditions under which they formed. E horizons may have formed in a wetter Last Interglacial paleoclimate, but they are still active in the present day.

References

- Akbulut, A. and Kadir, S. (2003). The geology and origin of sepiolite, palygorskite and saponite in Neogene lacustrine sediments of the Serinhisar-Acipayam Basin, Denizli, SW Turkey, *Clays and Clay Minerals* **51** (3): 279–292.
- Alexander, E. B. (1985). Estimating relative ages from iron-oxide/total-iron ratios of soils in the western PO Valley, Italy - A discussion, *Geoderma* **35**: 257–259.
- Allen, B. L. (1985). Micromorphology of Aridisols, in L. A. Douglas and M. L. Thompson (eds), *Soil Micromorphology and Soil Classification*, Soil Science Society of America, Madison, Wisconsin, pp. 197–216.
- Alonso-Zarza, A. M. (2003). Palaeoenvironmental significance of palustrine carbonates and calcretes in the geological record, *Earth-Science Reviews* **60**: 261–298.
- Alonso-Zarza, A. M. and Silva, P. G. (2002). Quaternary laminar calcretes with bee nests: evidences of small-scale climatic fluctuations, Eastern Canary Islands, Spain, *Palaeogeography, Palaeoclimatology, Palaeoecology* **178**: 119–135.
- Alvarez, A. (1984). Sepiolite: properties and uses, in A. Singer and E. Galan (eds), *Palygorskite-Sepiolite: Occurrences, Genesis and Uses*, Developments in Sedimentology 37, Elsevier Science Publishers, Amsterdam, pp. 253–287.
- Arduino, E. (1985). Estimating relative ages from iron-oxide/total-iron ratios of soils in the western PO Valley, Italy - A reply, *Geoderma* **35**: 257–259.
- Bain, J. A. (1971). Atterberg limits of clay, *Clay Minerals* **9**: 1–17.

- Banks, D., Parnachev, V. P., Frengstad, B., Holden, W., Karnachuk, O. V. and Vedernikov, A. A. (2004). The evolution of alkaline, saline ground- and surface waters in the southern Siberian steppes, *Applied Geochemistry* **19**: 1905–1926.
- Bigham, J. M., Jaynes, W. F. and Allen, B. L. (1980). Pedogenic degradation of sepiolite and palygorskite on the Texas High Plains, *Soil Science Society of America Journal* **44**: 159–167.
- Blank, R. R. and Fosberg, M. A. (1991). Duripans of the Owyhee Plateau Region of Idaho: genesis of opal and sepiolite, *Soil Science* **152**: 116–133.
- Blood, J. R. (2006). *Monitoring rehabilitation success on Namakwa Sands heavy minerals mining operation, Namaqualand, South Africa*, Master's thesis, University of Stellenbosch.
- Bockheim, J. G. (2005). Soil endemism and its relation to soil formation theory, *Geoderma* **129**: 109–124.
- Bockheim, J. G., Kelsey, H. M. and Marshall III, J. G. (1992). Soil development, relative dating, and correlation of Late Quaternary marine terraces in southwestern Oregon, *Quaternary Research* **37**: 60–74.
- Boettinger, J. L. and Southard, R. J. (1991). Silica and carbonate sources for Aridisols on a granitic pediment, western Mojave Desert, *Soil Science Society of America Journal* **55**: 1057–1067.
- Boggs, S. (1995). *Principles of Sedimentology and Stratigraphy*, second edn, Prentice Hall, Englewood Cliffs, N.J.
- Borchardt, G. (1989). Smectites, in J. B. Dixon and S. B. Weed (eds), *Minerals in the Soil Environment*, second edn, SSSA Book Series, no. 1, Soil Science Society of America, Madison, Wisconsin, pp. 675–727.
- Bosak, T., Souza-Egipsy, V. and Newman, D. K. (2004). A laboratory model of abiotic peloid formation, *Geobiology* **2** (3): 189–198.
- Bouza, P. J., Simón, M., Aguilar, J., del Valle, H. and Rostagno, M. (2007). Fibrous-clay mineral formation and soil evolution in Aridisols of northeastern Patagonia, Argentina, *Geoderma* **139**: 3850.

- Bradley, W. F. (1940). The structural scheme of attapulgite, *American Mineralogist* **25**: 405–410.
- Braissant, O., Cailleau, G., Aragno, M. and Verrecchia, E. P. (2004). Bacterially induced mineralization in the tree *Milicia exelsa* (Moraceae): its causes and consequences to the environment, *Geobiology* **2** (1): 59–66.
- Braissant, O., Cailleau, G., Dupraz, C. and Verrecchia, E. P. (2003). Bacterially induced mineralization of calcium carbonate in terrestrial environments: the role of exopolysaccharides and amino acids, *Journal of Sedimentary Research* **73** (3): 485–490.
- Braissant, O., Verrecchia, E. P. and Aragno, M. (2002). Is the contribution of bacteria to terrestrial carbon budget greatly underestimated?, *Naturwissenschaften* **89**: 366–370.
- Brauner, K. and Preisinger, A. (1956). Struktur und Entstehung des Sepioliths, *Tschermaks Mineralogische und Petrographische Mitteilungen* **6**: 120–140.
- Brindley, G. W. (1959). X-ray and electron diffraction data for sepiolite, *American Mineralogist* **44**: 494–500.
- Brindley, G. W., Bish, D. L. and Wan, H. M. (1977). The nature of kerolite, its relation to talc and sepiolite, *Mineralogical Magazine* **41**: 443–452.
- Brochier, J. E., Villa, P., Giacomarra, M. and Tagliacozzo, A. (1992). Shepherds and sediments: geo-ethnoarchaeology of pastoral sites, *Journal of Anthropological Archaeology* **11**: 47–102.
- Buczynski, C. and Chafetz, H. S. (1987). Siliciclastic grain breakage and displacement due to carbonate crystal growth: an example from the Lueders Formation (Permian) of north-central Texas, USA, *Sedimentology* **34**: 837–843.
- Bühmann, C., Nell, J. P. and Samadi, M. (2004). Clay mineral associations formed under Mediterranean-type climate in South Africa, *South African Journal of Plant and Soil* **21** (3): 166–170.
- Buol, S. W., Hole, F. D., McCracken, R. J. and Southard, R. J. (1997). *Soil Genesis and Classification*, fourth edn, Iowa State University Press, USA.

- Burgers, C. (1975). Heuweltjies (kraaltjies) in die Westelike Provinsie. Unpublished report of the Cape Department of Nature Conservation, Cape Town.
- Bustillo, M. A. and Alonso-Zarza, A. M. (2007). Overlapping of pedogenesis and meteoric diagenesis in distal alluvial and shallow lacustrine deposits in the Madrid Miocene Basin, Spain, *Sedimentary Geology*. Article in press, doi:10.1016/j.sedgeo.2006.12.006.
- Bustillo, M. A. and Bustillo, M. (2000). Miocene silcretes in argillaceous playa deposits, Madrid Basin, Spain: petrological and geochemical features, *Sedimentology* **47**: 1023–1037.
- Cailleau, G., Braissant, O., Dupraz, C., Aragno, M. and Verrecchia, E. P. (2005). Biologically induced accumulations of CaCO₃ in orthox soils of Biga, Ivory Coast, *Catena* **59** (1): 1–17.
- Calvet, F. and Julia, R. (1983). Pisoids in caliche profiles of Tarragona (NE Spain), in T. Peryt (ed.), *Coated Grains*, Springer-Verlag, Berlin, pp. 456–473.
- Canti, M. G. (1997). An Investigation of Microscopic Calcareous Spherulites from Herbivore Dungs, *Journal of Archaeological Science* **24**: 219–231.
- Canti, M. G. (1998). The Micromorphological Identification of Faecal Spherulites from Archaeological and Modern Materials, *Journal of Archaeological Science* **25**: 435–444.
- Carrick, P. and Krüger, R. (2007). Restoring degraded landscapes in lowland Namaqualand: Lessons from the mining experience and from regional ecological dynamics, *Journal of Arid Environments* **70** (4): 767–781.
- Castanier, S., Le Métayer-Levrel, G. and Perthuisot, J. (1999). Ca-carbonates precipitation and limestone genesis - the microbiogeologist point of view, *Sedimentary Geology* **126**: 9–23.
- Chadwick, O. A., Hendricks, D. M. and Nettleton, W. D. (1987). Silica in duric soils: I. A depositional model, *Soil Science Society of America Journal* **51**: 975–982.
- Chadwick, O. A. and Nettleton, W. D. (1990). Micromorphological evidence of adhesive and cohesive forces in soil cementation, in L. A. Douglas (ed.),

- Soil micromorphology: a basic and applied science*, Developments in Soil Science, 19, Elsevier, Amsterdam, pp. 207–212.
- Chartres, C. J. (1985). A Preliminary investigation of hardpan horizons in north-west New South Wales, *Australian Journal of Soil Research* **23**: 325–337.
- Christ, C. L., Hathaway, J. C., Hostetler, P. B. and Shepard, A. O. (1969). Palygorskite: new X-ray data, *The American Mineralogist* **54**: 198–205.
- Christ, C. L., Hostetler, P. B. and Siebert, R. M. (1973). Studies in the system MgO-SiO₂-CO₂-H₂O (III): The activity-product constant of sepiolite, *American Journal of Science* **273**: 65–83.
- Coaton, W. G. H. (1981). Fossilised nests of Hodotermitidae (Isoptera) from the Clanwilliam district, Cape Province, *Journal of the Entomological Society of South Africa* **44** (2): 79–81.
- Compton, J. S. (2007). Holocene evolution of the Anichab Pan on the south-west coast of Namibia, *Sedimentology* **54**: 55–70.
- Cowling, R. M., Esler, K. J. and Rundel, P. W. (1999). Namaqualand South Africa - an overview of a unique winter rainfall desert ecosystem, *Plant Ecology* **142**: 3–21.
- Cowling, R. M. and Hilton-Taylor, C. (1999). Plant biogeography, endemism and diversity, in W. R. J. Dean and S. J. Milton (eds), *The Karoo: Ecological Patterns and Processes*, Cambridge University Press, Cambridge, England, pp. 42–56.
- Cowling, R. M. and Pierce, S. (1999). *Namaqualand: A Succulent Desert*, Fernwood Press.
- Cox, G. W., Lovegrove, B. G. and Siegfried, W. R. (1987). The small stone content of Mima-like mounds in the South African Cape Region: implications for mound origin, *Catena* **14**: 165–176.
- Davies, P. J., Bubela, B. and Ferguson, J. (1978). The formation of ooids, *Sedimentology* **25**: 703–730.
- D.B.C.M. (2000). Environmental Management Program Report (E.M.P.R.) - Namaqualand Mines. De Beers Consolidated Mines Ltd, Private Bag X01, KLEINZEE, 8282, telephone (+27) 807-1911.

- De Villiers, S. E. and Cadman, A. (2001). An analysis of the palynomorphs obtained from Tertiary sediments at Koingnaas, Namaqualand, South Africa, *Journal of African Earth Sciences* **33** (1): 17–47.
- Deer, W. A., Howie, R. A. and Zussman, J. (1992). *An Introduction to the Rock-Forming Minerals*, second edn, Longman Scientific and Technical, Essex, England, chapter Sheet Silicates, p. 285; 354.
- Dékány, I., Turi, L. and Nagy, A. F. J. B. (1999). The structure of acid treated sepiolites: small-angle X-ray scattering and multi MAS-NMR investigations, *Applied Clay Science* **14**: 141–160.
- Deocampo, D. M. (2005). Evaporative evolution of surface waters and the role of aqueous CO₂ in magnesium silicate precipitation: Lake Eyasi and Ngorongoro Crater, northern Tanzania, *South African Journal of Geology* **108**: 493–504.
- Desmet, P. G. (2007). Namaqualand A brief overview of the physical and floristic environment, *Journal of Arid Environments* **70**: 570–587.
- Díaz Torres, J. A., Añorbe Urmeneta, M., Suárez Barrios, M., Navarrete López-Cozar, J. and Martín Pozas, J. M. (1990). Presencia y génesis de los minerales fibrosos de la arcilla en las proximidades de Villamuriel de Cerrato, Provincia de Palencia. (Abstract in English), *Studia Geologica Salmanticensis* **26**: 7–25.
- Doner, H. E. and Lynn, W. C. (1989). Carbonate, halide, sulphate, and sulphide minerals, in J. B. Dixon and S. B. Weed (eds), *Minerals in the Soil Environment*, second edn, SSSA Book Series, no. 1, Soil Science Society of America, Madison, Wisconsin, pp. 279–330.
- Drees, L. R., Wilding, L. P., Smeck, N. E. and Senkayi, A. L. (1989). Silica in soils: quartz and disordered silica polymorphs, in J. B. Dixon and S. B. Weed (eds), *Minerals in the Soil Environment*, second edn, SSSA Book Series, no. 1, Soil Science Society of America, Madison, Wisconsin, pp. 913–872.
- Drever, J. I. (1997). *The Geochemistry of Natural Waters: Surface and Ground-water Environments*, third edn, Prentice Hall, Upper Saddle River, N.J.

- Ducloux, J., Delhoume, J. P., Petit, S. and Decarreau, A. (1995). Clay differential in Aridisols of northern Mexico, *Soil Science Society of America Journal* **59**: 269–276.
- Eberl, D. D., Jones, B. F. and Khoury, H. N. (1982). Mixed-layer kero-lite/stevensite from the Armagosa Desert, Nevada, *Clays and Clay Minerals* **30 (5)**: 321–326.
- Ece, Ö. I. and Çoban, F. (1994). Geology, occurrence and genesis of Eskişehir sepiolites, Turkey, *Clays and Clay Minerals* **42 (1)**: 81–92.
- Eckardt, F. D. and Schemenauer, R. S. (1998). Fog water chemistry in the Namib Desert, Namibia, *Atmospheric Environment* **32**: 2595–2599.
- Ellis, F. (1988). *Die Gronde van die Karoo*, PhD thesis, University of Stellenbosch.
- Ellis, F. (2002). Contribution of termites to the formation of hardpans in soils of arid and semi-arid regions of South Africa. Proceedings of the 17th World Congress of Soil Science, Bangkok, Thailand, August 2002, ABSTRACT GeoBase-ref.
- Ellis, F., de Clercq, W. P. and Engelbrecht, H. (2001). Soils associated with microrelief features (“heuweltjies”) occurring on an ancient land surface in the lower Berg River Valley. Paper delivered at the Soil Science Society of South Africa Congress, Pretoria.
- Ellis, F. and Lambrechts, J. J. N. (1994). Dorbank, a reddish brown hardpan of South Africa: a proto-silcrete? Poster paper presented at the 15th World Congress of Soil Science, Acapulco, Mexico.
- Ellis, F. and Schloms, B. H. A. (1982). A note on the dorbanks (duripans) of South Africa, *Palaeoecology of Africa* **15**: 149–157.
- Elprince, A. M., Mashhady, A. S. and Aba-Husayn, M. M. (1979). The occurrence of pedogenic palygorskite (attapulgitite) in Saudi Arabia, *Soil Science* **128 (4)**: 211–218.
- Esquivel, E. V., Murr, L. E., Lopez, M. I. and Goodell, P. C. (2005). TEM observations of a 30 million year old mountain leather nanofiber mineral composite, *Materials Characterization* **54 (4-5)**: 458–465.

- Eugster, H. P. and Hardie, L. A. (1978). Saline Lakes, *in* A. Lerman (ed.), *Lakes: Chemistry, Geology, Physics*, Springer-Verlag, New York, pp. 237–293.
- Eugster, H. P. and Jones, B. F. (1979). Behaviour of major solutes during closed-basin brine evolution, *American Journal of Science* **279**: 609–631.
- Faure, G. (1992). *Principles and Applications of Inorganic Geochemistry*, Macmillan Publishing Company, New York.
- Faure, G. (1998). *Principles and Applications of Geochemistry*, second edn, Prentice Hall, New Jersey, chapter 12: Mineral Stability Diagrams, pp. 172–199.
- Fernández-Díaz, L., Astilleros, J. M. and Pina, C. M. (2006). The morphology of calcite crystals grown in a porous medium doped with divalent cations, *Chemical Geology* **225**: 314–321.
- Fernandez-Marcos, M. L., Macías, F. and Guitián-Ojea, F. (1979). A contribution to the study of the stability of clay minerals from the soil solution composition at different pF values, *Clay Minerals* **14**: 29–37.
- Fey, M. V., O'Brien, R. D. and Mills, A. J. (2002). Rehabilitation of waste rock and overburden dumps, *Encyclopedia of Soil Science*, Marcel Dekker, Inc., New York, pp. 1115–1117.
- Flach, K. W., Nettleton, W. D., Gile, L. H. and Cady, J. G. (1969). Pedocementation: induration by silica, carbonates, and sesquioxides in the Quaternary, *Soil Science* **107** (6): 442–453.
- Folk, R. L. (1993). SEM imaging of bacteria and nannobacteria in carbonate sediments and rocks, *Journal of Sedimentary Petrology* **63** (5): 990–999.
- Folk, R. L. (1999). Nannobacteria and the precipitation of carbonate in unusual environments, *Sedimentary Geology* **126**: 47–55.
- Francis, M. L., Fey, M. V. and Ellis, F. (2004). Sepiolite formation in soils of the Namaqualand coastal plain, South Africa, *Berichte der Deutschen Mineralogischen Gesellschaft (Beihefte zum (Supplement to the) European Journal of Mineralogy)* **16**: 40.

- Francis, M. L., Fey, M. V., Prinsloo, H. P., Ellis, F., Mills, A. J. and Medinski, T. V. (2007). Soils of Namaqualand: compensations for aridity, *Journal of Arid Environments* **70** (4): 588–603.
- Gac, J. Y., Droubi, A., Fritz, B. and Tardy, Y. (1988). Geochemical behaviour of silica and magnesium during the evaporation of waters in Chad, *Chemical Geology* **19**: 215–228.
- Galan, E. and Carretero, M. I. (1999). A new approach to compositional limits for sepiolite and palygorskite, *Clays and Clay Minerals* **47** (4): 399–409.
- Galan, E. and Ferrero, A. (1982). Palygorskite-sepiolite clays of Lebrija, southern Spain, *Clays and Clay Minerals* **30** (3): 191–199.
- Garrels, R. M. and Mackenzie, F. T. (1967). Origin of the chemical composition of some springs and lakes, in R. F. Gould (ed.), *Equilibrium Concepts in Natural Water Systems*, Advances in Chemistry Series 67, American Chemical Society, Washington, D.C., pp. 222–242.
- Golden, D. C., Dixon, J. B., Shadfan, H. and Klippenberger, L. A. (1985). Palygorskite and sepiolite alteration to smectite under alkaline conditions, *Clays and Clay Minerals* **33** (1): 44–50.
- González-Muñoz, M. T., Ben Chekroun, K., Ben Aboud, A., Arias, J. M. and Rodríguez-Gallego, M. (2000). Bacterially induced Mg-calcite formation: role of Mg²⁺ in development of crystal morphology, *Journal of Sedimentary Research* **70** (3): 559–564.
- Goudie, A. S. (1983). Calcrete, in A. S. Goudie and K. Pye (eds), *Chemical Sediments and Geomorphology: Precipitates and Residua in the Near-Surface Environment*, Academic Press, London, pp. 93–131.
- Goudie, A. S. (1996). Organic agency in calcrete development, *Journal of Arid Environments* **32**: 103–110.
- Gozález, L., Ibarra, L. M., Rodríguez, A., Moya, J. S. and Valle, F. J. (1984). Fibrous silica gel obtained from sepiolite by HCl attack, *Clay Minerals* **19**: 93–98.
- Gutiérrez-Castorena, M. d. C., Stoops, G., Ortiz-Solorio, C. A. and Sánchez-Guzmán, P. (2006). Micromorphology of opaline features in soils on the

- sediments of the ex-Lago de Texcoco, México, *Geoderma* **132** (1-2): 89–104.
- Hallmark, C. T., Wilding, L. P. and Smeck, N. E. (1982). Silicon, in A. L. Page, R. H. Miller and D. R. Keeney (eds), *Methods of Soil Analysis, Part 2. Chemical and Microbiological Properties*, second edn, Agronomy Monograph no. 9, ASA-SSSA, Madison, USA, pp. 263–273.
- Harden, J. W. (1982). A quantitative index of soil development from field descriptions: examples from a chronosequence of soils in central California, *Geoderma* **28**: 1–28.
- Hardie, L. A. and Eugster, H. P. (1970). The evolution of closed-basin brines, *Mineralogical Society of America Special Publication* **3**: 273–290.
- Harmse, J. T. and Swanevelder, C. J. (1987). Spatial variation in the granulometric properties of Sandveld aeolianites, *Annals of the Geological Survey of South Africa* **21**: 51–58.
- Hartnady, C. J. H. and Von Veh, M. W. (1990). Tectonostratigraphic and structural history of the Late Proterozoic-Early Palaeozoic Gariep Belt, Cape Province, South Africa, *Guidebook Geocongress '90 Geological Society of South Africa* **PO1**: 1–49.
- Harvie, C. E., Møller, N. and Weare, J. H. (1984). The prediction of mineral solubilities in natural waters: the Na-K-Mg-Ca-H-Cl-SO₄-OH-HCO₃-CO₃-CO₂-H₂O system to high ionic strengths at 25° C, *Geochimica et Cosmochimica Acta* **48**: 723–751.
- Harvie, C. E. and Weare, J. H. (1980). The prediction of mineral solubilities in natural waters: the Na-K-Mg-Ca-Cl-SO₄-H₂O system from zero to high concentration at 25° C, *Geochimica et Cosmochimica Acta* **44**: 981–997.
- Hay, R. L., Hughes, R. E., Kyser, T. K., Glass, H. D. and Liu, J. (1995). Magnesium-rich clays of the meerschaum mines in the Amboseli Basin, Tanzania and Kenya, *Clays and Clay Minerals* **43** (4): 455–466.
- Hay, R. L., Pexton, R. E., Teague, T. T. and Kyser, T. K. (1986). Spring-related carbonate rocks, Mg clays and associated minerals in Pliocene deposits of the Armagosa Desert, Nevada and California, *Geological Society of America Bulletin* **97**: 1488–1503.

- Hay, R. L. and Reeder, R. J. (1978). Calcretes of Olduvai Gorge and the Ndolanya Beds of northern Tanzania, *Sedimentology* **25**: 619–673.
- Hay, R. L. and Stoessell, R. K. (1984). Sepiolite in the Amboseli Basin of Kenya: A new interpretation, in A. Singer and E. Galan (eds), *Palygorskite-Sepiolite: Occurrences, Genesis and Uses*, Developments in Sedimentology 37, Elsevier Science Publishers, Amsterdam, pp. V–VI.
- Hay, R. L. and Wiggins, B. (1980). Pellets, ooids, sepiolite and silica in three calcretes of the southwestern United States, *Sedimentology* **27**: 559–576.
- Hayashi, H., Otsuka, R. and Imai, N. (1969). Infrared study of sepiolite and palygorskite on heating, *American Mineralogist* **54**: 1613–1624.
- Heineken, T. J. E. (1981). Estuaries of the Cape. Part 2: Synopsis of Available Information on Individual Systems. Report no.2: Buffels (CW3), CSIR Research Report 401, Stellenbosch.
- Hobsan, W. A. and Dahlgren, R. A. (1998). A quantitative study of pedogenesis in California vernal pool wetlands (Chapter 7), *Quantifying Soil Hydromorphy*, Soil Science Society of America, Madison, Wisconsin, USA, pp. 107–127. SSSA Special Publication Number 54.
- Holzmueller, E. J., Jose, S. and Jenkins, M. A. (2007). Relationship between *Cornus florida* L. and calcium mineralization in two southern Appalachian forest types, *Forest Ecology and Management* **245**: 110–117.
- Horwath, J. L. and Johnson, D. L. (2006). Mima-type mounds in southwest Missouri: Expressions of point-centered and locally thickened biomantles, *Geomorphology* **77**: 308–319.
- Horwath, J. L. and Johnson, D. L. (2007). Erratum to “Mima-type mounds in southwest Missouri: Expressions of point-centered and locally thickened biomantles” [Geomorphology 77 (2006) 308319], *Geomorphology* **83**: 193–194.
- Inglès, M., Salvany, J. M., Muñoz, A. and Pérez, A. (1998). Relationship of mineralogy to depositional environments in the non-marine Tertiary mudstones of the southwestern Ebro Basin (Spain), *Sedimentary Geology* **116**: 159–176.

- Jamoussi, F., Aboud, A. B. and López-Galindo, A. (2003). Palygorskite genesis through silicate transformation in Tunisian continental Eocene deposits, *Clay Minerals* **38**: 187–199.
- Jenkins, M. A., Jose, S. and White, P. S. (2007). Impacts of an exotic disease and vegetation change on foliar calcium cycling in Appalachian forests, *Ecological Applications* **17**: 869–881.
- Jones, B. F. and Galan, E. (1988). Sepiolite and palygorskite, in S. W. Bailey (ed.), *Hydrous Phyllosilicates*, Vol. 19 of *Reviews in Mineralogy*, Mineralogical Society of America, pp. 631–674.
- Jones, B. F., Hanor, J. S. and Evans, W. R. (1994). Sources of dissolved salts in the central Murray Basin, Australia, *Chemical Geology* **111**: 135–154.
- Jungerius, P. D., van den Ancker, J. A. M. and Múcher, H. J. (1999). The contribution of termites to the microgranular structure of soils on the Uasin Gishu Plateau, Kenya, *Catena* **34**: 349–363.
- Kampunzu, A. B., Ringrose, S., Huntsman-Mapila, P., Harris, C., Vink, B. W. and Matheson, W. (2007). Origins and palaeo-environments of Kalahari duricrusts in the Moshaweng dry valleys (Botswana) as detected by major and trace element composition, *Journal of African Earth Sciences* **48**: 199–221.
- Kavas, T., Sabah, E. and Çelik, M. S. (2004). Structural properties of sepiolite-reinforced cement composite, *Cement and Concrete Research* **34**: 2135–2139.
- Keller, W. D. (1982). Kaolin - A most diverse rock in genesis, texture, physical properties, and uses, *Geological Society of America Bulletin* **93**: 27–36.
- Khademi, H. and Mermut, A. R. (1999). Submicroscopy and stable isotope geochemistry of carbonates and associated palygorskite in Iranian Aridisols, *European Journal of Soil Science* **50**: 207–216.
- Khoury, H. N., Eberl, D. D. and Jones, B. F. (1982). Origin of magnesium clays from the Armagosa Desert, Nevada, *Clays and Clay Minerals* **30** (5): 327–336.
- Kittrick, J. A. (1971). Soil solution composition and stability of clay minerals, *Soil Science Society of America Proceedings* **35**: 450–454.

- Klappa, C. F. (1980). Rhizoliths in terrestrial carbonates: classification, recognition genesis and significance, *Sedimentology* **27**: 613–629.
- Knoll, A. H., Strother, P. K. and Ross, S. (1988). Distribution and diagenesis of microfossils from the Lower Proterozoic Duck Creek Dolomite, Western Australia, *Precambrian Research* **38**: 257–279.
- Knox, G. J. (1977). Caliche profile formation, Saldanha Bay (South Africa), *Sedimentology* **24**: 657–674.
- Land Type Survey Staff (1987). Land Types of the maps 2816 Alexander Bay; 2818 Warmbad; 2916 Springbok; 2918 Pofadder; 3017 Garies; 3018 Loeriesfontein. Memoirs on the Agricultural Natural Resources of South Africa No. 9.
- Laurie, H. (2002). Optimal transport in central place foraging, with an application to the overdispersion of *heuweltjies*, *South African Journal of Science* **98**: 141–146.
- Léveillé, R. J., Fyfe, W. S. and Longstaffe, F. J. (2000). Unusual secondary Ca-Mg-carbonate-kerolite deposits in basaltic caves, Kauai, Hawaii, *The Journal of Geology* **108**): 613–621.
- Léveillé, R. J., Longstaffe, F. J. and Fyfe, W. S. (2002). Kerolite in carbonate-rich speleothems and microbial deposits from basaltic caves, Kauai, Hawaii, *Clays and Clay Minerals* **50** (4): 514–524.
- Litaor, M. I., Mancinelli, R. and Halfpenny, J. C. (1996). The influence of pocket gophers on the status of nutrients in Alpine soils, *Geoderma* **70**: 37–48.
- Litchfield, W. H. and Mabbutt, J. A. (1962). Hardpan in soils of semi-arid Western Australia, *Journal of Soil Science* **13**: 148–159.
- Loisy, C., Verrecchia, E. P. and Dufour, P. (1999). Microbial origin for pedogenic micrite associated with a carbonate paleosol (Champagne, France), *Sedimentary Geology* **126**: 193–204.
- Lopez-Galindo, A., Ben Aboud, A., Fenoll Hach-Ali, P. and Casas Ruiz, J. (1996). Mineralogical and geochemical characterization of palygorskite from Gabasa (NE Spain). Evidence from a detrital precursor, *Clay Minerals* **31**: 33–44.

- Lovegrove, B. G. and Siegfried, W. R. (1986). Distribution and formation of Mima-like earth mounds in the western Cape Province of South Africa, *South African Journal of Science* **82**: 432–436.
- Lovegrove, B. G. and Siegfried, W. R. (1989). Spacing and origin(s) of Mima-like earth mounds in the Cape Province of South Africa, *South African Journal of Science* **85**: 108–112.
- Macumber, P. G. (1983). *Interactions between ground water and surface systems in northern Victoria*, PhD thesis, Melbourne University.
- Mahood, K. (2003). *Strip mining rehabilitation by translocation in arid coastal Namaqualand, South Africa*, Master's thesis, University of Stellenbosch.
- Martin De Vidales, J. L., Pozo, M., Alia, J. M., Garcia-Navarro, F. and Rull, F. (1991). Kerolite-stevensite mixed-layers from the Madrid Basin, Central Spain, *Clay Minerals* **26**: 329–342.
- Martínez-Ramírez, S., Puertas, F. and Blanco Varela, M. T. (1995). Carbonation processes and properties of a new lime mortar with added sepiolite, *Cement and Concrete Research* **25** (1): 39–50.
- Martínez-Ramírez, S., Puertas, F. and Blanco Varela, M. T. (1996). Stability of sepiolite in neutral and alkaline media at room temperature, *Clay Minerals* **31**: 225–232.
- McBride, M. B. (1994). *Environmental Chemistry of Soils*, Oxford University Press.
- McDaniel, P. A., Bathke, G. R., Buol, S. W., Cassel, D. K. and Falen, A. L. (1992). Secondary Manganese/Iron ratios as pedochemical indicators of field-scale throughflow water movement, *Soil Science of America Journal* **56**: 1211–1217.
- Mees, F. (1999). Unsuitability of calcite spherulites as indicators of subaerial exposure, *Journal of Arid Environments* **42**: 149–154.
- Mehra, O. P. and Jackson, M. L. (1960). Iron oxide removal from soils and clays by a dithionite-citrate system buffered with sodium bicarbonate, *Proceedings of the 7th National Conference on Clays and Clay Minerals*, Pergamon Press, New York, pp. 317–327.

- Mermut, A. R., Arshad, M. A. and St. Arnaud, R. J. (1984). Micropedological study of termite mounds of three species of macrotermes in Kenya, *Soil Science of America Journal* **48**: 613–620.
- Midgley, G. F. and Musil, C. F. (1990). Substrate effects of zoogenic soil mounds on vegetation composition in the Worcester-Robertson valley, Cape Province, *South African Journal of Botany* **56** (2): 158–166.
- Midgley, G., Hannah, L., Roberts, R., MacDonald, D. and Allsopp, J. (2001). Have Pleistocene climate cycles influenced species richness patterns in the greater Cape Mediterranean Region?, *Journal of Mediterranean Ecology* **2**: 137–144.
- Midgley, G. and Hoffman, T. (1991). Heuweltjies: nutrient factories, *Veld and Flora* **September**: 72–75.
- Midgley, J. J., Harris, C., Hesse, H. and Swift, A. (2002). Heuweltjie age and vegetation change based on $\delta^{13}\text{C}$ and $\delta^{14}\text{C}$ analyses, *South African Journal of Science* **98**: 202–204.
- Mifsud, A., Huertas, F., Barahona, E., Linares, J. and Fornés, V. (1979). Test de couleur pour la sepiolite, *Clay Minerals* **14**: 247–248.
- Milton, S. J. and Dean, W. R. J. (1990). Mima-like mounds in the southern and western Cape: are the origins so mysterious?, *South African Journal of Science* **86**: 207–208.
- Monger, H. C. and Adams, H. P. (1996). Micromorphology of calcite-silica deposits, Yucca Mountain, Nevada, *Soil Science Society of America Journal* **60**: 519–530.
- Monger, H. C. and Daugherty, L. A. (1991). Neoformation of palygorskite in a southern New Mexico Aridisol, *Soil Science Society of America Journal* **55**: 1646–1650.
- Monger, H. C., Daugherty, L. A. and Gile, L. H. (1991a). A microscopic examination of pedogenic calcite in an Aridisol of Southern New Mexico, *Soil Science Society of America Special Publication* **26**: 37–60.
- Monger, H. C., Daugherty, L. A., Lindemann, W. C. and Liddell, C. M. (1991). Microbial precipitation of pedogenic carbonate, *Geology* **19**: 997–1000.

- Monger, H. C. and Gallegos, R. A. (2000). Biotic and abiotic processes and rates of pedogenic carbonate accumulation in the southwestern United States - relationship to atmospheric CO₂ sequestration, *in* R. Lal, J. M. Kimble, H. Eswaran and B. A. Stewart (eds), *Global Climate Change and Pedogenic Carbonates*, Lewis Publishers, Boca Raton, Florida, pp. 273–289.
- Moody, L. E. and Graham, R. C. (1994). Pedogenic processes in thick sand deposits on a marine terrace, central California, *in* D. L. Cremeens, R. B. Brown and J. H. Huddleston (eds), *Whole Regolith Pedology*, Soil Science Society of America, Madison, Wisconsin, USA, pp. 57–74. SSSA Special Publication Number 34.
- Moore, J. M. and Picker, M. D. (1991). Heuweltjies (earth mounds) in the Clanwilliam district, Cape Province, South Africa: 4000-year-old termite nests, *Oecologia* **86**: 424–432.
- Mosaddeghi, M. R., Hajabbasi, M. A. and Khademi, H. (2006). Tensile strength of sand, palygorskite and calcium carbonate mixtures and interpretation with the effective stress theory, *Geoderma* **134**: 160–170.
- Munsell Color Company (1975). Munsell Soil Color Charts. Munsell Color, Baltimore, Maryland.
- Murphy, J. and Riley, H. P. (1962). A modified single solution method for the determination of phosphate in natural waters, *Analytica Chimica Acta* **27**: 31–36.
- Nash, D. J. and McLaren, S. J. (2003). Kalahari valley calcretes: their nature, origins, and environmental significance, *Quaternary International* **111**: 3–22.
- Nash, D. J. and Shaw, P. A. (1998). Silica and carbonate relationships in silcrete-calcrete intergrade duricrusts from the Kalahari of Botswana and Namibia, *Journal of African Earth Sciences* **27(1)**: 11–25.
- Nathan, Y., Bentor, Y. K. and Würzburger, U. (1970). Vein palygorskites in Isreal and Sinai, their origin and symmetry, *Israel Journal of Chemistry* **9**: 469–476.

- Ndeinoma, A. (2006). *Mycorrhiza re-establishment on post mined rehabilitated areas of the Brand se Baai Succulent Karoo vegetation*, Master's thesis, University of Stellenbosch.
- Neaman, A. and Singer, A. (2004). The effects of palygorskite on chemical and physico-chemical properties of soils: a review, *Geoderma* **123**: 297-303.
- Netterberg, F. (1969). *The Geology and Engineering Properties of South African Calcretes*, PhD thesis, University of the Witwatersrand.
- Nettleton, W. D., Olson, C. G. and Wysocki, D. A. (2000). Paleosol classification: Problems and solutions, *Catena* **41**: 61-92.
- Nordstrom, D. K., Plummer, L. N., Wigley, T. M. L., Wolery, T. J., Ball, J. W., Jenne, E. A., Bassett, R. L., Crerar, D. A., Florence, T. M., Fritz, B., Hoffman, M., Holdren, G. R. Jr., Lafon, G. M., Mattigod, S. V., McDuff, R. E., Morel, F., Reddy, M. M., Sposito, G. and Thraillkill, J. (1979). A comparison of computerized chemical models for equilibrium calculations in aqueous systems, in E. A. Jenne (ed.), *Chemical modeling in aqueous systems, speciation, sorption, solubility, and kinetics*, Symposium Series 93, American Chemical Society, Washington, D.C., pp. 857-892.
- Olivier, J. (2002). Fog-water harvesting along the West Coast of South Africa: A feasibility study, *Water SA* **28** (4): 349-360. Available on <http://www.wrc.org.za>.
- Ouhadi, V. R. and Yong, R. N. (2003). The role of clay fractions of marly soils on their post stabilization failure, *Engineering Geology* **70**: 365-375.
- Owliaie, H. R., Abtahi, A. and Heck, R. J. (2006). Pedogenesis and clay mineralogical investigation of soils formed on gypsiferous and calcareous materials, on a transect, southwestern Iran, *Geoderma* **134** (1-2): 62-81.
- Parkhurst, D. L. and Appelo, C. A. J. (1999). User's guide to PHREEQC (Version 2). A computer program for speciation, batch-reaction, one-dimensional transport, and inverse geochemical calculations: U.S. Geological Survey Water-Resources Investigations Report 99-4259, *Technical report*. <http://water.usgs.gov/software/>.

- Parkington, J., Baxter, A., Cartwright, C., Cowling, R. M. and Meadows, M. (2000). Palaeovegetation at the last glacial maximum in the western Cape, South Africa: wood charcoal and pollen evidence from Elands Bay Cave, *South African Journal of Science* **96**: 543–546.
- Partridge, T. C. and Maud, R. R. (1987). Geomorphic evolution of southern Africa since the Mesozoic, *South African Journal of Geology* **90** (2): 179–208.
- Partridge, T. C. and Maud, R. R. (2000). Macro-scale geomorphic evolution of southern Africa, in T. C. Partridge and R. R. Maud (eds), *The Cenozoic of Southern Africa*, Oxford University Press, pp. 3–18.
- Pether, J. (1994). *The Sedimentology, Palaeontology and Stratigraphy of Coastal-Plain Deposits at Hondeklip Bay, Namaqualand, South Africa*, Master's thesis, University of Cape Town.
- Pether, J., Roberts, D. L. and Ward, J. D. (2000). Deposits of the West Coast, in T. C. Partridge and R. R. Maud (eds), *The Cenozoic of Southern Africa*, Oxford University Press, pp. 33–54.
- Phillips, S. E., Milnes, A. R. and Foster, R. C. (1987). Calcified filaments: an example of biological influences in the formation of calcrete in South Australia, *Australian Journal of Soil Research* **25**: 405–428.
- Phillips, W. R. and Griffen, D. T. (1981). *Optical Mineralogy: The Nonopaque Minerals*, W H Freeman & Co., San Francisco.
- Picker, M. D., Hoffman, M. T. and Leverton, B. (2007). Density of *Microhodotermes viator* (Hodotermitidae) mounds in southern Africa in relation to rainfall and vegetative productivity gradients, *Journal of Zoology* **271**: 37–44.
- Pickford, M. and Senut, B. (1997). Cainozoic mammals from coastal Namaqualand, South Africa, *Palaeontologia Africana* **34**: 199–217.
- Pickford, M. and Senut, B. (2000). *Geology and Palaeobiology of the Namib Desert, Southwestern Africa: Geology and History of Study*, Vol. 1 of *Memoir 18*, Geological Survey of Namibia.
- Pitzer, K. S. (1973). Thermodynamics of electrolytes, I. Theoretical basis and general equations, *Journal of Physical Chemistry* **77** (2): 268–277.

- Pitzer, K. S. (1979). Theory: ion interaction approach, *in* R. M. Pytkowicz (ed.), *Activity Coefficients in Electrolyte Solutions*, Vol. 1, CRC Press, Inc., Boca Raton, Florida, pp. 157–208.
- Plummer, L. N., Parkhurst, D. L., Fleming, G. W. and Dunkle, S. A. (1988). A computer program incorporating Pitzer's equations for calculation of geochemical reactions in brines: U.S. Geological Survey Water-Resources Investigations Report 88-4153, *Technical report*. <http://water.usgs.gov/software/>.
- Poole, C. J. (1999). *Growth and Nutrition of Bruniaceae*, Master's thesis, University of Stellenbosch.
- Post, J. L. (1985). Identification of calcium oxalate crystals using alizarin red S stain, *Archives of Pathology and Laboratory Medicine* **109** (2): 186–189.
- Pozo, M. and Casas, J. (1999). Origin of kerolite and associated Mg clays in palustrine-lacustrine environments. The Esquivias deposit (Neogene Madrid Basin, Spain), *Clay Minerals* **34**: 395–418.
- Prinsloo, H. (2005). *Alteration of the soil mantle by strip mining in the Namaqualand Strandveld*, Master's thesis, University of Stellenbosch.
- Ranson, M. D. and Bidwell, O. W. (1990). Clay movement and carbonate accumulation in Ustolls of central Kansas, USA, *in* L. A. Douglas (ed.), *Soil micromorphology: a basic and applied science*, Developments in Soil Science, 19, Elsevier, Amsterdam, pp. 417–423.
- Raz, S., Weiner, S. and Addadi, L. (2000). Formation of high-magnesian calcites via an amorphous precursor phase: possible biological implications, *Advanced Materials* **12** (1): 38–42.
- Reheis, M. C., Sowers, J. M., Taylor, E. M., McFadden, L. D. and Harden, J. W. (1992). Morphology and genesis of carbonate soils on the Kyle Canyon fan, Nevada, U.S.A., *Geoderma* **52**: 303–342.
- Reider, R. G., Huss, J. M. and Miller, T. W. (1996). A groundwater vortex hypothesis for mima-like mounds, Laramie Basin, Wyoming, *Geomorphology* **16**: 295–317.

- Lobry de Bruyn, L. A. and Conacher, A. J. (1990). The role of termites and ants in soil modification: a review, *Australian Journal of Soil Research* **28**: 55–93.
- Rodas, M., Luque, F. J., Mas, R. and Garzon, M. G. (1994). Calcretes, palycretes and silcrete in the paleogene detrital sediments of the Duero and Tajo Basins, Central Spain, *Clay Minerals* **29**: 273–285.
- Rode, A. A. (1969). *Theory of Soil Moisture Properties of Soils and Movement of Soil Moisture*, IPST, Jerusalem. Translated from the Russian 1965 edition.
- Rogers, J., Pether, J., Molyneux, R., Hill, R. S., Kilham, J. L. C., Cooper, G. and Corbett, I. B. (1990). Cenozoic geology and mineral deposits along the west coast of South Africa and the Sperrgebiet, *Guidebook Geocongress '90 Geological Society of South Africa* **PR1**: 1–111.
- Roux, A. L. and Odendaal, F. J. (1992). Report on the study of natural recovery of overburden dumps on D.B.C.M. properties in Namaqualand, *Technical report*. Unpublished report, Geology Department, De Beers Consolidated Mines Ltd, Private Bag X01, KLEINZEE, 8282, telephone (+27) 807-1911.
- Sánchez, C. and Galán, E. (1995). An approach to the genesis of palygorskite in a Neogene-Quaternary continental basin using principle factor analysis, *Clay Minerals* **30**: 225–238.
- Sanz, M. E. (1996). *Sedimentología de las Formaciones Neógenas del Sur de la Cuenca de Madrid*, Ministerio de Fomento, Cedex Madrid.
- Sariiz, K. and Isik, I. (1995). Meerschaum from Eskişehir Province, Turkey, *Gems & Gemology* **31** (1): 42–51.
- Sauer, D., Glatzel, S., Kühn, J., Zarei, M. and Stahr, K. (submitted). Micro-morphology of duricrusts in soils of the Alentejo (Portugal), .
- Sauer, D. and Stahr, K. (2004). Formation of calcretes and silcretes in the Alentejo (Portugal) and consequences for the landscape, ecosystems and land use, *Eurosoil Proceedings*, University of Freiburg.
- Schmidt, A. (2002). *Strip-mine rehabilitation in Namaqualand*, Master's thesis, University of Stellenbosch.

- Schmiedel, U. and Jürgens, N. (1999). Community structure on unusual habitat islands: quartz-fields in the Succulent Karoo, South Africa, *Plant Ecology* **142**: 57–69.
- Schwertmann, U. and Taylor, R. M. (1989). Iron Oxides, in J. B. Dixon and S. B. Weed (eds), *Minerals in the Soil Environment*, second edn, SSSA Book Series, no. 1, Soil Science Society of America, Madison, Wisconsin, pp. 379–438.
- Schwertmann, U. (1993). Relationship between iron oxides, soil color and soil formation, in J. M. Bigham and E. J. Coilkosz (eds), *Soil Color*, Soil Science Society of America, Madison, Wisconsin, USA, pp. 51–69. SSSA Special Publication Number 31.
- Scott, D. F., du Toit, B., Johnston, M. A. and Burns, M. E. R. (1995). Soil leaching trials on overburden soil from Kleinzee and Koingnaas, *Technical report*. Report FOR-C 283, CSIR, Division of Forest Science and Technology, prepared for De Beers Consolidated Mines Ltd, Private Bag X01, KLEINZEE, 8282, telephone (+27) 807-1911.
- Scott, D. F. and Johnston, M. A. (1994). The effects of mining on soil properties and the ability of the soil to support vegetation after mining at Kleinzee and Koingnaas, on the west coast of South Africa., *Technical report*. Report FOR-C 253, CSIR, Division of Forest Science and Technology, prepared for De Beers Consolidated Mines Ltd, Private Bag X01, KLEINZEE, 8282, telephone (+27) 807-1911.
- Seong-Joo, L. and Golubic, S. (1999). Microfossil populations in the context of synsedimentary micrite deposition and acicular carbonate precipitation: Mesoproterozoic Gaoyuzhuang Formation, China, *Precambrian Research* **96**: 183–208.
- Siesser, W. G. (1973). Diagenetically formed ooids and intraclasts in South African calcretes, *Sedimentology* **20** (4): 539–551.
- Siffert, B. and Wey, R. (1962). Synthèse d'une sepiolite a temperature ordinaire, *Comptes rendus de l'Académie des sciences* **254**: 1460–1462.
- Singer, A. (1989). Palygorskite and sepiolite group minerals, in J. B. Dixon and S. B. Weed (eds), *Minerals in the Soil Environment*, second edn, SSSA

- Book Series, no. 1, Soil Science Society of America, Madison, Wisconsin, pp. 829–872.
- Singer, A. (2002). Palygorskite and sepiolite, in J. B. Dixon and D. G. Schulze (eds), *Soil Mineralogy with Environmental Applications*, third edn, SSSA Book Series, no. 7, Soil Science Society of America, Madison, Wisconsin, pp. 555–583.
- Singer, A. and Galan, E. (1984). *Palygorskite-Sepiolite: Occurrences, Genesis and Uses*, Developments in Sedimentology 37, Elsevier Science Publishers, Amsterdam.
- Singer, A., Ganor, E., Dultz, S. and Fischer, W. (2003). Dust deposition over the Dead Sea, *Journal of Arid Environments* **53**: 41–59.
- Singer, A., Kirsten, W. and Bühmann, C. (1992). Occurrence of sepiolite in the northern Transvaal, South Africa, *South Africa Journal of Geology* **95**: 165–170.
- Singer, A., Kirsten, W. and Bühmann, C. (1995). Fibrous clay minerals in the soils of Namaqualand, South Africa: characteristics and formation, *Geoderma* **66**: 43–70.
- Singer, A. and Norrish, K. (1974). Pedogenic palygorskite occurrences in Australia, *American Mineralogist* **59**: 508–517.
- Singer, A., Stahr, K. and Zarei, M. (1998). Characteristics and origin of sepiolite (Meerschaum) from Central Somalia, *Clay Minerals* **33**: 349–362.
- Slabber, M. H. (1945). *'n Grondopname in die Malmesbury-Piketberg streek*, PhD thesis, University of Stellenbosch (D.Sc. (Agric.)).
- Smith, M. and Compton, J. S. (2004). Origin and evolution of major salts in the Darling pans, Western Cape, South Africa, *Applied Geochemistry* **19**: 645–664.
- Soil Classification Working Group (1991). *Soil Classification: A Taxonomic System for South Africa*, second edn, Department of Agricultural Development, Republic of South Africa. Memoirs on the Agricultural Natural Resources of South Africa, Vol. 15.

- Soil Survey Staff (1999). *Soil Taxonomy: a basic system of classification for making and interpreting soil surveys*, second edn, Natural Resources Conservation Service, United States Department of Agriculture. Agric. Handbook No. 436.
- Spackman, L. K. and Munn, L. C. (1984). Genesis and morphology of soils associated with formation of Laramie Basin (Mima-like) mounds in Wyoming, *Soil Science Society of America Journal* **48**: 1384–1392.
- Stahr, K., Kühn, J., Trommler, J., Papenfuß, K.-H., Zarei, M. and Singer, A. (2000). Palygorskite-cemented crusts (palycretes) in Southern Portugal, *Australian Journal of Soil Research* **38**: 169–188.
- Stoessell, R. K. (1988). 25° C and 1 atm dissolution experiments of sepiolite and kerolite, *Geochimica et Cosmochimica Acta* **52**: 365–374.
- Stoessell, R. K. and Hay, R. L. (1978). The geochemical origin of sepiolite and kerolite at Amboseli, Kenya, *Contributions to Mineralogy and Petrology* **65**: 255–267.
- Stone, E. L. and Comerford, N. B. (1994). Plant and animal activity below the solum, in D. L. Cremeens, R. B. Brown and J. H. Huddleston (eds), *Whole Regolith Pedology*, Soil Science Society of America, Madison, Wisconsin, USA, pp. 57–74. SSSA Special Publication Number 34.
- Stoops, G. (1964). Application of some pedological methods to the analysis of termite mounds, in A. Bouillon (ed.), *Etude sur les Termites africains*, Lovanium, Kinshasa, pp. 379–398.
- Stoops, G. (2003). *Guidelines for the Analysis and Description of Soil and Regolith Thin Sections*, Soil Science Society of America, Madison, Wisconsin, USA.
- Suarez, M., Robert, M., Elsass, F. and Martin Pozas, J. M. (1994). Evidence of a precursor in the neoformation of palygorskite - new data by analytical electron microscopy, *Clay Minerals* **29**: 255–264.
- Sullivan, L. (1994). Clay coating formation on impermeable materials: deposition by suspension retention, in A. J. Ringrose-Voase and G. S. Humphreys (eds), *Soil Micromorphology: Studies in Management and Genesis*, Developments

- in *Soil Science* 22, Elsevier, Amsterdam, pp. 373–380. Proceedings of the IX International Working Meeting on Soil Micromorphology, Townsville, Australia, July 1992.
- Summerfield, M. A. (1983a). Petrography and diagenesis of silcrete from the Kalahari Basin and Cape Coastal Zone, southern Africa, *Journal of Sedimentary Petrology* **53**: 895–909.
- Summerfield, M. A. (1983b). Silcrete, in A. S. Goudie and K. Pye (eds), *Chemical Sediments and Geomorphology: Precipitates and Residua in the Near-Surface Environment*, Academic Press, London, pp. 59–91.
- Summerfield, M. A. (1983c). Silcrete as a palaeoclimatic indicator: evidence from southern Africa, *Palaeogeography, Palaeoclimatology, Palaeoecology* **41**: 65–79.
- Tankard, A. J. (1966). *The Namaqualand Coastal Deposits with special reference to the area between the Groen and Buffels rivers*. B.Sc Project, University of Natal.
- Tankard, A. J. (1975). *The late Cenozoic History and Palaeoenvironments of the coastal margin of the southwestern Cape Province*, PhD thesis, Rhodes University, Grahamstown.
- Tankard, A. J. and Rogers, J. (1978). Late Cenozoic palaeoenvironments on the west coast of southern Africa, *Journal of Biogeography* **5**: 319–337.
- Ten Cate, H. (1966). *Die gronde van die Overhex-Nuy gebied naby Worcester*, Master's thesis, University of Stellenbosch (M.Sc. (Agric)).
- Thellier, C., Fritz, B., Paquet, H., Gac, J. Y. and Clauer, N. (1988). Chemical and mineralogical effects of saline water movement through a soil during evaporation, *Soil Science* **146** (1): 22–29.
- Timpson, M. E., Richardson, J. L., Keller, L. P. and McCarthy, G. J. (1986). Evaporite mineralogy associated with saline seeps in southwestern North Dakota, *Soil Science Society of America Journal* **50**: 490–493.
- Tinely, K. L. (1985). Coastal Dunes of South Africa. SA Nat. Scientific Programmes Report no.109. FRD Council for Scientific and Industrial Research, Pretoria.

- Torres-Ruíz, J., López-Galindo, A., González-López, J. M. and Delgado, A. (1994). Geochemistry of Spanish sepiolite-palygorskite deposits: genetic consideration based on trace elements and isotopes, *Chemical Geology* **112**: 221–245.
- Tracy, S. L., François, C. J. P. and Jennings, H. M. (1998a). The growth of calcite spherulites from solution I. Experimental design techniques, *Journal of Crystal Growth* **193**: 374–381.
- Tracy, S. L., François, C. J. P. and Jennings, H. M. (1998b). The growth of calcite spherulites from solution II. Kinetics of formation, *Journal of Crystal Growth* **193**: 382–388.
- Usai, M. R. and Dalrymple, J. B. (2003). Characteristics of silica-rich pedofeatures in a buried paleosol, *Catena* **54**: 557–571.
- van der Eyk, J. J., Macvicar, C. N. and de Villiers, J. M. (1969). *Soils of the Tugela Basin*, Natal Town and Regional Planning Reports, Volume 15, Town and Regional Planning Commission, Natal.
- Van der Merwe, C. R. (1940). Soil groups and sub-groups of South Africa. Science Bulletin of the Department of Agriculture of South Africa no. 231/Chemistry series of the Dept. of Agriculture and Forestry no. 165; Originally presented as the author's thesis (D. Sc. University of Stellenbosch, 1940).
- Van Houten, F. B. (1973). Origin of red beds: a review 1961-1972, *Annual Review of Earth and Planetary Sciences* **1**: 39–61.
- Van Scoyoc, G. E., Serna, C. J. and Ahlrichs, J. L. (1979). Structural changes in palygorskite during dehydration and dehydroxylation, *American Mineralogist* **64**: 215–223.
- Van Zinderen Bakker, E. M. (1976). The evolution of late-Cenozoic paleoclimates of southern Africa, *Palaeoecology of Africa* **9**: 160–202.
- Vanden Heuvel, R. C. (1964). The occurrence of sepiolite and attapulgite in the calcareous zone of a soil near Las Cruces, New Mexico, *Thirteenth National Conference on Clays and Clay Minerals (Clays and Clay Minerals)* **13**: 193–207.

- Verrecchia, E. P., Dumont, J. and Verrecchia, K. E. (1993). Role of calcium oxalate biomineralisation by funghi in the formation of calcretes: a case study from Nazareth, Israel, *Journal of Sedimentary Petrology* **63** (5): 1000–1006.
- Verrecchia, E. P., Freytet, P., Verrecchia, K. E. and Dumont, J. (1995). Spherulites in calcrete laminar crusts: biogenic CaCO₃ precipitation as a major contributor to crust formation, *Journal of Sedimentary Research* **A65** (4): 690–700.
- Verrecchia, E. P. and Le Coustumer, M. (1996). Occurrence and genesis of palygorskite and associated clay minerals in a Pleistocene calcrete complex, Sde Boqer, Negev Desert, Israel, *Clay Minerals* **31**: 183–202.
- Verrecchia, E. P. and Verrecchia, K. E. (1994). Needle-fiber calcite: a critical review and a proposed classification, *Journal of Sedimentary Research* **A64** (3): 650–664.
- VetPath Veterinary Pathologists (2004). Nephrotoxins in Cattle in Southern Africa. Available at http://www.vetpath.co.za/large_16_nephrotoxins_in_cattle.htm. Email: info@vetpath.co.za; modified 2004, last accessed 2007.
- Von Damm, K. L. and Edmond, J. M. (1964). The occurrence of sepiolite and attapulgite in the calcareous zone of a soil near Las Cruces, New Mexico, *Thirteenth National Conference on Clays and Clay Minerals (Clays and Clay Minerals)* **13**: 193–207.
- Walker, T. R. (1967). Formation of red beds in modern and ancient deserts, *Geological Society of America Bulletin* **78**: 353–368.
- Walker, T. R. and Honea, R. M. (1969). Iron content of modern deposits in the Sonoran Desert: a contribution to the origin of red beds, *Geological Society of America Bulletin* **80**: 535–544.
- Wang, Y., Nahon, D. and Merino, E. (1993). Geochemistry and dynamics of calcrete genesis in semi-arid regions, *Chemical Geology* **107**: 349–351.
- Washburn, A. L. (1988). Mima mounds: an evaluation of proposed origins with special reference to the Puget Lowland, *Technical report*. Washington Division of Geology and Earth Resources, Report of Investigations, vol. 29.

- Watkeys, M. K. (1999). Soils of the arid south-western zone of Africa, *in* W. R. J. Dean and S. J. Milton (eds), *The Karoo: ecological patterns and processes*, Cambridge University Press, Cambridge, pp. 17–26.
- Watson, J. P. (1962). The soil below a termite mound, *Journal of Soil Science* **13** (1): 46–51.
- Watts, N. L. (1977). Pseudo-anticlines and other structures in some calcretes of Botswana and South Africa, *Earth Surface Processes* **2**: 63–74.
- Watts, N. L. (1978). Displacive calcite: Evidence from recent and ancient calcretes, *Geology* **6**: 699–703.
- Watts, N. L. (1980). Quaternary pedogenic calcretes from the Kalahari (southern Africa): mineralogy, genesis and diagenesis, *Sedimentology* **27**: 661–686.
- Weather Bureau (1988). Climate of South Africa: Climate Statistics up to 1984, *Technical report*. Department of Environment Affairs, Pretoria.
- Weaver, C. E. and Beck, K. C. (1977). Miocene of the S.E. United States: a model for chemical sedimentation in a peri-marine environment, *Sedimentary Geology* **17**: 1–234.
- Weaver, R. M., Syers, J. K. and Jackson, M. L. (1968). Determination of silica in citrate-bicarbonate-dithionite extracts of soils, *Soil Science Society of America Proceedings* **32**: 497–501.
- White, J. (1979). *Introduction to the Principles and Practice of Soil Science*, Blackwell, Oxford.
- Wieder, M. and Yaalon, D. H. (1974). Effect of matrix composition on carbonate nodule crystallization, *Geoderma* **11**: 95–121.
- Wieder, M. and Yaalon, D. H. (1982). Micromorphological fabrics and developmental stages of carbonate nodular forms related to soil characteristics, *Geoderma* **28**: 203–220.
- Wollast, R., Mackenzie, F. T. and Bricker, O. P. (1968). Experimental precipitation and genesis of sepiolite at earth surface conditions, *The American Mineralogist* **53**: 1645–1662.

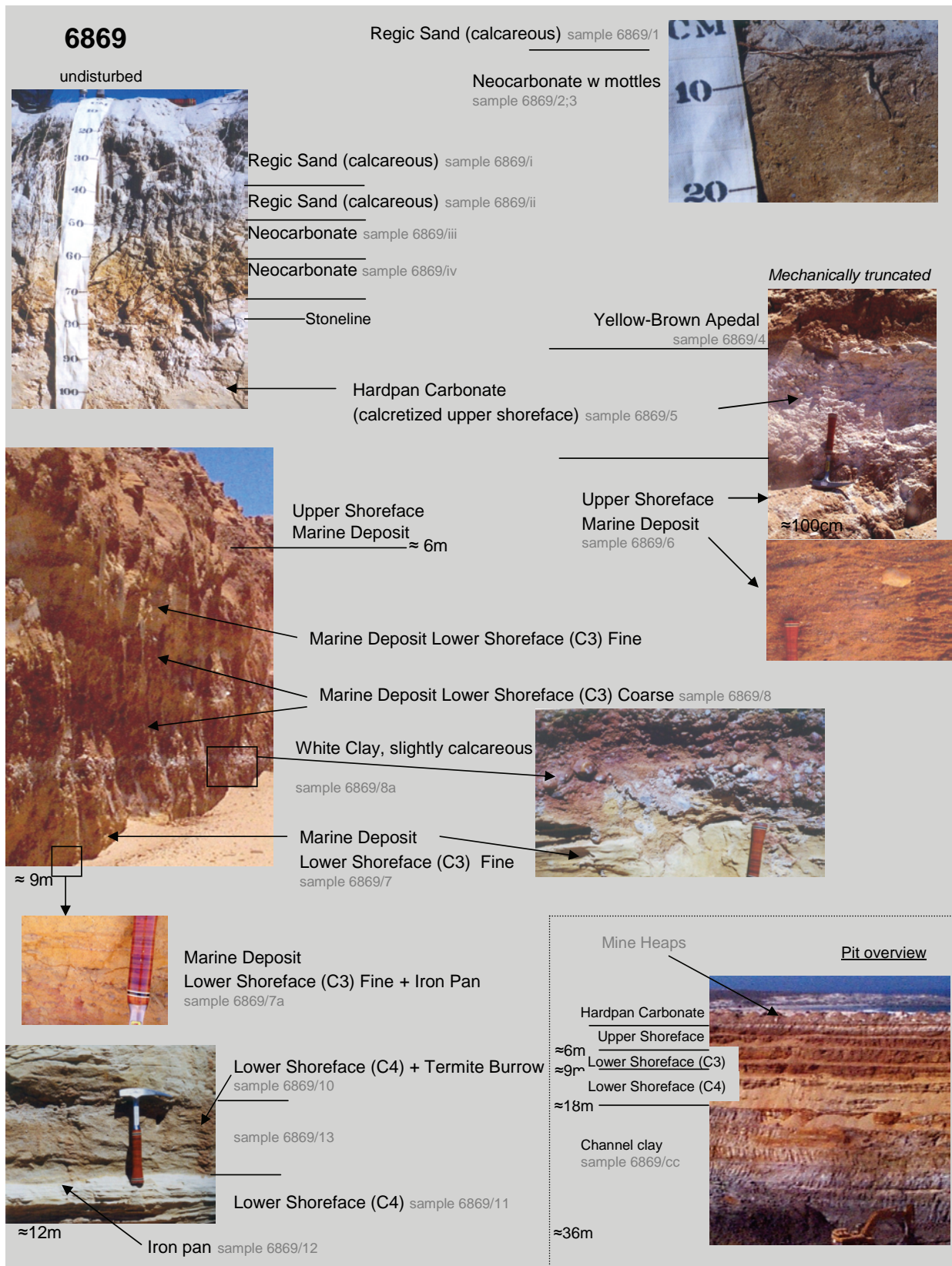
- World Reference Base for Soil Resources (WRB) (1998). World Soil Resources Reports no 84, Food and Agricultural Organization of the United Nations (FAO), Rome.
- Wright, V. P. and Tucker, M. E. (1991). Calcretes: an introduction, *in* V. P. Wright and M. E. Tucker (eds), *Calcretes*, Reprint Series Volume 2 of the International Association of Sedimentologists, Blackwell Scientific Publications, Oxford, pp. 1–22.
- Wright, V. P., Turner, M. S., Andrews, J. E. and Spiro, B. (1993). Morphology and significance of super-mature calcretes from the Upper Old Red Sandstone of Scotland, *Journal of Geological Society of London* **150**: 871–883.
- Yaalon, D. H. (1981). On the aeolianite-red sands relationship in coastal Natal, *Proceedings of the 6th Conference of S.A.S.Q.U.A. (The Southern African Society for Quaternary Research)*, Balkema, Pretoria, pp. 145–148.
- Yaalon, D. H. and Wieder, M. (1976). Pedogenic palygorskite in some arid (calciorthid) soils of Israel, *Clay Minerals* **11**: 73–80.
- Yalçın, H. and Bozkaya, Ö. (1995). Sepiolite-palygorskite from the Hekimhan region (Turkey), *Clays and Clay Minerals* **43** (6): 705–717.
- Zaaboub, N., Abdeljaouad, S. and Lopez-Galindo, A. (2005). Origin of fibrous clays in Tunisian Paleogene continental deposits, *Journal of African Earth Sciences* **43** (5): 491–504.

Appendix A

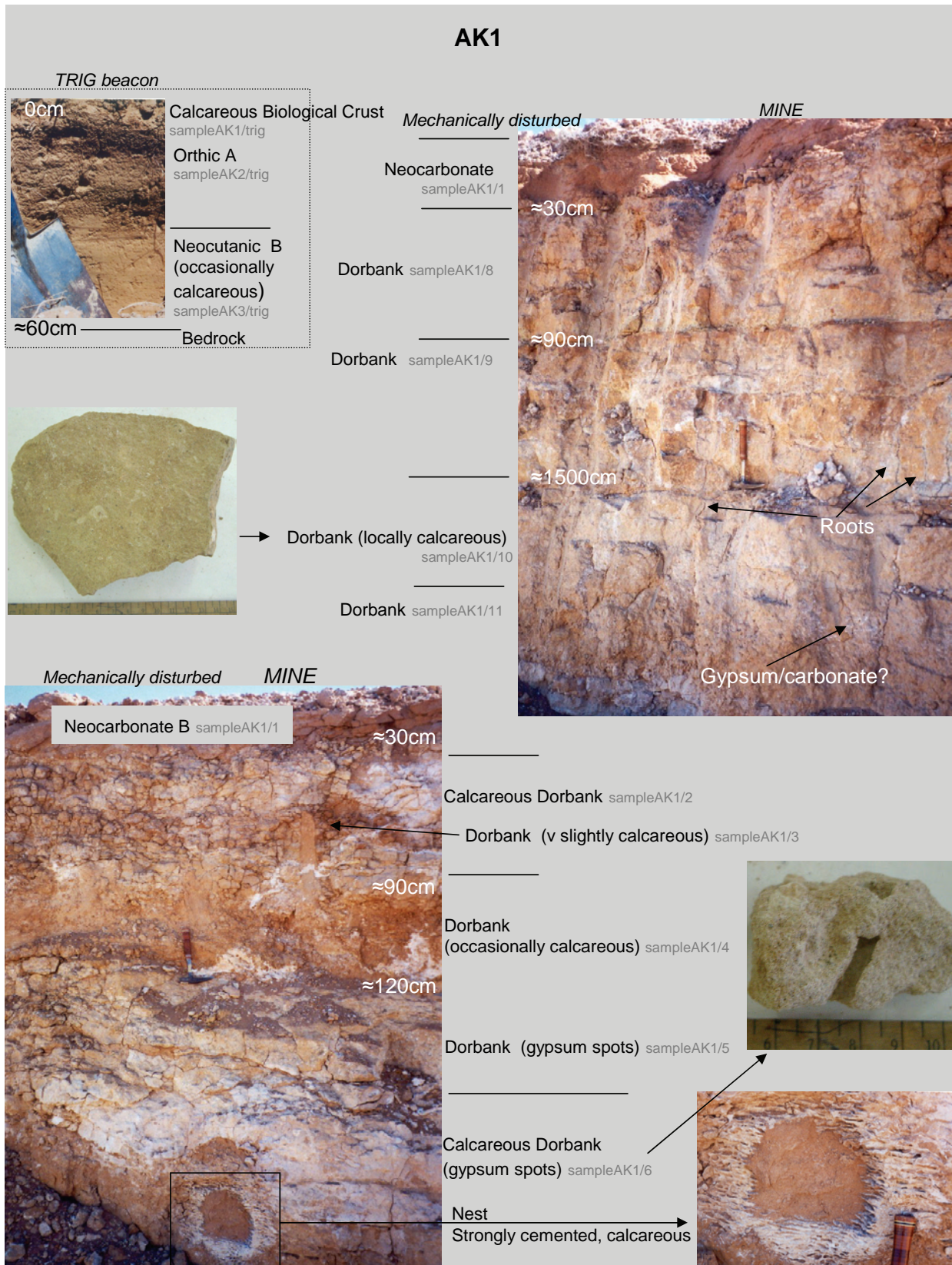
Photographs of soil profiles: BMC and KNC

Soil profiles taken in the Buffels Marine Complex (BMC) in the Kleinzee-Port Nolloth area, and the Koingnaas Complex (KNC) further south in the Koingnaas-Hondeklip Bay area.

Photographs of the Knersvlakte and Strandfontein heuweltjie are in the text.

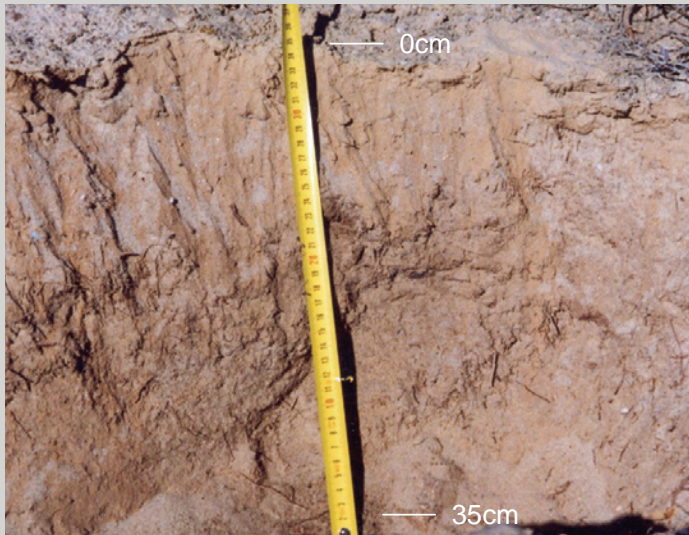


KNC: Profile 6869



BMC: Profile AK1

AK61H

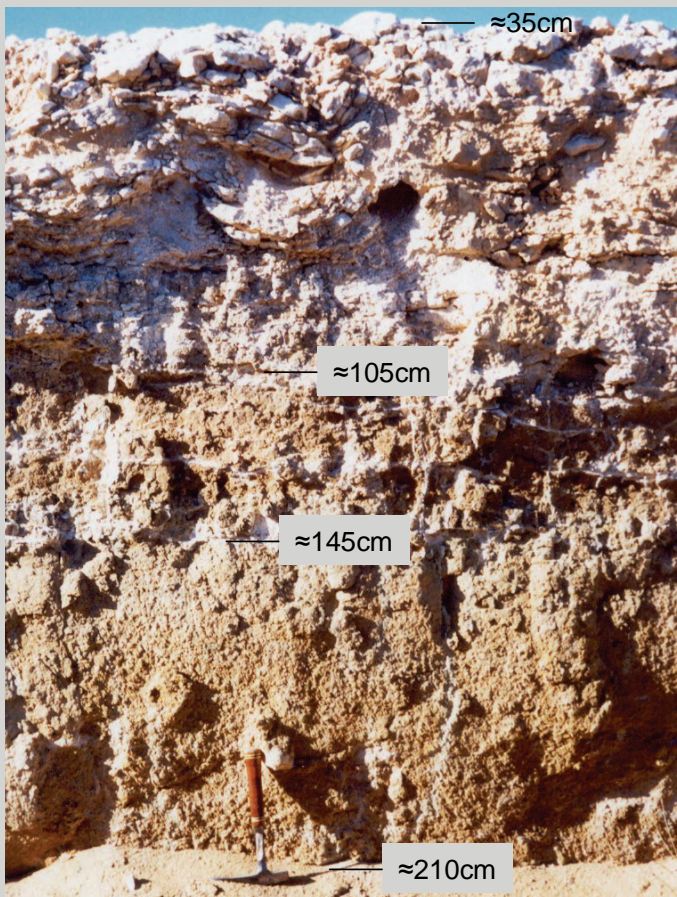


Biological Crust

Orthic A (calcareous) sample AK61H/4



Hardpan/Soft Carbonate sample AK61H/1

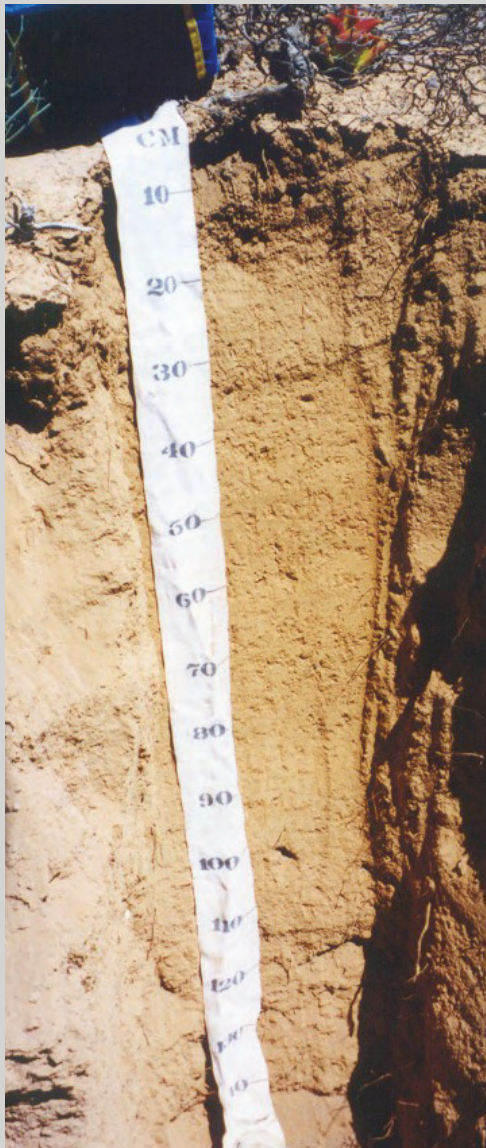


Blocky Calcretized Sediment sample AK61H/2

Marine deposit (salt efflorescence)
Sample AK61H/3

BMC: Profile AK61H

DL88



Surface Biological Crust

non-calcareous

calcareous

Bleached A sample DL88/1

Neocarbonate B sample DL88/2

Dorbank sample DL88/3

BMC: Profile DL88

KV196T



Orthic A sample KV196T/A
tunnels
≈20cm

Red Apedal B sample KV196T/B

Red Apedal B
sample KV196T/1

Dorbank sample KV196T/2

Dorbank sample KV196T/3

Calcareous Dorbank
sample KV196T/4

Hardpan/Soft Carbonate sample KV196T/5

Soft Dorbank sample KV196T/6 (≈KV196T/7?)

Soft Dorbank sample KV196T/7 (≈KV196T/6?)

Dorbank
+gypsum
sample KV196T/8

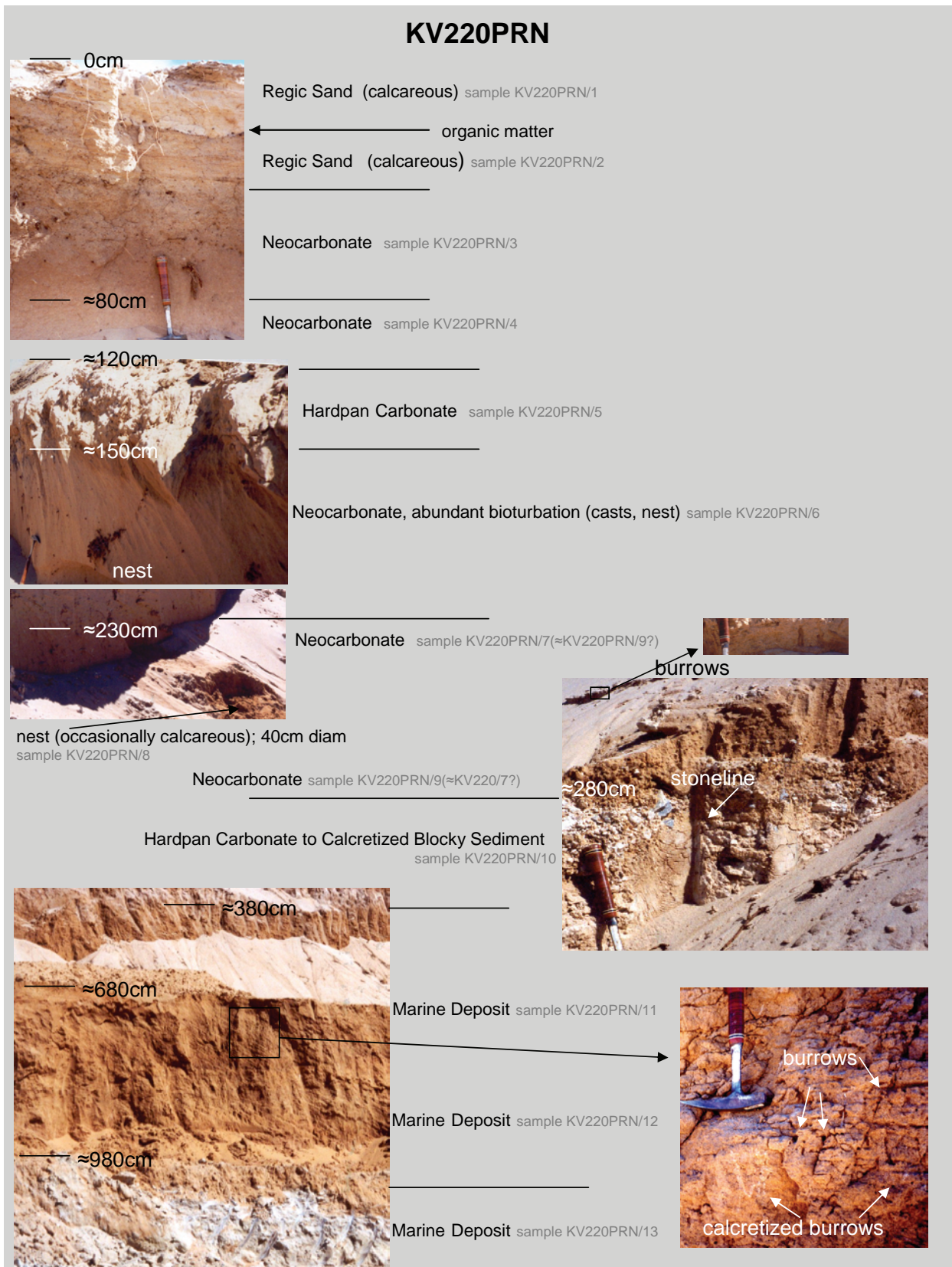
Dorbank
sample KV196T/9



Gypsum

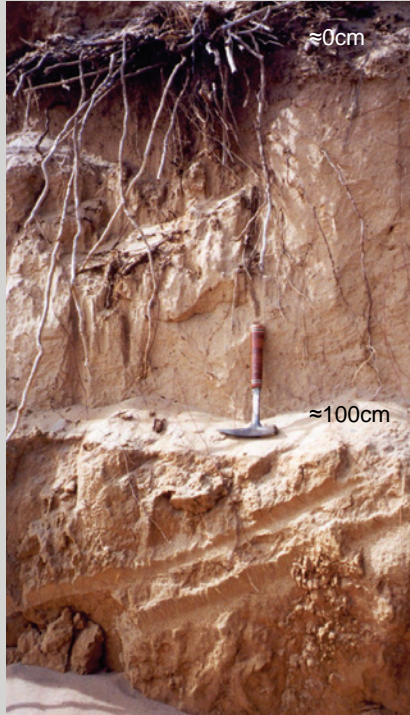
Marine Deposit sample KV196T/10

BMC: Profile KV196T



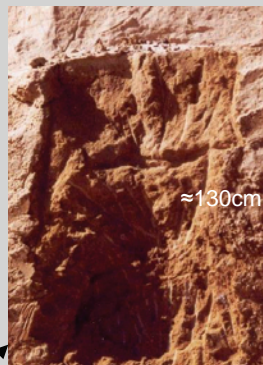
BMC: Profile KV220PRN

LKC1-5



Regic Sand sample LKC1-5/A

Regic Sand sample LKC1-5/B



Neocutanic B
sample LKC1-5/1

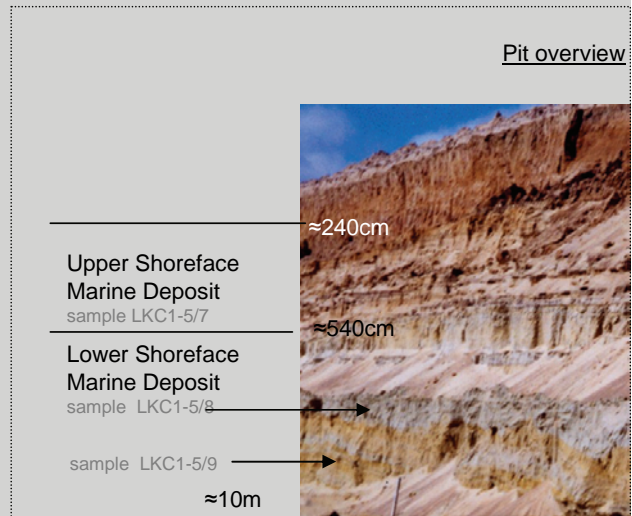
Neocutanic, Luvic
sample LKC1-5/3



Gleyed sand
sample LKC1-5/4

Sedimentary
sample LKC1-5/5

Sedimentary
sample LKC1-5/6



Pit overview

Upper Shoreface
Marine Deposit
sample LKC1-5/7

Lower Shoreface
Marine Deposit
sample LKC1-5/8

sample LKC1-5/9

≈10m

KNC: Profile LKC1-5

OBT

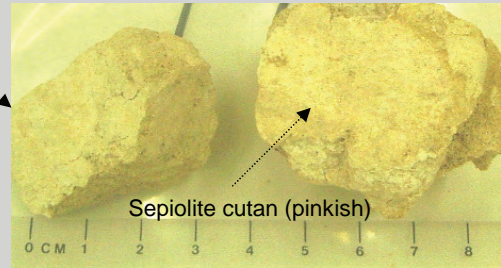


Regic Sand (deflation) (calcareous) sample OBT/1

Orthic A (calcareous) sample OBT/2

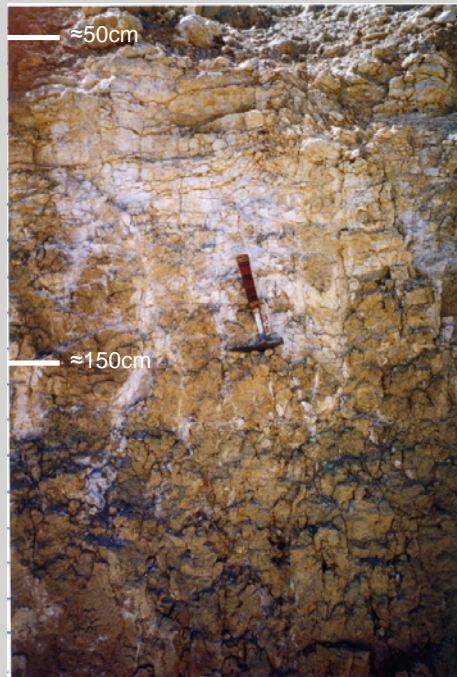
Neocarbonate B sample OBT/3

Hardpan Carbonate



Sepiolite cutan (pinkish)

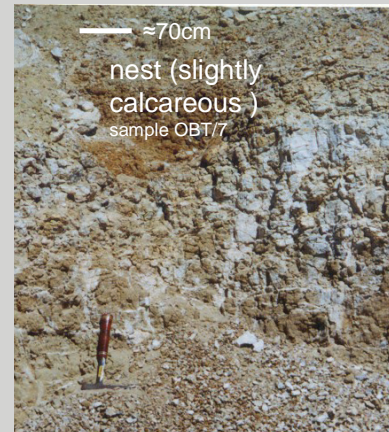
disturbed



Hardpan Carbonate to
Blocky Calcretized
Sediment
sample OBT/4 (sepiolite cutan)

Blocky Calcretized
Sediment sample OBT/5

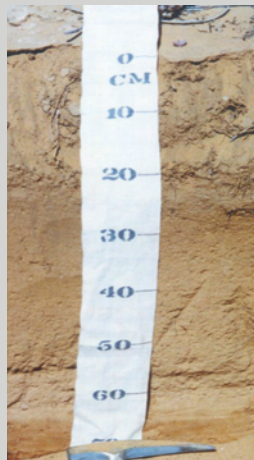
Sedimentary sample OBT/6



≈70cm

nest (slightly
calcareous)
sample OBT/7

SK11

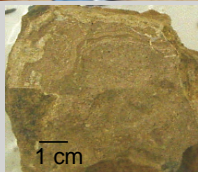


Orthic A
sample SK11/A

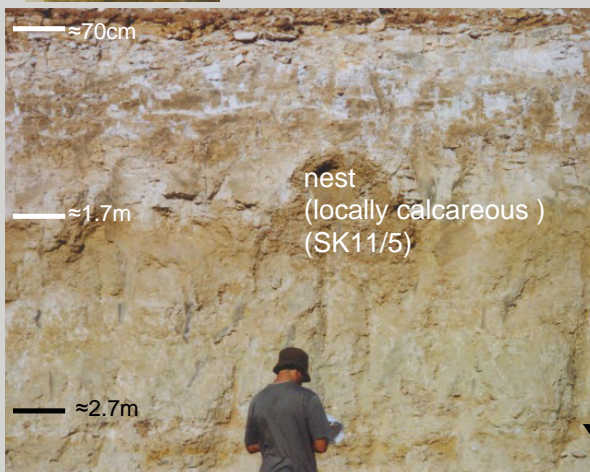
Yellow-Brown Apedal B
sample SK11/B

Gleyed Sand sample SK11/C

Neocutanic sample SK11/D



Sepiocrete
sample SK11/E



disturbed

Sepiocrete sample SK11/1

Blocky Calcretized Sediment sample SK11/6;2

Hardpan Carbonate sample SK11/3 (≈SK11/9?)

Neocarbonate sample SK11/4a

Neocarbonate sample SK11/4b

Sedimentary (locally calcareous) sample SK11/7

Iron pan sample SK11/10

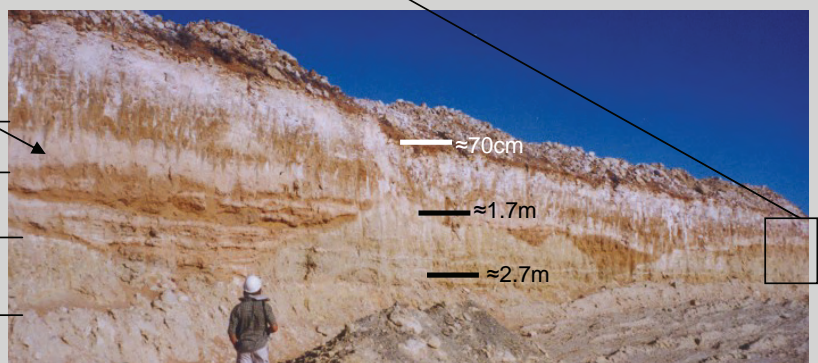


Hardpan Carbonate sample SK11/9
(≈SK11/3?)

Channel and/or bioturbation
sample SK11/8

Sedimentary sample SK11/11

Sedimentary sample SK11/12



BMC: Profile SK11

SL4-1



Orthic A sample SL4-1/1

Yellow-Brown Apedal B sample SL4-1/2

Gleyed Sand sample SL4-1/3

Neocutanic sample SL4-1/4

Yellow-Brown Apedal B sample SL4-1/2

Gleyed Sand sample SL4-1/3

Neocutanic sample SL4-1/4

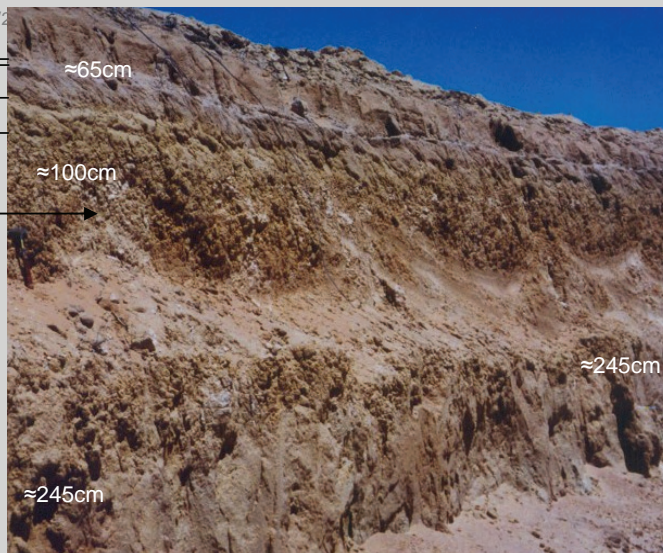
Slightly Gleyed Sand? sample SL4-1/5

Pedocutanic sample SL4-1/6

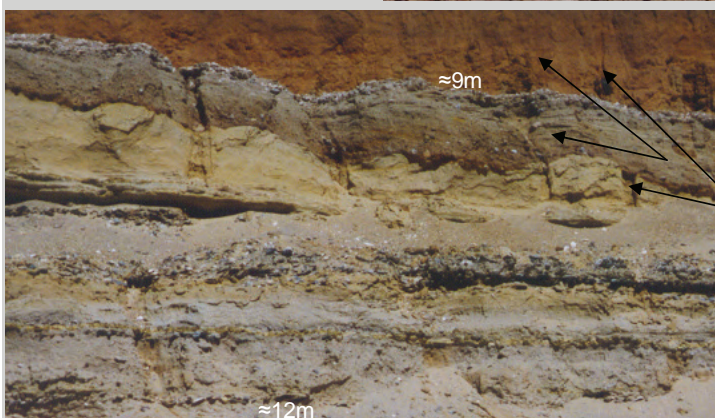
Pedocutanic +Carbonate

sample SL4-1/7

Pedocutanic sample SL4-1/8



Marine Deposit
Upper Shoreface
sample SL4-1/9



Marine Deposit
Upper Shoreface

Marine Deposit Lower Shoreface (calcareous)
sample SL4-1/10

Termite Burrows

Marine Shells – storm deposit

Marine Deposit Lower Shoreface (calcareous)
sample SL4-1/11

KNC: Profile SL4-1

SN30



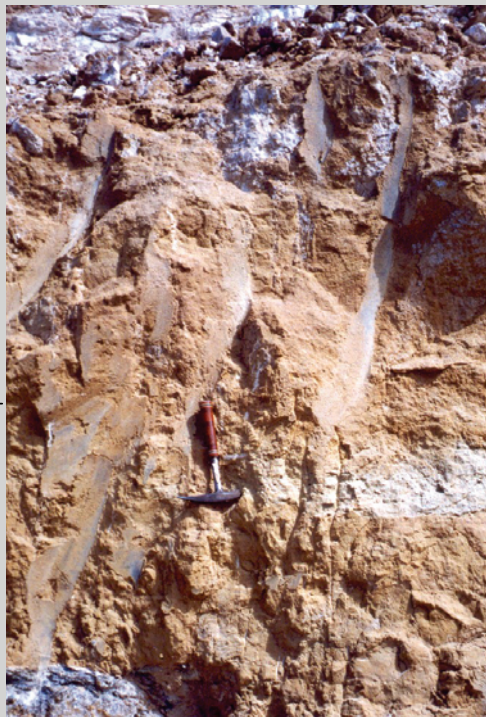
Regic Sand sample SN30/A

Neocarbonate B sample SN30/B



Hardpan Carbonate sample SN30/2

≈110cm



Upper Shoreface Marine Deposit sample SN30/3

sample SN30/5

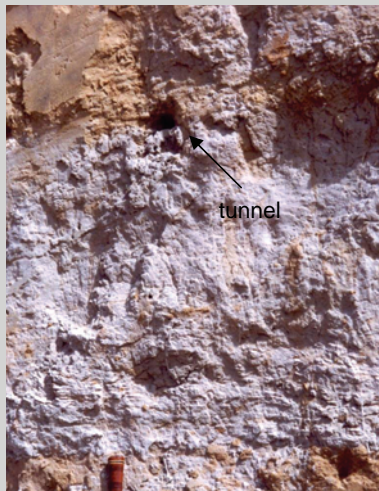
sample SN30/4

sample SN30/5

≈200cm

Lower Shoreface Marine Deposit

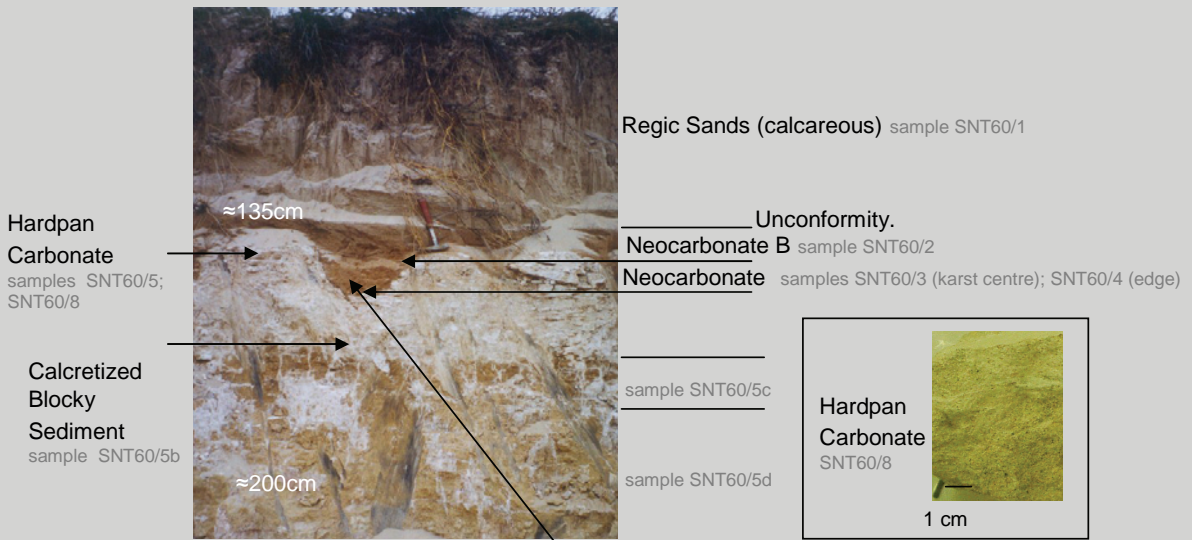
≈290cm



sample SN30/6

KNC: Profile SN30

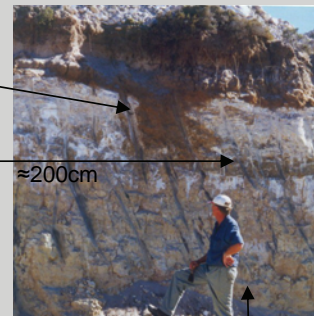
SNT60



Dissolution features



Calcretized Blocky Sediment (incl terrestrial fossil bone) sample SNT60/6



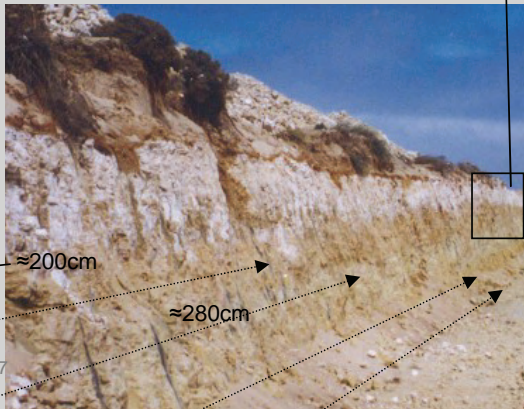
Hardpan Carbonate samples SNT60/5-5d

Calcretized Blocky Sediment sample SNT60/7

Sedimentary sample SNT60/10

Sedimentary sample SNT60/11

Sedimentary sample SNT60/12



KNC: Profile SNT60

SPNT



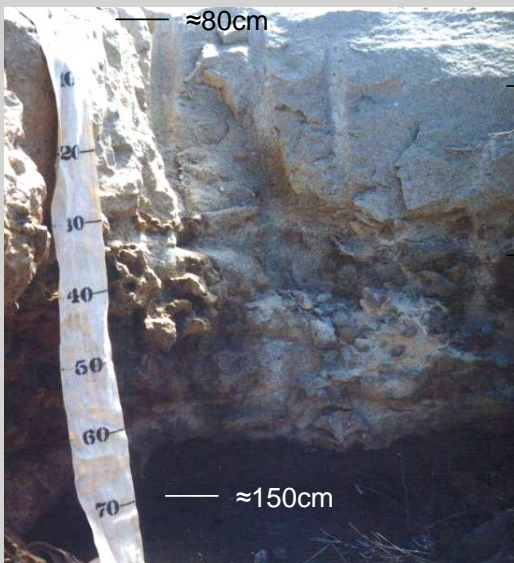
Regic sand (calcareous) sample SPNT/3

Orthic A (calcareous) sample SPNT/1

Neocarbonate B sample SPNT/2

moist

Hardpan Carbonate



disturbed

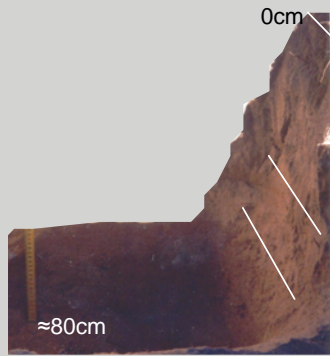
Hardpan Carbonate
sample SPNT/4

Hardpan Carbonate
sample SPNT/5



KNC: Profile SPNT

TP231L



Orthic A (calcareous) sampleTP231L/A

≈30cm

E (calcareous) sampleTP231L/E

≈50cm

Neocarbonate B sampleTP231L/B



New Profile

Regic Sand (calcareous) (disturbed?) sampleTP231L/1

Unconformity

Neocarbonate sampleTP231L/2

Hardpan Carbonate sampleTP231L/3

≈200cm



Marine deposit - structure possibly from bioturbation

Abundant tunnels; carbonate-filled tunnels sampleTP231L/4

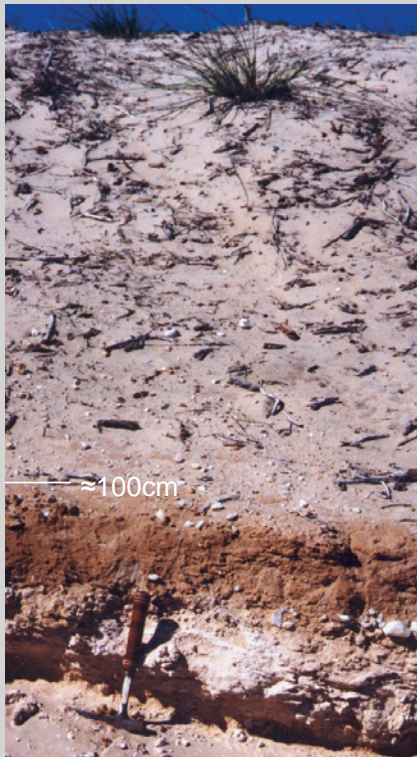


≈15m

Marine deposit sampleTP231L/3

BMC: Profile TP231L

TP266Q



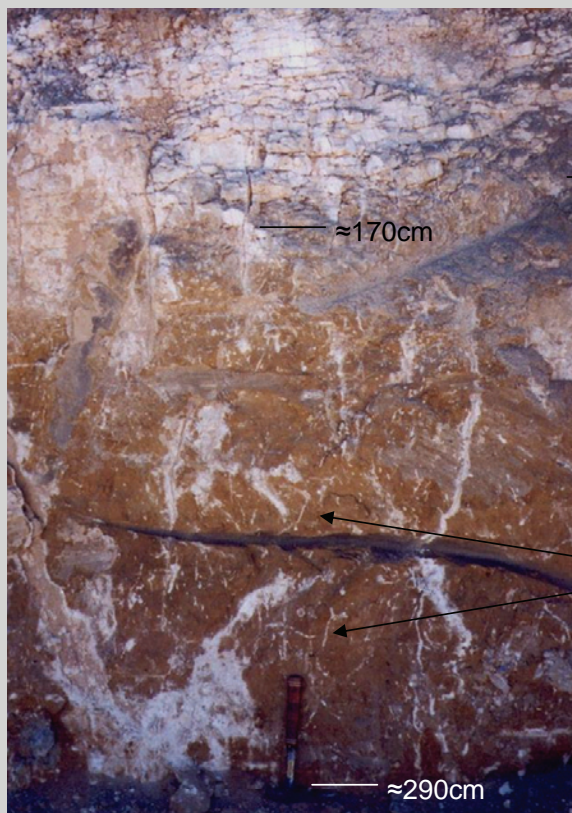
Regic Sand (calcareous) sample TPQ266/5

Unconformity

Neocarbonate B sample TPQ266/4

Stoneline

Hardpan Carbonate sample TPQ266/3



Hardpan Carbonate sample TPQ266/1



Possibly Marine sample TPQ266/2

Calcretised burrows

BMC: Profile TP266Q